

Biophysical Studies of Lipid Membranes and their Interactions with Amyloid Peptides

by

Elizabeth Drolle

A thesis

presented to the University of Waterloo

in fulfillment of the

thesis requirements for the degree of

Doctor of Philosophy

in

Biology

Waterloo, Ontario, Canada, 2015

© Elizabeth Drolle 2015

Author's Declaration

This thesis consists of material all of which I authored or co-authored: see Statement of Contributions included in the thesis. This is a true copy of the thesis, including any required final revisions, as accepted by my examiners.

I understand that my thesis may be made electronically available to the public.

Statement of Contributions

This work presented in this thesis was primarily done by myself, but there are portions of work presented that were done in collaboration with other students and scientists. Certain chapters of this thesis have been previously published in academic, peer-reviewed journals; for each of these published portions, I was a first author of the work. Each chapter begins with a detailed description of the work and a contribution statement, outlining my role in the work as well as the role of any collaborators, if applicable. Briefly:

Chapter Two: Review paper co-written with two others and myself. I modified this paper and adapted several figures to minimize overlap with other published works included in this thesis; the majority of the resulting chapter was done by me.

Chapter Three: This neutron scattering study was carried out, and the data were analyzed and written up primarily by me, with the assistance of an expert in the field at the nuclear reactor. Supplementary material done by collaborators is included to support the neutron scattering findings.

Chapter Four: Preliminary data for this AFM study was collected in equal part by me and my co-first-author. However, after preliminary results were obtained, all the experiments were repeated multiple times and I introduced a new system before my co-author and I jointly wrote the manuscript. Minor modifications to the manuscript were done to minimize certain contributions from my coauthor.

Chapter Five: This study was done primarily by me with the assistance of a postdoctoral fellow who is an expert in FM-KPFM; he assisted in KPFM imaging and analysis.

Chapter Six: For this work, I had an undergraduate assistant who, under my supervision and direction, participated in sample preparation and analysis.

Chapter Seven: This chapter was done primarily by me but includes a small portion on electrophysiology study of the membrane carried out by collaborators at Dalhousie University.

Abstract

Amyloid beta peptides are known to form amyloid fibrils which are implicated in more than 20 currently incurable neurodegenerative diseases, including Alzheimer's, Huntington's and Parkinson's. The proposed mechanism of amyloid fibril formation involves protein unfolding and formation of amyloid β -sheet aggregates. Although fibril plaque formation is associated with biological membranes *in vivo*, the role of membrane heterogeneity - and especially the effect of cholesterol and lipid rafts - in the process of amyloid fibril formation and toxicity is not well understood. Therefore, research in this area is of great interest and necessity. Cholesterol is a well-known sterol, which is found in eukaryotic membranes and is important for membrane structure and function. It has been shown that an increased level of cholesterol may lead to various disorders. It is my hypothesis that cholesterol may alter the interaction of plasma membrane with membrane-interacting biomolecules such as amyloid beta and may play an important role in amyloid toxicity.

In this thesis, I used multiple methods of investigation, including neutron scattering, atomic force microscopy, the Langmuir-Blodgett trough, and frequency modulated-Kelvin probe force microscopy, to study both simple and complex lipid systems. The thesis is organized in such a way that it begins with looking at the simple systems of a single to a few lipids and proceed to examine more complex systems, with multiple constituents.

Through these methods, it was found that cholesterol and melatonin have opposite effects on altering membrane thickness. Lipid properties like head group charge and lipid phase were shown to define the size and the amount of amyloid clusters when incubated on single lipid systems, and the presence of cholesterol resulted in cholesterol-induced electrostatic domains that can cause targeted binding of amyloid. It was also shown that cholesterol has measureable effects on membrane properties even in systems more complex than just a single lipid. Finally, through the development of models to mimic healthy and Alzheimer's diseased states of the membrane, it was shown that the models differed in properties and also had differential interactions with amyloid in terms of electrophysiology and amyloid accumulation.

The goal of this thesis is to investigate the nanoscale effects of both cholesterol, and the interactions of lipids in complex mixtures on the physical and electrical properties of model lipid membranes, especially nanoscale heterogeneity of the membrane and membrane domains, and how these altered properties affect binding of A β and amyloid fibril formation on the surface of lipid membranes. The results will help to understand the role of membrane nanoscale heterogeneity in the molecular mechanism of amyloid toxicity and therefore will help towards the development of new approaches for the prevention and treatment of neurodegenerative diseases.

Acknowledgments

I first and foremost want to thank my supervisor, Dr. Zoya Leonenko, for taking me under her wing as a nervous undergraduate student and giving me countless opportunities to increase my skills, knowledge, and confidence. Her passion for investigation and experimentation is what first attracted me to her research and that, along with her dedication and genuine care and concern for her students, is what kept me wanting to continue to work with her for the past years. I also would like to thank NSERC, OGS, and the Waterloo Institute for Nanotechnology (WIN) for the funding opportunities they have granted me throughout the past five years.

Thank you to my committee members: Dr. Bernard Glick; Dr. Barbara Moffatt; and Dr. Maud Gorbet. I am very fortunate to have had three such accomplished and respected researchers and human beings involved in this journey of mine, helping me along every step of the way with invaluable insight and direction.

There are many collaborative partners and instrument and research scientists that I have had the pleasure of working with over the past five years, both on projects and on helping me to increase essential skills. I would especially like to thank Dr. Norbert Kučerka for his hard work and dedication to our joint projects, which, I am happy to say, are continuing on to this day.

To my lab-mates (and adopted lab-mates) past and present, including Brenda, Robbie, Francis, Vince, Simon, Keely, and Ravi to just name a few, and especially my long-time partner in crime Erin: thank you so much for the support, assistance, collaborations, and stress-relief you have given me throughout this process. But most of all, thank you for your friendship; I'm unquestionably lucky to have come out at the end of this process with not only some data, but also a group of wonderful people I am honoured to call my friends.

Last but certainly not least, I want to thank my parents, Ronnie and Hugh, my brother and sister-in-law, Chris and Katerina, my life-long best friend Ashley, and Richard; I love you all so much and could not have asked for a better support group throughout this journey that was full of ups and downs. I would not be the person I am today without all of you.

Table of Contents

Author’s Declaration	ii
Statement of Contributions	iii
Abstract	iv
Acknowledgments	vi
List of Tables	xi
Chapter Six	xii
Chapter Seven	xii
List of Figures	xii
Chapter One	xii
Chapter Two	xii
Chapter Three	xii
Chapter Four	xiii
Chapter Five	xiv
Chapter Six	xiv
Chapter Seven	xiv
List of Abbreviations	xvi
Chapter 1.0: Introduction and Methods	1
1.1 The Cell Membrane	2
1.1.1 Cell Membrane Structure and Function	2
1.1.2 Model Membranes	3
1.2 Cholesterol in the Membrane	3
1.2.1 Lipid Raft Hypothesis	4
1.2.2 Effect of Cholesterol on Membrane Properties.....	5
1.3 Alzheimer’s Disease	6
1.3.1 Amyloid Fibril Formation: Molecular Mechanism.....	6
1.3.2 Peptide Interactions with the Membrane	7
1.4 Experimental Methods and Sample Preparation	9

1.4.1 Langmuir Blodgett Monolayer Technique	9
1.4.2 Atomic Force Microscope	11
1.4.3 Kelvin probe force microscopy	12
1.4.4 Neutron Scattering	13
1.5 Goals of Thesis and Objective of Research.....	16
Chapter 2.0: Review - The use of atomic force microscopy to study molecular mechanisms of amyloid fibril formation and toxicity in Alzheimer's disease	18
1.1 Introduction	20
1.1.1 Alzheimer's Disease	20
1.1.2 Nanotechnology and Atomic Force Microscopy	24
2.2 Atomic Force Microscopy to Study Amyloid Fibril Formation and Toxicity in Alzheimer's Disease.....	26
2.2.1 AFM Imaging of Fibrils and Oligomers	26
2.2.2 Effect of Surfaces on Amyloid Fibril Formation.....	28
2.2.3 Effect of Lipid Membrane on Amyloid Fibril Formation.....	34
2.3 Summary	48
Chapter 3.0 Comparative Effects of Cholesterol and Melatonin on the Physical Properties of the Lipid Membrane	49
3.1 Overview	51
3.2 Introduction	51
3.3 Materials and Methods	55
3.3.1 Sample Preparations	55
3.3.2 Small-Angle Neutron Diffraction.....	56
3.3.3 Small-Angle Neutron Scattering	58
3.4 Results.....	60
Chapter 4.0 - Amyloid-β Aggregation on Model Lipid Membranes: An Atomic Force Microscopy Study	73
4.1 Overview	75
4.2 Introduction	75
4.3 Materials and Methods	77
4.3.1 Lipid bilayer preparation	77
4.3.2 Amyloid- β Incubation	78

4.3.3 Atomic force microscopy imaging	78
4.3.4 Image analysis	79
4.3.5 Statistical analysis	79
4.4 Results	79
4.5 Discussion	86
4.6 Conclusion	91
Chapter 5.0 Nanoscale Electrostatic Domains in Cholesterol-Laden Lipid Membranes Create a Target for Amyloid Binding	92
5.1 Overview	94
5.2 Introduction	94
5.3 Experimental Details.....	95
5.3.1 Supported lipid bilayers and amyloid binding.....	95
5.3.2 Supported lipid monolayers.....	95
5.3.3 Atomic force microscopy	96
5.3.4 Frequency Modulated Kelvin probe force microscopy (FM-KPFM)	96
5.3.5 Data Processing software and statistical analysis	97
5.4 Results and Discussion	98
Chapter 6.0 Effect of Cholesterol on Topographical and Electrostatic Domains in Complex Lipid Mixtures.	103
6.1 Introduction	105
6.2 Materials and Methods:.....	111
6.2.1 Lipid solution preparation.....	111
6.2.2 Supported lipid monolayers preparation on the Langmuir-Blodgett trough.....	112
6.2.3 Atomic force microscopy (AFM) and frequency modulated-Kelvin probe force microscopy (FM-KPFM).	112
6.2.4 Image processing and analysis.....	112
6.3 Results and Discussion	113
Chapter 7.0 Multicomponent lipid membrane models mimicking “healthy” and “diseased” neuronal membrane states for the study of amyloid toxicity in Alzheimer’s disease.	126
7.1 Introduction	128
7.2 Materials and Methods	132

7.2.1 Lipid solution preparation.....	132
7.2.2 Supported lipid monolayers for Atomic force microscopy (AFM) and Kelvin probe force microscopy (KPFM) imaging.....	132
7.2.3 Supported lipid bilayers and amyloid incubation for AFM imaging.....	133
7.2.4 AFM and KPFM - Monolayer Samples.....	133
7.2.5 AFM/KPFM Data Processing and Analysis.....	134
7.2.6 Planar lipid bilayers for Black Lipid Membrane (BLM) study.....	134
7.2.7 BLM recording and data analysis.....	134
7.3 Results and Discussion	135
7.4 Conclusions	151
Chapter 8.0 :Thesis Conclusions.....	154
Chapter 9.0: Future Work.....	157
References	159
Appendix A: Additional Information on Sample Preparation.....	185
A.1 Monolayer Formation via Langmuir-Blodgett Deposition.....	186
A.1.1 Solid-Supporting Sample Formation (on a Mica Substrate)	186
A.1.2 Trough Cleaning Procedures	188
A.1.3 Kelvin Compatible Samples.....	189
A.2 Membrane Formation via Vesicle Fusion	189
A.2.1 Preparing a Vesicle Solution	189
A.2.2 Membrane Preparation using Vesicle Solution	191
A.3 Amyloid Preparation	192
A.4 Buffer Preparation	193

List of Tables

Chapter Six

<i>Table 6.1: Lipid Mixtures Studied and Their Respective Lipid Ratios.</i>	<i>.....Page 111</i>
<i>Table 6.2: Summary of the Effect of Cholesterol on All Systems Studied.</i>	<i>.....Page 124</i>

Chapter Seven

<i>Table 7.1: Structures and Properties of Lipids Studied.</i>	<i>.....Page 136</i>
<i>Table 7.2: Detailed description of complex lipid systems studied.</i>	<i>.....Page 137</i>
<i>Table 7.3: Summary of Statistical Analysis of Mixed Lipid Monolayer Samples</i>	<i>.....Page 142</i>
<i>Table 7.4: Amyloid Deposition Over Time.</i>	<i>.....Page 149</i>
<i>Table 7.5: Summary of Results</i>	<i>.....Page 152</i>

List of Figures

Chapter One

Figure 1.1: Cholesterol in the Membrane.Page 4
Figure 1.2: Lipid Phases.Page 5
Figure 1.3: Schematic Model of Amyloid-Beta (1-40) Interaction with the Membrane.Page 8
Figure 1.4: Depiction of the action of a Langmuir-Blodgett trough.Page 10
Figure 1.5: Schematic depicting the set up of stacks of bilayers for neutron scattering analysis.Page 14
Figure 1.6: Neutron Scattering in ActionPage 16

Chapter Two

Figure 2.1: Schematics of AFMPage 26
Figure 2.2: Amyloid peptide Aβ (1-42) incubated in solution for 24 hours and then deposited on mica and imaged in airPage 28
Figure 2.3: Small scan size images of AFM topography of Aβ aggregates formed on modified surfacesPage 32
Figure 2.4: Schematic showing amyloid origin and the mechanism of the amyloid fibril formation and toxicityPage 34
Figure 2.5: Schematic showing proposed mechanisms of Amyloid interactions with lipid membrane.Page 37
Figure 2.6: Molecular dynamics simulation and AFM images of Aβ induced ion channels.Page 47

Chapter Three

Figure 3.1: Semi-log plot of a rocking curve (points) corresponding to the first order diffraction peak from aligned multi-bilayers (DOPC with 9 mol% melatonin).Page 57
Figure 3.2: Log-log plot of SANS data obtained for A) DPPC bilayers doped with different amounts of cholesterol (data from the N5 instrument) and B) DOPC bilayers doped with melatonin (measuredPage 59

<i>on the CG-3 Bio-SANS instrument).</i>	
<i>Figure 3.3: Schematics illustrating the proposed locations of cholesterol and melatonin in the lipid membrane: (A) cholesterol, (B) melatonin.</i>	<i>.....Page 61</i>
<i>Figure 3.4: Neutron Scattering Length Density (NSLD) profiles of DOPC bilayers with increasing concentrations of cholesterol (A) and melatonin (C), as well as DPPC with increasing concentrations of cholesterol (B) and melatonin (D).</i>	<i>.....Page 62</i>
<i>Figure 3.5: Neutron Scattering Length Density Profiles.</i>	<i>.....Page 65</i>
<i>Figure 3.6: Thicknesses of DOPC (top) and DPPC (bottom) bilayers upon the addition of cholesterol (left) and melatonin (right).</i>	<i>.....Page 67</i>
<i>Figure 3.7: Molecular dynamics simulations of DPPC and DOPC bilayers with and without melatonin.</i>	<i>.....Page 69</i>
<i>Figure 3.8: Density profiles for one bilayer leaflet calculated from MD simulations for DPPC (a) and DOPC (b) membranes at T=300 K.</i>	<i>.....Page 70</i>

Chapter Four

<i>Figure 4.1: Schematic, showing a supported bilayer on mica interacting with Aβ₁₋₄₂ in solution.</i>	<i>.....Page 80</i>
<i>Figure 4.2: Aβ1-42, 500μg/mL in buffer was allowed to incubate in solution.</i>	<i>.....Page 81</i>
<i>Figure 4.3: Comparison of AFM topography images of DPPC bilayer under different conditions</i>	<i>.....Page 82</i>
<i>Figure 4.4: AFM topography images of Aβ aggregates formed on DPPC (A), DOPG (B), DOTAP (C), and DOPC (D) bilayers after 24 h of incubation.</i>	<i>.....Page 83</i>
<i>Figure 4.5: Statistical analysis of Aβ oligomer volume adsorbed onto supported lipid bilayer DPPC, DOPC, DOPG, and DOTAP respectively at 1 h, 6 h, and 24 h of incubation time.</i>	<i>.....Page 84</i>
<i>Figure 4.6: Height distribution of Aβ oligomers formed on supported lipid bilayers, DPPC, DOPC, DOPG, and DOTAP after 1 h and 24 h of incubation with Aβ peptide solution.</i>	<i>.....Page 85</i>
<i>Figure 4.7: The structure and charge distribution in the lipid head group for lipids used</i>	<i>.....Page 90</i>

Chapter Five

Figure 5.1: 3D-Cross-sectional analysis emphasizing the importance of surface roughness parameters S_k and S_{vk}Page 97
Figure 5.2: AFM topography images of Aβ binding to the lipid membranePage 99
Figure 5.3: AFM and corresponding FM-KPFM images of lipid monolayers with and without cholesterol.Page 101

Chapter Six

Figure 6.1: Schematic of Possible Monolayer Arrangement in a Three-Component Lipid System in the Presence of CholesterolPage 114
Figure 6.2: AFM and corresponding FM-KPFM illustrating the effect of cholesterol on both the topography and electrical surface potential of a lipid mixture of DPPC and DOPC.Page 115
Figure 6.3: AFM and corresponding FM-KPFM illustrating the effect of cholesterol on both the topography and electrical surface potential of a lipid mixture of POPC and SM.Page 118
Figure 6.4: AFM and corresponding KPFM illustrating the effect of cholesterol on both the topography and electrical surface potential of a lipid mixture of DPPC, POPC, and SM.Page 119
Figure 6.5: Smaller scale image of AFM and corresponding KPFM data for a DPPC-POPC-SM-Chol sample.Page 121
Figure 6.6: AFM and corresponding FM-KPFM illustrating the effect of cholesterol on both the topography and electrical surface potential of a lipid mixture of DPPC and negatively charged DOPG.Page 122

Chapter Seven

Figure 7.1: Comparison of topography and electrical surface potential results for each system studied.Page 139
Figure 7.2: Experimental Set Up of a Black Lipid Membrane (BLM) Experiment.Page 143

<i>Figure 7.3: Ion currents observed across the membrane with “Healthy” lipid composition (A), “Diseased 1” lipid composition (B); and “Diseased 2” lipid composition (C).</i>	<i>.....Page 145</i>
<i>Figure 7.4: Comparison of the membrane conductance induced by 5 μM of Aβ on different model membranes at voltage amplitude of 50 mV.</i>	<i>.....Page 146</i>
<i>Figure 7.5: Schematic of amyloid beta interacting with a model membrane.</i>	<i>.....Page 147</i>
<i>Figure 7.6: Comparison of Amyloid Incubation on Three Different Model Membranes for Increasing Time Periods (1 and 6 Hours).</i>	<i>.....Page 148</i>

List of Abbreviations

Abbreviation	Term
Methods	
AFM	Atomic Force Microscopy
KPFM	Kelvin probe force microscopy
FM-KPFM	Frequency modulated Kelvin probe force microscopy
NS	Neutron Scattering
LB	Langmuir Blodgett (Trough)
MD	Molecular Dynamics (Simulation Studies)
BLM	Black Lipid Membrane
Lipids	
DPPC	Dipalmitoylphosphatidylcholine
DOPC	1,2-Dioleoyl-sn-glycero-3-phosphocholine
DOPG	1,2-dioleoyl-sn-glycero-3-phospho-(1'-rac-glycerol) (sodium salt)
DOTAP	1,2-dioleoyl-3-trimethylammonium-propane (chloride salt)
POPC	1-palmitoyl-2-oleoyl-sn-glycero-3-phosphocholine
SM	Sphingomyelin
Chol	Cholesterol
GM1	Monosialotetrahexosylganglioside
Additional Terms	
Ra	Average roughness
(Δ)h	(difference in) height
(Δ)V	(difference in) electrical surface potential

Chapter 1.0: Introduction and Methods

Plasma membranes – also known as cell membranes – are complex structures, composed of phospholipids, membrane-bound proteins and other lipids, such as sterols and steroids (Singer & Nicolson 1972). The cell membrane is involved in a vast number of biological processes, including but not limited to: cell signaling, cellular adhesion, and molecular transport (Singer & Nicolson 1972). It is also the first line of defense for the cell against invading species. Because of the wide array of processes that the membrane is involved in, the biological membrane properties – both physical and chemical – are extremely important when it comes to understanding certain membrane functions of cells, as well as cellular defense in relation to many diseases, including Alzheimer's disease. The proposed mechanism of amyloid fibril formation involves protein misfolding and the interaction of amyloid β -sheet aggregates, oligomers, and fibrils with the membrane. It has been shown that *in vivo*, there is an association of fibril plaque formation with biological membranes; however, the role of membrane heterogeneity - and especially the effect of cholesterol and lipid rafts – in amyloid fibril formation and toxicity is not yet well understood.

1.1 The Cell Membrane

1.1.1 Cell Membrane Structure and Function

The cell membrane is composed primarily of lipids and proteins. Lipids are the main constituents of plasma membranes, and eukaryotic cells contain three classes of lipids: glycerophospholipids (usually present in levels of 40 to 60 mol%); sphingolipids (usually present in levels of 10 to 20 mol%) and cholesterol (usually present in levels of 30 to 40 mol%) (McMullen et al, 2004). The term *phospholipid* describes a lipid molecule that contains a hydrophilic 'head' group that contains a phosphate group and a hydrophobic alkyl 'tail' region. When forming a membrane, these molecules orient themselves in a tightly packed bilayer such that the hydrophilic head groups are facing outwards into the extracellular fluid or cytoplasm and the hydrophobic alkyl tail regions face inwards, shielded from the fluid.

1.1.2 Model Membranes

Biological membranes are very complex – they can differ widely in several aspects when it comes to lipids alone, including differences in lipid head-group structure, the length of their hydrocarbon chain, degree of saturation of the acyl-chain, and mode of attachment of the hydrocarbon chains as well as composition; the complexity only increases when it comes to the other major components of membranes, like proteins. Therefore, model membranes are widely used to study these complex systems (Ohvo-Rekilä et al, 2002). Model membranes are bilayers that have a defined composition (composed of one or several lipids, often with no protein present) and are formed through artificial means, such as vesicle fusion or Langmuir-Schaeffer methods (Leblanc & Huo, 2006); they are used in order to help give a simplified system to study in order to help eliminate variables that may lead to unclear results. One of the most common methods of using model membranes is through the use of supported lipid bilayers on solid substrates or vesicle fusion (Leonenko et al, 2001). Another commonly used lipid model is lipid monolayers, which are systems that are one lipid molecule thick (essentially one leaflet of a lipid membrane), and which can also be used to study lipid systems in a simplified form.

1.2 Cholesterol in the Membrane

A cholesterol molecule is made up of four fused rings (shown in Figure 1.1) with an alterable conformation, indicating some flexibility in the rings (Yeagle 1985). The presence of a hydroxyl group gives cholesterol a polar region, while the presence of an alkyl tail gives it a non-polar hydrophobic region. Cholesterol orients itself perpendicular to the membrane of mammalian cells (parallel to the hydrophobic chains of the phospholipid molecules, as shown in Figure 1.1) (Yeagle 1985). Cholesterol is found in biological membranes in non-random distribution in domains or pools. These regions are thought to be important for the maintenance of membrane structure and function (Mukherjee & Chattopadhyay 2005). These pools – microdomains in the lipid membrane that are known as lipid rafts – are enriched in cholesterol and are tightly packed (more so than the surrounding components of the membrane) and compartmentalize certain cellular processes, like signalling-molecule assembly, membrane fluidity influence, and the trafficking of membrane proteins, as well as

act as an anchor region for important components (like proteins) that are involved in these cellular processes (Giordani et al, 2008).

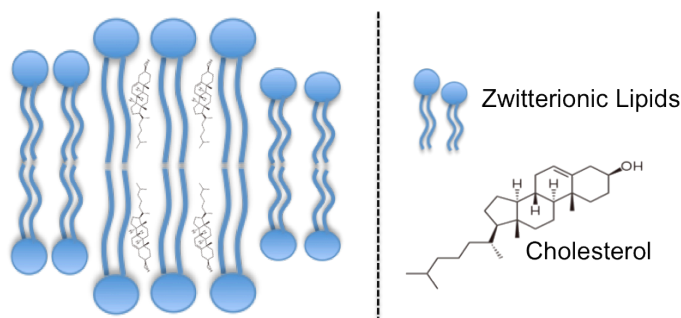


Figure 1.1: Cholesterol in the Membrane. This schematic illustrates how cholesterol orients itself into the tail group region of lipid molecules, with its hydrophilic -OH group end pointed towards the lipid head groups, and its alkyl, hydrophobic tail region shielded within the lipid tail groups. As an average lipid molecule is between 2 and 3 nm in length, this image is greatly enlarged in terms of scale.

1.2.1 Lipid Raft Hypothesis

The idea of the presence of these non-uniform regions in the membrane is known as the “lipid raft hypothesis”; it suggests that the lipids are able to form these domains (i.e. aggregates) in the membrane because of specific and preferential interactions between the lipid molecules. These interactions are due to the differing physical properties of the different lipid molecules involved, which are dependent on lipid structure and chain saturation (these factors define the ordering of the lipid tails at room temperature, as well as phase [discussed later] and the transition [melting] temperature) (Ohvo-Rekilä et al, 2002). The physical properties of a lipid determine how tightly it is able to pack together with other lipid molecules – molecules that pack tightly together have a higher melting temperature, while molecules that pack loosely together have a lower melting temperature. Studies supporting the idea of the lipid raft hypothesis tend to come from three sources: (1) the isolation of “detergent resistant membrane” (DRM) fractions of human and animal membranes; (2) the disruption in animal and human cell function when cholesterol is depleted from the membrane; and (3) the non-random distributions of raft-associated proteins within the membrane (McMullen et al, 2004).

1.2.2 Effect of Cholesterol on Membrane Properties

Cholesterol's interaction with the lipid molecules in both monolayers and in bilayers has been widely studied and extensive information has been gathered about these interactions. Cholesterol's effects are highly dependent on the properties of the lipid molecules making up the membrane. It has numerous effects on the membrane, including the ability to alter the physio-chemical properties of the membrane and the order of the membrane, among others. One of the most important properties of cholesterol is its role in the formation of lipid rafts and raft-like domains.

The effect of cholesterol on the membrane is dependent on what phase the lipid molecules are in. This property of a lipid molecule is highly dependent on two factors: the structure of the acyl chain portion of the lipid molecule (as the acyl chain length increases, the transition temperature increases) as well as the degree of saturation of the lipid molecule (as the degree of saturation decreases with the increasing presence of double and triple bonds in the acyl chain, the transition temperature decreases) (Ohvo-Rekilä et al, 2002). For example, in the liquid-crystalline state (or the “fluid phase”, L_α), cholesterol causes an increase in the lipid molecules' degree of orientational order and decreases their rate of motion – the increased order of the acyl chains translates into an increase of membrane thickness (Ohvo-Rekilä et al, 2002). In contrast, in the gel-phase (L_β), cholesterol decreases the orientational order and increases the rates of motion of the lipid molecules (McMullen et al, 2004). Cholesterol is known to induce an intermediate state, between fluid phase and gel phase, known as “liquid-ordered” or L_o , which can be visualized in Fig 1.2. Cholesterol's effects are discussed in further detail in Chapter 2 of this thesis.

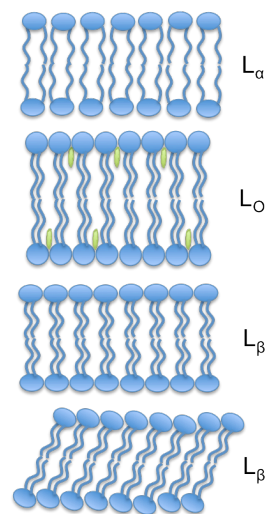


Figure 1.2: Lipid Phases. Membrane segments of fluid phase (L_α), gel phase (L_β), gel phase tilted (L_β'), and cholesterol induced liquid-ordered phase (L_o) lipids are shown (adapted from McMullen et al, 2004).

1.3 Alzheimer's Disease

Alzheimer's disease (AD), named such because of its first identification by German scientist Alois Alzheimer, is a progressive neurodegenerative disease that is associated with deterioration of memory and cognitive function (Whitehouse et al, 1982). The prevalence of Alzheimer's cases worldwide is only increasing, with current modeling studies (based on a multistate probabilistic model) suggesting there are approximately 26.6 million occurrences in 2006 (Brookmeyer et al, 2007). This number is expected to quadruple by the year 2050, giving a frequency of 1 in 85 people being diagnosed with AD (Brookmeyer et al, 2007). Because of its rapid increase in prevalence in today's population, finding a treatment for this incurable disease is of vital interest to the medical community.

One of the main features of Alzheimer's disease is amyloid-beta protein plaques (accumulations) in neuronal cell membranes and cerebral blood vessels (Puglielli et al, 2003).

1.3.1 Amyloid Fibril Formation: Molecular Mechanism

Amyloid-beta ($A\beta$) fibrils are the product of the cleavage of APP (amyloid precursor protein, NCBI gene ID: 351) by a secretase, whose activity may be modulated by the lipid environment, which also may alter the function of the secretase enzyme (Eckert et al, 2010).

$A\beta$ is actually a collective term that is used to identify a seed, aggregate, plaque, or fibril that has a characteristic structure – the cross β -sheet. Through a series of polymerization, elongation, and bundling, amyloid fibrils are formed, which are just essentially elongated amyloid twisted fibrils that are characteristically about 10 nm in diameter and over 100 nm – up to microns – in length (Chiang et al, 2008; Sipe & Cohen 2000). When these fibrils aggregate together, they form *plaques*; these plaques have been found in the affected tissues of over 20 diseases and are insoluble, affecting a great number of the regular tissue functions (Chiang et al, 2008; Sipe & Cohen 2000). The fibrils are found on the surface of neurons aggregated together in the form of plaques and when stained, originally served as a signature for diagnosing a patient with Alzheimer's disease post mortem (Sipe & Cohen 2000). This

process of membrane interaction with amyloid species can be seen in Chapter 2 of this thesis, Figure 2.4.

1.3.2 Peptide Interactions with the Membrane

The manner with which A β peptides interact with a cell membrane is of great importance to understanding the molecular mechanism of the disease itself. The membrane is the primary defense of the cell against any potential harmful species and the mechanism of interaction of A β peptides is intimately related to the mechanism of amyloid toxicity, and this mechanism is currently not well understood. This area of research recently attracted great interest but publications are still limited when compared to the study of peptide-peptide interaction in solution.

Interaction of the A β peptide with the membrane can be envisioned as either through adsorption to the surface or through partial or full insertion into the membrane, which can be seen in Figure 1.3, or full insertion into the membrane leading to the formation of an ion pore or ion channel. Using ^{31}P MAS NMR (magic angle spinning nuclear magnetic resonance) and CD (circular dichroism) spectroscopy, it has been found that A β (1-40) will bind electrostatically to a monolayer system at the air-water interface that is exhibiting a negative potential; increasing the content of acidic lipids in the monolayer decreases the surface charge (making it more negative), which can lead to increased accumulation of A β peptide on the surface of the lipid system in β -sheet resembling aggregates (Bokvist et al, 2004). Insertion of the A β peptide into the lipid system has also been shown to be greatly affected by surface charge. In neutral monolayers, only a short segment of the peptide (a hydrophobic portion) will insert into the monolayer; when surface charge decreases, it allows for electrostatic anchoring of the surface charged residues and this allows for more of the peptide to insert into the monolayer (Bokvist et al, 2004). This charge dependence investigated by Bokvist et al. in a monolayer study is extrapolated to a bilayer system and is illustrated in Figure 1.3.

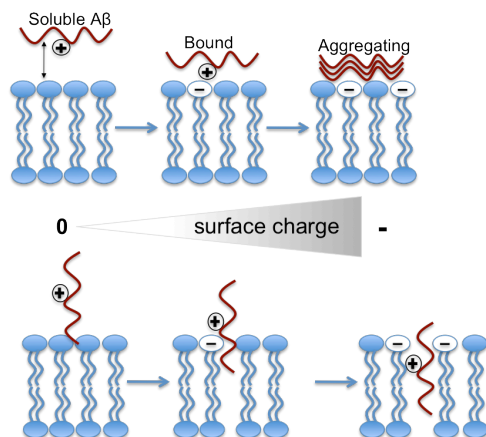


Figure 1.3: Schematic Model of Amyloid-Beta (1-40) Interaction with the Membrane (adapted from Bokvist et al, 2004). This image illustrates the idea that increasing surface charge of a bilayer can affect A β interactions, both in terms of aggregation atop the membrane (adsorption) and penetration of the amyloid peptide into the membrane.

A β has been shown to have effects on the lipid membrane, including alterations in membrane fluidity (Eckert et al, 2010). Other observations include A β compromising the integrity of the membrane, causing leakage (lipid monolayer studies) and alteration of ionic homeostasis by integration into the membrane to form ion channels (single lipid bilayer and liposome studies) (Ambroggio et al, 2005; Arispe 2004)

Cholesterol concentration has been shown to affect the insertion of A β_{1-40} into the membrane. Ji et al. (Ji et al, 2002b) studied this using both monolayer research and membranes formed through phospholipid vesicle fusion and, using mass spectrometry, electron microscopy, and circular dichroism, they found that at concentrations less than 30 mol%, A β_{1-40} tends to stay in its beta-sheet structure; at concentrations above, A β_{1-40} can insert spontaneously into the membrane. It has also been shown that A β_{1-40} insertion in the membrane may prevent fibril formation (Ji et al, 2002b) as well as insertion being increased in a low pH environment (Ji et al, 2002a).

Previous studies using the atomic force microscope have also shown the preferential accumulation of A β_{1-42} to gel phase lipids when introduced to a pre-supported mixed lipid membrane (Choucair et al, 2007). Cell culture studies with cholesterol and amyloid plaques in human neuroblastoma cells have also shown the possibility that increased cholesterol

content reduces membrane disruption (alteration of function) by the amyloid plaques (Cecchi et al, 2009). This group used confocal laser microscopy, anisotropy fluorescence, and atomic force microscopy and found that A β oligomers interacted with membrane rafts and that a moderate increase in the cholesterol content in the membrane – leading to an increased cholesterol content in the rafts – tended to decrease amyloid-induced membrane modifications in the lipid rafts (Cecchi et al, 2009).

The cell membrane is a very a complex structure, as is the amyloid peptide itself. Despite the great interest this area has attracted, only simple lipid systems have been studied to date; these do not fully allow one to address the question of lipid complexity and specifically the presence of nanodomains on the interaction of a lipid membrane with amyloid beta peptides. As such, much remains left to be discovered about the interactions of amyloid and the membrane, despite very large amounts of research being done in this area, to truly address these question, the use of more complex mixtures are needed in order to closer approach the complexity of the cell membrane. This is a challenging task that requires the use of advance methods and instrumentation in order to resolve these nanoscale structures.

1.4 Experimental Methods and Sample Preparation

1.4.1 Langmuir Blodgett Monolayer Technique

The Langmuir-Blodgett trough is a specialized apparatus that allows for the compression of molecular monolayers arranged on a liquid subphase. The trough allows the user to carry out three key techniques: (1) the formation of monolayers of amphiphilic molecules (like phospholipids) at the air-water interface; (2) to study the surface tension of these monolayer films; and (3) to deposit monolayers or multilayers onto a solid support that can then be studied through different methods, including microscopy (Martin & Szablewski 2001).

The trough, made of a hydrophobic substance, like PTFE or Delrin, consists of a shallow basin with a well in the middle that is filled with Nanopure or Ultrapure water (Ah-Fat et al, 1994). It also has two moveable barriers that are slightly submerged in the fluid. When a solution containing an amphiphilic molecule is spread using a Hamilton syringe on the surface of the liquid in the trough; it quickly spreads out across the water and orients itself

such that the hydrophilic heads interact with the water and the hydrophobic tails orient away from the water at the air-water interface (Ah-Fat et al, 1994). The trough also contains a pressure sensor that monitors the pressure exerted by the molecular film to monitor the surface tension (or compression). As the barriers are moved inward or outwards, there is a reduction or increase in the surface area that the molecules can occupy in the trough, resulting in a change in tension/pressure that is monitored by the pressure sensor. The relationship between surface tension and surface pressure for the trough is given by the following equation:

$$P = \gamma_0 - \gamma$$

Where P is the surface pressure being measured; γ_0 is the “ideal surface tension” - the surface tension for the pure Nanopure water subphase, which under ideal conditions, is 72.8 mN/m; and γ is the surface tension measured on the trough with a sample present at the air-water interface of the subphase (Martin & Szablewski 2001).

The movement inwards of the barriers in the trough with a monolayer on the surface of the subphase can be visualized in Figure 1.4A.

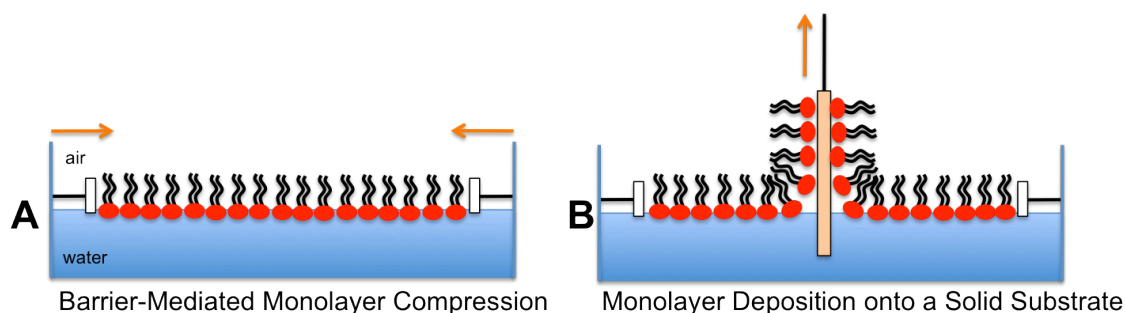


Figure 1.4: Depiction of the action of a Langmuir-Blodgett trough (not to scale). (A) shows the formation of a monolayer atop the surface of the trough’s subphase at the air water interface, with the barrier arms starting to reduce available surface area, arranging the lipid molecules into a continuous ordered monolayer. (B) shows the ability of the trough to create a monolayer deposition onto a solid substrate by passing the solid substrate through the monolayer via a movable dipping mechanism.

The trough can be set up to maintain a specific pressure of the film via a pressure control. This method is used in deposition, so that the pressure remains constant as a sample of the monolayer is retrieved. To carry out this retrieval, a solid substrate is obtained (often silica, mica or glass) and attached to the dipping mechanism of the trough, which is essentially a long arm that is attached to a motor gearbox. Attached to the horizontal arm is a vertical clamp with which the solid substrate is held. Movement of the dipping arm allows the solid substrate to be dipped in and out of the trough (Ah-Fat et al, 1994; Martin & Szablewski 2001). With each dip, molecules from the surface of the trough attach to the substrate in a monolayer, creating samples of specific layer thickness. The creation of the initial first monolayer can be seen in Figure 1.4B.

Sample Preparation Utilizing the Trough

Please see appendix A for in-depth descriptions of how the trough can be utilized for the preparation of supported lipid monolayer samples, which can then be analyzed using the atomic force microscope or the Kelvin probe force microscope.

1.4.2 Atomic Force Microscope

Atomic Force Microscopy (AFM) allows for topographical imaging of surfaces with nanoscale resolution; it utilizes a scanning probe (which consists of a cantilever with a sharp tip at the end) to physically scan the sample and create an image based on the interactions between the probe and the surface of the sample (Binnig & Quate 1986; Meyer 1992; Rugar & Hansma 1990; Zhong et al, 1993). The tip of the cantilever scans along the surface of the sample and, as it physically interacts with surface features, the forces of interaction cause deflection of the cantilever (Binnig & Quate 1986; Meyer 1992; Rugar & Hansma 1990; Zhong et al, 1993). This deflection is monitored through a laser that is directed at the top of the cantilever in the location directly above the tip (Binnig & Quate 1986; Meyer 1992; Rugar & Hansma 1990; Zhong et al, 1993). The laser is then reflected back to a multi-segment photodiode which detects the laser spot and, more specifically, the movement of this laser spot due to changes in deflection of the cantilever as forces between it and the sample change due to differing surface features (Binnig & Quate 1986; Meyer 1992; Rugar & Hansma 1990; Zhong et al, 1993). These forces may include, but are not limited to:

electrostatic interactions; van der Waals forces; capillary forces, and dipole-dipole interactions. This can be seen in the following chapter, in Figure 2.1.

Modes of AFM Imaging: Contact and Intermittent Contact Mode

There are multiple modes of AFM that can be utilized. In the static, or contact mode, the tip is in contact with the surface of the sample while the probe scans; it is essentially being gently dragged across the surface. The deflection measured is used to adjust the cantilever height when the sample height differs, to ensure that the tip doesn't break off and that the tip remains in contact with the surface (Garcia & Perez 2002; Zhong et al, 1993). While contact mode is very useful for some samples, it has several disadvantages, especially for soft biological samples, like lipids, as the sample may be destroyed if improper settings are used.

To avoid these disadvantages of contact mode, lipids are often scanned using tapping, or intermittent contact, mode. In this method, the cantilever oscillates, causing the tip to quickly move up and down (Garcia & Perez 2002; Zhong et al, 1993). As the tip moves over the surface, it intermittently touches the surface of the sample, producing information of the topography of the sample, without dragging across it and causing any damage (Garcia & Perez 2002; Zhong et al, 1993).

For samples being scanned in liquid, this method can be difficult because the movement of the apparatus to maintain cantilever oscillation can cause vibrations in the liquid. These vibrations can lead to inconsistencies in results and, essentially, bad images. To overcome this, one can use 'MAC' mode – magnetic alternating current. In this method, the cantilever has a magnetic coating and its oscillation is achieved through magnetic drive, thus eliminating the need for acoustic oscillation of the whole apparatus. This allows for tiny oscillations of the cantilever only without disturbance of the fluid in the liquid cell.

1.4.3 Kelvin probe force microscopy

The Kelvin probe force microscope (KPFM) is an extension of scanning probe microscopy that combines the capabilities of the AFM with the Kelvin method, allowing for measurement of the work function in metals or, more specific to our uses, the electrical surface potential in non metals.

The set up of the KPFM is heavily based on the AFM set up (previously described) but utilizes a conductive probe and a conductive substrate with a voltage applied between them. As the cantilever scans over the surface of the sample, we can measure contact potential differences and extract differences in work function in metals or in electrical surface potential of the sample (Nonnenmacher et al, 1991).

Typically, KPFM is carried out in lift or “hover” mode – the probe is not in direct contact with the sample and is a certain distance away from the sample surface at all times; it is also done in two scans – an initial AFM scan and a second KPFM scan, usually at a distance of 50 to 100 nm above the surface, to ensure for only electrostatic interactions. However, it has been found that this method does not give high enough resolution and sensitivity for the study of biological systems (Moores et al, 2010). A specialization of the KPFM – frequency modulated-KPFM - does have this higher resolution and sensitivity necessary for biological systems and is more advantageous for such applications. In FM-KPFM, a small modulation frequency (F_{mod}) is applied in addition to the main resonance frequency (F_0), which produces sidebands $F_0 - F_{\text{mod}}$ (Zerweck et al, 2005). We use the main resonance frequency for topography and the side bands for FM-KPFM, giving that higher sensitivity and resolution (Zerweck et al, 2005). This method also allows for simultaneous AFM and KPFM imaging.

One minor drawback for KPFM is that, currently, it is unable to operate in biologically relevant conditions – for example, it cannot be used in aqueous solutions, which would be typical of cellular membranes or cells in general. As a result, samples must be analyzed in an air environment, which is well suited for the study of lipid monolayers. Nonetheless, valuable information of biological systems can be gathered using the KPFM and then this information can be extrapolated and inferred to a system under biologically relevant conditions.

1.4.4 Neutron Scattering

Neutron scattering methods are widely used to study periodical stacks of model lipid membranes. *Neutron scattering* is a broad term that describes methods that investigate materials through the scattering of free neutrons by matter. There are different types of neutron scattering that are classified based on the change in energy over the course of the

experiment: if there is no change in the energy of the neutron from the start to the finish of the experiment, it is known as elastic neutron scattering (also known as neutron diffraction); if during the scattering process, some energy of the neutron is gained or lost, it is known as inelastic neutron scattering (Rauch & Petrascheck 1979; Bacon 1962).

Elastic neutron scattering, or neutron diffraction, is often used for determining structures, which is ideal for “crystal” structures – samples with a three-dimensional periodic array of atoms, or more simply put, samples that repeat themselves, like stacks of bilayers (Kučerka et al, 2007; Kučerka et al, 2009). These stacks, which can be thought of as planes, are equally spaced from one another; this spacing is denoted as “d”; the thickness of each plane (in this example, the thickness of the bilayers) is denoted as “D”. A visualization of these planar, repeated structures are shown in Figure 1.5.

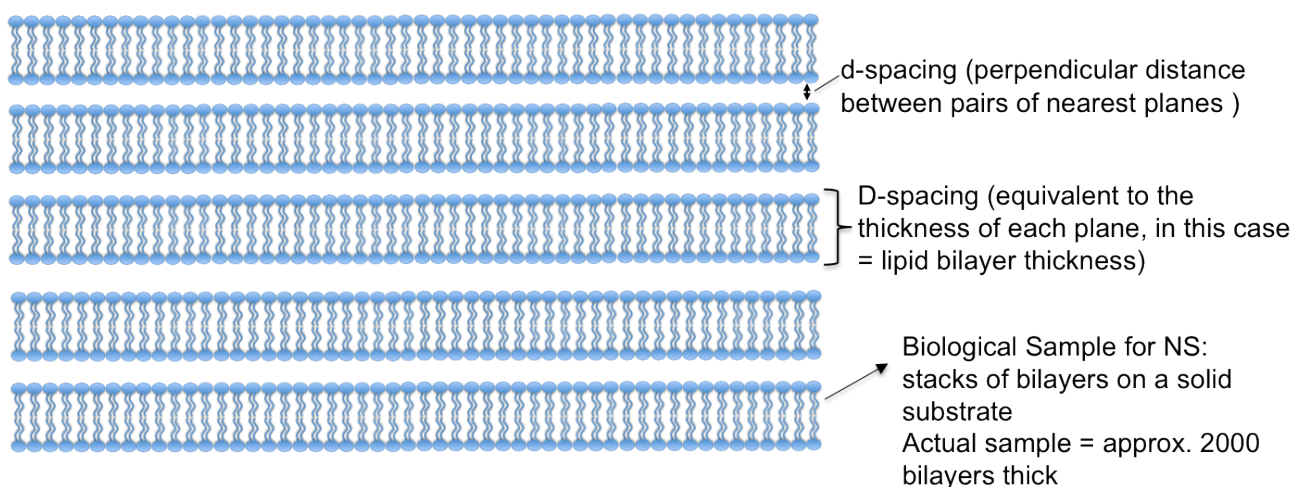


Figure 1.5: Schematic depicting the set up of stacks of bilayers for neutron scattering analysis. This image gives an example of a small section of the stacks of lipid bilayers atop one another, as would be found in a typical set up of a neutron scattering investigation into lipid bilayers. The spacing between pairs of nearest planes (in this case, planes being bilayers) is known as d/D-spacing and is indicated in this image. Please note that for actual experiments, the actual number of bilayers stacked atop one another is approximately 2000.

When the beam of neutrons is directed at the sample, the neutrons pass through a monochromator, which only allows neutrons of predetermined wavelength to pass through, and then reaches the sample of repeating planar units (Kučerka et al, 2007; Kučerka et al,

2009). The neutrons interact with the nuclei present and are scattered in different directions with every nucleus that they come into contact with. These scattered neutron waves interfere with one another, either constructively (overlapping waves combine together, yielding stronger peaks) or destructively (subtract from one another, yielding weaker peaks), producing a wave pattern that is read by a detector that is position sensitive, giving information that can then be analyzed for useful information (Pfleegor & Mandel 1967). In general, the analysis of this scattering of neutrons can be used to give information about the structure of the material being studied and the periodicity and position of the atoms, and their position relative to one another. One such piece of structural information that can be obtained is the d-spacing, by using Bragg's Law:

$$2 d \sin \theta = n \lambda.$$

where θ the angle between the wave/vector of the incident plane wave \mathbf{k} and the lattice planes, λ its wave length and n is an integer, the order of the reflection (Bragg & Bragg 1913). This is more clearly explained in Figure 1.6, which shows how the neutrons interact with each plane in a periodical sample and those that are scattered back in specific planes reach the detector.

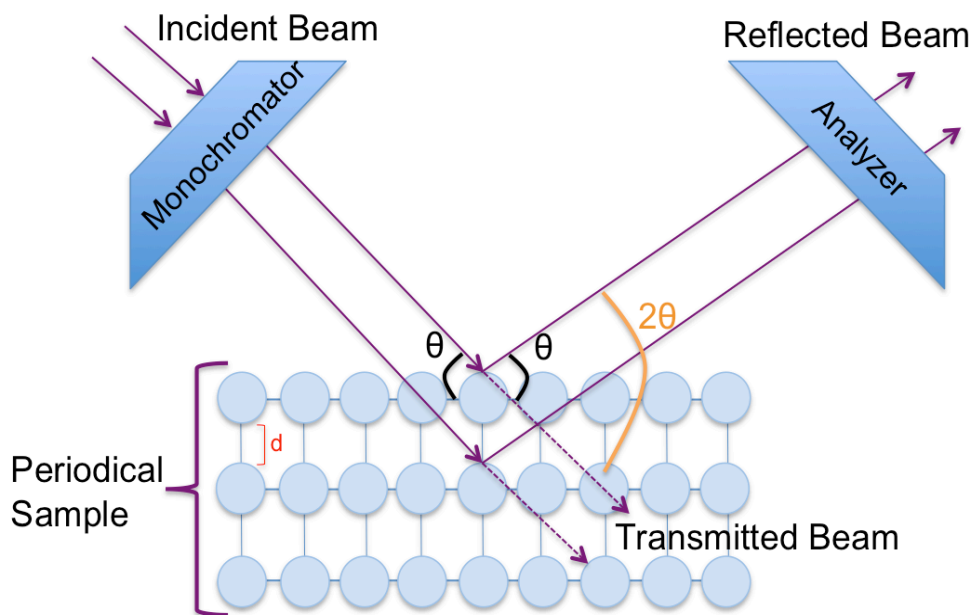


Figure 1.6: Neutron Diffraction in Action (not to scale). This figure illustrates the beam of neutrons, passing through a monochromator, interacting with the nuclei present in the planar sample. Those that are scattered interfere with one another, producing a specific wave pattern that is read by the analyzer. Through analysis of this wave pattern, useful information can be obtained, like the d spacing.

Overall, the use of neutron scattering is very desirable for the study of periodical structures as it is non-destructive to the sample, the neutrons are highly penetrating, and for the wide array of characteristics that neutrons can be used to study (including lattice dynamics, molecular dynamics, magnetic fluctuations, and so on).

1.5 Goals of Thesis and Objective of Research

The general objective of this thesis is to elucidate more on the indirect interaction of amyloid peptides with the membrane in relation to Alzheimer's toxicity; that is, we are interested in the effect of the lipids of the cell membrane themselves on amyloid fibril formation, as opposed to direct interaction with the membrane via protein receptors, etc. One area of particular interest with regards to the lipid membrane is the degree to which the composition

of the membrane, and in particular the presence and amount of cholesterol and lipid domains, affects membrane interaction with amyloid.

The specific objectives of this thesis are:

1. Give an in depth review of the use of the atomic force microscope on amyloid fibril formation and toxicity, especially in relation to Alzheimer's disease, to show that this is a heavily researched area and yet, there is still much left to discover in order to elucidate the cause of this disease and most importantly, in order to develop a treatment or cure.
 - a. This is outlined in Chapter 2 of this thesis
2. Investigate the effect of cholesterol itself on physicochemical properties of the membrane in comparison with the unknown effects of melatonin, as both molecules have been linked to amyloid toxicity
 - a. This is outlined in Chapter 3 of this thesis
3. Determine the effect of lipid composition on amyloid fibril formation and accumulation; specifically, study the effect of lipid head group charge and lipid phase at room temperature on amyloid interactions with the membrane
 - a. This is outlined in Chapter 4 of this thesis

Determine the effect of cholesterol (if any) on a single lipid system on amyloid fibril formation and interactions with the membrane

- b. This is outlined in Chapter 5 of this thesis
4. Characterize the structure and properties of increasingly complex multi-component lipid monolayer systems; specifically, study topography of the mixtures and electrical surface potential in order to find a suitable system to mimic neuronal cellular membranes
 - a. This is outlined in Chapter 6 of this thesis
5. Develop model lipid membrane systems that mimic healthy vs. diseased neuronal cell membranes; study the structure and physicochemical properties of the models in monolayer and bilayer form, and in the interactions of amyloid with the membrane
 - a. This is outlined in Chapter 7 of this thesis

Chapter 2.0: Review - The use of atomic force microscopy to study molecular mechanisms of amyloid fibril formation and toxicity in Alzheimer's disease

Note: the majority of this chapter was reproduced with modifications with permission from {Drolle E, Hane F, Lee B, Leonenko Z. 2014. Atomic force microscopy to study molecular mechanisms of amyloid fibril formation and toxicity in Alzheimer's disease. *Drug Metab. Rev.*, 46(2): 207-223.} © {2014} Informa Pharmaceutical Science.

Summary of Published Work: The goal of the review was to write a review on AFM being used for Alzheimer's disease research. We reviewed work from our lab and leading contributors from around the world. This in depth review attempted to illustrate the benefits of using atomic force microscopy for study at the nanoscale and outline that vast research has been done using atomic force microscopy in the study of amyloid fibril formation and in Alzheimer's disease, and yet, there is still much left to discover.

Contributions: This published manuscript was co-written by myself and Dr. Francis Hane, with Brenda Lee responsible for original authorship of the figures. For this thesis, the applicable figures were redone and the manuscript was reworked, with some portions not as relevant to my current research removed, in order to focus on the portions of this manuscript written primarily by me. All authors were involved in the final editing of the manuscript prior to publication.

Abstract

Alzheimer's disease (AD) is a devastating neurodegenerative disease characterized by dementia and memory loss, for which no cure or effective prevention are currently available. Neurodegeneration in AD is linked to formation of amyloid plaques found in brain tissues of Alzheimer's patients during post-mortem examination. Amyloid plaques are composed of amyloid fibrils and small oligomers - insoluble protein aggregates. Although amyloid plaques are found on the neuronal cell surfaces, the mechanism of amyloid toxicity is still not well understood. Currently it is believed that the cytotoxicity is a result of the non-specific interaction of small soluble amyloid oligomers (rather than longer fibrils) with the plasma membrane. In recent years, nanotechnology has contributed significantly to understanding the structure and function of lipid membranes and to the study of the molecular mechanisms of membrane-associated diseases. We review the current state of research, including applications of the latest nanotechnology approaches, on the interaction of lipid membranes with the amyloid- β ($A\beta$) peptide in relation to amyloid toxicity. We discuss the interactions of $A\beta$ with model lipid membranes with a focus to demonstrate that composition, charge and phase of the lipid membrane, as well as lipid domains and rafts, affect the binding of $A\beta$ to the membrane and contribute to toxicity. Understanding the role

of the lipid membrane in Alzheimer's disease at the nanoscale and molecular level will contribute to the understanding of the molecular mechanism of amyloid toxicity and may aid into the development of novel preventive strategies to combat Alzheimer's disease.

1.1 Introduction

1.1.1 Alzheimer's Disease

Alzheimer's Disease (AD) is a neurodegenerative disorder which results in progressive cognitive impairment, including dementia, personality changes, judgment, language skills and memory loss, eventually resulting in the death of the individual. AD is a member of the family of protein misfolding diseases. The 27 protein misfolding diseases identified to date all have an implicated protein that misfolds and aggregates to cause a specific pathology (Sipe et al, 2010; Stefani, 2012). AD is associated with the amyloid- β ($A\beta$) peptide. Other diseases in the protein misfolding disease family include Parkinson's disease (α -synuclein), Creutzfeldt-Jacobs (PrPc), Pulmonary Alveolar Proteinosis (SP-C), and diabetes (insulin) (Sipe et al, 2010).

The symptoms associated with AD were first identified by Alois Alzheimer in 1907 (Alzheimer, 1907). A significant period of time elapsed between Dr. Alzheimer's identification of the disease and significant progress in the study of AD; it was not until the mid to late 1980s that any real progress on Alzheimer's disease was made, with the discovery that the $A\beta$ peptide is correlated with AD symptoms (Masters et al, 1985; Tanzi et al, 1988) and the advancement of the amyloid hypothesis (Selkoe, 1991). Pathologically, AD is identified by the presence of extracellular amyloid plaques and intracellular neurofibrillary tangles (NFT) in the brain tissues during post-mortem examination. It has been shown that $A\beta$ is the primary constituent of these amyloid plaques, which are found extracellularly, and that hyper-phosphorylated tau protein is the primary constituent in NFT's, which are found intracellularly (Selkoe 1991). Considerable effort has been put into characterizing these plaques in order to elucidate the molecular pathways of $A\beta$ aggregation, with a shared goal of identifying therapeutic approaches to slow the onset of AD. At the micro- and nanoscales, the neuronal plaques consist of amyloid fibrils, which are protein structures with cross-linked beta-strands stacked together. Mature fibrils are a series of protofibrils that are twisted

around one another and reach lengths of up to several micrometers, with a diameter of roughly 5-10 nm (Antzutkin et al, 2000). In the past, these fibrils were believed to be causal to AD. However, recent research has demonstrated that these fibrils are relatively inert compared to amyloid oligomers, which are much smaller than the fibrils (Ono et al, 2009). Whether these oligomers are a precursor to the amyloid fibril or lie along an off-pathway reaction coordinate is a matter of contemporary debate (Yamaguchi et al, 2010). By the turn of the last century, research results began to show that neuronal synapses were most affected by amyloid neurotoxicity by impairing potentiation as a result of the interaction between amyloid oligomers and the neuronal synapse (Walsh et al, 2004; Walsh & Selkoe, 2004). Concurrently, various groups reported that the misfolding of amyloid proteins was not an abnormal occurrence; rather, it is an intrinsic property of the backbone of any polypeptide chain (Dobson & Karplus, 1999). In addition, it was shown that cytotoxicity is a generic effect of all amyloid oligomers (Bucciantini et al, 2002) and is associated with the initial misfolding of oligomers setting off the amyloid cascade (Kayed et al, 2003; Stefani, 2012).

Post mortem examinations of patients with Alzheimer's symptoms have shown a reduction in the physical size of the temporal and frontal lobes, hippocampus and amygdala – the regions involved in memory and learning process. This cerebral atrophy is the direct result of neuronal apoptosis and synaptic atrophy appearing concurrently with the presence of amyloid plaques and tau tangles (Mattson 2004). In addition, inflammatory cytokines formed by degenerating neurons and activated microglia around the amyloid plaques may contribute to the symptoms associated with Alzheimer's disease (Mattson, 2004).

Despite extensive research into AD and A β , no clear mechanism of action has been uniformly accepted, and little progress has been made in developing pharmaceuticals that eliminate, prevent, or even significantly slow the devastation caused by AD. In the past, the presence of amyloid plaques in the brain, which showed apple green birefringence when stained with Congo Red, was the definitive post mortem diagnoses for AD (Serrano-Pozo et al, 2011). Many cadavers display post-mortem cerebral amyloid plaques even though the living person never presented any Alzheimer's symptoms. Conversely, some people diagnosed with Alzheimer's disease do not have any amyloid plaques post-mortem (Davinelli et al, 2011). This inconsistency can be caused by either false diagnoses or poor

specificity of the classical Alzheimer's signs post-mortem. Currently, the clinical diagnosis for AD is based on accepted mental and cognitive testing or MRI imaging when large areas of the brain are already damaged. Approximately 90% of patients diagnosed with AD are found to have AD on autopsy (Knopman et al, 2001). Recent advances have shown promise in making an AD diagnosis using cerebrospinal fluid or blood for patients who have not yet presented with AD symptoms, for example, by looking for the presence of A β 42 (De Meyer et al, 2010). Some groups are now suggesting that large fibril plaques could play a protective role (Esparza et al, 2013; Yang et al, 2013). Therefore more effort in elucidating the molecular mechanism of AD and amyloid toxicity is highly desired, considering that the number of AD patients is constantly growing with the elderly population.

Although the exact mechanism by which A β produces neurodegenerative symptoms remains unclear, amyloid fibril formation has been studied extensively as a cause and a signature of AD. The proposed mechanism of amyloid fibril formation involves cleavage of the trans-membrane amyloid precursor protein (APP) (O'Brien & Wong 2011). When APP fragments (such as A β 35, A β 40, A β 42) become exposed to cellular fluids, they misfold into amyloid fibrils - thin insoluble fibers made up of the A β peptide arranged in a cross beta sheet structure (Berhanu & Hansmann 2012). Fibrils are hypothesized to form through a sequence of aggregation processes from monomers and oligomers, but whether oligomers are precursors to fibrils or form along a separate pathway is a subject of current research and academic debate.

Most early research on fibrillogenesis has been devoted to characterizing the formation of oligomers and fibrils in aqueous solution, where the effect of temperature, pH, and other factors were studied (Kusomoto et al, 1998; Stine et al, 2002). Recent research indicated that fibril plaque formation and neurotoxicity are associated with biological membranes *in vivo*. A β neurotoxicity was first identified in the 1980s with the discovery that A β is the prime constituent in amyloid plaques (Allsop et al, 1983; Glenner & Wong 1984; Masters et al, 1985; Hardy & Allsop 1991). Neurotoxicity is associated with A β interactions with neuron cells and results in neuronal cell death. The exact mechanism of this neurotoxicity is still under debate and several mechanisms have been discussed in literature: 1) the inflammatory effect of A β on the cell membrane (Verdier & Penke 2004); 2) oxidative

stress (Mutisya et al, 1994); 3) effect of metals (Sayre et al, 1999); 4) specific and non-specific interactions with cellular and lipid membranes (Lin et al, 2001; Kaye et al, 2003; Wang et al, 2004; Sokolov et al, 2006); as well as 5) the damaging effect of A β on DNA (Geng et al, 2010).

It has been shown that sequence of A β also contributes to the toxicity (Buchsteiner 2012). Even though there is only a 2 amino acid difference in the primary structure of A β (1-40) and A β (1-42), there are distinct differences in both the aggregation pathway (Bitan et al, 2003) and the toxicity levels (Dahlgren et al, 2002) between the two isoforms. A β (1-42) has a higher aggregation rate, higher propensity to bind metal ions, and higher toxicity levels than A β (1-40) (Bitan et al, 2003; Bush & Tanzi 2008).

When considering the role of cell membrane in amyloid toxicity, it is important to note that amyloid deposits are known to affect the synapse and are not uniform in the cerebral parenchyma, but A β is uniformly expressed and A β (1-42) is a normal constituent of all cerebrospinal fluid and is present in non-AD patients. Secondly, amyloid deposition increases with age, yet amyloid production does not (i.e. there is no change in the rate of the cleavage of APP into the A β peptides). It appears that processes which clear amyloid deposits are diminished with age, as are mechanisms to protect against redox effects (Bush & Tanzi 2008). A difference between A β production and A β clearance is likely an underlying factor in the AD disease process (Greenough et al, 2012).

A large portion of the toxicity of A β comes from its association with and ability to cause membrane disruption and damage. Research by Lal's group indicates that oligomeric A β can form ion channels in lipid membranes, resulting in higher levels of intracellular calcium (Lin et al, 2001). Perturbations in membrane fluidity have been also suggested by Kremer et al. (Kremer et al, 2000) and Muller et al. (Muller et al, 1998). Free radical production has been identified by Butterfield et al. (Butterfield et al, 1999) and changes in lipid metabolism have been demonstrated by Koudinov et al. (Koudinov et al, 1998). Other examples of cellular damage by amyloid include: changing of membrane permeability (Abramov et al, 2011), induction of cell apoptosis (Loo et al, 1993), the formation of ion channels in cell membrane altering ion homeostasis (Arispe et al, 1993), the production of toxic levels of

hydrogen peroxide (Behl et al, 1994), and the thinning of the membrane (Sokolov et al, 2006).

These studies indicated that the mechanism of membrane toxicity induced by A β is very complex and still poorly understood (Berthelot et al, 2013). These studies also demonstrate the need to elucidate the role of the lipid membrane surface in the mechanism of amyloid fibril formation and toxicity at the nanoscale and molecular level. High-resolution imaging techniques such as atomic force microscopy provide a powerful nanotechnology method with which to approach this challenging task.

1.1.2 Nanotechnology and Atomic Force Microscopy

Nanotechnology has contributed to the progress of modern medicine, contributing significantly to understanding the molecular mechanisms of disease and the development of novel methods for diagnostics and cure, which has resulted in the development of the modern discipline of nanomedicine. We focus here specifically on one nanotechnology method - atomic force microscopy (AFM). AFM is a member of the scanning probe microscopy (SPM) family, which includes more than 20 scanning probe methods, such as scanning tunneling microscopy (STM), Kelvin probe force microscopy (KPFM), near-field scanning optical probe microscopy (NSOM) and many other methods that appeared with the development of nanotechnologies. SPM has proven to be a remarkable tool for advancing Alzheimer's research (Connolly & Smith 2010). It has also provided definitive nanoscale insight into the structure of amyloid fibrils, oligomers and their interactions with lipid membrane and each other (Lal & Arnsdorf 2010). AFM and related SPM methods employ a sharp scanning probe (AFM tip), which is rastered over the surface of the sample. The probe is attached to a flexible beam (cantilever), which interacts with the sample through various forces (van der Waals, electrostatic). These forces are detected at each point following the deflection of the cantilever (Figure 2.1) and are used to produce a nanoscale 3D image with single molecule level resolution (Binnig et al, 1986). The resolution of these methods is not limited by the diffraction of light as in optical microscopy, but is instead limited by the sharpness of the scanning probe, typically 2-10 nm. However, even atomic resolution can be achieved with an appropriate tip (Binnig et al, 1986). With AFM, high-resolution three-

dimensional images of biomolecules in physiologically relevant conditions can be obtained. In addition to imaging, AFM can be used in force spectroscopy mode, which allows the measurement of forces between the tip and the sample as the probe is brought repeatedly to and from the sample surface. This method allows for the studying of important mechano-elastic properties of the sample (including live cells) such as Young's modulus and adhesion (Burke et al, 2013). Because these physical properties of the cell are related to cellular function, AFM can thus be used to study biomechanical processes of the cell in order to understand not only cell morphology, but also cellular processes such as migration and division (Radmacher 2007). Work by Burke et al. demonstrated that amyloid proteins decreased localized Young's moduli and adhesive properties in lipid membranes. (Burke et al, 2013). When the molecules of interest are attached to the probe, binding forces between two individual molecules can be measured (Benoit et al, 2000; Hinterdorfer & Dufrene 2006; Hane et al, 2013). AFM has been widely used to study various biological samples such as lipid membranes, cells, DNA and proteins (Hansma & Hoh 1994).

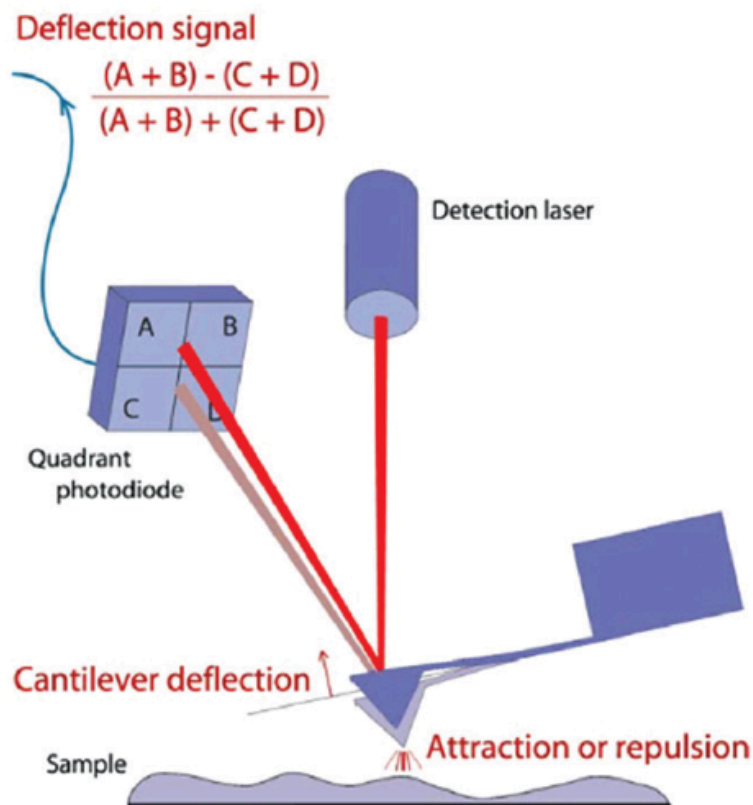


Figure 2.1: Schematics of AFM. Adapted from JPK Instruments AFM Handbook, 2005 (Image reproduced with permission to *Drug Metabolism Reviews* (DMR) from JPK Instruments, <http://www.jpk.com>).

2.2 Atomic Force Microscopy to Study Amyloid Fibril Formation and Toxicity in Alzheimer's Disease

In this section we review our recent work and other AFM studies in relation to AD and amyloid toxicity.

2.2.1 AFM Imaging of Fibrils and Oligomers

AFM has provided researchers with the nanoscale morphology of amyloid structures, revealing truly remarkable details into the etiology of neurodegenerative protein misfolding diseases. Much research has been done to characterize these fibrils and small oligomers with AFM imaging, beginning with work done by Krafft's group comparing fibrils imaged by

EM to fibrils imaged by AFM (Stine et al, 1996). The authors were able to show the axial periodicity of the fibril structure, confirming structures obtained using electron microscopy techniques and confirming the fibril diameter to be 5-12 nm (Stine et al, 1996). With the increased resolution provided by AFM, many other groups were also able to obtain higher quality images of amyloid fibrils and oligomers (Harper et al, 1997; Wang et al, 2003; Mastrangelo et al, 2006; Segers-Nolten et al, 2007; Adamcik et al, 2010; Moores et al, 2011; Xiang et al, 2012; Norlin et al, 2012; Irwin et al, 2013; Ridgley & Barone 2013; Goldsbury 1999; Campioni et al, 2010).

Amyloid fibril formation has been studied extensively in solution where the interaction between peptide molecules is mainly considered. According to the amyloid hypothesis (Petkova et al, 2005; Chiti et al, 2006), interactions between amyloidogenic peptides in solution results in the formation of small oligomers and long fibrils with twisted morphology (Lansbury 1997; Blackley et al, 1999; Chiti & Dobson 2006; Moores et al, 2011), which elongate by attaching monomer units to the end of growing protofibrils. A left-handed helical twist in the fibril structure and a periodicity of 43 nm was reported (Lansbury 1997). Interestingly, the structures of fibrils formed in solution are different from the protofibrils formed on surfaces (Blackley et al, 2000; Zhu et al, 2002; Rocha et al, 2005). Mastrangelo et al. used AFM to track the growth of amyloid oligomers on substrates (Mastrangelo et al, 2006), demonstrating that fibrils form as self-dimerizing monomers stack upon one another. We showed that after 24 hours of incubation in solution, A β (1-42) forms fibrils that are long, continuous, and twisted together into helices (Figure 2.2) with a continual increase in the length and height of amyloid fibrils both as a function of time and of peptide concentration in solution. The AFM images demonstrate that in addition to the large fibrils, small oligomers are also present in solution. Lansbury and colleagues suggested that there may be different pathways for fibril and oligomer formation, prompted by their observations that only certain prefibrillar species, when added to monomeric solution, “seed” the solution and accelerate aggregation time by having the solution skip the lag phase of aggregation. Importantly, it was reported that fibrils formed in solution are identical in structure to fibrils isolated from Alzheimer’s diseased cerebral plaques (Lansbury 1997).

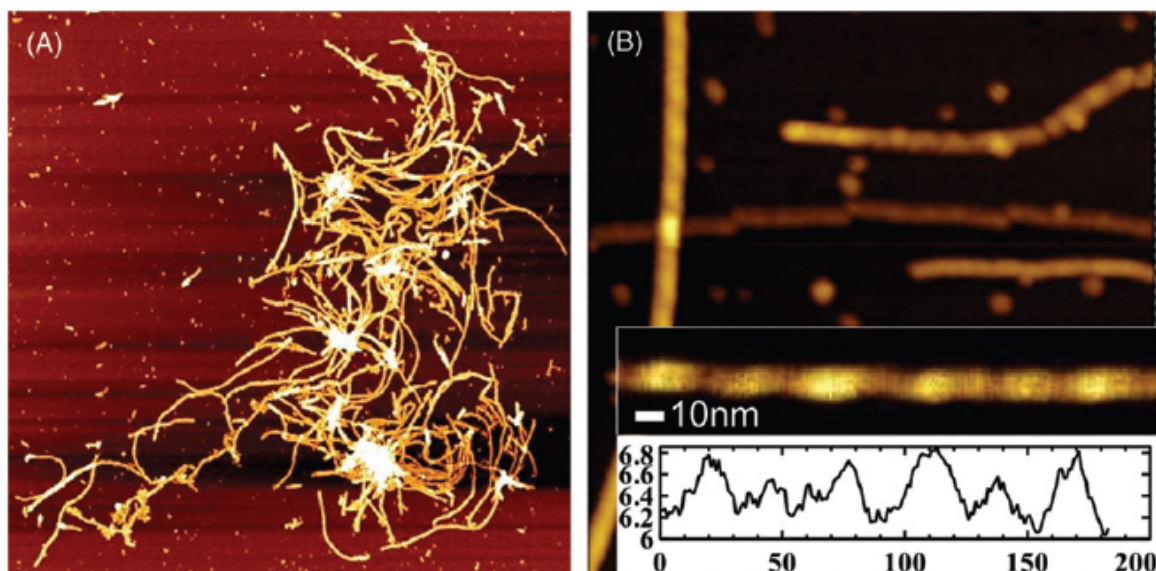


Figure 2.2: Amyloid peptide A β (1-42) incubated in solution for 24 hours and then deposited on mica and imaged in air. A 5x5 μm scan area (A) of the surface shows many fibrils and large fibril clusters, ranging from 100 nm to several μm . A high-resolution image (B) shows that the fibrils are tightly wound together forming helices, scan size is 500 by 500nm. (Figure 2.2 (B) - reprinted with permission to *DMR* from Moores B, Drolle E, Attwood SJ, Simons J, Leonenko Z. [2011]. Effect of surfaces on amyloid fibril formation. *PLoS ONE*, 6(10):e25954).

A number of factors have been identified that alter the kinetics of amyloid fibril formation in solution: lowered pH, increased temperature and agitation as well as increased concentration of amyloid have all been shown to accelerate amyloid aggregation (Harper & Lansbury 1997; Buell et al, 2012; Crespo et al, 2012). It has also been shown that the toxicity of amyloid species is highly dependent on the structural flexibility and exposure of hydrophobic residues of the peptide (Campioni et al, 2010).

2.2.2 Effect of Surfaces on Amyloid Fibril Formation

It has been emphasized that amyloid peptides may interact with the surfaces of lipid membranes. This theory has initiated numerous studies aiming to elucidate the effect of surfaces on amyloid fibril formation.

A growing number of recent research contributions emphasized the importance of cell membrane surfaces (Terzi et al, 1995; Dobson 2001; Lin et al, 2001; Yip et al, 2001; Sharp et al, 2002; Kaye et al, 2004; Quist et al, 2005; Ambroggio et al, 2005; Ege et al, 2005; Cordy et al, 2006; Choucair et al, 2007) for amyloid toxicity and in particular the role of electrostatic interactions between the lipid membrane and amyloid-forming proteins (Yanagisawa et al, 1995; Choo-Smith et al, 1997; Kakio et al, 2002). While cell membrane surfaces are extremely important in amyloid toxicity, interpreting results from heterogeneous and complex systems like plasma membranes is often very difficult. Chemically modified surfaces with well-defined functionality can serve as initial simplified models to elucidate the effect of surfaces on amyloid binding and fibril formation, including electrostatic interactions.

Surfaces play a crucial role in amyloid fibril formation for many amyloidogenic peptides. The size and shape of amyloid aggregates and fibrils, formed on surfaces, as well as the kinetics of their formation, are affected by the physicochemical nature of the surface. A number of surfaces including nanoparticles (Linse et al, 2007; Pronchik et al, 2010), graphite (Brown et al, 2002) and mica (Zhu et al, 2002) have been studied to determine their effect on fibril formation. Surfaces have been shown to significantly accelerate the formation of amyloid fibrils for a variety of peptides compared to incubation in solution (Powers & Kelly 2001; Zhu et al, 2002). This phenomenon may be attributed to increased local concentrations caused by surface interactions forcing peptide diffusion into a 2D plane (Shen et al, 2012). In addition to accelerating fibril formation, several authors reported that surfaces have an effect on the structure of fibrils (Zhu et al, 2002, Qin et al, 2007, Goldsbury et al, 1999, Blackley et al, 2000, Blackley et al, 1999). For many peptides, fibrils formed on surfaces lack the twisted and intertwined morphology, which is characteristic of fibrils grown in solution (Blackley et al, 2000), α -synuclein, and SMA (Zhu et al, 2002). The mechanism of fibril formation on surfaces includes nucleation and elongation (Zhu et al, 2002; Blackley et al, 2000; Blackley et al, 1999; Kowalewski et al, 1999), where protofibrils elongate in various directions radiating from the central core, resulting in branched structures (Zhu et al, 2002; Blackley et al, 2000; Moores et al, 2011).

Multiple studies have illustrated the important role that surfaces play in amyloid fibril formation; however, these data are difficult to compare due to different research groups conducting their studies under varying experimental conditions, such as pH, temperature, surface type and peptide type (Uversky et al, 2001; Giacomelli & Norde 2005; McMasters et al, 2005; Qin et al, 2007, Yokoyama & Welchons 2007; Hammarstrom et al, 2008). Along with experimental conditions, limited surface types studied (Powers & Kelly 2001) make comparisons for the same type of amyloid proteins difficult (Zhu et al, 2002, Hammarstrom et al, 2008).

Electrostatic interactions with surfaces are of high importance, considering that A β is a charged (-3), polar molecule at physiological pH (pI=5.5) (Rauk 2009) This is especially relevant as many membrane surfaces are charged and may therefore influence amyloid aggregation through electrostatic forces (Yanagisawa et al, 1995; Choo-Smith et al, 1997; Kakio et al, 2002).

Using AFM, we studied the electrostatic and hydrophobic interaction of A β (1-42) with three different surfaces: hydrophobic (CH₃); negatively charged (COOH); and positively charged (NH₂) surfaces at pH 7.8, at 37°C, in order to provide a direct comparison on the effect of these surfaces (Moores et al, 2011). A progressive accumulation of A β deposits with time was observed on all three surfaces (Moores et al, 2011). We showed that the surface charge and hydrophobicity affects the structure, amount and surface coverage of A β deposits: hydrophobic CH₃ surfaces promoted the formation of amorphous aggregates while the charged NH₂ and COOH surfaces promoted small oligomers and small protofibrils. Interestingly, the structures of fibrils formed in solution are different from the protofibrils formed on surfaces (Blackley et al, 2000; Zhu et al, 2002; Rocha et al, 2005; Moores et al, 2011). Instead of characteristic twisted morphologies observed for fibrils formed in solution (Figure 2.2B), we observed formation of small oligomers, which covered the surface of substrate completely and formed a monolayer of densely packed oligomers (Figure 2.3). The presence of small oligomeric units on surfaces and in solutions was also reported by others (Blackley et al, 1999, Blackley et al, 2000, Rocha et al, 2005) for A β (1-40). Stable oligomers for both A β (1-40) and A β (1-42) were isolated also from brain and synthetic amyloid material. Dimeric (9 kDa) and trimeric (13.5 kDa) forms (Roher et al, 1996;

Blackley et al, 1999) of A β have been previously observed by size-exclusion chromatography, whereas incubation of monomeric A β has led to the separation of 4-, 19-, and 46-kDa fragments (Dyrks et al, 1993). There have also been reports from other groups of the presence of oligomer units (Levine 1995; Roher et al, 1996; Kuo et al, 1996). We observed the deposition of small oligomers on all surface types; however, the surface type influenced the shape and the size of the oligomers present. Interactions with the hydrophobic surface resulted in spherical oligomers with broader size distribution, while A β oligomers on charged surfaces were of triangular shape with a more narrow size distribution. This indicates that electrostatic interactions with the surfaces may affect the oligomer folding and therefore the shape of the smaller building blocks. Triangular shaped oligomers were proposed by simulations of trimers by Paravastu et al. (Paravastu et al, 2008). As well, Wang et al. (Wang et al, 2010) used molecular dynamics simulations to show that A β packing is affected by electrostatic interactions with surfaces; A β is relatively free to move at the CH₃ surfaces and may result in a more disordered surface than A β interaction with charged COOH- and NH₂-surfaces, in which stronger electrostatic interactions of the A β may result in more ordered appearance of the A β (Wang et al, 2010). Building of protofibrils later in time occurs by adding small spherical building blocks to the surface bound oligomers, (Figure 2.3A), which result to elongation in both directions and formation of fibrils with branched morphologies (Moore et al, 2011; Zhu et al, 2002; Blackley et al, 2000).

At longer times of incubation (22h), the density of larger amyloid clusters was observed to be highest on CH₃-modified surface, lower on COOH-modified surfaces and lowest on NH₂-modified surfaces (Moore et al, 2011).

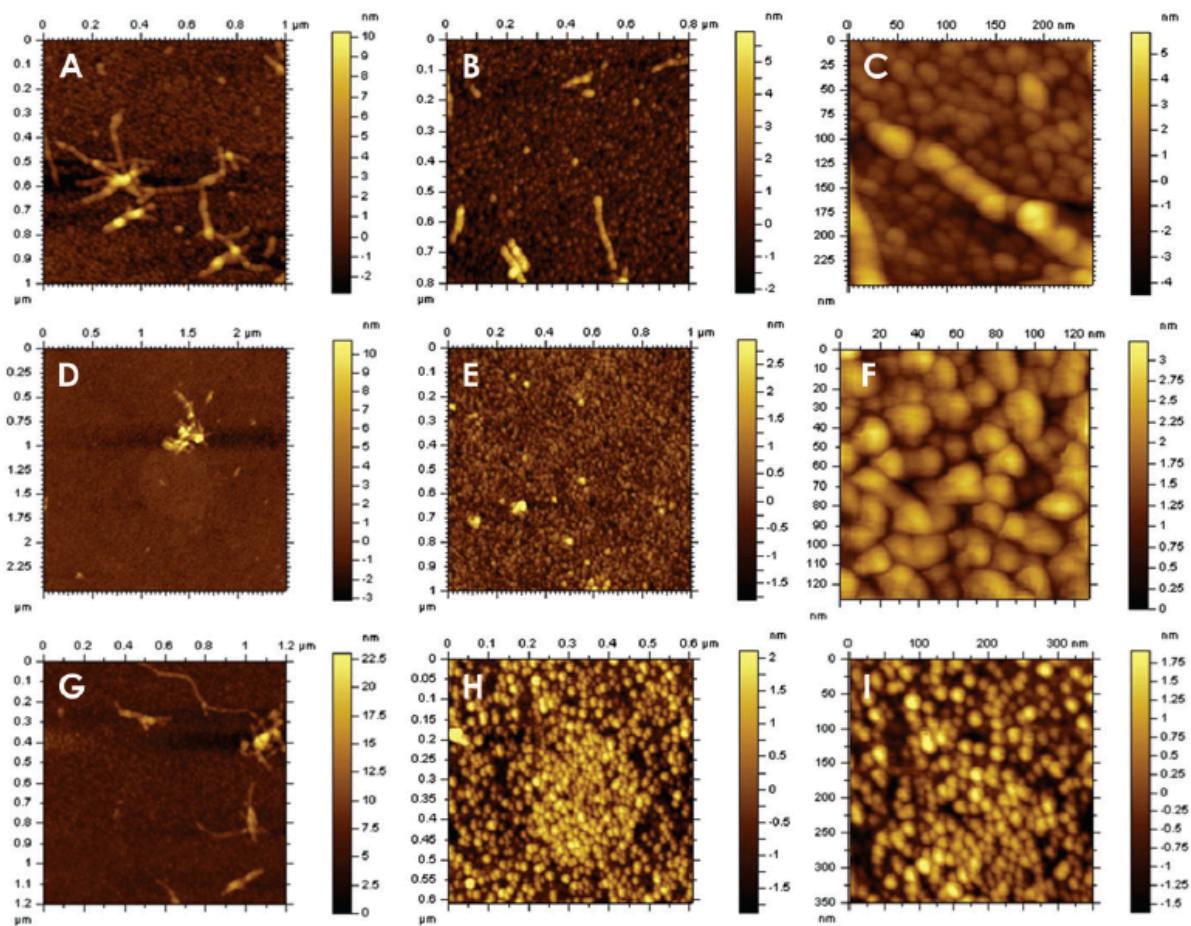


Figure 2.3: Small scan size images of AFM topography of $A\beta$ aggregates formed on modified surfaces: CH₃- (A-C), COOH - (D-F), and NH₂- (G-I) modified surfaces, after incubation with $A\beta$ 1-42 solution (500 $\mu\text{g}/\text{ml}$) for 1 hour at 37°C. (Image reproduced with permission to DMR from Moores B, Drolle E, Attwood SJ, Simons J, Leonenko Z. (2011). Effect of surfaces on amyloid fibril formation. PLoS ONE, 6(10):e25954).

It is clear that electrostatic interactions with surfaces directly influence A β fibril formation, which can be explained by the complex charge distribution in the A β peptide and its secondary structure dependence. The peptide has a net charge of -3, with six negatively charged residues and three positively charged residues, and an isoelectric point of approximately 5.5 (Rauk 2009). We showed that a complex charge distribution develops in oligomers (dimers and pentamers) as compared to monomers, (Moore et al, 2011). According to our analysis of electrostatic potential distribution (Moore et al, 2011), A β monomer, dimer or larger oligomers all differ in their surface charge distribution. In a monomeric α -helix structure the charge is fairly evenly distributed to prevent a dipole from forming. A larger collective polarity (likely occurring as a result of the misfolding), which induces stronger electrostatic surface interactions, is observed in oligomers in β -sheet conformations, as well as preferential ordering of the oligomers on the surfaces. This may be the driving force for oligomer binding and the reason for the more ordered and fibril-like structures that are seen on charged surfaces, compared to hydrophobic CH₃-modified surfaces. This may have an effect on binding of A β to charged or polar lipid molecules, which compose biomembranes.

Therefore, based on this analysis, we conclude that α -helical peptide clusters preferentially form on the hydrophobic CH₃ surface, and β -sheet clusters of various sizes form on the negatively charged COOH and positively charged NH₂ surfaces. This correlates with findings by other authors: McMasters et al. (McMasters et al, 2005), investigated amyloid fibril formation of the A β peptide on chemically modified mica bearing positively or negatively charged, or hydrophobic functional groups at pH 11.5 (chosen as a high pH inhibits aggregation in solution so results only be based on surface-mediated aggregation) and showed that all surfaces cause adsorption/deposition of A β (10-35) peptide. Deposits were composed of peptides in β -sheet, β -turn, random coil and α -helical conformation. The equilibrium on hydrophobic monolayer was shifted towards an α -helix form. This is consistent also with findings by Giacomelli et al. (Giacomelli et al, 2005), who showed that conformation of the A β (1-40) peptide (at pH 7 and 10, at 25°C) strongly depends on the hydrophobicity of the surface. They observed intramolecular α -helix formation due hydrophobic interactions on the Teflon surfaces in contrast to intermolecular β -sheet formation due to electrostatic interactions on the mica surfaces (Giacomelli et al, 2005).

2.2.3 Effect of Lipid Membrane on Amyloid Fibril Formation

AFM along with other studies confirmed the proposed mechanism of amyloid fibril formation and demonstrated the formation of A β oligomers and fibrils from monomeric solution of A β . The structure of both oligomers and fibrils formed in solution and on surfaces has been extensively studied at the nanoscale and at a great detail. Yet, the mechanism of amyloid toxicity still is not well understood.

Amyloid fibril formation is a multiple state process, which starts with the cleavage of the amyloid fragments from the transmembrane amyloid precursor protein (APP), misfolding of A β monomers which form various structures, such as unfolded clusters, beta-sheet oligomers, larger fibrils and amyloid plaques. Due to the close proximity to the cell surfaces, these amyloid aggregates may interact strongly with the membrane. Increasing evidence supports the hypothesis that the state of the cell membrane (composition, morphology and other physicochemical properties) plays an important role in amyloid toxicity and Alzheimer's disease. This mechanism is outlined in Figure 2.4.

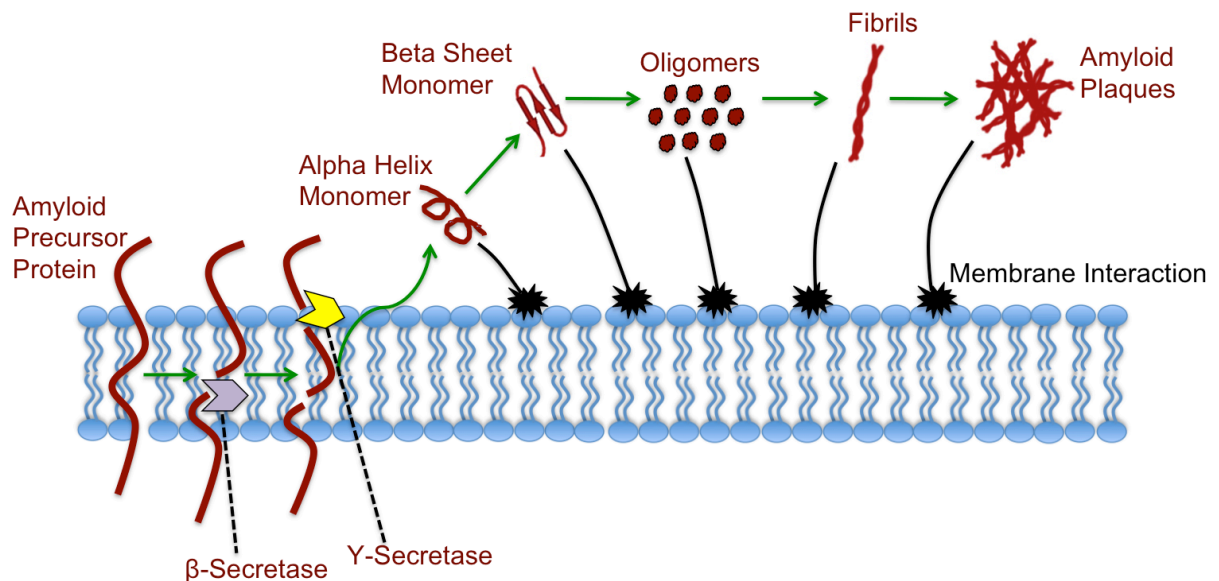


Figure 2.4: Schematic showing amyloid origin and the mechanism of the amyloid fibril formation and toxicity. (adapted from Drolle et al, 2014)

To account for role of the cellular membrane, whose composition is known to change with age and in AD (Wells et al, 1995; Farooqui et al, 1995; Selkoe, et al, 1980; Farooqui et al, 1988; Bartzokis et al, 2004), it has been hypothesized that within the cellular membrane itself, raft domains, enriched in cholesterol and sphingolipids, may constitute the environment in which amyloid-forming proteins cluster, thus increasing amyloid aggregation and toxicity.

A growing number of recent research contributions suggest the importance of the lipid membrane for amyloid fibril formation and toxicity (Cordy et al, 2006; Sharp et al, 2006; Ege et al, 2005; Yip et al, 2001 Abramov et al, 2011; Tofoleanu & Buchete 2012; Kinnunen et al, 2009; Sasahara et al, 2013).

These studies emphasize the effect of charged lipids, pH, metal cations, and cholesterol on the effectiveness of fibrillogenesis, suggesting interactions between the lipid membrane and amyloid are important. The stronger interaction of amyloid oligomers with cell membranes may induce the higher toxicity and thus disruption of the membrane function. Therefore, by controlling membrane properties, one may prevent the amyloid toxic effect and disease initiation. It is necessary to continue systematic studies in order to understand the physico-chemical properties of the cell and model membrane and the role they play in the amyloid toxicity.

Biological membranes are very complex structures, mainly composed of phospholipids and enriched with multiple trans-membrane proteins and sterols assembled in rafts. Due to this complexity, lipid bilayers and monolayers are widely used to mimic biological membranes (Ohvo-Rekilä et al, 2002) in order to study their structure and interaction with biomolecules, including amyloid peptides, nanoparticles and drugs (Yip et al, 2001; Bonn et al, 2004; Choucair et al, 2007; Hane et al, 2011).

Electrostatic and hydrophobic interactions between amyloid oligomers and lipid membranes play an important role during initial amyloid pathogenesis. Several groups have focused their efforts on elucidating the role of electrostatic and hydrophobic interactions of A β peptides with model lipid membranes and monolayers. Using a combination of ^{31}P MAS NMR (magic angle spinning nuclear magnetic resonance) and CD (circular dichroism)

spectroscopy, Bokvist et al. suggested fundamental differences in the functional organization of supramolecular A β (1–40) membrane assemblies for two different scenarios with potential implication in AD: A β peptide can either be firmly anchored in a membrane upon proteolytic cleavage, preventing release and aggregation, or it can have fundamentally adverse effects when bound to membrane surfaces by undergoing accelerated aggregation, causing neuronal cell death (Bokvist et al, 2004). Their results suggested that two different molecular mechanisms of peptide–membrane assemblies are involved in A β pathophysiology with the finely balanced type of A β –lipid interactions against release of A β from neuronal membranes and production of toxic β -structured aggregates. Therefore, pathological interactions of A β with neuronal membranes might not only depend on the oligomerization state of the peptide, but also on the type and nature of the supramolecular A β –membrane assemblies (Bokvist et al, 2004).

In one interesting study, Bokvist et al. proposed that A β interacts with lipid membranes by binding and insertion of the peptide in its monomeric form into the lipid membrane. It was hypothesized that these processes are driven by the interplay between electrostatic and hydrophobic interactions. This finding correlates with previous research on lipid monolayers showing that electrostatic interactions with negatively charged lipids increase peptide adsorption onto the monolayer at the air-water interface (Maltseva et al, 2005). It has also been proposed that the strong electrostatic interaction between the peptide and negatively charged lipids drives the peptide deep into the monolayer (Ege et al 2005). Other authors (Quist et al, 2007; Jang et al, 2010; Lin et al, 2001; Jang et al, 2011) proposed that membrane can be damaged due to the creation of ion channels or pores, which induce cell malfunction by an unregulated toxic ion current (Abramov et al, 2011). In summary, the mechanism of A β toxicity is still not well understood, showing a discrepancy between suggested non-specific membrane alteration (Williams et al, 2011) and ion-channel formation suggested on the base of membrane reconstituted A β (Lin et al, 2001; Jang et al, 2011), and contradictory non-ion channel but membrane perforation alteration mechanisms (Sepulveda et al, 2010).

In addition, molecular dynamics simulations by Jang et al suggested various steps of membrane disorder due to the binding of A β peptides (Jang et al, 2013). Summarizing these

studies, we propose that the molecular mechanism of A β toxicity involves several pathways of A β interactions with the lipid membrane: 1) binding of A β monomers and oligomers to the surface of lipid membrane and accumulation of A β deposits on the surface of lipid membrane without destroying membrane structure or integrity (Figure 2.5A); 2) penetration of A β into the membrane, creating disorder in the membrane structure and inducing unstructured defects and perforation, (Figure 2.5B); and 3) induction of ion channels by A β (Figure 2.5C). We postulate that the prevalence of one pathway over another and the significance of the induced damage may strongly depend on the physical and chemical properties of the lipid membrane itself. Thus the membrane structure and integrity may be important factors to take into account while considering strategies to overcome AD and related neurodegenerative disease.

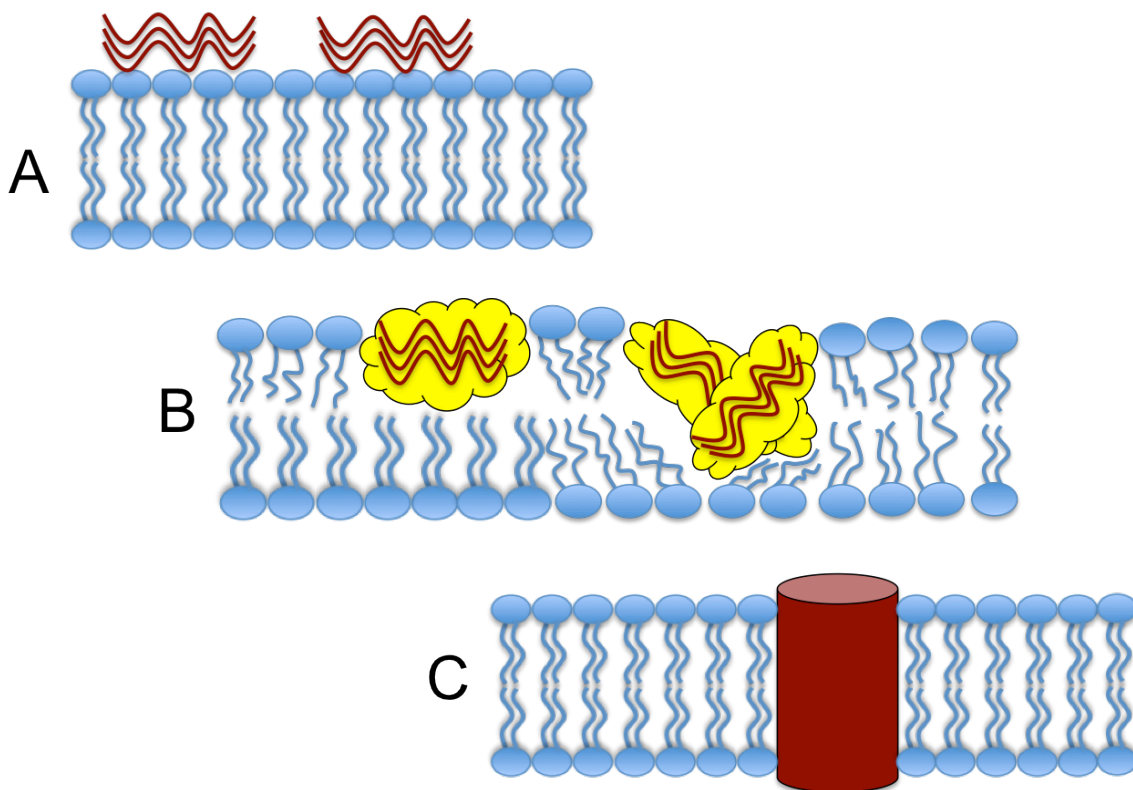


Figure 2.5: Schematic showing proposed mechanisms of Amyloid interactions with lipid membrane. A - adsorption of A β on the surface of lipid membrane, building deposits on the top of membrane, B - partially penetrating inside the membrane, inducing membrane disorder and irregular pores, C - ion channel formation. (adapted from Drolle et al, 2014)

While other methods have been employed to approach this challenging task, AFM has been especially useful as it provided the possibility to directly visualize interactions of A β with the lipid membrane at the nanoscale and in physiologically relevant conditions.

Using AFM, it has been demonstrated that lipid composition, the phase of lipid membrane and presence of cholesterol-induced domains (rafts) affect amyloid aggregation (Drolle et al, 2012; Choucair et al, 2007; Hane et al, 2011; Lal et al, 2007; Sheikh et al, 2012; Yip et al, 2002; Gorbenko et al, 2006; Goldsbury et al, 1999)

2.2.3.1 Lipid Composition

Previously, we used AFM to investigate how time and membrane composition affected the aggregation of A β -42 on model phospholipid membranes, in particular looking at the effects of lipid head group charge and lipid membrane phase. AFM helped to directly resolve the nanoscale structure of amyloid oligomers and fibrils as well as the structure of planar supported lipid bilayers before and after incubation with A β -42. In order to study how amyloid binding is affected by lipid charge and phase, we used the following: neutral, gel phase, dipalmitoylphosphatidylcholine (DPPC); neutral, fluid phase 1,2-dioleoyl-*sn*-glycero-3-phosphocholine (DOPC); anionic, 1,2-dioleoyl-*sn*-glycero-3-[phospho-*rac*-(3-lysyl(1-glycerol)) (DOPG); and cationic, 1,2-dioleoyl-3-trimethylammonium-propane (DOTAP). This study will be discussed in full detail in chapter four of this thesis, but in summary, we showed interactions of the A β oligomers with the membrane surface were affected by the charge on the lipid head group, changing the rate of adsorption and causing membrane disruption. We observed that A β accumulates progressively in a similar manner on the surface of the zwitterionic, gel phase DPPC and anionic, fluid phase DOPG membranes, according to the schematic in Figure 2.5A. In contrast to DPPC and DOPG, amyloid aggregates incubated on cationic, fluid phase DOTAP and zwitterionic, fluid phase DOPC permeate into the membrane to a greater extent than DPPC and DOPG. This observation correlates with the scenario proposed in Figure 2.5B. Furthermore, we observed more membrane disruptions on the DOTAP and DOPC membranes compared to the DPPC and DOPG membranes. We attributed this difference to the electrostatic interactions between the lipid membranes and the A β and also to the difference in the phase of the lipid membranes.

Both DPPC and DOPC have identical charge and type of head group but exist in different phases at room temperature: DPPC is in a gel phase characterized by higher order in lipid tails, and DOPC is in fluid phase characterized by less ordered lipid tails and large dynamics of lipid molecules (Ohvo-Rekilä et al, 2002).

Our data correlates with findings by other authors, including Estelrich (Estelrich et al, 2012) and Bokvist (Bokvist et al, 2004), who observed stronger stabilizing interactions with negatively charged lipid models. Molecular dynamics simulations by Poojari et al. also demonstrated that zwitterionic and anionic lipid surfaces promote A β stability in the bilayer (Poojari et al, 2013). The affinity of A β for anionic lipids has been shown to affect the amyloidosis process (Maltseva et al, 2005). Ege reported that cationic lipids can bind A β just as readily as anionic lipids (Ege & Lee 2004). This correlates with our data that A β binds to both positively and negatively charged surfaces (Moores et al, 2011) as well to positively and negatively charged membranes (Hane et al, 2011).

In solution, A β reaches a reversible equilibrium of monomers and unstructured aggregates in random coils and oligomeric β sheet structures. Research by Terzi has demonstrated that in the presence of negatively charged membrane lipids, this random coil and β sheet equilibrium shifts almost completely toward the β sheet conformation (Terzi et al, 1995). It was hypothesized by Terzi et al that this equilibrium shift is a result of the positively charged part of the A β peptide being attracted to the anionic lipids in the membrane forming a higher local surface concentration of the peptide on the surface (Terzi et al, 1995). A combination of increased surface concentration and specific alignment of the peptide creates ideal conditions for the formation of amyloid fibrils. This process may act as a catalyst, reducing the activation energy required to correctly position the peptide chains, or the presence of the membrane may shift the thermodynamic equilibrium to favour the β sheet conformation (Terzi et al, 1995). We showed that the charge distribution in A β 42 changes upon oligomer formation, making it a more pronounced dipole or multipole with growing oligomer size (Moores et al, 2011). This makes interactions with either cationic or anionic lipid membrane more preferable.

In addition, we demonstrated that membranes in the fluid phase, both cationic DOTAP and zwitterionic DOPC, bind A β and show larger penetration of A β into the membrane, compared to gel phase membranes, producing larger defects in the membrane. This is illustrated in the schematic in Figure 2.5B. In addition, Kremer et al. demonstrated that A β changes membrane fluidity upon binding and that A β membrane-interactions do not depend on charge interactions (Kremer et al, 2001). This group and others showed that the lipid phase appears to be influential in the ability of A β to bind and penetrate the lipid bilayer (Choucair et al, 2007; Hane et al, 2011; Ahyayauch et al, 2012).

The fragment of peptide itself is important for the interactions of A β with lipid membrane. Ionov et al (Ionov et al, 2010) found that A β (1–28) preferentially interacts with the hydrophilic part of the model membranes, while A β (25–40) locates itself in the hydrophobic core of the bilayer where it reduces the order of phospholipid packing.

In summary, the charge and the phase of the lipid membrane as well as the structure of A β itself are important factors for A β interactions with lipid membrane (Ionov et al, 2010; Choucair et al, 2007; Hane et al, 2011; Ahyayauch et al, 2012; Ege et al, 2005; Maltseva et al, 2005), which is an important initial step of amyloid fibril formation in the AD brain (Yanadisawa et al, 1995) and in vitro (Terzi et al, 1995; Choo-Smith & Surewicz 1997).

2.2.3.2 Effect of Cholesterol

Studies of A β interactions with membranes are of great interest to researchers because the plasma membrane serves as the site of the accumulation of amyloid plaques. Earlier, we reviewed the data where model membranes of simple composition were studied in this relation, focusing on lipid charge and phase. However, because of the great complexity of membranes, the presence of lipid rafts and sterols may have an important effect on amyloid binding and toxicity. Cholesterol is an essential component for the formation of rafts within the membrane, and therefore, its effect on the interactions of amyloid with the membrane could be a key component of the molecular mechanism of amyloid toxicity. Although amyloid fibril plaque accumulation occurs on the surface of plasma membranes *in vivo*, the role of cell membrane rafts and their composition on A β fibril formation and toxicity are still not well understood.

Cholesterol is known to regulate various important functions of the membrane and is involved in signaling, molecule assembly, membrane fluidity and membrane protein trafficking (Lingwood & Simons 2010; Giordani et al, 2008). The effect of cholesterol on the membrane is very complex and is still a matter of debate, mainly because of various factors that influence its effect, including the type and phase of membrane lipids (Ohvo-Rekilä et al, 2002) and the concentration of cholesterol (Lipowski et al, 1995). Previous works (Ohvo-Rekilä et al, 2002; Demel & Kruyff 1976; McMullen et al, 2004; Bonn et al, 2004; Cadenhead et al, 1985) have demonstrated that cholesterol plays a key role in controlling the fluidity, permeability, and mechanical strength of the lipid membrane, as well as interfering with lipid phase transitions. These effects are also dependent on cholesterol concentration.

It has been hypothesized that lipid raft domains in cell membranes, enriched with cholesterol and sphingolipids, could provide an environment which promotes A β binding and amyloid formation. It has been shown that soluble A β aggregates bind to raft microdomains enriched by clusters of gangliosides (Williamson et al, 2008) and mediate membrane oxidative damage (Zampagni et al, 2010). A growing number of recent research contributions suggest the importance of the lipid rafts in amyloid fibril formation and toxicity (Cordy et al, 2006; Sharp et al, 2002; Ege et al, 2005; Yip et al, 2001). These studies emphasize the effect of charged lipids, pH, metal cations, and cholesterol on the effectiveness of fibrillogenesis, suggesting that electrostatic interactions between the lipid membrane and amyloid proteins are important. The role of electrostatic interactions and detailed understanding of lipid electrostatic non-homogeneity is of particular interest in this regard. A recent study by Sheikh et al. also suggests that membrane interactions with A β monomers in the membrane greatly depend on cholesterol content, as well as lipid composition and phase state (Sheikh et al, 2012). In this study, cholesterol's presence in systems of DOPC and DPPC caused an increase in the initial kinetics of the area coverage of amyloid- β on the lipid bilayer surface by as much as two orders of magnitude, which suggests an increased membrane affinity for amyloid when cholesterol is present (Sheikh et al, 2012). Indeed, a recent molecular dynamics simulation study has shown that cholesterol can act as a promoter for membrane-amyloid interactions because its presence makes the binding process of amyloid to the membrane more energetically favourable (Yu et al, 2012).

Although cholesterol is an important constituent of lipid rafts (Zampagni et al, 2010), the role of cholesterol is not clear in the molecular mechanism of amyloid toxicity. In fact, the effect of cholesterol on amyloid toxicity in relation to Alzheimer's disease is controversial. On one hand, research has shown an adverse effect of cholesterol on amyloid toxicity: membranes containing sterols, such as cholesterol, have been shown to activate the fibrillogenesis of A β suggesting a specific sterol binding site that accelerates amyloid aggregation (Ryan et al, 2012). In addition, lipid membranes can catalyze the conversion of monomeric A β into toxic amyloid aggregates (Relini et al, 2009). Interactions with the cell membrane, especially in areas containing cholesterol-rich lipid rafts, are considered important for neurotoxicity (Kakio et al, 2003). Fahrenholz and colleagues amongst others have shown that cholesterol increases the cleavage of A β from APP (Kojro et al, 2001; Fassbender et al, 2001). Cholesterol has been shown to influence the fluidity of total brain extract and the extent of A β fibrillogenesis (Yip et al, 2001). This data showed a correlation between membrane cholesterol level and A β cell surface binding leading to cell death (Yip et al, 2001). Furthermore, Abramov's group (Abramov et al, 2011) reported that the addition of A β to lipid bilayers caused a calcium ion conductance that was significantly higher in membranes containing cholesterol. They concluded that increasing membrane cholesterol significantly increased A β -induced neuronal and astrocytic cell death. On the other hand, however, cholesterol has been reported to have a neuroprotective effect against A β (Yip et al, 2001; Arispe et al, 2002) and inhibit the formation of amyloid induced ion channels (Lin et al, 2002). Similarly, studies with cholesterol and amyloid plaques in human neuroblastoma cells have shown the possibility that increased cholesterol content reduces membrane perturbation by the amyloid plaques (Cecchi et al, 2009).

Cholesterol has been reported to alter the penetration of A β into the lipid bilayer (Dante et al, 2006) and monolayers (Ji et al, 2002). Notably, 20% of cholesterol completely inhibits monomeric A β (25-35) membrane insertion (Dante et al, 2006). The mechanism by which cholesterol attracts A β to the cell membrane is believed to be by increasing hydrogen bonding between A β and DPPC accelerating incorporation into the cell membrane (Abramov et al, 2011). Once cholesterol is present, cholesterol-A β interactions compete with inter-protein A β interactions and do not accelerate A β aggregation (Zhao et al, 2012). MD simulations indicate that A β 40 prefers to reside on the surface of the cell membrane as

opposed to inserting into cholesterol-depleted membranes. In cholesterol rich membranes, A β (1-40) inserts only partially (Qiu et al, 2011). Amyloid insertion and ion channel formation will be further expanded upon in the next section of this review.

As mentioned previously, the role of electrostatic interactions within lipid membranes and a detailed understanding of lipid electrostatic non-homogeneity is of great interest in studying the interaction of charged species such as A β with the membrane. We recently reported that cholesterol has an interesting electrostatic effect on model lipid monolayers (Drolle et al, 2012) and in Bovine Lipid Extract Surfactant (BLES) surfactant, a complex lipid-protein mixture (Gunasekara et al, 2010; Finot et al, 2010). We demonstrated that cholesterol induces electrostatic domains in supported lipid-protein films of BLES surfactant (Finot et al, 2010), which results in surfactant failure. These intriguing electrostatic properties of cholesterol on membrane structure may be crucial in understanding the interaction of the plasma membrane with amyloid forming peptides.

In order to study the role of cholesterol-induced domains on A β -membrane interactions we used high-resolution AFM and model single lipid membranes in the absence and presence of cholesterol. We used also Frequency Modulated Kelvin Probe Force Microscopy (FM-KPFM) (Zerweck et al, 2005; Moores et al, 2010), a modification of AFM, to resolve electrical surface potential maps in DOPC monolayer with and without cholesterol in order to elucidate the role of electrostatic domains.

This study is discussed in full detail in chapter five of this thesis, but in short, we found that in the pure DOPC bilayer, A β deposits were small, spherical and spread across the lipid membrane surface in a uniform distribution with no discernible preferential binding sites or clustering. However, when looking at a DOPC membrane with 20% cholesterol, amyloid fibril formation was no longer uniform; we observed nanoscale islands or domains loaded with amyloid deposits and surrounded by smooth areas of lipid bilayer void of A β deposits, seemingly formed as a result of the amyloid deposits binding to the membrane in a non-uniform and rather selective manner. The presence of single fibrils protruding from the clustered domains were clearly visible, indicating that cholesterol promotes much stronger preferential binding of A β . Our data correlates well with the previously mentioned recent

study by Sheikh, who reported that binding of A β to the membrane was increased two orders of magnitude when cholesterol was present in the membrane (Sheikh et al, 2012), and a recent molecular dynamics simulation study, which has shown that membrane cholesterol makes the binding process of amyloid to the membrane more energetically favorable (Yuet et al, 2012).

We ascribed this targeted binding of amyloid in the presence of cholesterol to cholesterol-induced nanoscale electrostatic domains. To look specifically at the role of the electrostatic effect of cholesterol, we used FM-KPFM. FM-KPFM is a powerful technique which, as we demonstrated earlier, is the only technique suitable of mapping the local electrical surface potential of complex self-assembled biological films with a lateral resolution of a few nanometers and sensitivity of a few millivolts in air at normal humidity (Zerweck et al, 2005; Moores et al, 2010). In addition to high sensitivity and high resolution, FM-KPFM also has the advantage of allowing both the topography and surface potential to be collected simultaneously on the same location of the same samples, allowing for easy comparisons.

Using this highly sophisticated technique, we resolved nanoscale electrostatic domains in DOPC with 20% cholesterol monolayer samples that were not present in monolayer samples of pure DOPC. Considering the charged nature of A β and complex nature of electrical charge distribution in oligomers (Moores et al, 2011), it can be ascertained that electrostatic domains created in the DOPC lipid membrane by cholesterol attract the A β peptide, thus inducing the formation of the non-uniform islands or domains that are heavily loaded with amyloid deposits.

As shown earlier, cholesterol produces similar nanoscale electrostatic domains in lung surfactant, which leads to surfactant failure (Finot et al, 2010; Leonenko et al, 2006). These electrostatic domains create a distinct electrical potential, which affects the interaction of the surfactant film with charged species (Finot et al, 2010). We demonstrated that this previously unknown electrostatic effect of cholesterol is not limited to only lung surfactant films but extends to model lipid monolayers and lipid membranes and can greatly affect the interaction of A β peptides with the surface of lipid membrane.

We propose that this electrostatic effect of cholesterol on the monolayer has an important role in cholesterol-lipid systems and may be present in other, more complex systems as well. This earlier unknown electrostatic effect of cholesterol may serve as a driving force for amyloid targeted attack on lipid membranes and therefore may be involved in the mechanism of amyloid toxicity.

2.2.3.3 Ion channels

In addition to binding and penetrating into the membrane, A β may interact with membrane forming ion channels, shown schematically in Figure 5C. These ion channels destabilize cellular ionic homeostasis and induce cell pathophysiology and degeneration, characteristic of amyloid diseases.

Lal and colleagues provided strong evidence supporting this hypothesis, first proposed by Arispe (Arispe et al, 2004), that cellular dyshomeostasis caused by ion channels was responsible for at least some of the symptoms associated with AD. Quist used AFM to image tetrameric and hexameric oligomeric structures formed by A β in reconstituted membranes, which resemble the ion channels in cell membranes. By using atomic force microscopy, circular dichroism, gel electrophoresis, and electrophysiological recordings, they showed the presence of ion channels in lipid membranes is a common feature of the proteins implicated in neurodegenerative disorders such as Alzheimer's disease, Parkinson's disease, and frontotemporal dementia (Quist et al, 2005). Amyloid molecules, including A β -40, alpha-synuclein, ABri, ADan, serum amyloid A, and amylin undergo supramolecular conformational change, and in reconstituted membranes, they form morphologically compatible ion-channel-like structures, which elicit single ion-channel currents. Kaye et al, referred to such ion-like structures as annular protofibrils (APF), a distinct off-pathway structure (Kayed et al, 2009). Interestingly enough, even though APFs are structurally similar, they have shown that these structures are not nearly as membrane-permeable as the fibrillar precursors termed prefibrillar oligomers (PFOs).

Using the unique combination of AFM and electrical recording, Lal's group resolved their structures with AFM and showed that these ion channels, induced by assembly of A β in the membrane, have a distinct ion current activity when an electric potential is applied (Quist et al, 2007). For these experiments, Lal's group designed a special AFM liquid cell with two compartments separated by a silicon membrane with microfabricated nanopores of diameter 70-100nm, on which the lipid bilayer can be deposited, while both compartments are immersed in buffer. Two electrodes are positioned in each compartment in order to apply a defined potential to measure membrane permeability or ion current induced in the membrane by A β . AFM imaging and ion current recording can be done on the same single ion pore with this approach (Quist et al, 2007).

Later, the Lal and Nussinov groups provided more evidence supporting the ion channel mechanism for Alzheimer's disease (Jang et al, 2010). Using solid-state NMR, AFM imaging and molecular dynamics simulations they demonstrated that small A β oligomers insert into the cell membrane, forming toxic ion channels and destabilizing the cellular ionic homeostasis. Using MD simulations, Jang modeled a β -barrel-like organization for these channels. β -Barrels are common in transmembrane toxin pores, typically consisting of a monomeric chain forming a pore, organized in a single-layered β -sheet with antiparallel β -strands and a right-handed twist. Their MD data in comparison with AFM images support a β -barrel channel organization for A β channels. Different from the transmembrane β -barrels where the monomers are folded into a circular β -sheet with antiparallel β -strands stabilized by the connecting loops, these A β barrels consist of multimeric chains forming double β -sheets with parallel β -strands, where the strands of each monomer are connected by a turn (Figure 2.6). The A β barrels adopt the right-handed β -sheet twist but still break into heterogeneous, loosely attached mobile subunits, in good agreement with AFM images, which allows for unregulated, hence toxic, ion flux.

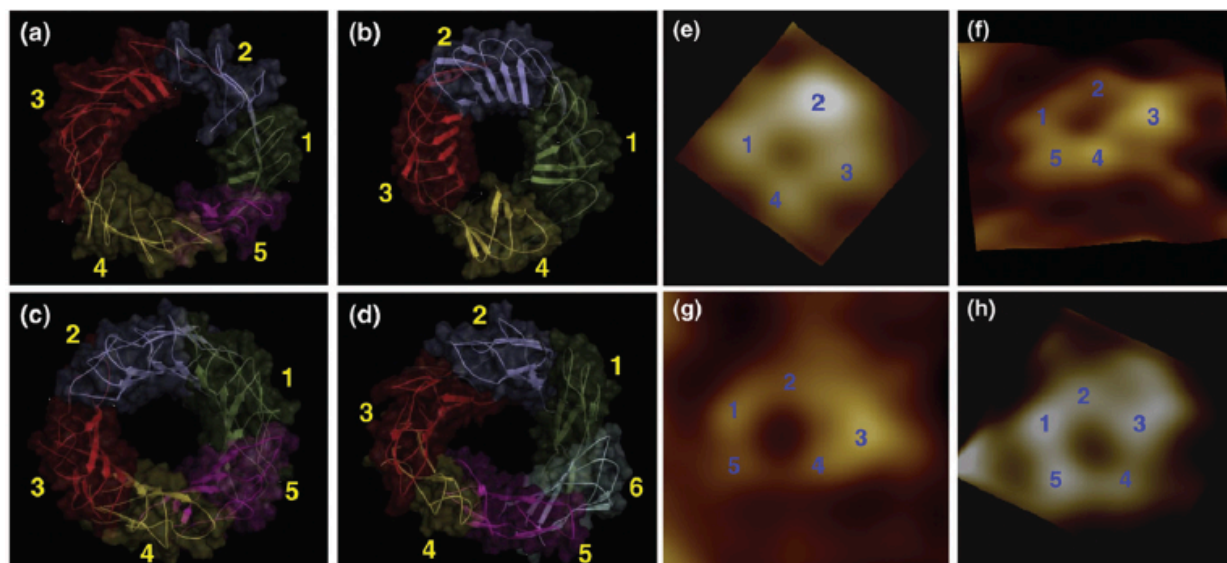


Figure 2.6: Molecular dynamics simulation and AFM images of A β induced ion channels. Side-by-side comparison between the computational barrels and the experimental channels. The simulated barrel structures with highlighted subunits for the 20-mer p3 (a), p3h (b), N9 (c), and N9h (d) barrels. The averaged barrels in the surface representation are shown in the view along the membrane normal. AFM images of p3 (e and f) and N9 (g and h) barrels show four or five subunits, consistent with the simulated barrels. Image sizes are 15 \times 15 and 23 \times 23 nm², respectively. (Figure reproduced from Jang et al, *J. Mol. Biol.* (2010) 404, 917–934 with DMR permission to use).

The β -barrel channel structure reported by Jang (Jang et al, 2010) is rare in eukaryotes but is found in the mitochondrial (which is believed to be a bacterial relic) outer membrane and is known as a voltage-dependent anionic channel (Thinnes et al, 1989; Bay et al, 2002; Casadio et al, 2002). Such anionic channels have a two-state voltage-dependent gating mechanism opening and closing the pore, inducing cytotoxicity and apoptosis (Shulga et al, 2009; Abu-Hamad et al, 2009). These studies are in agreement with electrophysiology data by Abramov (Abramov et al, 2011) who reported that addition of A β to lipid bilayers causes ion conductance, which was significantly higher in membranes containing cholesterol. They concluded that incorporation of A β into membranes and the ion channels created by A β are promoted by membrane cholesterol, which significantly increased A β -induced [Ca²⁺] current, leading to neuronal and astrocytic cell death. Other theoretical work (Pannuzzo et al, 2013) report significant change in membrane curvature due to amyloid binding and

formation of non-channel defects, which resemble conical holes inside the membrane. Such defects can also result to increased membrane permeability and ion currents. This case corresponds to the membrane damage seen on a DOPG membrane, as discussed in section 2.2.3.1 (Lipid Composition).

These studies show that A β ion channels can serve as candidates for understanding the neurotoxicity of Alzheimer's disease and secondly, they highlight the possibility of drug design targeting these amyloid ion channels. The formation of these channels and their activity are dependent on the properties of lipid membrane and in particular on the presence of membrane cholesterol.

2.3 Summary

In summary, we reviewed the major aspects of A β interactions with lipid membrane in relation to amyloid toxicity and Alzheimer's disease, with a specific focus on AFM studies, which provide nanoscale insight into the molecular mechanism of these interactions. We have shown that it is now increasingly accepted that A β interacts with the membrane in a complex mechanism where several pathways are possible: accumulation on the surface of the lipid membrane (Figure 2.5A), penetration into the membrane, causing disorder in lipid organization (Figure 2.5B), and formation of ion pores and ion channels, which leads to unregulated ion leakage and, ultimately, cell death (Figure 2.5C).

Overall, the role of the lipid membrane in the molecular mechanism of amyloid toxicity is very important in the pathogenesis of AD and may provide avenues for the development of preventive and treatment strategies to combat Alzheimer's disease and other amyloid induced neurodegenerative disorders.

Chapter 3.0 Comparative Effects of Cholesterol and Melatonin on the Physical Properties of the Lipid Membrane

Note: this chapter was reproduced with modifications with permission from {Drolle E, Kučerka N, Hoopes MI, Choi Y, Katsaras J, Karttunen M, Leonenko Z. 2013. Effect of melatonin and cholesterol on the structure of DOPC and DPPC membranes. *Biochim. Biophys. Acta*, 1828: 2247 – 2254.} © {2013} Elsevier.

Aim of Published Work

In this study, we compared the effects of cholesterol and melatonin on two single lipid systems – DPPC and DOPC. Cholesterol's effect on the membrane is well known, but melatonin's effects are still relatively undiscovered. As studies have shown, melatonin may have a neuroprotective effect while cholesterol's effect in this regard is still controversial; as a result, the comparison of cholesterol and melatonin is of great interest to neurodegenerative research.

Contributions

Under the supervision of Dr. Z. Leonenko, I set up a collaboration with a research scientist at the NRC, Dr. N. Kučerka, to do this comparison study using neutron scattering methods. I was responsible for experimental design and traveled to the nuclear reactor in Chalk River, ON to carry out the actual neutron scattering experiments. With the assistance of Dr. N. Kučerka, I made the numerous samples and carried out the neutron scattering experiments myself as well as wrote this manuscript. Data analysis was done using analysis software available in Chalk River and was carried out by Dr. Kučerka; I was trained by Dr. Kučerka in this analysis and assisted in carrying it out while I was present at the nuclear facility.

To supplement the NS data we collected, we invited Dr. M. Karttunen and his postdoctoral fellow Dr. M. Hoopes to collaborate; they conducted molecular dynamic simulations for our systems to support the observations made through neutron scattering. In this description of our study, we refer to this work by Karttunen and Hoopes to further support our NS findings.

Summary and Conclusions

Our neutron scattering and the supplemented molecular dynamics data both confirmed that melatonin causes a disordering in the lipid hydrocarbon chains, which increases membrane fluidity and thereby decreases the thickness of the bilayer. This effect on the membrane is opposite that of cholesterol, which has a commonly agreed upon ordering and thickening effect.

3.1 Overview

An important initial step in studying the effect of biomolecules on peptide-membrane interactions is accurately determining the effect that the biomolecules themselves have on the membrane in general, in the absence of any peptide. This is important because, due to the complexity of lipid membranes, both lipid composition and the presence of small biomolecules may cause changes in membrane structure and physicochemical properties; these alterations may, in turn, affect membrane-peptide interactions. Recent evidence of amyloid toxicity studies has revealed that melatonin and cholesterol both have effects on amyloid interaction with the membrane and associated damage. While cholesterol's effect on the membrane has been widely studied, its effect on amyloid fibril formation and toxicity is still debated (Puglielli et al, 2003; Cecchi et al, 2009). Melatonin has been suggested to have a neuroprotective effect against amyloid toxicity but the mechanism of this protection is not understood. The effect of both melatonin and cholesterol on 1,2-dioleoyl-sn-glycero-3-phosphocholine (DOPC) and 1,2-dipalmitoyl-sn-glycero-3-phosphocholine (DPPC) model membranes were compared. The comparison studies were conducted using small-angle neutron diffraction (SAND) from oriented lipid multi-layers, small-angle neutron scattering (SANS) from unilamellar vesicles experiments and supplemented with Molecular Dynamics (MD) simulations. It was found that melatonin causes disordering in the lipid hydrocarbon chains, thus increasing membrane fluidity and causing a decrease in the thickness of the bilayer. This is in direct opposition to the commonly agreed upon ordering and thickening effect of cholesterol (Bonn et al, 2004; Demel & De Kruffyff 1976; Kučerka et al, 2007; McMullen et al, 2004; Ohvo-Rekilä et al, 2002).

3.2 Introduction

The cell membrane is the first line of defense against invading species, and is a key to understanding disease, including amyloid toxicity that is commonly associated with Alzheimer's disease. Small molecules, such as cholesterol and melatonin incorporate into the lipid matrix and are known to alter the membrane's structure and its physical properties (Bongiorno et al, 2005; Severcan et al, 2005). These changes to the membrane subsequently affect its functionality and its interactions with biomolecules. While the interaction of

cholesterol with membranes has been extensively studied, the effect of melatonin on the structure of lipid membranes is not well understood. Structural studies detailing the effects of melatonin and cholesterol on membranes are, however, of great importance because both molecules have been linked to amyloid toxicity associated with Alzheimer's disease.

Alzheimer's disease (AD) is a neurodegenerative disease and a major form of dementia that becomes more prevalent with increasing age. AD is associated with the formation of plaques and insoluble amyloid fibrils, which are composed of amyloid-beta ($A\beta$) proteins folded into β -sheets, found on the surface of neuronal plasma membranes (Mucke & Selkoe, 2012). Recent studies have shown the lipid membrane to be extremely important in enabling amyloid fibril formation and its ensuing toxicity (Di Paolo & Kim 2011; Friedman et al, 2009; Gellermann et al, 2005).

In both human and animal studies, melatonin has been shown to have a protective role against AD, namely slowing the development of disease by, for example, providing anti- β -amyloid aggregation capabilities (Dragicevic et al, 2011; Karasek 2004; Olcese et al, 2009; Rosales-Corral et al, 2012). However, the underlying molecular mechanism of this protective effect is not well understood. Melatonin is a pineal hormone that is produced in the human brain and is responsible for maintaining the circadian rhythm and regulating the sleep-wake cycle (Benloucif et al, 2008). In addition to its well-known anti-oxidative effects, melatonin is known for its involvement in intracellular signal transduction, regulation of cell death and cell proliferation (Kondratova & Kondratov 2012). The protective mechanism of melatonin against AD may involve a nonspecific interaction of melatonin with the membrane (Severcan et al, 2005), although its effects on lipid membranes remain inconclusive and controversial. It has also been reported that melatonin decreases the gel-to-fluid phase transition temperature in a number of different lipid systems, implying that melatonin increases membrane disorder (de Lima et al, 2010; de Lima et al, 2007; Garcia et al, 1997; Saija et al, 2002; Severcan et al, 2005). In contrast, slower membrane dynamics have been reported in DPPC bilayers (Severcan et al, 2005), rat brain homogenate (Akkas et al, 2007; Sahin et al, 2007), and in DMPC membranes (Costa et al, 1997; de Lima et al, 2007). Garcia et al reported the stabilizing effect of melatonin in synergy with other drugs on mitochondrial membrane (García et al, 1998). These important, but somewhat contradictory,

results therefore necessitate further studies regarding melatonin's effects on biologically relevant membrane systems, especially in terms of trying to determine where these contractions in results arise.

Although a number of *in vitro* studies have demonstrated the above-mentioned protective effects of melatonin against A β , including studies at the cellular level (Dragicevic et al, 2011; Feng & Zhang 2004; Poeggeler et al, 2001) the underlying mechanisms of melatonin's protective action have yet to be adequately explained. For example, Galano et al. emphasized the importance of antioxidant action of melatonin (Galano et al, 2011); Bongiorno et al. have shown that melatonin may compete with cholesterol for binding to lecithin, and that it may even displace cholesterol from the phospholipid bilayer (Bongiorno et al, 2005). Melatonin's ability to control cholesterol content, and therefore membrane rigidity, may thus reduce the effects of cholesterol on the membrane, as well as cholesterol-mediated processes (Rosales-Corral et al, 2012). Previous studies (Benloucif et al, 2008; Bongiorno et al, 2005; de Lima et al, 2010; de Lima et al, 2007; Di Paolo & Kim 2011; Friedman et al, 2009; Garcia et al, 1997; Gellermann et al, 2005; Karasek 2004; Kondratova & Kondratov 2012; Mucke & Selkoe 2012; Olcese et al, 2009; Rosales-Corral et al, 2012; Severcan et al, 2005) have demonstrated melatonin's ability to non-specifically bind to and interact with the lipid membrane and to alter its biophysical properties. In addition to its anti-oxidative protection, the biophysical effects of melatonin on the membrane may also contribute to its cell protective qualities and thus deserves further investigation. This study specifically focuses on the non-specific biophysical effect of melatonin on model membranes with the purpose of comparing it to the effect of cholesterol.

In contrast to melatonin's protective abilities, it has been shown that cholesterol, when in a membrane, can enhance amyloid binding and fibril formation (Puglielli et al, 2003). However, depending on the type of lipid (in terms of charge and saturation) and the type of amyloid peptide (for example, A β ₁₋₄₀ vs A β ₁₋₄₂), others have reported that cholesterol hinders the insertion of amyloid peptides into lipid membranes (Dante et al, 2006). It was recently shown that cholesterol induces non-homogeneous binding of the amyloid peptide to the lipid membrane and formation of membrane defects (Drolle et al, 2012). Sheikh et al also reported enhanced membrane solubilization and defect formation when cholesterol was

present in a model membrane (Sheikh et al, 2012). On a cellular level, cholesterol has been shown to reduce the toxic effect of amyloid plaques on neuroblastoma cells (Cecchi et al, 2009). Therefore, in order to better understand how melatonin and cholesterol affect the interaction of biomolecules – e.g., amyloid fibrils – with the membrane, it is necessary to systematically determine the effects that these molecules have on membrane structure.

Cholesterol is a well-known sterol that usually orients itself parallel to the bilayer lipids, the exception being in bilayers with polyunsaturated fatty acids, where cholesterol sequesters into the middle of the bilayer (i.e., orthogonal to the bilayer normal) (Harroun, Katsaras, & Wassall, 2006). According to the lipid rafts hypothesis, cholesterol is an important constituent of lipid rafts (Kučerka et al, 2009; McMullen et al, 2004; Niemela et al, 2007; Ohvo-Rekilä et al, 2002; Radhakrishnan et al, 2000). Rafts saturated with cholesterol and sphingolipids, as well as saturated lipids such as 1,2-dipalmitoyl-*sn*-glycero-3-phosphocholine (DPPC), are thought to compartmentalize certain cellular processes, including cell signalling, molecular assembly and membrane protein trafficking, and require the presence of cholesterol in order to form (Giordani et al, 2008; McMullen et al, 2004; Ohvo-Rekilä et al, 2002). Cholesterol has also been shown to affect membrane permeability and fluidity, as well as the mechanical properties of model membranes (Bonn et al, 2004; Demel & De Kruyff 1976; Kučerka et al, 2007; McMullen et al, 2004; Ohvo-Rekilä et al, 2002). Factors affecting cholesterol's influence on membranes include its concentration and lipid membrane composition (Kučerka et al, 2010; Ohvo-Rekilä et al, 2002; Sackmann 1995).

Neutron scattering has been extensively used to study the structure of model lipid membranes. The technique has been used to accurately determine various bilayer structural parameters (e.g., lipid area, bilayer thickness), cholesterol's location in an multilayers, and its interactions with different lipids, to name a few (Karmakar & Raghunathan 2003; Kučerka et al, 2008; Lemmich et al, 1997; Levy & Briggman 2007; Marrink et al, 2008). To the best of our knowledge, neutron scattering has not been previously used to study the effect of melatonin on model membranes, nor how cholesterol's effects on membranes differ from those of melatonin. Surprisingly, there are no computer simulation studies of the effect of melatonin on membranes. To the best of our knowledge, the present study is the first to

address the molecular mechanisms of melatonin-lipid and melatonin-cholesterol-lipid interactions using Molecular Dynamics (MD) simulations in comparison with Neutron Scattering experiments.

3.3 Materials and Methods

3.3.1 Sample Preparations

1,2-dipalmitoyl-*sn*-glycero-3-phosphocholine (DPPC), 1,2-dioleoyl-*sn*-glycero-3-phosphocholine (DOPC), melatonin and cholesterol were purchased from Sigma-Aldrich (St. Louis, MO) in powder form. All other chemicals used were of reagent grade.

Lipids were solubilized in a 1:1 solution of chloroform: TFE (trifluoroethanol) with the requisite amount of cholesterol or melatonin (reported here in molar fractions) placed in a glass vial at total lipid concentrations of between 25 and 30 mg/mL. Approximately 15 mg of pure lipid; a mixture of lipid and cholesterol; or a mixture of lipid and melatonin (thin film thickness of ~ 0.001 cm when spread onto a 25 x 60 mm² silicon wafer), was deposited onto a silicon wafer and rocked during evaporation of the organic solvent in a glove box to form samples of highly oriented multilayer stacks (Tristram-Nagle 2007). The remaining solvent was removed by placing the oriented samples under vacuum prior to diffraction measurements.

Samples of unilamellar vesicles (ULVs) were prepared for study by small angle neutron scattering (SANS). Lipids were mixed with cholesterol/melatonin in chloroform, and then solutions were dried, initially in a stream of inert gas (e.g., Ar or N₂) and subsequently under vacuum. The resulting lipid film was hydrated using the requisite amount of 100% D₂O, resulting in a solution with a total lipid concentration of 20 mg/mL. The dispersions of self-assembled multilamellar vesicles (MLVs) were then extruded through polycarbonate filters populated with 50nm pores using an Avanti extruder (Avanti Polar Lipids, Alabaster, AL). This procedure has been shown to yield reasonably monodisperse ULVs with a mean diameter of ~ 60 nm (Kučerka et al, 2007).

3.3.2 Small-Angle Neutron Diffraction

Neutron diffraction data was collected at the Canadian Neutron Beam Centre's (CNBC) N5 beamline, which is located at the National Research Universal (NRU) reactor (Chalk River, Ontario, Canada). Neutrons of 0.237 nm wavelength were selected by the (002) reflection of a pyrolytic graphite (PG) monochromator, and a PG filter was used to eliminate higher order reflections. Incoming neutrons were collimated into a rectangular beam of dimensions 6x50 mm², and scattering angles were determined via the sample angle θ and the detector angle Φ . Samples were placed in an airtight sample cell and hydrated with saturated K₂SO₄ (97% relative humidity) solutions using a series of different neutron contrast D₂O/H₂O mixtures (i.e., 70%, 40%, and 8% D₂O) at 25°C.

The stability of the sample over the duration of the experiment was confirmed by the reproducibility of the diffraction data, whereby lamellar repeat spacings and peak intensities (i.e., for a given quasi-Bragg reflection) remained constant, indicating that the bilayer structure was unaltered. Alignment quality for each sample was assessed using the Gaussian width of rocking curves [i.e., the sample was rotated through an angle θ , while the detector remained fixed at a given angle (Φ)]. Figure 3.1 shows a typical rocking curve with a sharp central peak (mosaic spread of Gaussian width $\sim 0.05^\circ$) corresponding to large lateral domains of highly oriented multi-bilayers (Kučerka et al, 2009). This narrow peak sits atop a broad peak (Gaussian width $\sim 0.5^\circ$) consisting of scattering from much smaller domains with a broader distribution of orientations (Als-Nielsen & McMorrow 2001).

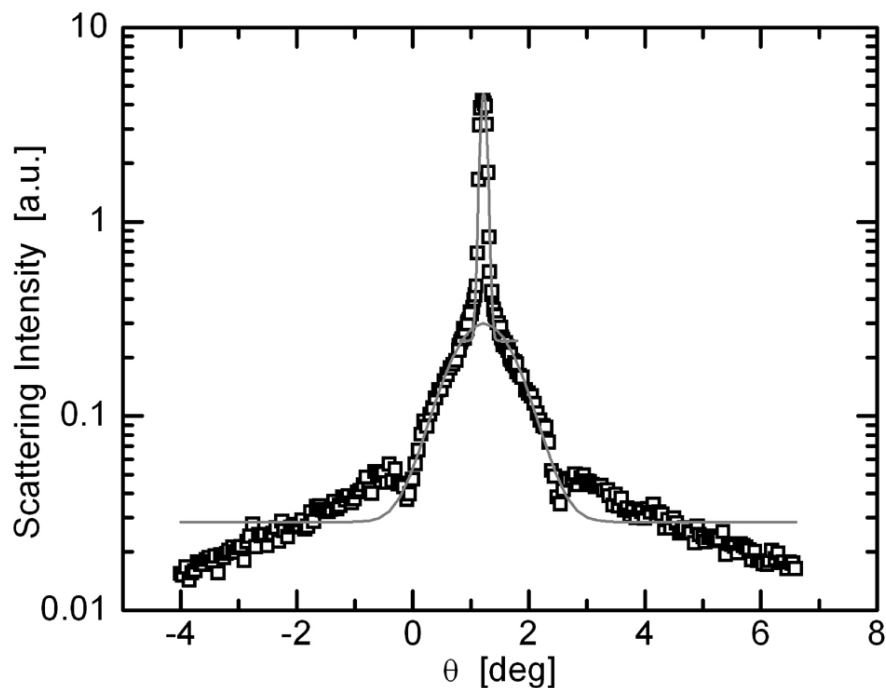


Figure 3.1: Semi-log plot of a rocking curve (points) corresponding to the first order diffraction peak from aligned multi-bilayers (DOPC with 9 mol% melatonin). The width of the peak (gray lines) indicates the quality of the sample's alignment. Note that the neutron signal drops at two points along the curve, both as a result of increased neutron absorption, which occurs when the sample is parallel to the incident (i.e., $\theta=0$) or the diffracted (i.e., $\theta=\Phi$) neutron beam.

Diffraction curves were obtained using θ - 2θ scans, i.e., where the detector is always positioned at $\Phi=2\theta$. Typically five quasi-Bragg orders were detected, which were fitted to Gaussians and an additional second-order polynomial function associated with the background. Integrated intensities for the different quasi-Bragg peaks were corrected for incident neutron flux, sample absorption, and the Lorentz correction, as described elsewhere (Kučerka et al, 2009). The phases of the corrected form factors were deduced through the systematic replacement of H_2O by D_2O in the hydrating solution, whereby the bilayer form factors measured at different contrast conditions change linearly as a function of D_2O content (Worcester & Franks 1976). Finally, neutron scattering length density (NSLD) profiles were calculated via the Fourier transform of the scattering form factors, while absolute scale NSLD profiles were not determined. This procedure results in NSLD profiles

that can be used to determine the characteristic features of bilayers. Moreover, the profiles obtained for samples hydrated with 8% D₂O solution show only the bilayer, and are not obscured from scattering by the solvent (in 8% D₂O the water contribution to the NSLD is zero). These profiles are thus best used to extract the membrane's fine structural details (i.e., lipid head-groups peak-peak distance across the bilayer, D_{HH}).

3.3.3 Small-Angle Neutron Scattering

Neutron scattering data were collected at the CNBC's N5 triple-axis spectrometer, which was adapted for SANS measurements (Nieh et al, 2008), and at the CG-3 Bio-SANS instrument (Lynn et al, 2006) located at Oak Ridge National Laboratory (ORNL). In the case of the N5 instrument, 4 Å wavelength neutrons were selected using a PG monochromator, and the scattered neutrons were detected using a 32 wire detector positioned at five predetermined angles (i.e., $\Phi=1.5, 3.3, 5.1, 6.9,$ and 8.7), covering a scattering range of $0.008 \text{ \AA}^{-1} < q < 0.270 \text{ \AA}^{-1}$. In the case of the CG-3 instrument, 6 Å wavelength neutrons were selected using a mechanical velocity selector, while two different sample-to-detector distances (i.e., 2.5 and 15.3 m) were used to cover a total scattering vector of $0.004 \text{ \AA}^{-1} < q < 0.370 \text{ \AA}^{-1}$. The two different experimental setups provided data of comparable quality (see Figure 3.2), although the dedicated SANS CG-3 instrument resulted in better quality high q data.

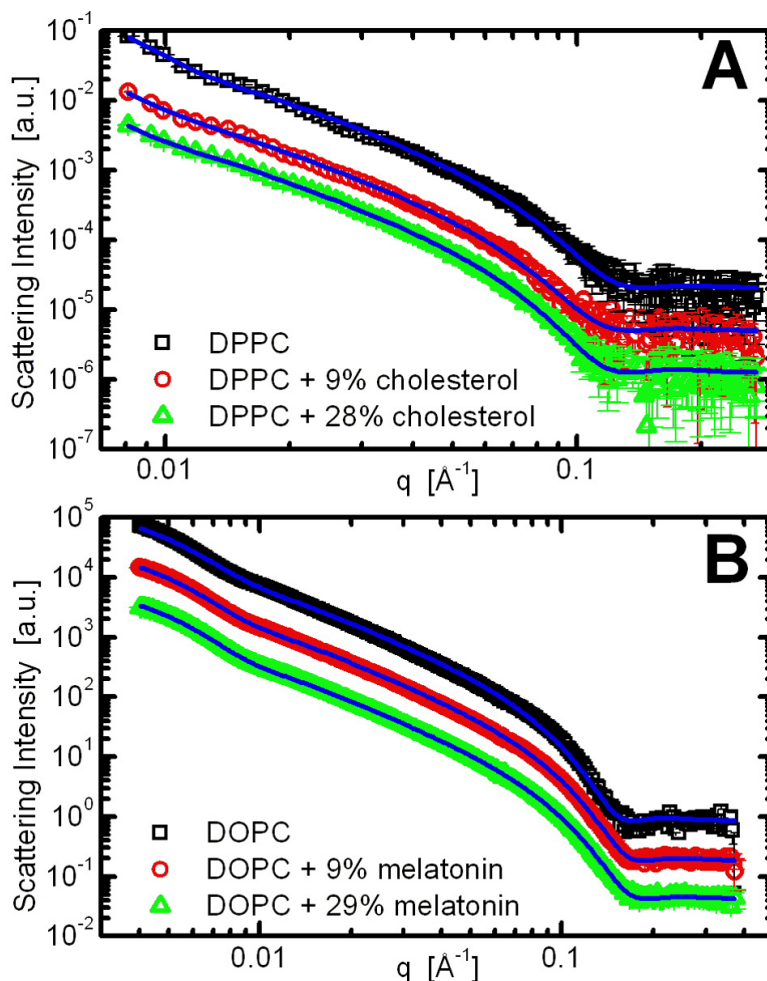


Figure 3.2: Log-log plot of SANS data obtained for A) DPPC bilayers doped with different amounts of cholesterol (data from the N5 instrument) and B) DOPC bilayers doped with melatonin (measured on the CG-3 Bio-SANS instrument). The blue solid lines are best fits to the data (open symbols). The SANS curves are shifted from each other (by a factor of 4) for better visualization.

SANS measurements were carried out using ULVs dispersed in 100% D_2O solution - as opposed to H_2O . D_2O is often used in neutron experiments in order to decrease the large incoherent scattering that results from hydrogen atoms, and to increase the contrast between the hydrating water and the lipid bilayer – which is also rich in hydrogen. As a result, the system is best described by a three component strip model made up of pure water (outside the lipid bilayer), a bilayer core of pure hydrocarbons, and a region where the lipid head-groups are inter-dispersed with water. This type of strip model analysis (Kučerka et al,

2004) has been used successfully to study the effect of cholesterol on DOPC bilayers (Kučerka et al, 2007). However, in the present study, the sharp interfaces separating the different strips were substituted with smooth error functions that represent a more realistic picture of membranes (Kučerka et al, 2010). As a result, a bilayer thickness that corresponds to the steric thickness of the bilayer is reported. It should be noted that this thickness is different from the D_{HH} obtained from SAND (described above; SAND shows distance between head groups while SANS shows steric thickness), and it is thus more appropriate to focus on the relative changes taking place within these different membrane thickness parameters, rather than the absolute values.

3.4 Results

In order to determine how melatonin affects membrane structure, and to compare these changes to those induced by cholesterol, a model was created of simplified bilayers containing either melatonin or cholesterol. It is well known that cholesterol when incorporated into a lipid bilayer partitions into the hydrocarbon chain region with its hydrophilic hydroxyl head-group residing in close proximity to the lipid head-groups (Léonard et al, 2001; Martinez-Seara et al, 2008; Yeagle 1985) (Figure 3.3A). It has also been proposed that melatonin may integrate itself into the head-group region of the lipid bilayer (Vânia R de Lima et al, 2010), as shown in Figure 3.3B.

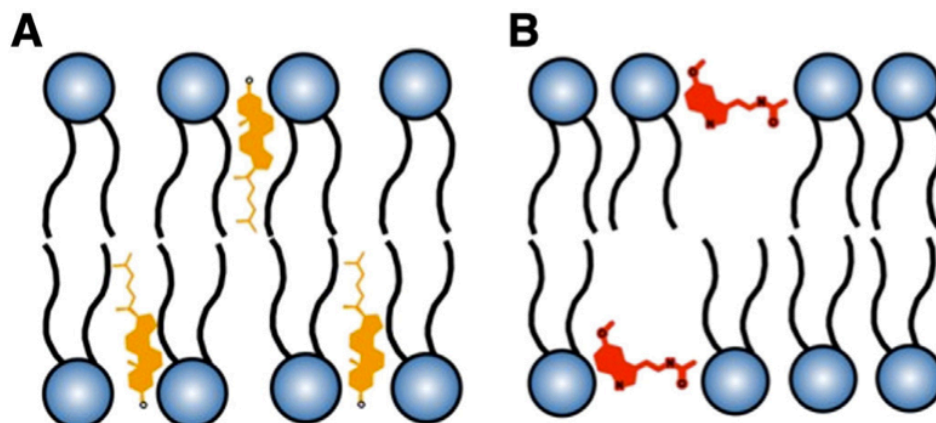


Figure 3.3: Schematics illustrating the proposed locations of cholesterol and melatonin in the lipid membrane: (A) cholesterol, (B) melatonin.

The SAND data obtained from oriented stacks of multi-bilayers and SANS data from ULV dispersions provide a more detailed description of the changes in bilayer structure incurred by the incorporation of cholesterol or melatonin into a lipid bilayer.

Figure 3.4 shows the NSLD profiles of lipid bilayers obtained from SAND measurements. In the case of these samples, varying amounts of cholesterol or melatonin were added (in equivalent molar ratio amounts), and the samples were hydrated using solutions with different neutron contrasts. The 8% D₂O solution results in NSLD profiles whose scattering can be exclusively attributed to the lipid bilayer, with no contribution from the bulk water.

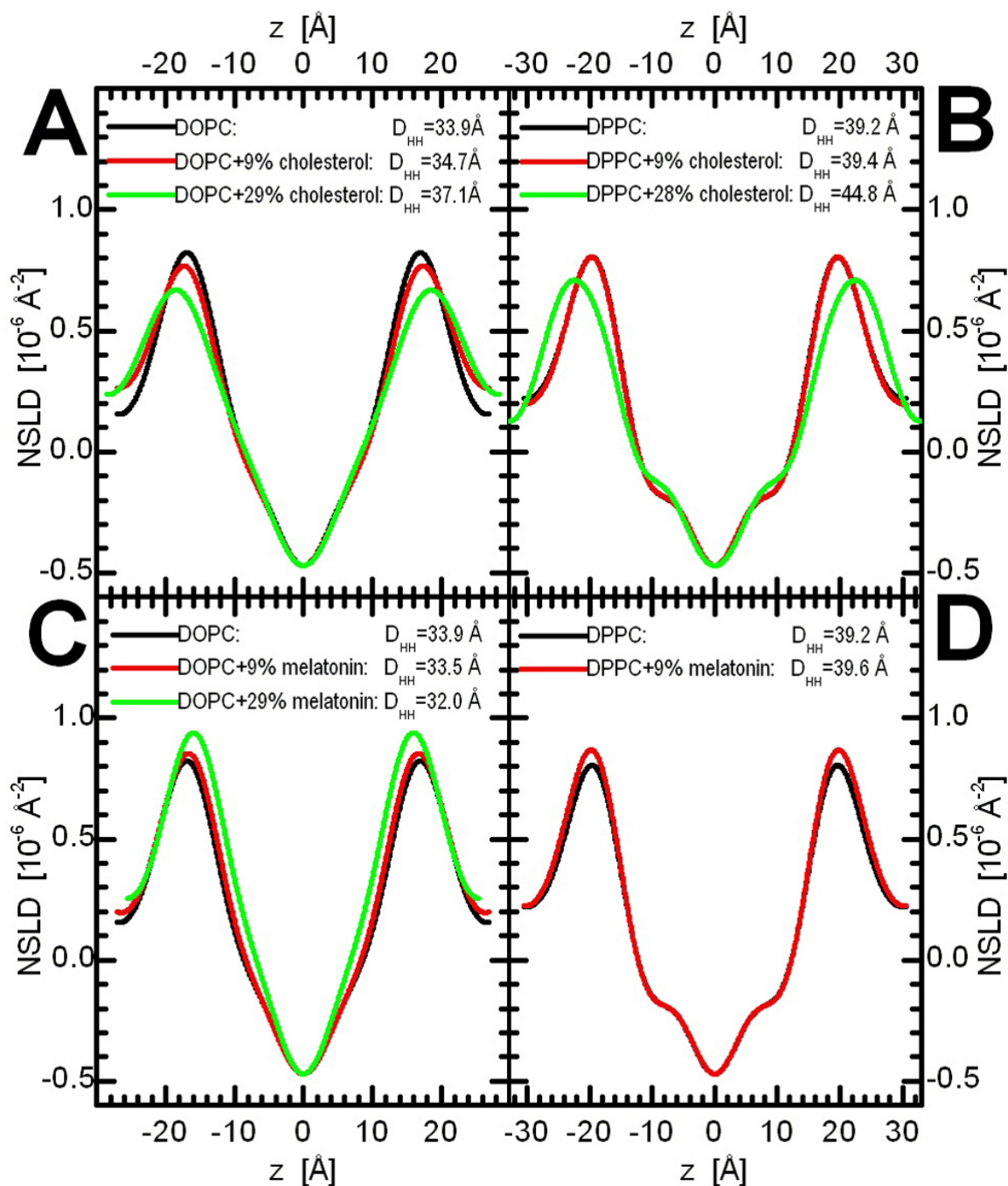


Figure 3.4: Neutron Scattering Length Density (NSLD) profiles of DOPC bilayers with increasing concentrations of cholesterol (A) and melatonin (C), as well as DPPC with increasing concentrations of cholesterol (B) and melatonin (D). Profiles are of bilayers hydrated with 8% D_2O , and deliberately centred at $z=0 \text{ \AA}$ to allow for the direct comparison of the lipid head-group peak-peak distance (D_{HH}) of the different samples.

The bilayer thickening effect as a result of cholesterol is well documented (Kučerka et al, 2007; Kučerka et al, 2009; Martinez-Seara et al, 2008; Worcester & Franks 1976), and the results presented here (Figure 3.4A and 3.4B) are in good agreement with previous published data. Figure 3.4A and 3.4B clearly illustrate the changes taking place in the lipid head-group peak-to-peak distance (D_{HH} , in which neutron interactions show maximum scatter at their head group region; as such, the two peaks present in a NSLD profile are indicative of head group location and as such, the distance between them can be interpreted as bilayer thickness) as a function of increasing amounts of cholesterol in DOPC (Figure 3.4A) and DPPC (Figure 3.4B) bilayers. D_{HH} is a good indicator of bilayer thickness, and corresponds to the distance separating head groups from opposing bilayer leaflets. It is clear that D_{HH} progressively increases with increasing amounts of cholesterol in the case of both bilayers (Figures 3.4A and 3.4B). Although cholesterol does not initially result in any significant change to D_{HH} , this change becomes more pronounced with increasing amounts of cholesterol. In the absence of cholesterol, the D_{HH} of the DOPC bilayer (Figure 3.4A) is 33.9 Å, and increases to 34.7 Å and 37.1 Å at 9% and 29% cholesterol, respectively. A similar trend of increasing thickness is seen in DPPC bilayers (Figure 3.4B): D_{HH} of the pure DPPC bilayer is 39.2 Å, and increases to 39.4 Å and 44.8 Å at 9% and 28% cholesterol, respectively.

Figures 3.4C and 3.4D show NSLD profiles for DOPC and DPPC bilayers, respectively, with increasing amounts of melatonin. In contrast to the effect by cholesterol, increasing amounts of melatonin in the lipid bilayer result in a progressive decrease in lipid bilayer thickness.

In the case of DOPC bilayers, for example, D_{HH} decreases from 33.9 Å in pure DOPC bilayers to 33.5 Å and 32.0 Å in DOPC bilayers with 9% and 29% melatonin, respectively (Figure 3.4C). In DPPC bilayer with the lowest concentration of melatonin studied here (9%), it appears that melatonin causes only a slight increase in D_{HH} - i.e., pure DPPC has a D_{HH} of 39.2 Å, while DPPC with 9% melatonin increases to 39.6 Å. However, due to difficulties in preparing oriented DPPC samples, high quality data from DPPC bilayers with higher concentrations of melatonin was not able to be collected. Therefore, only the data from ULV samples to report on how increasing amounts of cholesterol affected the D_{HH} of

DPPC bilayers was used.

SANS data from ULV samples have been successfully used to study cholesterol's effects on DOPC bilayers (Kučerka et al, 2007; Kučerka et al, 2009). As mentioned, SANS experiments were carried out using ULVs dispersed in 100% D₂O in order to improve the scattering contrast between the lipid bilayer and its surrounding water. By fitting the SANS data with an appropriate model, one can obtain NSLD profiles that differ from the ones obtained from oriented stacks of bilayers hydrated with 8% D₂O solution. In other words, in the ULV case with 100% D₂O the water molecules are part of the overall bilayer structure. As such, the obtained bilayer thickness (D_S) corresponds to the bilayer's steric thickness, which also includes the water molecules penetrating into the bilayer's head-group region.

Analysis of the ULV cholesterol data obtained by SANS is in agreement with the data obtained from the diffraction experiments. Bilayer thickness D_S increases with increasing cholesterol concentration for both DOPC (Figure 3.5A) and DPPC bilayers (Figure 3.5B). In case of DPPC bilayers (Figure 3.5B) D_S increases from 57.0 Å, to 59.6 Å, to 60.2 Å at 0%, 9% and 28% cholesterol, respectively. This result agrees well with the known ordering effect that cholesterol has on saturated and monounsaturated phosphatidylcholine bilayers, where lipid chain ordering increases as a result of interactions with the rigid cholesterol molecule.

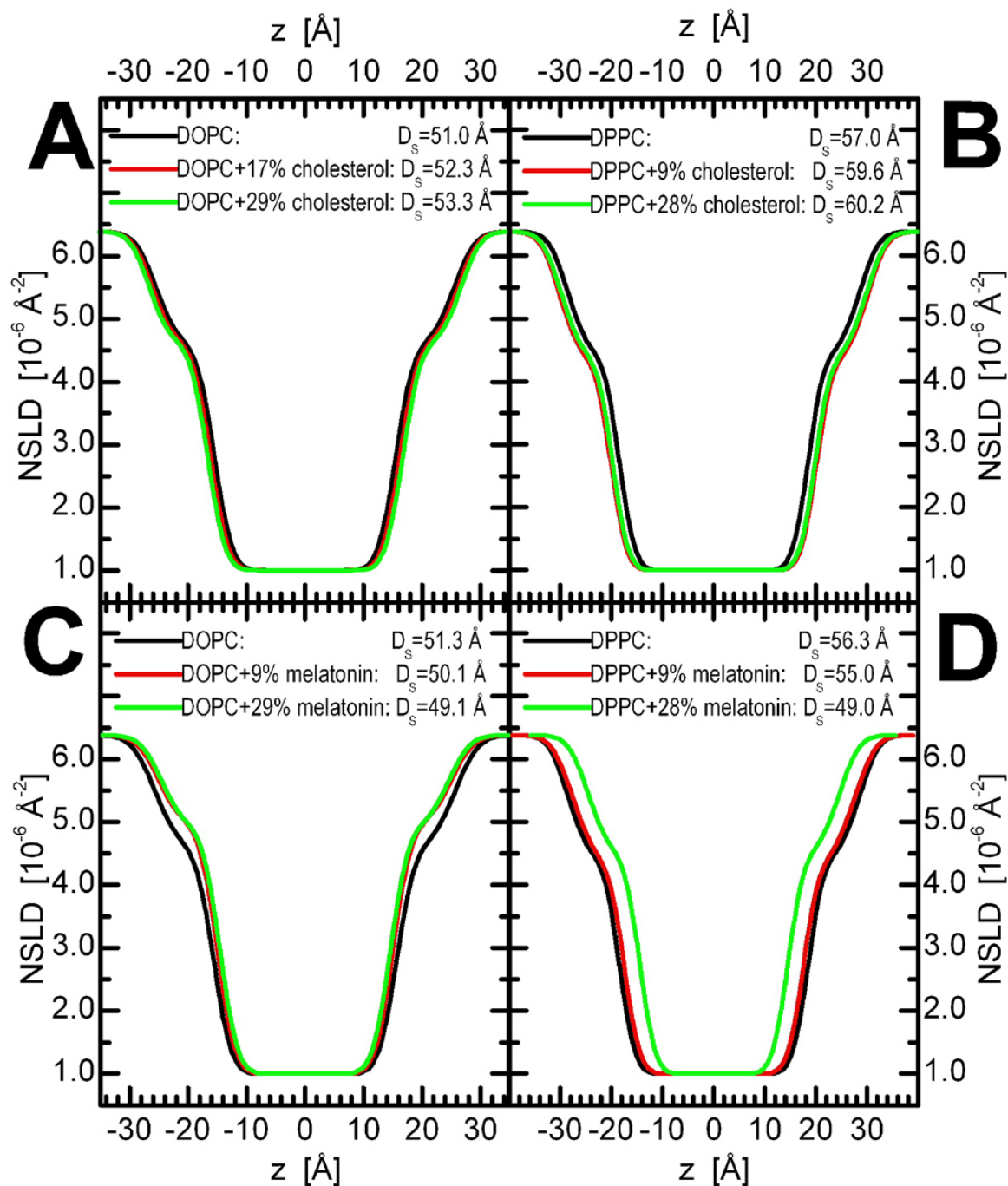


Figure 3.5: Neutron Scattering Length Density Profiles. The plots are results of fitting a smooth strip model to SANS data from DOPC (A) [adapted from (30)] and DPPC (B) [data from the N5 instrument] bilayers with increasing amounts of cholesterol. Panels C and D show the effect of melatonin on DOPC and DPPC bilayers, respectively [measured on the CG-3 Bio-SANS instrument]. ULVs were extruded in 100% D_2O .

Importantly, the SANS studies of DOPC and DPPC bilayers with increasing amounts of melatonin show that both membranes undergo progressive thinning as a function of increasing amounts of melatonin (Figure 3.5C and 3.5D respectively). In the case of pure DOPC, D_S has a value of 51.3 Å, which decreases to 50.1 Å and 49.1 Å upon the addition of 9% and 28% melatonin, respectively. A similar thinning trend is observed for the DPPC systems: the pure DPPC bilayer has a D_S of 56.3 Å, but the addition of 9% and 28% melatonin caused D_S to decrease, respectively to 55.0 Å and 49.0 Å. This result is in support of the notion that melatonin incorporates itself into the bilayer's head-group region, as shown in Figure 3.3B. According to this scheme, melatonin acts as a spacer between lipid head-groups, causing the free volume in the bilayer's hydrocarbon region to increase. This free volume is then readily taken up by the disordered hydrocarbon chains at the expense of their effective length (i.e., reduced bilayer thickness).

Figure 3.6 summarizes the different neutron data. Although it has been pointed out that the two bilayer thicknesses (i.e., D_{HH} and D_S) differ in their definition, their relative changes are directly comparable. Figure 3.6 shows that there is very good agreement between D_{HH} and D_S as a function of increasing concentration of cholesterol or melatonin – i.e., increased amounts of cholesterol cause the bilayer to thicken, while melatonin has the exact opposite effect on bilayer thickness.

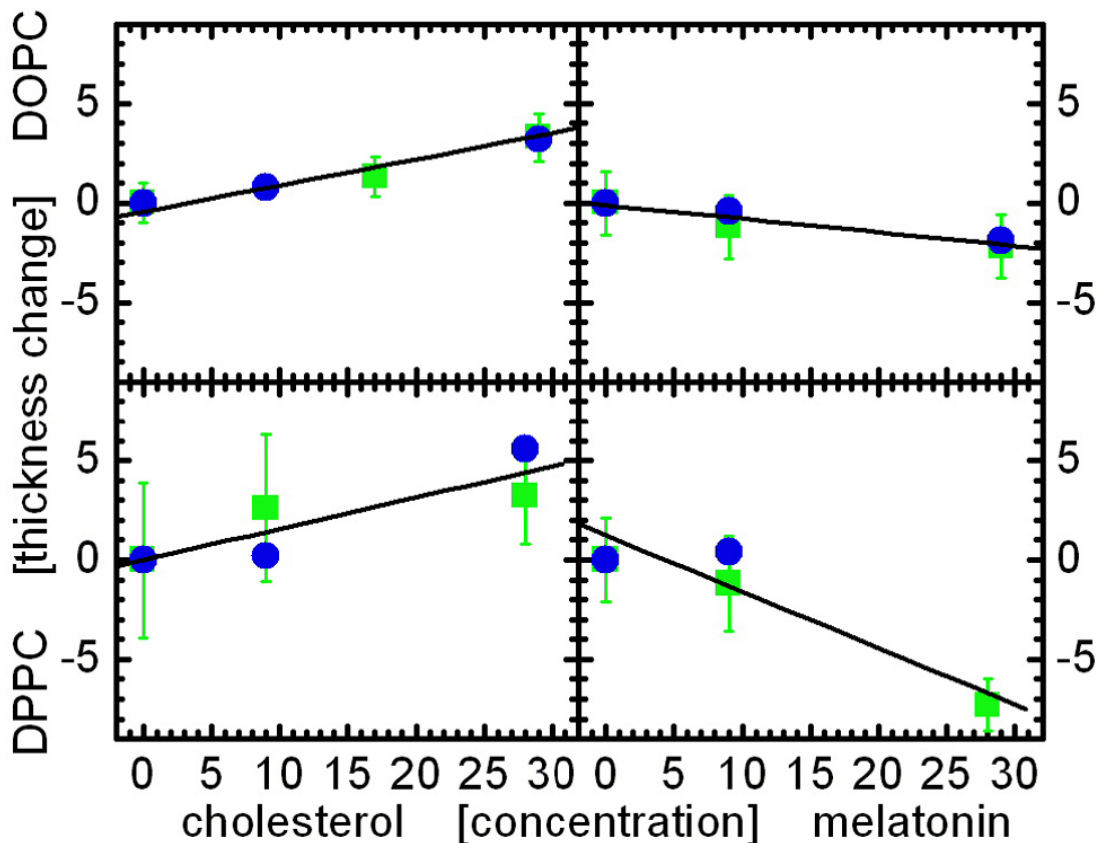


Figure 3.6: Thicknesses of DOPC (top) and DPPC (bottom) bilayers upon the addition of cholesterol (left) and melatonin (right). Blue circles represent changes to the D_{HH} thickness obtained from SAND, while green squares correspond to changes in the D_s thickness obtained from SANS. Black lines are fits to the data.

Lipid membrane thickness is a structural parameter that is needed to accurately determine other bilayer structural parameters, and is directly related to lipid-lipid, and lipid-protein interactions in biomembranes. The experimental results confirm the previously reported and well-known bilayer thickening effect induced by cholesterol (see Figure 3.6). This is a direct result of the hydrocarbon chains experiencing increased order due to their interactions with the rigid cholesterol molecules. Interestingly, the experimental results show, for the first time, that the addition of melatonin has the exact opposite effect, i.e., melatonin causes bilayer thinning (Figure 3.6). This is most likely due to melatonin introducing disorder within the membrane by increasing the area per lipid as it incorporates itself among the lipid head-groups. This notion is also supported by the encroachment of water molecules deeper

into the membrane (shown in Figure 3.5C and 3.5D).

To confirm these findings and to further elucidate structural details on effect of melatonin and cholesterol on model lipid bilayers, the results were compared to MD simulations conducted by collaborators, Dr. M. Hoopes and Dr. M. Karttunen. In their work, which is in agreement with the experimental SANS and SAND data, MD simulations show that cholesterol increases the order in both DOPC and DPPC bilayers (Drolle et al, 2013). In contrast to cholesterol, melatonin decreases the order in both bilayers, which can be seen in Figure 3.7, which is a reproduction of their work (Drolle et al, 2013).

Figure 3.7 illustrates the findings of Hoopes and Karttunen on the structure of DPPC and DOPC bilayers with and without melatonin at a temperature of 300K. At this temperature, a pure DPPC bilayer exists in the gel phase (T_m of DPPC is 314 K) and a pure DOPC bilayer exists in the fluid phase ($T_m=253$ K). The figure clearly demonstrates that the presence of melatonin induces local disorder in the lipid tails, i.e., it melts the gel phase of the pure DPPC system (Figure 3.7A vs Figure 3.7B). The pure DPPC system has a number of lipids in the liquid phase (Figure 3.7A). This is due to the fact that the time to complete the phase transition longer than simulation time. The melatonin-containing system is different (Figure 3.7B): all of the melatonin containing regions are in the liquid phase, i.e., melatonin increases fluidity of the system. The areas that do not contain melatonin remain in the gel phase. At 300K, DOPC already exists in the liquid state (Figure 3.7C), therefore effect of melatonin is readily apparent (Figure 3.7D) To determine whether or not melatonin has a further fluidizing effect on DOPC, Hoopes and Karttunen further investigated the occurrence of bilayer thinning and changes to area per lipid.

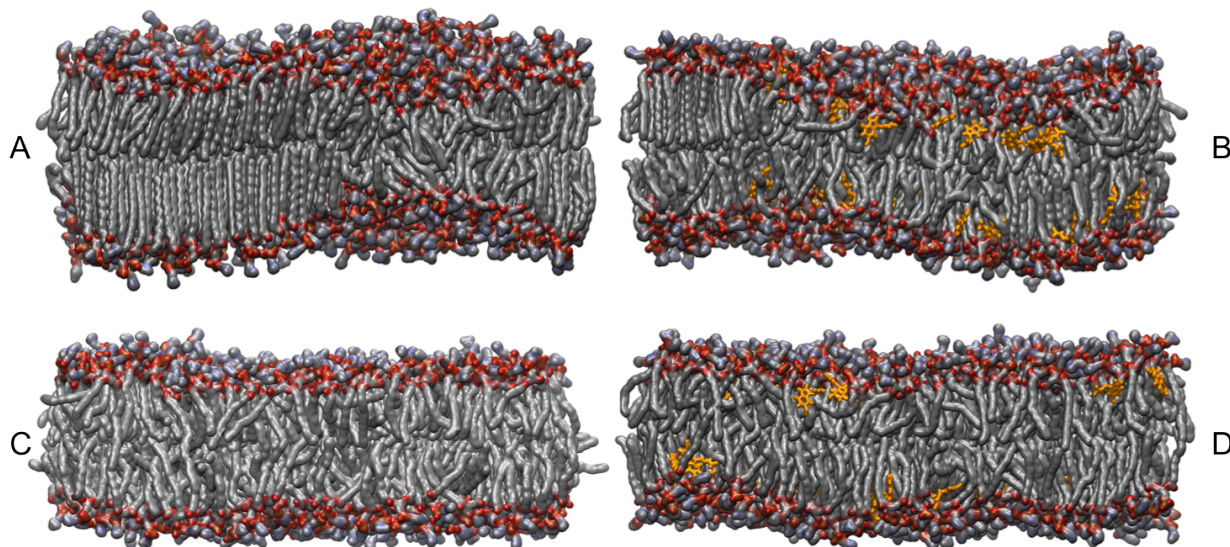


Figure 3.7: Molecular dynamics simulations of DPPC and DOPC bilayers with and without melatonin. A and C represent DPPC and DOPC membranes respectively, while B shows DPPC with melatonin and D shows DOPC with melatonin.

DPPC (top) and DOPC (bottom) bilayers. Left: pure systems: A - DPPC, C - DOPC. Right: with melatonin: B – DPPC-mel, D – DOPC-mel. Melatonin molecules are shown in orange. Snapshots were after 400 ns of MD simulation at $T=300$ K. The total simulation time for each system was 500 ns. Note the gel phase on the left hand side in the pure DPPC system (for DPPC, $T_m = 314$ K). Melatonin appears to enhance and maintain local fluidity. This is clearly visible in the DPPC membrane with melatonin (top right). Since the DOPC system is above its main phase transition ($T_m = 253$ K), the effects of melatonin are more subtle. This figure is a reproduction of work done by Dr. M. Karttunen and Dr. M. Hoopes (Drolle et al, 2013) and is included for support of the NS data.

MD data in Figure 3.8 show that melatonin's (orange line) preferred location is just inside the crossover region describing the lipid headgroups and the fatty acid chains. Figure 3.8 shows that for DPPC (Figure 3.8A) bilayers the peak density is decreased when melatonin is present. For DOPC (Figure 3.8B), the peak density of the lipid tails is increased when melatonin is added (solid lines: no melatonin, dashed lines: with melatonin). In the simulations for DPPC, the thickness of the membrane increased with the addition of melatonin from $D_{HH} = 39.8 \pm 0.1$ Å to 40.9 ± 0.5 Å. For DOPC, the thickness went from

$D_{HH} = 37.0 \pm 0.1 \text{ \AA}$ to $37.6 \pm 0.5 \text{ \AA}$ with the addition of melatonin. The area of the pure DOPC bilayer was $67.4 \pm 0.4 \text{ \AA}^2$. Addition of melatonin lead to an increase to $69.4 \pm 0.5 \text{ \AA}^2$. The trends observed upon the addition of melatonin are in excellent agreement with the experimental results. In addition, the trends observed in neutron scattering upon addition of cholesterol are in perfect agreement with previous simulations (Alwarawrah, Dai, & Huang, 2010; Martinez-Seara, Róg, Karttunen, Vattulainen, & Reigada, 2010). Thus, it can be concluded that the simulations provide an accurate picture of melatonin's location and effect on both DPPC and DOPC bilayers: melatonin interacts with the headgroups and does not penetrate deeply into the hydrophobic core.

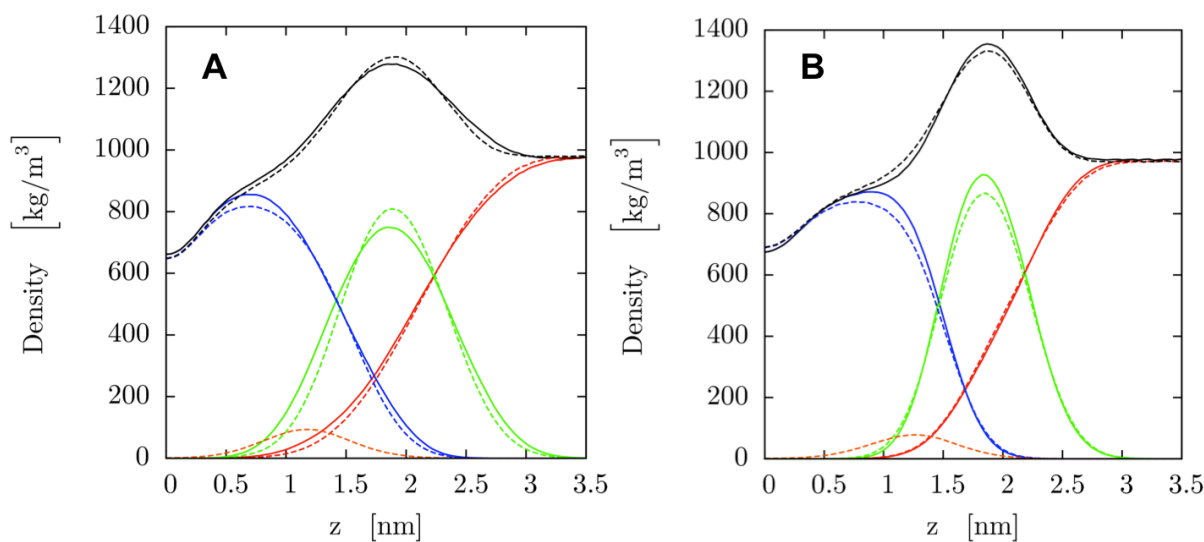


Figure 3.8: Density profiles for one bilayer leaflet calculated from MD simulations for DPPC (a) and DOPC (b) membranes at T=300 K. Zero denotes the membrane center. Pure membranes are represented by solid lines and ones with melatonin by dashed lines: Black: The total density, red: solvent, green: head groups, and blue: lipid tails, and orange: melatonin. This figure is a reproduction of work done by Dr. M. Karttunen and Dr. M. Hoopes (Drolle et al, 2013) and is included for support of the NS data.

Both experimental and theoretical data are in good agreement and show that the effect of melatonin on bilayer thickness is opposite to that of cholesterol. Both experimental data and comparative MD simulations performed by collaborators show that cholesterol has the ordering effect and increases the thickness of bilayer. In contrast to cholesterol, melatonin

decreases the order and decreases the thickness in both bilayers, thus inducing the increased fluidity in the model membrane. The observation of these structural changes may prove to be important for other studies on amyloid toxicity, as they may lend some insight into understanding the molecular mechanism of melatonin protection in Alzheimer's disease. For example, melatonin levels in the body have been shown to decrease with age (Sack et al, 1986). As Alzheimer's disease is more prevalent later in life, the effects of melatonin and cholesterol on lipid membrane become very important as their amounts in membranes also change with age. Both cholesterol and melatonin have implications in amyloid toxicity and Alzheimer's progression in animal and cell studies (Di Paolo & Kim 2011; Kondratova & Kondratov 2012), although the molecular mechanism of their action is not well understood. Considering the role of cell membrane in amyloid toxicity, it is important also to note that amyloid deposits are known to affect the synapse (Lorenzo & Yankner 1996; Walsh & Selkoe 2004), where fluidity of lipid membrane is very important for the propagation of action potential signal from one neuron cell to another, which occurs through the fusion of synaptic vesicles. These results can, for the first time, provide an understanding for the possible structural changes taking place within biological membranes. The effects of melatonin on membrane structure may have consequences similar to those of cholesterol reducing drugs. Studies have also shown that membrane cholesterol levels may regulate the toxic effects of amyloid beta, and that cholesterol reducing agents, such as mevastatin, methyl- β -cyclodextrin or filipin, are able to reverse or diminish such toxic effects (Abramov et al, 2011). Melatonin has also been shown to significantly decrease cholesterol absorption and total cholesterol levels (Hussain 2007), in addition to its ability in reducing amyloid toxicity. Amyloid toxicity is directly related to the damage that amyloid produces in cell membranes. It has also been shown previously (Drolle et al, 2012) that amyloid binding, the first step in amyloid toxicity (Simakova & Arispe 2007), is affected by cholesterol, i.e. the presence of cholesterol increases damage to the membrane, and in good agreement with data by Sheikh et al (Sheikh et al, 2012). Choucair et al. also reported that the phase of the lipid membrane is important for amyloid binding and demonstrated that amyloid peptide preferentially binds to thicker and less fluid membranes (Choucair et al, 2007).

In summary, this work has shown that melatonin decreases bilayer thickness and increases the head group area, resulting in more fluid and disordered bilayers, in contrast to the well-

known condensation effect of cholesterol. Based on these results, it is hypothesized that melatonin may counteract cholesterol's membrane ordering effect, and thus may affect amyloid binding, which leads to the membrane damage, associated with amyloid toxicity. The present results help in understanding the mechanism by which cholesterol and melatonin may affect the properties of biological membranes, and they could be used to better understand the mechanism of interaction of membranes with amyloid peptides in relation to amyloid toxicity and AD.

Chapter 4.0 - Amyloid- β Aggregation on Model Lipid Membranes: An Atomic Force Microscopy Study

Note: this chapter was reproduced with modifications with permission from {Hane F, Drolle E, Gaikwad R, Faught E, Leonenko Z. 2011. Amyloid- β Aggregation on Model Lipid Membranes: An Atomic Force Microscopy Study. *J. Alzheimer's Dis.*, 26: 485 – 494.} © {2011} IOS Press.

Aim of Published Work

In this study, we compared the aggregation of amyloid-beta (1-42) on four different single lipid systems, which differed from one another in phase at room temperature and head group charge. For each system, we looked at amyloid incubations at three time points to see how the progression of fibrilization is affected by these parameters.

Experimental Design and Collaborations

Under the supervision of Dr. Z. Leonenko, Francis Hane and I (co-first-authors for this work) were responsible for experimental design of this project. Each system was studied at least in triplicate, with both co-authors each completing at least one full set of experiments. We performed AFM experiments on two different AFMs and cross-sectional statistical analysis on lipid membranes and amyloid incubations on lipid membranes to determine the effect of lipid charge and phase on fibril formation. Dr. Gaikwad (PDF at UW at the time) assisted with statistical analysis and lent his AFM expertise and E. Faught assisted with sample preparation.

Please note that this chapter includes some overlap with material presented in the MSc thesis of F. Hane. His thesis includes preliminary work of this study that was a joint collaboration between the two of us. After the submission and defense of his thesis, work on this investigation continued, with full sets of experiments redone and an additional system (DOPC) introduced as well as the use of an additional AFM (whereas in the preliminary data, we only conducted experiments on one AFM). Despite the possibility of some overlap in data explanation, there is no overlap in the figures included in this chapter or in the article published with what is included in F. Hane's MSc thesis.

Summary and Conclusions

Using AFM, we observed a similar increasing accumulation of amyloid aggregates on the surface of neutral DPPC gel phase membrane as on the surface of fluid phase negatively charged DOPG membrane. Interactions of aggregates with positively charged fluid DOTAP membrane and neutral fluid phase DOPC membrane did not show a similar accumulation pattern to DPPC and DOPG; instead, we observed amyloid deposits with reduced height on

the DOTAP and DOPC membranes, which suggests a fusing of $A\beta_{1-42}$ into the lipid membrane surface. This work shows that phase and charge have an effect on the interactions of amyloid species with the membrane.

4.1 Overview

Amyloid fibril formation is generally associated with many neurodegenerative disorders, including Alzheimer's disease (AD). Although fibril plaque formation is associated with biological membranes *in vivo*, the role of the cell surfaces in amyloid fibril formation and the molecular mechanism of amyloid toxicity are not well understood. Understanding the details of amyloid interaction with lipid membrane may shed light on the mechanism of amyloid toxicity. Using atomic force microscopy (AFM), this study investigated aggregation of amyloid- β_{1-42} ($A\beta_{1-42}$) on model phospholipid membranes as a function of time and membrane composition. Neutral, 1,2-dipalmitoyl-sn-glycero-3-phosphocholine (DPPC) and 1,2-dioleoyl-sn-glycero-3-phosphocholine (DOPC), anionic - 1,2-dioleoyl-sn-glycero-3-phospho-(1 -rac-glycerol) (sodium salt) (DOPG), and cationic - 1,2-dioleoyl-3-trimethylammonium-propane (DOTAP), were used to study the effect of lipid type on amyloid binding. This study shows that both the charge on the lipid head group and lipid phase affect the interaction of amyloid oligomers with the membrane surface changing the rate of adsorption and causing changes in membrane structure and structure of amyloid deposits. This study shows that amyloid aggregates progressively accumulate in a similar manner on the surface of neutral DPPC gel phase membrane and on the surface of fluid phase negatively charged DOPG membrane. In contrast to DPPC and DOPG, positively charged fluid DOTAP membrane and neutral fluid phase DOPC membrane contain amyloid deposits with reduced height, which suggests fusing of $A\beta_{1-42}$ into the lipid membrane surface.

4.2 Introduction

AD is a progressive neurological disease that is characterized by dementia, memory loss, and mental degradation believed to be associated with neuronal amyloid plaques. The primary constituent of these amyloid plaques is the amyloid- β ($A\beta$) peptide, which is cleaved from the amyloid- β protein precursor ($A\beta$ PP) (Kang et al, 1987). Normally, $A\beta$ is in an α -helical

form (Kalberg et al, 2001) but can misfold into β sheets and aggregate leading to the formation of amyloid oligomers or fibrils. No clear reason as to the cause of this misfolding has been identified (Carrell 1998). The cascading process leading from an α -helical native protein to mature amyloid fibrils runs through several possible oligomeric intermediate structures. Recent research indicates that these intermediate oligomers have higher neurotoxicity than the more inert mature amyloid fibrils (Lambert et al, 1998; Kaye et al, 2003; Dalgren et al, 2002; Roher et al, 1996; Campioni et al, 2010).

Although fibril plaque formation is associated with biological membranes *in vivo*, the majority of research has been done on amyloid fibril formation in solution, where the role of membrane surfaces has not been considered (Dobson 2001, Johansson 2003, Chiti & Dobson 2006, Blackley et al, 1999). Therefore, despite recent research efforts, the exact mechanism of A β interactions with lipid membranes is still not well understood (Walsh et al, 2002). Several studies reported in the last few years demonstrated that A β peptide when reconstituted into a model lipid membrane may form ion pores or channels in membrane bilayers (Lin et al, 2001; Quist et al, 2005; Arispe 2004) and increase the membrane fluidity (Kremer et al, 2000) as well as induce the thinning and reduce the conductance of the cell membrane (Sokolov et al, 2006). In addition, factors such as lipid rafts, cholesterol, pH, and salt have been shown to affect amyloid fibril formation (Cordy et al, 2006; Sharp et al, 2002; Yip et al, 2001; Choucair et al, 2007; Neugroschl & Sano 2010; Cirtain et al, 2003; Cruz et al, 2005). Previously, several groups focused their efforts on elucidating the role of interactions of various A β peptides with model lipid membrane and monolayers. Bokvist and colleagues (2004) suggested two methods in which A β interacts with lipid membranes: binding of monomeric peptide to the lipid membrane and insertion of peptide into the lipid membrane, and hypothesized that the interplay between electrostatic and hydrophobic interaction drives these processes. Their results suggested pathological interactions of A β with neuronal membranes might not only depend on the oligomerization state of the peptide, but also on the type and nature of the supramolecular A β -membrane assemblies (Bokvist et al, 2004). Previous research on lipid monolayers has also shown the importance of electrostatic interactions between negatively charged lipids and A β peptide at the air-water interface (Maltseva et al, 2005; Ege et al, 2005; Ionov et al, 2010). Ege et al. (2005) have shown that aggregation of A β_{1-40} can take place at considerably lower concentrations when

exposed to phospholipid monolayers at the air-water interface, as compared to bulk peptide in solution. Earlier research has shown that the interaction of A β with lipid membrane is the initial step of amyloid fibril formation in AD brain (Yanagisawa et al, 1995) and in vitro (Terzi et al, 1995; Choo-Smith & Surewicz 1997).

The phase of the lipid membrane may also play an important role when interactions of A β with lipid membrane are considered. A key feature of a membrane, which is defined by the lipid phase, is its relative fluidity (i.e., mobility) of the lipid molecules within the membrane (Feigenson 2006). The three major lipid phases are classified as following: the Lo (liquid ordered, induced by cholesterol); the La (liquid-disordered); the gel phase, (L β) (Feigenson 2006; Lingwood & Simons 2010). The fluidity of the lipid membrane defines the membrane melting transitions (Koynova & Caffrey 2002) and has an important impact on membrane. The phase of the lipid membrane may also be a defining feature for the interaction of amyloid forming peptides. It has been reported recently that fluorescently labeled A β ₁₋₄₂ binds preferentially to the gel phase domains in the mixed DPPC/DOPC bilayer (Choucair et al, 2007), although the fibril formation was inhibited by the fluorescent label attached to A β ₁₋₄₂ peptide.

In this work, AFM is used to elucidate the effect of lipid composition (headgroup charge and phase) on interaction of A β ₁₋₄₂ with supported lipid bilayers.

4.3 Materials and Methods

4.3.1 Lipid bilayer preparation

1, 2-dipalmitoyl- sn-glycero-3-phosphocholine (DPPC), 1, 2-dioleoyl- sn-glycero-3-phospho-(1'- *rac*-glycerol) (sodium salt) (DOPG), 1,2-dioleoyl- sn-glycero-3-phosphocholine (DOPC), and 1,2-dioleoyl-3-trimethylammonium-propane (DOTAP) lipids were purchased from Avanti Polar Lipids (Alabaster, AL) in powder form. Lipid vesicle solution was prepared by adding 0.5 mg of dry lipid in 1mL of ultrapure water. The lipid solution was stirred for 15 min, followed by 10 min of sonication. This stirring/sonication procedure was repeated until the lipid solution was clear which indicated vesicle formation. In order to produce planar supported bilayer 100 μ L of vesicle solution was placed on freshly

cleaved mica. Vesicles were allowed to fuse for 10–15 min to achieve full bilayer coverage. The sample was washed with ultrapure water to remove unbound vesicles, leaving supported lipid bilayer on mica. Samples of each lipid bilayer (DPPC, DOPC, DOPG and DOTAP) were imaged with the atomic force microscope in liquid to ensure uniformity of the bilayer. One sample of each lipid was rinsed hard with a stream of ultrapure water, causing “nanoholes” in the lipid bilayer. When imaged with the AFM, these samples with holes showed a bilayer height of approximately 5 nm indicating formation of a lipid bilayer.

4.3.2 Amyloid- β Incubation

A β_{1-42} was purchased from rPeptide Inc. (Bogart, GA). The peptide was pretreated to ensure the monomeric form of the peptide was being utilized (Fezoui et al, 2000). For the incubations, 1mL of HEPES buffer (50 mM, pH 7.8) was added to a 0.5 mg vial of A β_{1-42} . The solution was sonicated for 1 minute as directed by rPeptide instructions. 100 μ L of A β_{1-42} solution was placed on the lipid bilayers and allowed to incubate at room temperature for the defined time periods of 1 h, 6 h, and 24 h. At the conclusion of incubation time, excess peptide was gently rinsed 3 times with 50 μ L of ultrapure water. Nanopure water was added in sufficient quantity to cover the mica slide for imaging with the atomic force microscope.

4.3.3 Atomic force microscopy imaging

AFM is a nanoscale imaging technique, which employs a sharp probe scanning over a sample surface and allows for imaging the topographical features at the nanoscale and single molecule level in liquid at near physiological conditions. Samples with supported bilayers were placed in the AFM liquid cells as provided by JPK Instruments AG and Agilent Technologies. The liquid cells were filled with nanopure water, covering the entire sample. All samples were imaged in liquid using a tapping mode (JPK), or MacMode (Agilent) at lower set point to ensure gentle imaging which did not destroy the membrane samples. Veeco DNP-S cantilevers (spring constant 0.5–0.6 N/m) or Agilent Type II Mac Levers (spring constant 2.8 N/m) were used for imaging. Images were scanned at a line rate of 0.5 Hz. Instrument settings (such as set point) were adjusted throughout the scanning processes in order to optimize image quality.

4.3.4 Image analysis

Images were processed with Gwyddion image processing software (non-proprietary software, freely available online) or JPK image processing software (proprietary software). Images were leveled by subtracting a polynomial fit from the images, and some images were adjusted using the MinMax z-range and a low pass filter to improve image quality.

4.3.5 Statistical analysis

Statistical analysis of oligomer volume has been done using Image Metrology's SPIP software version 5.1.5. The larger fibrils and were neglected. The images were first corrected globally with an average polynomial fit of order 3 and then to remove observable steps between subsequent scan lines, the images were leveled using the LMS fit method of order 3. The images were then used for calculating the net volume of material using the height distribution histogram, which is the integral of the area under the histogram and normalized to the volume per surface area. Statistical analysis of oligomer height distribution was done using cross-section analysis within JPK images processing software. Several images with at least 100 measurements of oligomers and small protofibrils were used for each sample to determine the average height and height distribution.

4.4 Results

To mimic the interaction of A β with cell membrane, the interaction of A β_{1-42} peptide with a supported lipid model membrane were studied. When peptides are placed in close proximity to the lipid membrane several processes may occur: 1) the peptides may interact with each other in solution and form fibrils; 2) the peptide monomers and oligomers may interact with lipid head-groups and assemble onto the lipid surface, resulting in oligomers and small protofibrils bound to the lipid membrane. These processes are shown schematically on Figure. 4.1.

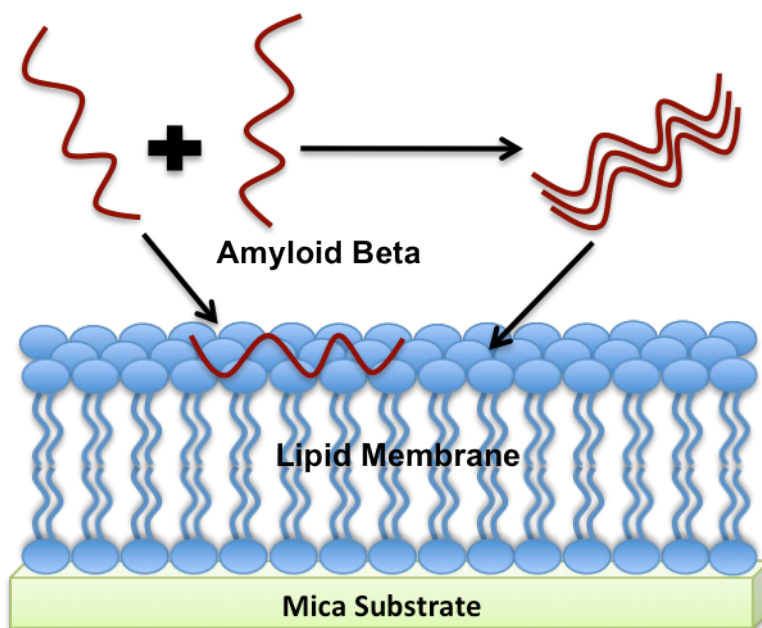


Figure 4.1: Schematic diagram showing a supported bilayer on mica interacting with A β ₁₋₄₂ in solution. Two processes may occur: 1) peptides interact with each other and oligomerize in solution; 2) Peptides interact with lipid surfaces (head groups) and assemble onto the lipid surface.

The first process—aggregation of amyloid peptides in solution—has been studied extensively (Dobson 2001, Johansson 2003, Chiti & Dobson 2006, Blackley et al, 1999). Control experiments were also performed for comparison. Figure 4.2A and 4.2B shows AFM images of the aggregation of A β ₁₋₄₂ when peptide was incubated in solution for periods of 1 and 24 h respectively. After incubation, a small droplet was placed on mica substrate for 5 min, gently rinsed with water, dried with nitrogen and imaged in air. At a short time of incubation (1h), the formation of oligomers and small protofibrils are observed (which are defined as a few oligomers linked linearly together to form short fibril (Dobson 2001, Blackley et al, 1999)), Figure 4.2A. As incubation time increases, (24 h) formation of longer mature amyloid fibrils are observed, Figure 4.2B.

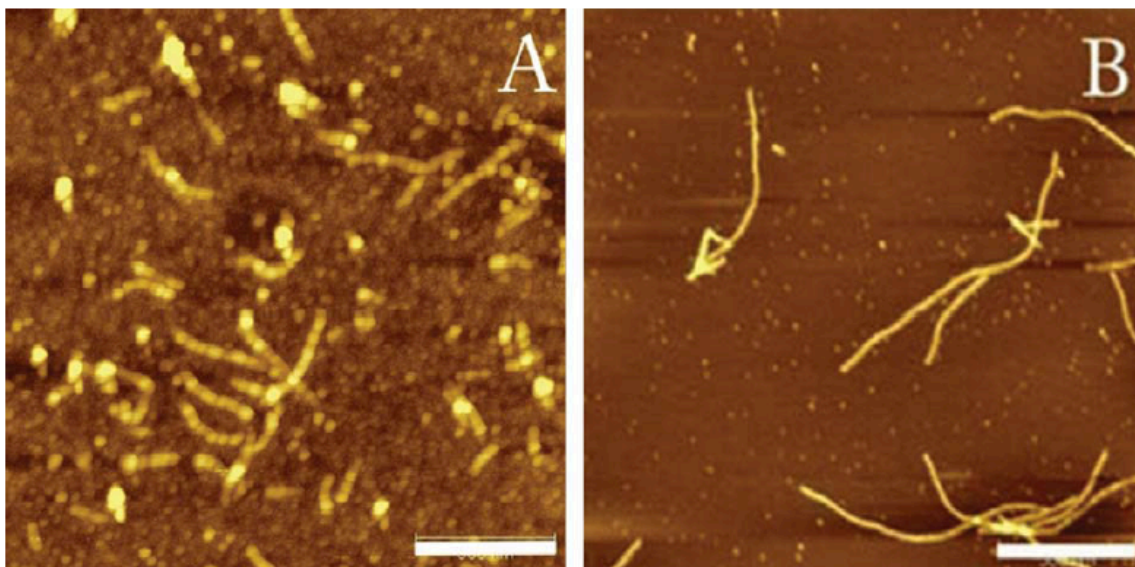


Figure 4.2: A β 1-42, 500 μ g/mL in buffer was allowed to incubate in solution. After defined time, 100 μ L of solution was deposited on mica for 5 min. After 5 min the mica was rinsed gently to remove excess of solution and imaged with AFM in liquid cell. Scale bar (white rectangle in bottom right of images) indicates 500 nm. A) Amyloid fibrils formed in solution after 1 h of incubation; B) - Amyloid fibrils formed in solution after 24 h of incubation.

Next, supported lipid bilayers were formed, composed of one of the four types of lipids: with neutral (or zwitterionic) head group – DPPC (gel phase) and DOPC (fluid phase), with anionic head group DOPG (fluid phase), and cationic head group DOTAP (fluid phase). Supported lipid bilayers were formed on mica by vesicle fusion, gently rinsed with water to remove excess vesicles solution, and imaged by AFM in liquid. The surfaces of the bilayers were very flat, which is characteristic of lipid bilayers composed of one lipid type. Cross section analysis shows all these surfaces within 400 pm of height differential. A DPPC bilayer with complete coverage is shown on Figure 4.3B. To confirm that a bilayer formed on the surface the samples were rinsed forcefully with a stream of water in order to produce holes in the supported bilayer. Figure 4.3A shows DPPC bilayer after such rinsing. The dark areas are the mica surface, where the lipid patches were removed by rinsing. The thickness of the bilayer was measured from cross-sections, and was about 5 nm, as expected for the DPPC bilayer measured by AFM.

After a smooth supported bilayer with complete coverage was formed on mica, 100 μ L of $A\beta_{1-42}$ solution was deposited, and incubated peptide solution in a liquid cell with supported bilayer for 10 minutes, and 1, 6, and 24 h. After each time the cell was rinsed gently with water and bilayer with $A\beta_{1-42}$ deposits was imaged immediately in liquid with AFM. Figure 4.3C shows AFM image of $A\beta_{1-42}$ accumulated on a DPPC bilayer after 1 h of incubation. Small round oligomers and short protofibrils were observed, no long mature fibrils were observed at 1 h of incubation for the DPPC bilayer, Figure 4.3C. Similar small oligomers and protofibrils growing with time were observed on the surfaces of DOPC, DOTAP and DOPG bilayers (images are not shown). The oligomers have a height 1–3 nm at 1 h incubation, Figure 4.3C.

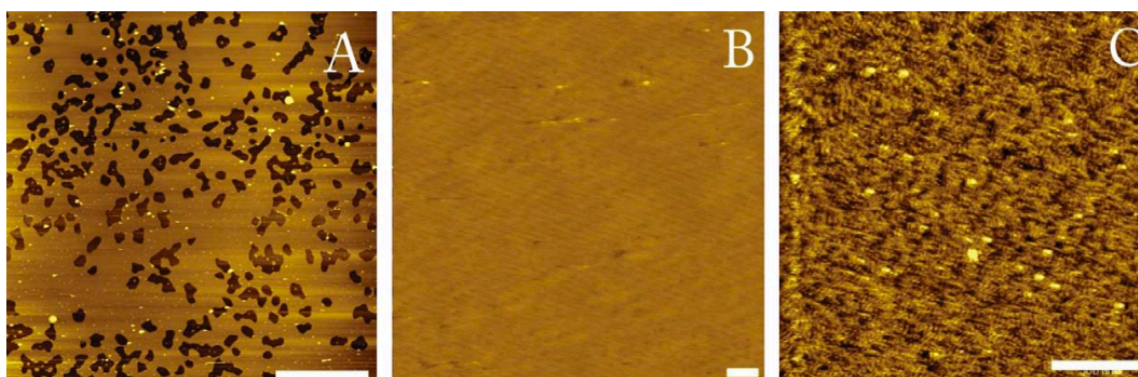


Figure 4.3: Comparison of AFM topography images of DPPC bilayer under different conditions. This image shows a DPPC bilayer: A) with holes, after hard rinsing; B) DPPC bilayer with complete surface coverage, after gentle rinsing; C) $A\beta$ deposits on DPPC bilayer with complete surface coverage after 1 h of incubation. Scale bar (white rectangle in bottom right of images) indicates 500 nm.

Figure 4.4 shows formation of $A\beta_{1-42}$ deposits on supported bilayers after 24 h of incubation imaged by AFM. A DPPC bilayer with amyloid deposits is shown in Figure 4.4A. For a DPPC bilayer at 24 h of incubation, an accumulation of small oligomers and short protofibrils was observed - similar to the observations at 1 h of incubation, Figure 4.3C. In addition, longer twisted fibrils are also visible at 24 h of incubation. The number of oligomers and short fibrils formed on DPPC bilayer surface increases steadily with incubation time, Figure 4.5. To account for this, the total volume of amyloid deposits

accumulated on lipid surfaces was calculated (Figure 4.5). Larger mature fibrils, presumably formed in solution at 24 h, were excluded from analysis. DPPC bilayer shows accumulation of amyloid deposits – the amyloid deposits volume increases from 1.47 ± 0.08 (10×10^7 nm³) at 1 h, to 4.07 ± 0.21 at 6 h and slowly increases to 4.55 ± 0.82 at 24 h as seen in Figure 4.5.

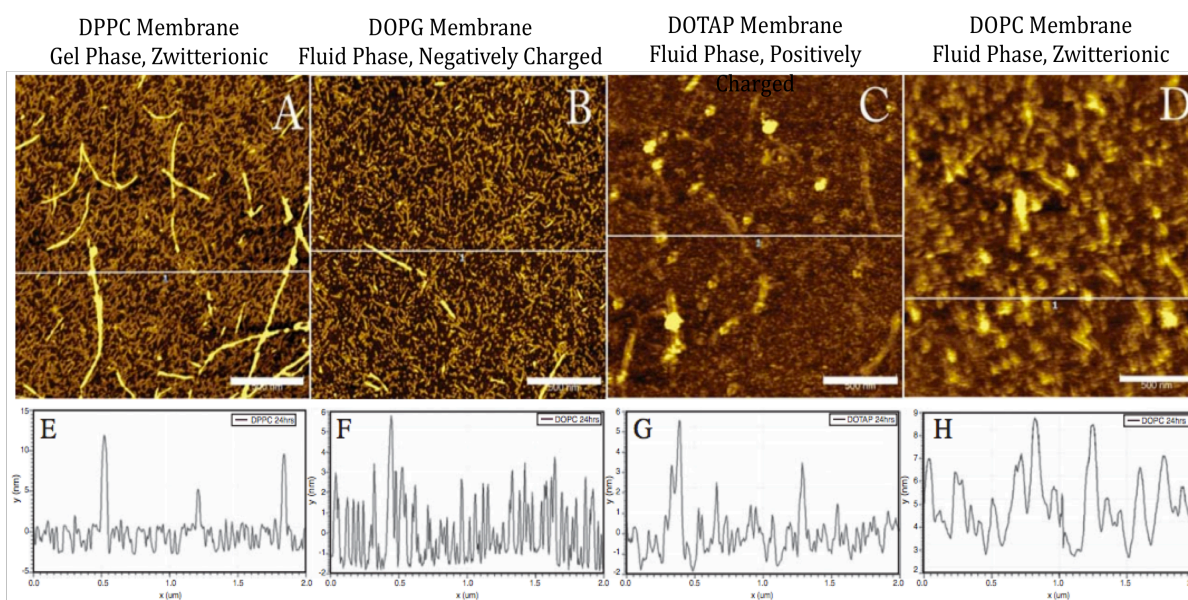


Figure 4.4: AFM topography images of Aβ aggregates formed on DPPC (A), DOPG (B), DOTAP (C), and DOPC (D) bilayers after 24 h of incubation. Cross-sections presented underneath the images show the height of protein aggregates measured above the lipid surface, DPPC- (E), DOPG- (F), DOTAP - (G), and DOPC (H), with the location of where the cross section was on the corresponding image indicated by the horizontal white line across the topography image. After incubation, bilayers with protein deposits were rinsed gently with water and imaged in liquid cell. Scale bar (white rectangle in bottom right of images) indicates 500 nm.

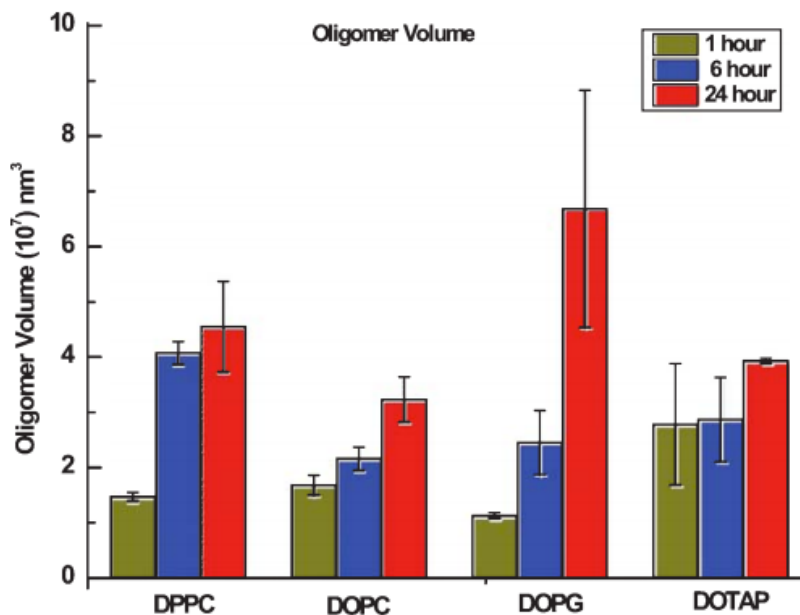


Figure 4.5: Statistical analysis of A β oligomer volume adsorbed onto supported lipid bilayer DPPC, DOPC, DOPG, and DOTAP respectively at 1 h, 6 h, and 24 h of incubation time. The oligomer volume is calculated on $5 \times 5 \mu\text{m}^2$ scan areas of the bilayers using SPIP software. Error bars are indicative of standard deviation.

Quantitative analysis of oligomer height distribution was done using cross-section analysis of AFM images, Figure 4.5D–F (where $n=100$ for each system). The results of statistical analysis of oligomer and protofibril height distribution deposited on all lipid bilayers are shown on Figure 4.6. For a DPPC supported bilayer the average height of A β deposits was changing from 1.15 ± 0.28 nm at 1 h to 4.45 ± 2.80 nm at 24 h of incubation. The length of oligomers and short protofibrils varied from 40 nm to 100 nm. In addition, longer mature fibrils start to form at 24 h of incubation on DPPC bilayer. These larger fibrils have a length up to 2–3 μm and are similar to the fibrils formed in solution at 24 h of incubation, Figure 4.2B.

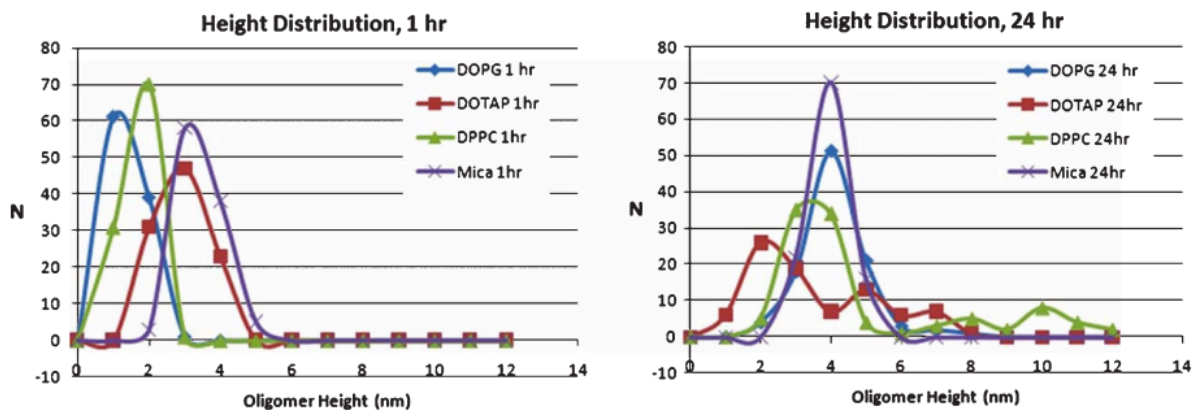


Figure 4.6: Height distribution of A β oligomers formed on supported lipid bilayers, DPPC, DOPC, DOPG, and DOTAP after 1 h and 24 h of incubation with A β peptide solution.

Figure 4.4B shows AFM topography image of A β_{1-42} deposits on a DOPG bilayer after 24 h of incubation. Similar to what is seen for DPPC (Figure 4.4A), it was observed that only small mostly round oligomers with a height of 0.97 ± 0.39 nm and short protofibrils (20–300 nm long) formed on the DOPG bilayer surface at 1 h of incubation (AFM images for this not shown here). After 24 h of incubation, both oligomers and short protofibrils with a length of 20–300 nm are still present and are well resolved by AFM. The measured height of oligomers and protofibrils increases to 3.60 ± 0.99 at 24 h of incubation. DOPG bilayer shows progressive accumulation of amyloid deposits; the volume increasing from 1.13 ± 0.05 (10×10^7 nm³) at 1 h, 2.45 ± 0.58 at 6 h (not pictured) and to 6.68 ± 2.15 at 24 h as seen in Figure 4.5.

In addition, few mature amyloid fibrils are observed on the very top of the bilayer, at 24 h of incubation, which range in length from 500 nm to 1 μ m. Figure 4.4C shows AFM topography image of A β_{1-42} deposits formed on DOTAP bilayers after 24 h of incubation. Small round oligomers are observed, as well as small protofibrils formed on the bilayer surface. The average height of the oligomers formed on DOTAP bilayer after 1 h of incubation is 2.40 ± 0.62 nm and does not change significantly with time (2.99 ± 1.78 nm after 24 h of incubation). Amyloid protofibrils increase in length as incubation time increases from 45–280 nm at 1 h, to 100–580 nm at 24 h of incubation. The volume of amyloid deposits on DOTAP bilayer is the largest at 1 h, 2.78 ± 1.10 (10×10^7 nm³)

compared to other bilayers, remains almost the same at 6 h, 2.87 ± 0.76 and slowly increases to 3.93 ± 0.05 at 24 h as seen in Figure 4.5. Longer fibrils with the length of up to 3 μm are also observed. Both oligomers and fibrils are not well resolved and seem to be buried into the bilayer as it is seen from cross-sections and height distributions. We are confident that blurriness of the images is not a result of the poor quality of AFM probe or AFM settings, as high-resolution imaging of nanoparticles and pure bilayers was possible immediately after imaging DOTAP- $\text{A}\beta_{1-42}$ assemblies.

Figure 4.4D shows AFM topography image $\text{A}\beta_{1-42}$ deposits on a DOPC bilayer after 24 h of incubation. Similar to what is seen for DOTAP (Figure 4.4C), small round oligomers as well as small protofibrils were found to have formed on the bilayer surface. The average height of the oligomers formed on DOPC bilayer after 1 h of incubation is measured as 1.81 ± 0.58 nm and changes with time to 3.7 ± 1.45 nm after 24 h of incubation. The volume of amyloid deposits on DOPC membrane progressively increases from 1.68 ± 0.18 (10×10^7 nm³) at 1 h, 2.16 ± 0.21 at 6 h and to 3.23 ± 0.41 at 24 h as seen in Figure 4.5. The average height of the fibrils, measured above the lipid surface is smaller when they are formed on fluid phase DOTAP bilayer (2.99 nm), DOPC bilayer (3.70 nm) and DOPG bilayer (3.60 nm), compared to fibrils formed on mica (4.42 nm) and DPPC bilayer (4.45 nm). Unlike for DPPC and DOPG, the height distribution of oligomers formed on DOPC and DOTAP becomes very wide at 24 h of incubation (Figure 4.6).

4.5 Discussion

The difference in fibril formation between $\text{A}\beta_{1-42}$ -incubated in solution and $\text{A}\beta_{1-42}$ -incubated on lipid bilayers is striking: fibrils formed in solution grow in length with time up to several microns long, Figure 4.2, are thin and show twisted morphology, characteristic for fibrils formed in solution (Blackley et al, 1999). Figure 4.2A shows $\text{A}\beta_{1-42}$, which have been incubated in solution for 1 h and deposited on mica. Compared to fibril formation in solution, amyloid aggregation is different on lipid surfaces. When $\text{A}\beta_{1-42}$ is incubated on lipid bilayers, small oligomers and short protofibrils are observed that are present at all times, while long fibrils, characteristic for incubation in solution, are rarely observed. This suggests higher propensity of oligomers to lipid surfaces compared to mature fibrils, which

correlates well with the earlier reported higher neurotoxicity of oligomers compared to fibrils (Lambert et al, 1998; Kaye et al, 2003; Dalgren et al, 2002; Roher et al, 1996; Campioni et al, 2010).

As shown in Figures 4.4A, on DPPC bilayer, progressive accumulation of oligomers and short protofibrils on the lipid surface are observed, indicated by an increase in the total volume of amyloid deposits (Figure 4.5). The oligomers are well resolved and the height of the deposits measured above the lipid surface increases with the time of incubation, which also indicates accumulation of oligomers and short protofibrils on the surface of DPPC bilayer, Figures 4.4A and 4.6. After 24 h of incubation of $A\beta_{1-42}$ on the DPPC bilayer, the surface is almost completely and uniformly covered by densely packed oligomers and short protofibrils. Some longer fibrils that we observed at 24 h of incubation on lipid surfaces resemble the long fibrils formed in solution and were likely also formed in solution above the lipid bilayer, and then adsorbed onto the bilayer surface. In the case of DOPG bilayers, oligomer volume increases slowly at 1 h and 6 h (Figure 4.5) and increases further at 24 h. Individual oligomers and protofibrils are well resolved by AFM on both DPPC and DOPG bilayers. Progressive accumulation of oligomers and short fibrils on the DOPG lipid surfaces are observed, similar to DPPC, Figure 4.6. This suggests that $A\beta_{1-42}$ binds to the lipid surfaces of DPPC and DOPG but does not fuse into the lipid membrane and does not disturb the surface of membrane. Both DPPC and DOPG lipid membrane act as a solid substrate, which binds and accumulates $A\beta_{1-42}$ oligomers without affecting the AFM resolution

DOTAP lipid surfaces show a different behavior. The oligomer volume (Figure 4.5) is highest at 1 h compared to other lipid type and saturates at 1 h. After this, it stays nearly the same at later times of incubation (6 h and 24 h). This means that initial binding and accumulation occurs faster on DOTAP bilayer, than on DOPC and DPPC, and the DOPG is the slowest at 1 h, which may indicate the preferable interaction of DOTAP positively-charged lipid heads with negatively charged amyloid monomers and oligomers. The height distribution does not increase progressively from 1 h to 24 h, but becomes broader, for DOTAP, Figure 4.6. This suggests that $A\beta_{1-42}$ oligomers may interact differently with DOTAP bilayer, in that they may penetrate into the bilayer headgroup area and disturb the flat surface of the bilayer, instead of simply accumulating on surface as observed on DPPC

and DOPG bilayers. This is revealed by AFM images, Figure 4.4C, which show no single well-resolved oligomers or protofibrils on DOTAP bilayer, as observed on DPPC and DOPG bilayers, but rather fused clusters which are presumably protein/lipid complexes. This lack of well resolved oligomers or protofibrils suggests stronger interaction between DOTAP lipids and A β ₁₋₄₂, compared to other lipid membrane, which changes the uniform flat surface of the bilayer to produce defects in the bilayer. It has been reported earlier that due to high fluidity and electrostatic interaction DOTAP lipids have strong interaction with charged DNA, which results into partial penetration of DNA into the bilayer headgroup area (Leonenko et al, 2004; Leonenko and Cramb 2002). Considering the complex charge distribution and total negative charge for A β ₁₋₄₂ monomer at neutral pH the interaction of A β ₁₋₄₂ with DOTAP lipids should be stronger and may cause similar bilayer deformation, resulting from clustering of positively charged DOTAP lipids around A β deposits. Slower progression of the amyloid deposition at 24 h can be also be explained by the fact that amyloids may neutralize the positive charge at the lipid headgroups upon binding and therefore reduce the electrostatic driving force for further adsorption on the surface.

The DOPC bilayer shows similar behavior as DOTAP in faster accumulation of oligomers in the first 6 h, and slower progression at 24 h, (see Figure 4.5), compared to DPPC and DOPG. Oligomers formed on DOPC are also not well resolved likely due to the partial fusion into the bilayer surface. Both lipid bilayers show wide distribution of oligomer sizes at 24 h. This suggests a stronger interaction of A β ₁₋₄₂ with lipid head groups and possible formation of lipid-protein clusters. It can be seen that all three fluid phase bilayers DOTAP (positive), DOPG (negative), and DOPC (neutral) bind A β ₁₋₄₂ effectively but show different degrees of membrane disturbance and a different order of A β ₁₋₄₂ deposits on the bilayer. While there is significant fusion of A β ₁₋₄₂ into DOTAP and DOPC bilayers upon binding observed, (Figures 4.4 and 4.5), binding of A β ₁₋₄₂ to the DPPC and DOPG bilayers was observed, but no disturbance of the bilayer. DPPC (gel phase) and DOPC (fluid phase) also show different results, although the charge on the head group is the same. This leads to the conclusion that not only the charge, but also the phase of the lipid membrane affects the interaction of A β ₁₋₄₂ with the membrane. These results correlate with the trend described in monolayers studies (Maltseva et al, 2005; Ege et al, 2005), indicating that A β ₁₋₄₀ interacts with charged lipids, but the insertion of the peptide depends on the compression of the monolayer, which

correlates with the bilayer phase (Maltseva et al, 2005). Binding was observed but no incorporation of $A\beta_{1-42}$ into the DPPC and DOPG bilayer, and disordering of DOTAP and DOPC bilayers, which most likely is a result of partial fusion of the peptide into the lipid head group area upon binding, Figures 4.4 and 4.5. Although DOPG and DOTAP bilayers are both fluid at room temperature, more ordered amyloid-lipid assemblies for DOPG membrane than for DOTAP are observed, which correlates with peptide ordering reported on negatively charged monolayers (Maltseva et al, 2005). Importantly, larger membrane disturbance due to penetration of $A\beta_{1-42}$ into the positively charged DOTAP bilayer than into the negatively charged DOPG bilayer are observed, Figure 4.5. This can be explained by the electrostatic interactions that may order the negatively charged peptide on the surface DOPG lipids. Although $A\beta_{1-42}$ is negatively charged at neutral pH (total charge -3), it has a complex distribution of charged and hydrophobic regions, which may result in different orientations of the monomers and oligomers on charged surfaces. Oriented alternating charges may result from the peptide-lipid arrangements on the DOPG membrane surfaces, which in turn may result into the ordering of the lipid phase, therefore reducing the fluidity of DOPG bilayer and degree of disturbance caused by amyloid deposits. Both DOTAP and DOPG bilayers normally exist in fluid phase at room temperature. The fluid-gel transition temperatures for DOPG and DOTAP are -18°C (Silvius 1982) and -11.9°C (Regelin 2000) respectively. The structures of the four lipids are shown in Figure 4.7. DOTAP bilayer has smaller head groups that repulse each other due to the positive charge and may be therefore more effectively disrupted by the negatively charged peptide oligomers interacting with the lipid head groups. Comparing neutral DOPC and DPPC bilayers, it is clear that the differences in phase produce different interaction with $A\beta_{1-42}$. DOPC is analogue of DPPC with similar neutral head group, but differs in saturation of the chains and exists in fluid phase at room temperature, while the DPPC is present in gel phase. DOPC bilayer behaves similarly to the fluid phase DOTAP bilayer accumulating broad distribution of oligomer sizes, which likely penetrate into the bilayer head group area, forming lipid-peptide clusters.

This demonstrates that both the phase and the charge of lipid membrane are important for binding and accumulation of $A\beta_{1-42}$ deposits on the surface of lipid membrane, which in turn may affect the morphology of lipid membrane surface and may lead to altering membrane potential upon amyloid binding.

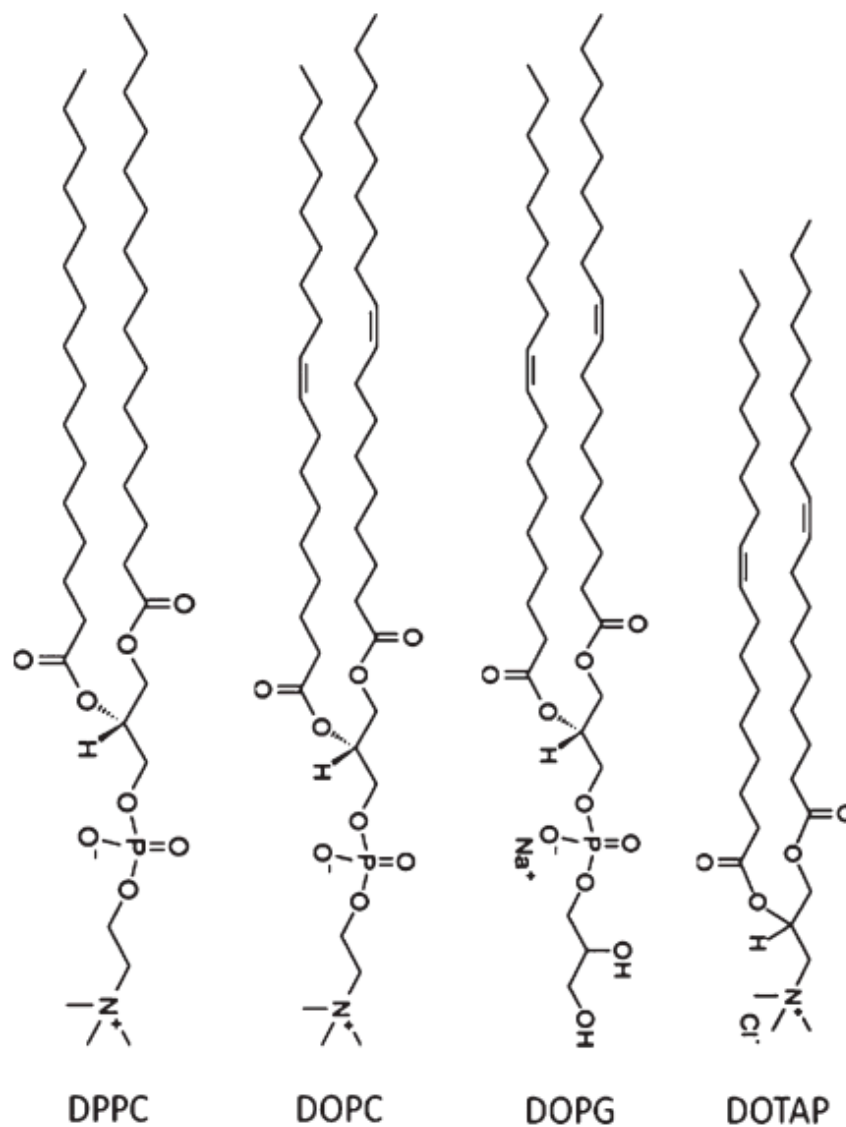


Figure 4.7: The structure and charge distribution in the lipid head group for lipids used: DPPC-1, 2-dipalmitoyl-sn-glycero-3-phosphocholine, DOPC-1, 2-dioleoyl-sn-glycero-3-phosphocholine, DOPG-1, 2-dioleoyl-sn-glycero-3-phospho-(1'-rac-glycerol) (sodium salt), DOTAP-1, 2-dioleoyl-3-trimethylammonium-propane. The structures are adapted from Avanti Polar Lipids website (<http://avantilipids.com>), where the lipids were purchased.

4.6 Conclusion

This work studied fibril formation of $A\beta_{1-42}$ on model supported lipid bilayers composed of positively charged (DOTAP), negatively charged (DOPG), and zwitterionic (DPPC and DOPC) lipids using high resolution atomic force microscopy. AFM images show binding and progressive accumulation of $A\beta_{1-42}$ oligomers and short protofibrils on the surface of zwitterionic lipid membrane DPPC and negatively charged lipid membrane DOPG. Fluid phase lipid bilayers (DOTAP (positively charged) and DOPC (neutral) show stronger interference with $A\beta_{1-42}$. Significant disturbance of the lipid membrane for positively charged fluid DOTAP bilayer and neutral fluid DOPC was also observed. This indicates the importance of electrostatic interactions as well as lipid membrane phase in amyloid-membrane interaction, which affect both the structure of amyloid aggregates and the structure of the lipid membrane itself.

Chapter 5.0 Nanoscale Electrostatic Domains in Cholesterol-Laden Lipid Membranes Create a Target for Amyloid Binding

Note: this chapter was reproduced with permission and minor modifications from {Drolle E, Gaikwad RM, Leonenko Z. 2012. Nanoscale Electrostatic Domains in Cholesterol-Laden Lipid Membranes Create a Target for Amyloid Binding. *Biophys. J.*, 103: L27 – L29.} © {2012} Cell Press.

Aim of Published Work

In this study, we looked at the effect of cholesterol on the interaction of amyloid-beta with DOPC lipid membranes. We carried out amyloid incubations for three increasing time periods on pure DOPC membranes and DOPC membranes with cholesterol and used atomic force microscopy (AFM) to visualize each system to compare the amount and type of amyloid accumulations with the membranes. We also studied both systems in monolayer form to look at the effect of cholesterol on the topography of the lipid system as well as the electrostatic surface potential map.

Experimental Design and Collaborations

Under the supervision of Dr. Z. Leonenko, I designed this experiment and carried out the sample preparation and membrane incubations, and wrote this manuscript. Post-doctoral fellow Dr. R. Gaikwad trained me in the use of frequency-modulated Kelvin probe force microscopy (FM-KPFM) and assisted greatly in the FM-KPFM monolayer study portion of this experiment, as well as statistical analysis of the samples.

Summary and Conclusions

Through AFM analysis, we saw that in the absence of cholesterol, amyloid interaction with the DOPC membrane was random and homogeneous; however, with the incorporation of cholesterol, amyloid interaction with the DOPC-Chol membrane was non-uniform and appeared to be selective. We hypothesized that this targeted binding was the result of electrostatic domains formed as a result of cholesterol's presence in the membrane. We used FM-KPFM to determine if these electrostatic domains were induced and show that cholesterol induces electrostatic domains in the membrane that likely induce targeted binding of amyloid to the membrane, as amyloid has a complex charge distribution.

5.1 Overview

Amyloid fibrils are associated with multiple neurodegenerative disorders, such as Alzheimer's disease. Although biological membranes are involved in fibril plaque formation, the role of lipid membrane composition in fibril formation and toxicity is not well understood. We investigated the effect of cholesterol on the interaction of model lipid membranes with amyloid β peptide ($A\beta$). With atomic force microscopy we demonstrated that binding of $A\beta$ (1–42) to DOPC bilayer, enriched with 20% cholesterol, resulted in an intriguing formation of small nonuniform islands loaded with $A\beta$. We attribute this effect to the presence of nanoscale electrostatic domains induced by cholesterol in DOPC bilayers. Using frequency-modulated Kelvin probe force microscopy, we were able to resolve these nanoscale electrostatic domains in DOPC monolayers. These findings directly affect the understanding of how the presence of cholesterol may induce targeted binding of amyloid deposits to biomembranes. It is postulated that this nonhomogeneous electrostatic effect of cholesterol has a fundamental nature and may be present in other lipid membranes and monolayers.

5.2 Introduction

Although amyloid fibril plaque accumulations have been observed on the surface neuronal cells *in vivo* in test subjects with Alzheimer's disease (Chiti & Dobson 2006; Roberson & Mucke 2006), the role of cell membrane composition and the presence of sterols on fibril plaque formation and toxicity are still not well understood. Studies have shown that amyloid interacts with the membrane and that it is vital in amyloid fibril formation and toxicity (Friedman et al, 2009; Jang et al, 2010). Although cholesterol is an important constituent of lipid rafts and is thought to regulate various important functions of the membrane (Lingwood & Simons, 2010), the role of cholesterol in the molecular mechanism of amyloid toxicity is not clear. Cholesterol has been shown to influence the fluidity of total brain extract, cell death and the extent to which $A\beta$ fibrillogenesis occurs (Yip et al, 2001). The effect of this sterol on the membrane is very complex and is still debated to this day (Bonn et al, 2004; Cadenhead 1985; Ohvo-Rekilä et al, 2002; Cecchi et al, 2009). We recently discovered an interesting electrostatic effect of cholesterol on pulmonary surfactant BLES (bovine lipid

extract surfactant) and showed that cholesterol inhibits surfactant function (Finot et al, 2010; Gunasekara et al, 2005). These intriguing electrostatic properties of cholesterol may be important for understanding the interaction of the plasma membrane with amyloid forming peptides. Lipid bilayers and monolayers are widely used to mimic biological membranes (Ohvo-Rekilä et al, 2002), in order to study their structure and interaction with biomolecules (Choucair et al, 2007; Hane et al, 2011; Yip et al, 2001).

5.3 Experimental Details

5.3.1 Supported lipid bilayers and amyloid binding

Phospholipid bilayers were supported on freshly cleaved mica (ruby, ASTMV-2 quality; Asheville-Schoonmaker Mica, Newport News, VA) by method of vesicle fusion (Leonenko et al, 2001) via alternating sonication and stirring procedures. Amyloid β (1-42) peptide (rPeptide, Bogart GA) was pretreated according to Fezoui procedure (Fezoui et al, 2000) to ensure the monomeric form and was suspended in HEPES buffer (50 mM, pH 7.8) at a concentration of 0.5 mg amyloid / mL of buffer. 100 μ L of amyloid solution was then added to the supported lipid membrane and incubated for 1 hour. Gentle rinsing ensured removal of excess amyloid solution, and then samples were imaged using MAC Mode AFM (Agilent) in water.

5.3.2 Supported lipid monolayers

Phospholipid monolayers were supported on freshly cleaved mica by Langmuir-Blodgett deposition. A mica slide was placed in a dipper arm of the Langmuir-Blodgett (LB) trough and lowered into the subphase (Nanopure water) of an LB trough from NIMA Technology (Coventry, United Kingdom). Solutions of lipid dissolved in chloroform were added to the subphase of the trough and allowed to spread and equilibrate on the subphase-air interface for 10 minutes. The monolayer was compressed at a speed 10 cm^2 /min to a pressure of 45 mN/m and the pressure kept constant as the dipper arm raised the mica through the interface at a speed of 2 mm/min. The mica slide was allowed to air-dry for 10 minutes before being placed in a desiccator for a 24-hour period, after which it was affixed on a conductive plate for AFM/KPFM imaging.

5.3.3 Atomic force microscopy

The AFM imaging of DOPC supported bilayers with and without cholesterol and Amyloid β (1-42) was performed in a liquid cell in Milli-Q water at room temperature using MAC mode imaging with an AFM/SPM-5500, Agilent Technologies, with type II MAC mode cantilevers with tip radius of ~ 5 nm and spring constant of ~ 2.8 N/m. AFM imaging of monolayers was simultaneously performed with FM-KPFM mode using SmartSPM (AIST-NT) in air at normal humidity (section FM-KPFM).

5.3.4 Frequency Modulated Kelvin probe force microscopy (FM-KPFM)

FM-KPFM is a Kelvin probe force microscopy technique for mapping the local electrostatic surface potential simultaneously with AFM topography images with superior resolution and sensitivity (few nm and few 10 mV) (Moores et al, 2010). Previously developed KPFM methods have limited application in biological research, whilst FM-KPFM has proven to be advantageous to study the surface potential maps in complex self-assembled biological films (Moores et al, 2010). The FM-KPFM imaging was performed using the NC-DFM mode with a SmartSPM 1000 system provided by AIST-NT. A standard PPP-EFM (Nanosensors) cantilever with a radius of curvature (< 30 nm) and spring constant ~ 2.8 N/m was used for imaging in ambient air at normal humidity.

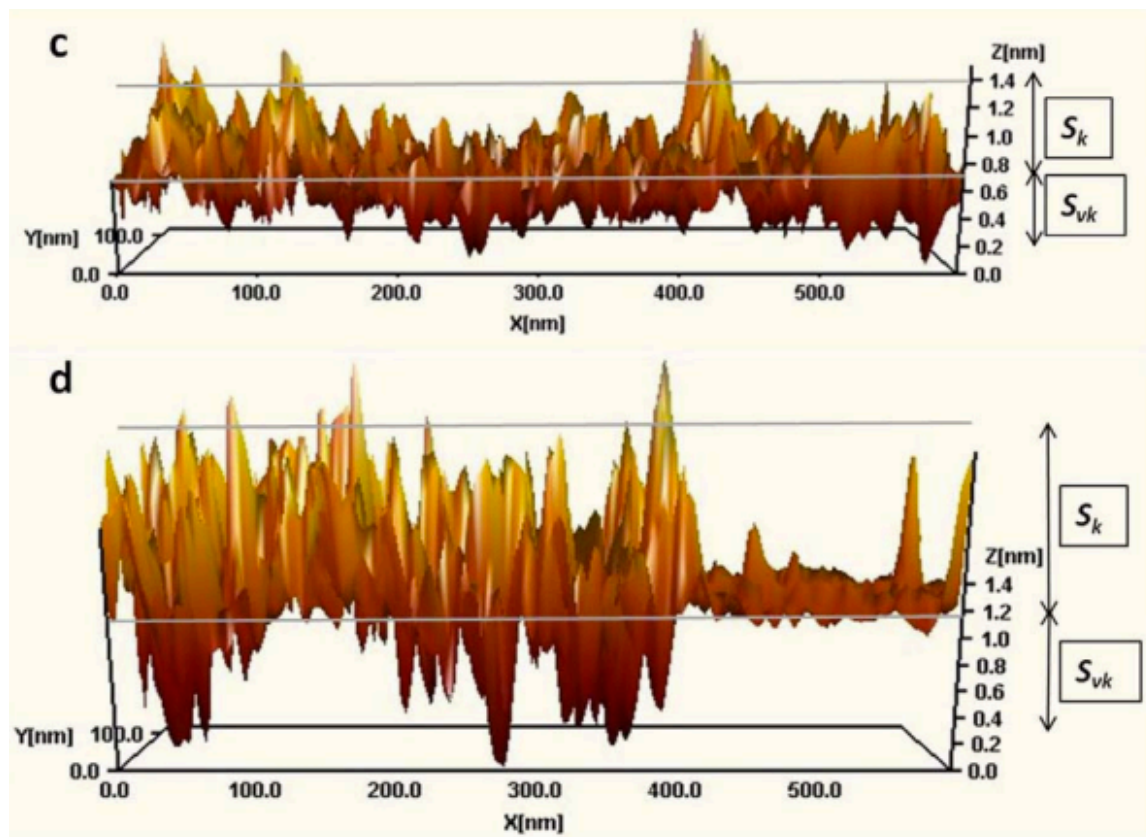


Figure 5.1: 3D-Cross-sectional analysis emphasizing the importance of surface roughness parameters S_k and S_{vk} of (c) pure DOPC membrane after 1hr incubation with $A\beta$ (1-42), (d) - DOPC membrane with 20% cholesterol after 1hr incubation with $A\beta$ (1-42)

5.3.5 Data Processing software and statistical analysis

Data collected using Agilent and AIST-NT AFM's was processed using Gwyddion v.2.25. The topography images were leveled by mean plane subtraction, corrected for line jumps and horizontal scar to nullify AFM artifacts caused while scanning with high resolution Z-scale (picometers). The images were processed to remove any polynomial background. The FM-KPFM images were not processed with any filters, to ensure the proper potential measurements; the raw data were used for cross section analysis using Gwyddion software. Statistical analysis of AFM topography images and surface roughness was done using SPIP software (v 5.1.6). In order to estimate the damaging effect of $A\beta$ deposits on the lipid membranes we evaluated the roughness parameters of the surface for both samples. We

calculated the core roughness depth, S_k , which is a measure of the nominal roughness (peak to valley) and the reduced valley depth, S_{vk} , which is a measure of the valley depth below the core roughness (Wang et al, 2006). Data was collected on $2 \mu\text{m} \times 2 \mu\text{m}$ high-resolution images of the membranes. The three dimensional AFM images (surface roughness) in Figures 5.2c and 5.2d show representative regions highlighting the contrast in surface roughness between the two types of sample. An enlarged version of Figure 5.2c and 5.2d are shown in Figure 5.1 - the 3D cross section of pure DOPC membrane after 1hr incubation with $A\beta$ (1-42) and DOPC membrane with 20% cholesterol after 1hr incubation with $A\beta$ (1-42) is shown here, below. The S_k parameter is slightly lower for pure DOPC membrane (0.7 ± 0.1 nm) than for cholesterol enriched DOPC membrane (0.8 ± 0.1 nm), which correlates with smoother surface of the membrane when there is no cholesterol present in the membrane. The S_{vk} parameter is significantly higher for cholesterol enriched DOPC membrane (0.5 ± 0.1 nm) than for pure DOPC membrane (0.24 ± 0.03 nm), which corresponds to a higher damage (deeper holes in the membrane) that $A\beta$ deposits produce in the membrane domains saturated with cholesterol. All experiments were repeated at least 3 times, 4-5 images were used for statistical analysis with no less than 100 measurements in each case ($N > 100$).

For the KPFM statistical analysis, random cross sections were taken on the Contact Potential Difference 1 (CPD1/KPFM channel) to measure the potential difference between the domain and the substrate manually. For quantitative purpose, no fewer than 50 cross sections were analyzed on 3 images and measured potential difference of approximately 120 domains ($N > 50$).

5.4 Results and Discussion

In this work, Atomic Force Microscopy (AFM) and Frequency-Modulated Kelvin Probe Force Microscopy (FM-KPFM) are used to investigate the effect of cholesterol on the structure of dioleoyl-sn-glycero-3-phosphocholine (DOPC) bilayers and monolayers and to study how this affects $A\beta$ (1-42) binding and fibril formation. DOPC bilayers with and without cholesterol were prepared as described in section 5.4, supported on mica, incubated with $A\beta$ (1-42) solution in buffer and then rinsed with water and imaged in water. As shown

in Figure 5.2a, A β deposits on the pure DOPC bilayers were small, spherical and uniformly distributed across the lipid membrane surface with no preferential binding sites or clustering. Amyloid fibril formation on DOPC membranes with 20% cholesterol showed quite different and striking results (Figure 5.2b) - amyloid deposits were binding to the lipid membrane in a non-uniform, selective manner which resulted in the formation of nanoscale islands or domains (10-100 nm in size) enriched with amyloid deposits (Figure 5.1).

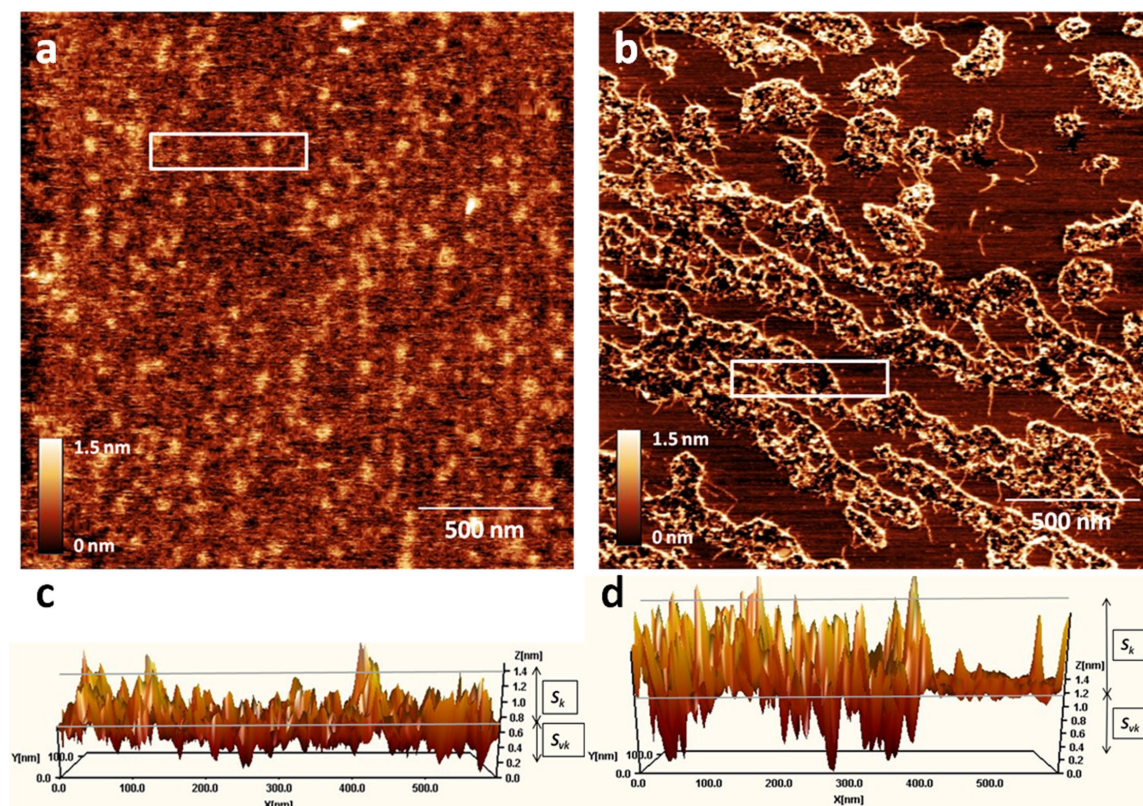


Figure 5.2: AFM topography images of A β binding to the lipid membrane: (a) pure DOPC membrane after 1hr incubation with A β (1-42), (b) DOPC membrane with 20% cholesterol after 1hr incubation with A β (1-42), surface roughness of the pure DOPC membrane with A β deposits (c), of the rectangular area marked in Figure 5.2a; and of the cholesterol enriched DOPC membrane with A β deposits (d) of the rectangular area marked in Figure 5.2b.

The amyloid deposits observed on the DOPC/cholesterol membrane were clusters of spherical oligomers and short fibrils. In order to estimate the disruptive effect of A β deposits on the lipid membranes, the roughness parameters of the membrane surfaces were evaluated for both samples. The surface of the pure DOPC membrane with A β deposits was relatively

smooth with A β deposits slightly sinking into the membrane (Figure 5.2a), which correlates with this group's previous data (Hane et al, 2011). The domains of clustered A β deposits on the DOPC/cholesterol bilayer showed rough surfaces corresponding to the domains saturated with A β deposits and smooth areas of pure membrane Figure 5.2c and d. The core roughness S_k (see experimental details, section 5.3.5, for further information) is slightly lower for pure DOPC membrane (0.7 ± 0.1 nm) than for cholesterol enriched DOPC membrane (0.8 ± 0.1 nm). The reduced valley depth S_{vk} is significantly higher for the cholesterol-enriched DOPC membrane (0.5 ± 0.1 nm) than for the pure DOPC membrane (0.24 ± 0.03 nm), which corresponds to increased damage (deeper holes produced) in the membrane by A β deposits.

It was reported that cholesterol induces a small thickening of the DOPC membrane (Kucerka et al, 2007; Drolle et al, 2013) which may result to the formation of topographical domains that were observe, which may indicate the coexistence of liquid-ordered and liquid-disordered phases (Lingwood & Simons, 2010). In addition, using FM-KPFM (Moores et al, 2010; Zerweck et al, 2005), this work shows that these domains are also electrostatic in nature (Figure 5.3). Figure 5.3 shows AFM topography (a and b) and FM-KPFM surface potential images (c and d) of pure DOPC monolayer (a and c) and monolayer with 20% cholesterol (b and d). The pure DOPC lipid monolayer is smooth (Figure 5.3a) and has uniform featureless surface potential (Figure 5.3c), while the DOPC lipid monolayer with 20% of cholesterol shows domains in topography (Figure 5.3b) and in surface potential (Figure 5.3d). These domains have a surface potential difference of 61 ± 8 mV measured from potential cross-sections (see experimental details, section 5.3).

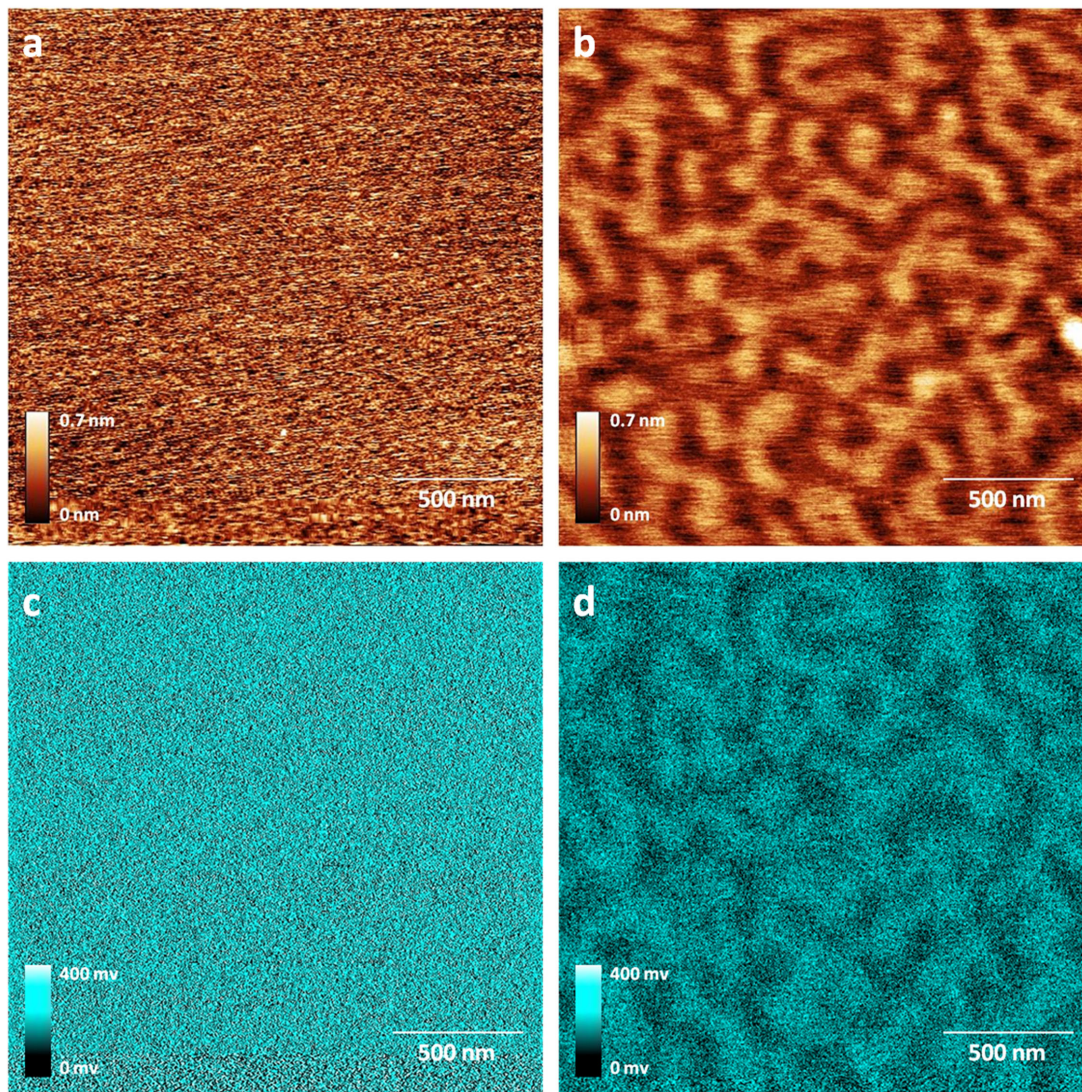


Figure 5.3: AFM and corresponding FM-KPFM images of lipid monolayers with and without cholesterol. AFM images depicting the topography of pure DOPC monolayer (a), and DOPC monolayer with 20% cholesterol (b) and the corresponding FM-KPFM images depicting surface potential distribution of pure DOPC monolayer (c), and DOPC monolayer with 20% cholesterol (d). AFM and FM-KPFM images were collected with SmartSPM (AIST-NT).

Considering the charged nature of A β (Moore et al, 2011), it is expected that electrostatic domains created in the DOPC lipid membrane by cholesterol attract the A β peptide, thus inducing non-homogeneous islands or domains densely packed with amyloid deposits, as shown on Figure 5.2b. Earlier, it was discovered that cholesterol-induced nanoscale electrostatic domains are crucial for the function of pulmonary surfactant and its interaction

with charged nanoparticles (Finot et al, 2010; Gunasekara et al, 2005). It is postulated that this previously unknown electrostatic effect of cholesterol is not specific to pulmonary surfactant films and extends to other self-assembled amphiphilic structures such as lipid monolayers and lipid membranes, and, therefore, can greatly affect the interaction of charged or polar biomolecules with the surface of lipid membrane. This work demonstrates that this electrostatic effect of cholesterol may serve as a driving force for amyloid targeted interactions with lipid membranes and if this is the case, suggests that cholesterol may be involved in the mechanism of amyloid toxicity.

Chapter 6.0 Effect of Cholesterol on Topographical and Electrostatic Domains in Complex Lipid Mixtures.

Summary

Interactions of biomolecules and peptides with cellular membranes are observed in numerous diseases, such as the interaction of amyloid fibrils with the membrane in Alzheimer's disease. Molecular arrangement of lipids and proteins in the biomembrane gives rise to a complex film morphology as well as regions of distinct electrical surface potential, which may rule many biological processes, as well as interactions of molecules with the cell. This is of particular interest in the research of certain diseases in which biomolecules interact with the membrane, such as in Alzheimer's disease involving the binding of amyloid peptides to the membrane.

Based on this interest, in this study, the effect of cholesterol and the effect of composition, lipid charge, and lipid phase on the monolayer structure and the electrical surface potential distribution is investigated. Atomic Force Microscopy (AFM) was used to study topographical features and frequency modulated-Kelvin Probe Force Microscopy (FM-KPFM) to resolve topographical and electrostatic nanoscale domains in the monolayer. Model monolayers composed of dipalmitoylphosphatidylcholine (DPPC), 1,2-dioleoyl-sn-glycero-3-phosphocholine (DOPC), 1-palmitoyl-2-oleoyl-sn-glycero-3-phosphocholine (POPC), 1,2-dioleoyl-sn-glycero-3-[phospho-rac-(3-lysyl(1-glycerol))] (DOPG), sphingomyelin, and cholesterol were studied. It was observed that cholesterol had a significant effect on the electrical surface potentials of the mixtures studied. This lends support to the idea that cholesterol plays an important role in the membrane in the creation of electrostatic domains that are involved in the interaction of the membrane with biomolecules, especially those that carry a charge.

Experimental Design and Contributions

Under the supervision of Dr. Z. Leonenko, I designed this experiment, carried out the experimentation and data analysis, and wrote this chapter in manuscript form to be submitted for publication to a peer-reviewed journal. For this project, I also had an undergraduate assistant, Keely Hammond, a summer NSERC student; I trained her in sample preparation,

AFM and FM-KPFM usage, and data analysis, which she assisted with, under my supervision and mentorship, for this project.

6.1 Introduction

In recent years, the model of the lipid membrane has changed from a bilayer composed of a uniform lipid mixture to a heterogeneous surface with distinct domains. Membrane domains are recognized as areas of distinct thickness and diameter, organization, physical properties, and lipid composition. Domains are responsible for many biological functions, stemming from their ability to bind and sequester functional membrane proteins, including initiation of signalling pathways, fusion with other membranes, and various sorting processes (Simons & Toomre 2000).

The first evidence of lipid domains was collected in the study of epithelial cells containing two membrane domains physically separated by tight junctions (Nusrat et al, 2000). Beyond physical separation, however, both biological and model lipid membranes contain smaller microdomains (rafts) that form independently of external organizational processes. Rafts form spontaneously in model membranes with mixed lipid composition, particularly in mixtures containing cholesterol and sphingolipids (Hooper 1999). The minimization of free energy in lipid packing, of short-range line tension along the boundaries between rafts and the rest of the membrane, and of long-range electrostatic repulsion between lipid dipoles drives the formation of lipid rafts (Sriram & Schwartz 2012). Combined, these effects are responsible for both the partitioning of saturated lipids and cholesterol into the raft regions (where tighter packing occurs) and the characteristic size of the rafts (Sriram & Schwartz 2012). Rafts are thicker than the surrounding membrane – due to the presence of cholesterol in the acyl chain region of the lipids – causing the chains to become fully extended in order to shield the hydrophobic cholesterol from water (Simons & Toomre 2000). Various methods have been used to determine the position and shape of rafts in the membrane, including atomic force microscopy (AFM), neutron scattering, fluorescence microscopy, and fluorescence resonance energy transfer (Veatch et al, 2004). Generally, rafts are categorized as being less than 1 micron in diameter; a recent AFM study of erythrocyte membranes found raft diameters to be within 100 - 300 nm (Cai et al, 2012). Others have found raft

diameters to be as small as 40 nm in both model systems and biological membranes (Sriram & Schwartz 2012). The organizational properties of rafts are linked to their phase state in the membrane. Lipid membranes often contain multiple phases, including the gel phase and various liquid crystalline phases. While the majority of membrane lipids exist in a liquid-disordered phase, raft lipids exist in a cholesterol-induced liquid-ordered phase, where they are characterized by a high degree of order in the acyl chains while retaining the freedom of lateral diffusive movement (Veatch et al, 2007). Effectively, the tails of liquid-ordered phase lipids are more densely and uniformly packed than those of liquid-disordered lipids, a process facilitated by the insertion of cholesterol between the acyl chains. This also results in thickening of the membrane and thus increased membrane stiffness within the domain (Bennett & Tieleman 2013). The kinks present in unsaturated acyl chains make them less suited to the liquid-ordered phase, explaining their tendency to remain outside lipid rafts at physiological temperatures (Veatch et al, 2004).

Membranes are polar structures and have an associated dipole moment. This dipole moment is generated between the electrically neutral acyl chains and the polar, occasionally charged head groups of individual lipid molecules (Langner & Kubica 1999). The head groups accumulate a hydration shell of water dipoles in aqueous solution, further enhancing the dipole effect (Langner & Kubica 1999). As one of several non-covalent interactions occurring at the surface of biological membranes, electrostatic forces are involved in many protein-lipid binding events. Mapping membrane surface potential is therefore useful in determining the mechanism of such binding events. This group's recent work using Kelvin Probe Force Microscopy (KPFM) has elucidated the presence of electrostatic domains in model membrane systems containing the unsaturated lipid DOPC and cholesterol that correlate with position of liquid-ordered domains, or presumptive lipid rafts (Drolle et al, 2012). These electrostatic domains have lower surface potential than the surrounding regions and preferentially interact with the charged amyloid-beta peptide (Drolle et al, 2012).

As a continuation of this work studying the electrostatic effect of cholesterol, this study moved to more complex systems that more accurately approaches the true complexity of a cell membrane to see if cholesterol has a similar effect. One area of interest is cholesterol's electrostatic effect when studying lipid rafts. A common model for the study of rafts contains

the lipids 1,2-dipalmitoyl-sn-glycero-3-phosphocholine (DPPC), 1,2-dioleoyl-sn-glycero-3-phosphocholine (DOPC), and cholesterol in various proportions. DOPC and DPPC contain two unsaturated and two saturated acyl chains respectively and are thus useful as representative low and high melting point lipids. DPPC mainly partitions into the liquid-ordered phase in the presence of cholesterol, while DOPC is found primarily in the liquid-disordered phase at physiological temperatures (Veatch et al, 2004). Cholesterol is responsible for keeping DPPC in a liquid-ordered phase rather than the gel phase it would prefer under cholesterol-free conditions, due to the insertion of cholesterol between the acyl chains of DPPC as described above (McMullen et al, 2004; Bennett & Tieleman 2013). Several studies have characterized the phase transitions of this system using deuterium NMR with vesicles containing DPPC-d62/DOPC/Chol and have defined a distinct region of coexistence of the two liquid phases, with cholesterol and DPPC in the liquid-ordered phase and DOPC in the liquid-disordered phase (Veatch et al, 2007; Davis et al, 2009). The presence of two phases corresponds with the presence of domains visualized with fluorescence microscopy (Veatch et al, 2004). Using deuterium NMR and fluorescence microscopy data, Juhasz et al. performed a quantitative comparison of the area covered by domains in giant unilamellar vesicles (Juhasz et al, 2009). Domain size has also been investigated using fluorescence microscopy and fluorescence resonance energy transfer (FRET) and ranges from fractions of a nanometer to tens of nanometers, depending on temperature, sample and solution composition, and measurement technique (Veatch et al, 2004; Suga & Umakoshi 2013; Brown et al, 2007; Aguilar et al, 2012). Neutron scattering experiments show a domain size of 15 nm in DPPC-d62-DOPC-Chol (27:45:28 mol%) multilamellar vesicles (Vogtt et al, 2010).

Cholesterol is also shown to associate preferentially with saturated acyl chains over unsaturated ones in molecular dynamics (MD) simulations (de Joannis et al, 2011; Bennett & Tieleman 2013). De Joannis et al. performed atomistic MD simulations of the DPPC-DOPC-Chol system and found cholesterol arranges itself normal to the bilayer surface (upright) at sufficiently high concentrations (de Joannis et al, 2011). DPPC has a higher affinity for upright cholesterol than tilted cholesterol; thus, greater ordering of DPPC molecules occurs at higher cholesterol concentrations (de Joannis et al, 2011). A coarse-grained MD simulation of DPPC-DOPC-Chol as a bilayer showed fast partitioning of the

mixture into raft-like domains, with the liquid-ordered domains (DPPC) being highly enriched in cholesterol and thicker than the surrounding DOPC regions (Risselada & Marrink 2008). Monolayer simulations showed phase separation similar to the bilayer model, again with cholesterol enrichment in the DPPC phase, at surface tensions from 1 - 30 mN/m (Baoukina et al, 2012). In both the monolayer and bilayer models, cholesterol drives the formation of the liquid-ordered phase by its preferential interactions with DPPC (Risselada & Marrink 2008; Baoukina et al, 2012). Increasing temperature in bilayer simulations and decreasing surface tension in monolayer simulations were shown to have similar effects on lipid packing and domain formation (Baoukina & Mendez-Villuendas 2009).

Along with DPPC-DOPC-Chol, there are currently many different lipid mixtures used as models for cellular membranes in order to study raft formation, vesicle fusion, and other cellular processes. Several features can be used to characterize model membranes, including phase diagrams (Veatch et al, 2005a; Veatch et al, 2004; Veatch et al, 2007), domain size (Brown et al, 2007), and surface potential (Hane et al, 2011). Mixtures used to study raft formation typically include both high and low melting temperature (T_m) phospholipids, where the low melting temperature lipid contains one or more unsaturated acyl chains, plus cholesterol to induce domain formation (Veatch et al, 2005a). Addition of sphingomyelin further enhances domain formation, due to additional hydrogen bonding opportunities with cholesterol (Veatch et al, 2005a). Sometimes, lipids containing a net charge are included in the mixture in order to study electrostatic interactions (Hane et al, 2011; Patel et al, 2009).

Multiple three-component or ternary mixtures have been used in the study of raft formation. The most common choice of high T_m phospholipid is DPPC, which as mentioned before contains two saturated acyl chains, while DOPC, with its two unsaturated acyl chains, is frequently chosen as the low T_m component. Another choice of low T_m phospholipid is 1-palmitoyl-2-oleoyl-*sn*-glycero-3-phosphocholine (POPC), which contains one saturated and one unsaturated acyl chain. The mixture DPPC-DOPC-Chol has a well-characterized phase diagram (Veatch et al, 2004). There is a clear region where liquid-disordered and liquid-ordered phases coexist, corresponding with the visible presence of rafts in fluorescence microscopy investigations (Veatch et al, 2004; Veatch et al, 2007). In contrast, the DPPC-

POPC-Chol model does not display liquid-ordered, liquid-disordered phase coexistence under the microscope or in fluorescence resonance energy transfer experiments (Brown et al, 2007). Instead, this mixture transitions directly from a liquid-disordered phase to a liquid-ordered phase at a specific composition (Brown et al, 2007). These two models have been compared to determine the effects of acyl chain saturation in the low T_m component on domain formation.

Inclusion of sphingolipids such as sphingomyelin (SM) in model membranes, as the high T_m , saturated component, facilitates domain formation by offering more hydrogen bonding sites for cholesterol than sites present in phospholipids. Hydrogen bonding occurs between cholesterol and the sphingosine region of sphingolipids, increasing the affinity of the lipid for the liquid-ordered phase (Veatch et al, 2005b). In biological membranes, the outer membrane leaflet is composed of saturated sphingolipids, phospholipids with one saturated and one unsaturated acyl chain, and cholesterol. Thus SM-POPC-Chol forms a biologically relevant membrane model (Bunge et al, 2008). From NMR spectroscopy studies, it is known that liquid-ordered and liquid-disordered phases coexist in this model, and domain formation or liquid-liquid phase coexistence can also be observed with fluorescence microscopy (Bunge et al, 2008). Overall, the phase behaviour of this mixture is similar to that of DPPC-DOPC-Chol (Veatch et al, 2005b); they are different in that SM-POPC-Chol preserves its liquid-liquid phase coexistence at slightly higher temperatures than DPPC-DOPC-Chol (Veatch et al, 2005b).

The presence of charged lipids in biological membranes is important for protein binding. In particular, negatively charged lipids, often found in the prokaryotic outer membrane leaflet, contribute to cationic peptide binding events in model systems (Joanne et al, 2009). Two examples of negatively charged lipids are 1,2-dioleoyl-*sn*-glycero-3-phospho-(1'-*rac*-glycerol) (DOPG), with two unsaturated acyl chains, and 1,2-dipalmitoyl-*sn*-glycero-3-phospho-(1'-*rac*-glycerol) (DPPG), with two saturated acyl chains, analogous to DOPC and DPPC respectively. Specific cationic peptides, including antimicrobial peptides and cell penetrating peptides, interact with the membrane surface in order to enter the cell (Joanne et al, 2009). They rely on electrostatic interactions between their positively charged domains and the negative charges on the lipid head groups to initiate the entry process (Joanne et al,

2009). One model membrane used to examine cationic peptide binding is the DPPC-DOPG-Chol system (Joanne et al, 2009). Interactions between negatively charged peptides and the DPPC-DOPG-Chol system have also been investigated (Hane et al, 2011). In the case of anionic amyloid peptides, the negative surface charge of the membrane slows the aggregation and oligomerization of the peptides (Hane et al, 2011). The phase transitions for this model have not been well characterized. However, those of the DOPC-DOPG-DPPC-DPPG-Chol system have been characterized, and the temperature and cholesterol content where liquid-liquid phase coexistence occurs was found to be similar to the zwitterionic DPPC-DOPC-Chol mixture (Kapoor et al, 2011).

Mapping the electrical surface potential of model lipid systems can reveal the presence of electrostatic domains whether or not the models contain lipids with a net charge. The Kelvin probe force microscopy (KPFM) technique is a high-resolution, sensitive method for detection of surface potential and has recently been used to map surface potential in model lipid systems (Finot et al, 2010; Moores et al, 2010). For example, the presence of cholesterol causes electrostatic domain formation in a pulmonary surfactant lipid mixture containing DPPC and anionic lipids (Finot et al, 2010; Moores et al, 2010). As well, the DOPC-Chol model system displays nanoscale electrostatic domains, and these may be involved in binding the anionic peptide amyloid- β , a peptide implicated in the mechanism of Alzheimer's disease (Drolle et al, 2012). Cholesterol is clearly involved in electrostatic domain formation in addition to its involvement in liquid-liquid phase coexistence.

This study shows both the topographical effect of cholesterol as well as its effect on surface potential in membranes of increasing complexity (beginning with two-lipid systems such as DPPC and DOPC), primarily using lipids that are commonly found in neuronal cell membranes. Research in this area has shown that the most common lipids in the neuronal cell membrane are saturated fatty acids, like DPPC, as well as 18:1 monounsaturated lipids, like DOPC (two 18:1 monounsaturated acyl chains) or POPC (one 18:1 monounsaturated acyl chain, with the other acyl chain fully saturated) (Soderberg et al, 1991; Prinetti et al, 2001). In the outer leaflet of the membrane, which is where this group's interest lies, cholesterol and sphingolipids are found in higher concentrations than in the inner leaflet (Vestergaard et al, 2008).

The monolayers studied were formed from mixtures of two or more of these lipids and studied the effect of cholesterol on the topography and electrical surface potential to determine if cholesterol had a similar effect of the creation of nanoscale electrostatic domains in each mixture.

6.2 Materials and Methods:

6.2.1 Lipid solution preparation.

Dipalmitoylphosphatidylcholine (DPPC), 1,2-dioleoyl-*sn*-glycero-3-phosphocholine (DOPC), 1-palmitoyl-2-oleoyl-*sn*-glycero-3-phosphocholine (POPC), 1,2-dioleoyl-*sn*-glycero-3-phospho-(1'-*rac*-glycerol) (sodium salt) (DOPG), sphingomyelin, and cholesterol were purchased from Avanti Polar Lipids (Alabaster, AL) in powder form. All other chemicals used, including chloroform and ethanol, were of reagent grade. Stock lipids were dissolved in chloroform at a concentration of 1 mg/mL and combined to form the mixtures shown in Table 6.1. These solutions were then used for monolayer deposition with the Langmuir-Blodgett trough.

Table 6.1: Lipid Mixtures Studied and Their Respective Lipid Ratios. This table outlines the 8 samples analyzed in this study; four different lipid systems in the absence and presence of cholesterol. The corresponding ratio of lipids to one another (based on weight) is given.

Lipids	Ratio (w/w)
DPPC-DOPC	607:393
DPPC-DOPC-Chol	560:346:94
POPC-SM	80:20
POPC-SM-Chol	80:10:10
DPPC-POPC-SM	40:40:20
DPPC-POPC-SM-Chol	40:40:10:10
DPPC-DOPG	50:50
DPPC-DOPG-Chol	40:40:20

6.2.2 Supported lipid monolayers preparation on the Langmuir-Blodgett trough.

For monolayer creation, phospholipids were deposited on fresh cleaved mica (Asheville-Schoonmaker Mica Co., Newport News, VA) using Langmuir-Blodgett deposition. In this method, phospholipid mixtures are added to the surface of liquid subphase; the molecules orient themselves into a monolayer on the subphase surface, and are then compressed via moveable barrier arms at a rate of $10 \text{ cm}^2/\text{min}$ to a pressure of 35 mN/m . At this pressure, the moveable dipper arm of the trough arm passes the mica substrate through the monolayer, utilizing vertical deposition in order to create a solid-supported monolayer, while the moveable barrier arms maintain the pressure of 35 mN/m . Samples were then allowed to dry in a dessicator environment for a minimum of 24 hours and affixed on a conductive plate prior to AFM/KPFM imaging.

6.2.3 Atomic force microscopy (AFM) and frequency modulated-Kelvin probe force microscopy (FM-KPFM).

Topography imaging (AFM) of the supported monolayers was performed simultaneously with electrical surface potential mapping (FM-KPFM) in air using intermittent contact mode on the AIST-NT SmartSPM, with a Micromasch chromium-gold coated cantilever (HQ:NSC14 / Cr-Au) with a resonance frequency of 160 kHz and a spring constant of 5.0 N/m . The use of FM-KPFM allows for higher resolution than typical KPFM techniques and allows for simultaneous AFM-KPFM imaging, both of which are essential for biological applications.

6.2.4 Image processing and analysis.

Image processing was carried out using AIST Image Analysis and Processing software. Images were levelled using plane levelling and lines were corrected by fitting the lines and removing scars (any image artifacts present). Statistics were also obtained using roughness analysis made available by the AIST Image Analysis and Processing software, as well as cross sectional analysis of multiple samples and scans for each combination. For analysis of FM-KPFM images, raw data was used; the images were not processed with any filters prior to the analysis in order to ensure that the potential measurements were accurate. All

quantitative results are presented as mean \pm standard error and differences in the presence of cholesterol are statistically significant based on a t-test statistical analysis with confidence level of at least 90%, unless otherwise indicated.

6.3 Results and Discussion

In order to study the effect of cholesterol on more complex lipid systems as well as the formation or abolishment of lipid domains, numerous samples were looked at with and without cholesterol. This study began with simpler samples, composed of two lipids, and increased sample complexity by adding more components. A schematic of a more complex lipid monolayer system is given in Figure 6.1. The image also depicts how difference in height and difference in electrical surface potential are measured. The difference in the heights (Δh) of the lipids and how they arrange themselves can be seen via the atomic force microscopy (AFM) topography analysis of the sample and the difference in electrical surface potential (ΔV) based on the same arrangements (though not visible in this image) is also measureable via frequency-modulated Kelvin probe force microscopy (FM-KPFM) electrical surface potential mapping.

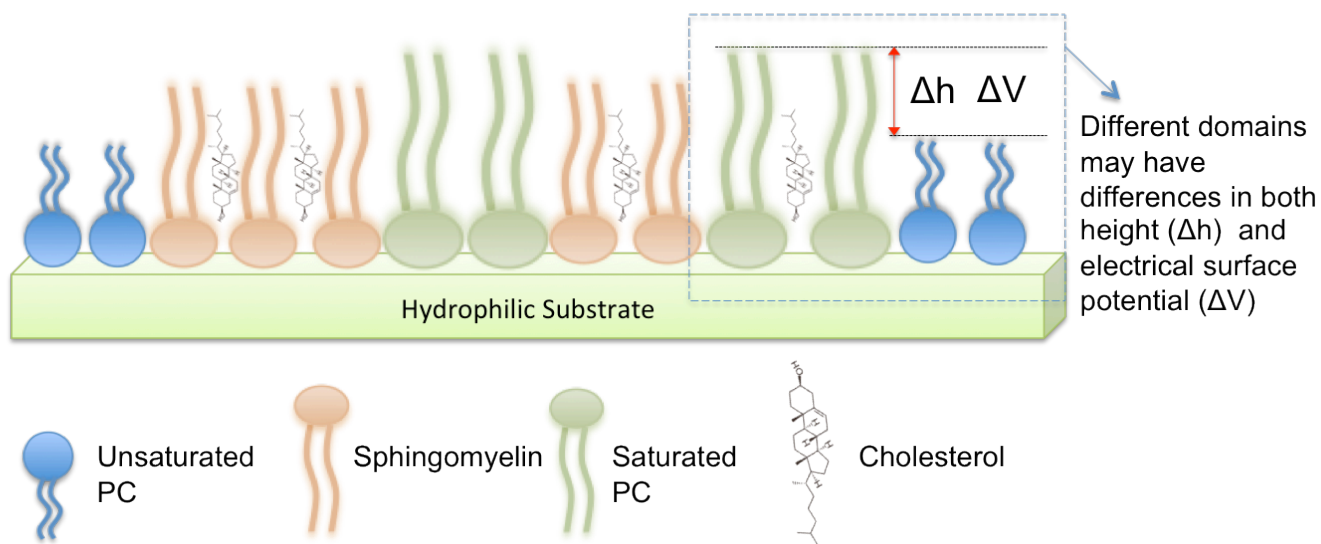


Figure 6.1: Schematic of Possible Monolayer Arrangement in a Three-Component Lipid System in the Presence of Cholesterol (not to scale). This image depicts a schematic of the most complex of the systems studied in this work – three lipids (unsaturated PC being POPC; saturated PC being DPPC; and sphingomyelin SM) in the presence of cholesterol. The hydrophilic head groups of the lipids interact with the hydrophilic surface of the mica substrate, resulting in the tail groups facing upwards into the air. The image also depicts how difference in height (Δh) is extracted from AFM topography and difference in electrical surface potential (ΔV) is determined using KPFM. Please note that this is a hypothesized model of how a portion monolayer may look in terms of arrangement and location of molecules in a monolayer.

The first system studied was a DPPC-DOPC mixture with and without cholesterol. As previously mentioned, DPPC-DOPC-Chol is a common, simple system used to form lipid rafts/domains. Without cholesterol present, prominent domain separation was observed, with larger areas corresponding to higher domains (Figure 6.2A). The difference in height between these domains (Δh , visualized in Figure 6.1) averaged 1.22 ± 0.03 nm. It is likely that higher domains correspond to DPPC molecules, as in their gel phase, the tail groups are more ordered and thus are slightly thicker than the disordered tail groups of fluid phase (also known as liquid disordered, L_d , phase) DOPC (Ohvo-Rekilä et al, 2002). These higher domains were much larger in size than the lower domains, reaching lateral dimensions of up

to 570 nm in length (i.e. X) and 775 nm in width (i.e. Y); the lower domains were less prevalent in the monolayer, with average X dimensions of 150 nm and Y dimensions of up to 350 nm. Each higher and lower domain present in the mixture has a distinct electrical surface potential. The difference in the electrical surface potential between the higher and lower domains was analyzed (ΔV , visualized in Figure 6.1). The average ΔV of the electrostatic domains was determined to be 41.6 ± 5.39 mV (potential map shown in Figure 6.2B). Note that this data is summarized for easy comparison in Table 6.2.

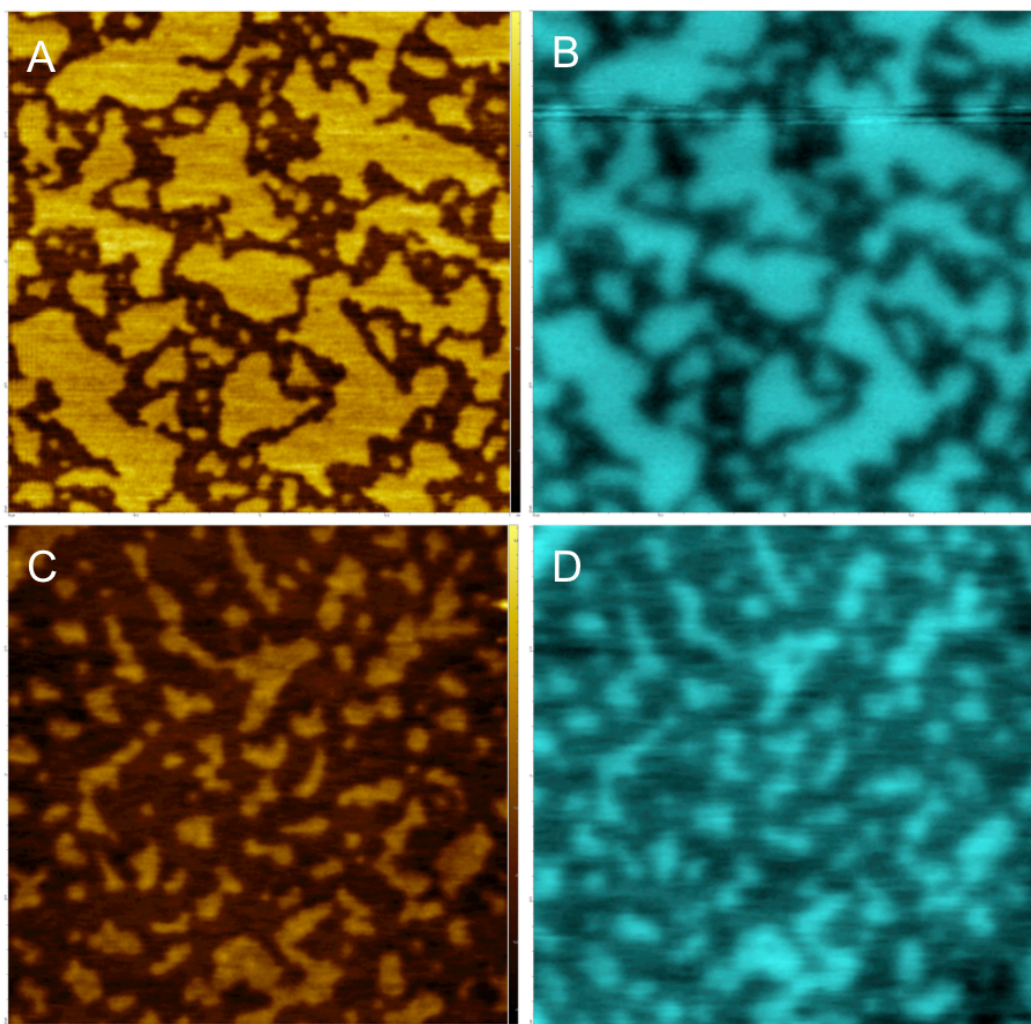


Figure 6.2: AFM and corresponding FM-KPFM illustrating the effect of cholesterol on both the topography and electrical surface potential of a lipid mixture of DPPC and DOPC. AFM images (A) and FM-KPFM images (B) of a DPPC-DOPC mixture (at a ratio of 607:393) are compared to topography captured by AFM and electrical surface potential captured by KPFM of

a DPPC-DOPC-Cholesterol sample (at a ratio of 560:346:94, images C and D respectively). AFM and KPFM images were scanned in air in ambient conditions. These images are 2 μm by 2 μm .

With the addition of cholesterol to the DPPC-DOPC system, the presence of small topographical domains on the monolayer samples were observed (Figure 6.2C) with an average Δh of the domains present of 0.97 ± 0.06 nm. This average Δh is slightly lower than that observed in the DOPC-DPPC system (1.22 nm). This is consistent with the idea that cholesterol causes slight disorder in the already ordered tail groups of gel phase lipid molecules such as DPPC by creating an intermediate liquid-ordered (L_o) phase (Ohvo-Rekilä et al, 2002). The idea that cholesterol molecules are clustered in higher concentration near the DPPC molecules than the DOPC molecules agrees with the idea that cholesterol prefers to interact with saturated rather than unsaturated lipids (with DPPC being fully saturated and DOPC being monounsaturated) (Ohvo-Rekilä et al, 2002). It also agrees with simulation studies done by Tieleman's group, which show a similar DOPC-DPPC-Chol system, with the cholesterol molecules organized in higher concentration with DPPC molecules rather than the DOPC molecules (Bennett & Tieleman 2013). The lower domains are much larger in size than those observed in the DPPC-DOPC sample, with dimensions of up to 600 by 450 nm (DPPC-DOPC dimensions were only up to 150 by 350 nm). This also supports the idea that cholesterol is interacting especially with the DPPC molecules and causing slightly disorder, resulting in increased lower domain presence in the sample.

The corresponding surface potential image (Figure 6.2D) shows distinct electrostatic domains where higher topographical domains correspond to areas of higher electrical surface potential. These electrostatic domains had an average ΔV of 67.25 ± 7.03 mV. This difference is larger than that observed in the DOPC-DPPC-Chol system, which had an average ΔV of 41.6 mV, supporting the idea that cholesterol has a measurable effect on the V of the mixed lipid system.

The next system investigated was another two-lipid system, POPC and sphingomyelin. POPC is similar to DOPC in terms of having a low transition temperature and is a common phospholipid in neuronal cell membranes (Soderberg et al, 1991; Prinetti et al, 2001). Sphingolipids are found in higher concentrations in the outer leaflet of the neuronal cell

plasma membrane; sphingomyelin (SM) is the most common type of sphingolipid (Vestergaard et al, 2008). In the POPC-SM system, there appears to very little difference in topography to observe, as can be seen in Figure 6.3A, though some topographical deviations do exist, as the average Δh was 0.35 ± 0.02 nm. Only minor fluctuations in differences in electrical surface potential were observed (Figure 6.3B), which were, on average, 22.07 ± 1.11 mV.

With the addition of cholesterol to the system, the emergence of some small, organized domains in topography are evident, almost double the average height of the fluctuations seen in the cholesterol-free sample, with an average Δh of 0.57 ± 0.05 nm, seen in Figure 6.3C. Because cholesterol is well known to interact preferentially with SM over POPC and other phospholipids, these small domains present in the system are likely the areas that are rich in interacting SM-Chol molecules, with the slightly lower regions being more concentrated in the L_d phase POPC (Ohvo-Rekilä et al, 2002). In V , fluctuations are observed that are slightly more organized than in the cholesterol-free POPC-SM sample, with areas of difference in electrical surface potential (Figure 6.3D) aligning weakly with features seen in topography (Figure 6.3C). The average ΔV for this POPC-SM-Chol system was determined to be 35.70 ± 2.02 mV, a larger average difference than observed in the POPC-SM system, showing that once again, cholesterol has a measurable effect on the electrostatic non-homogeneity of a lipid system.

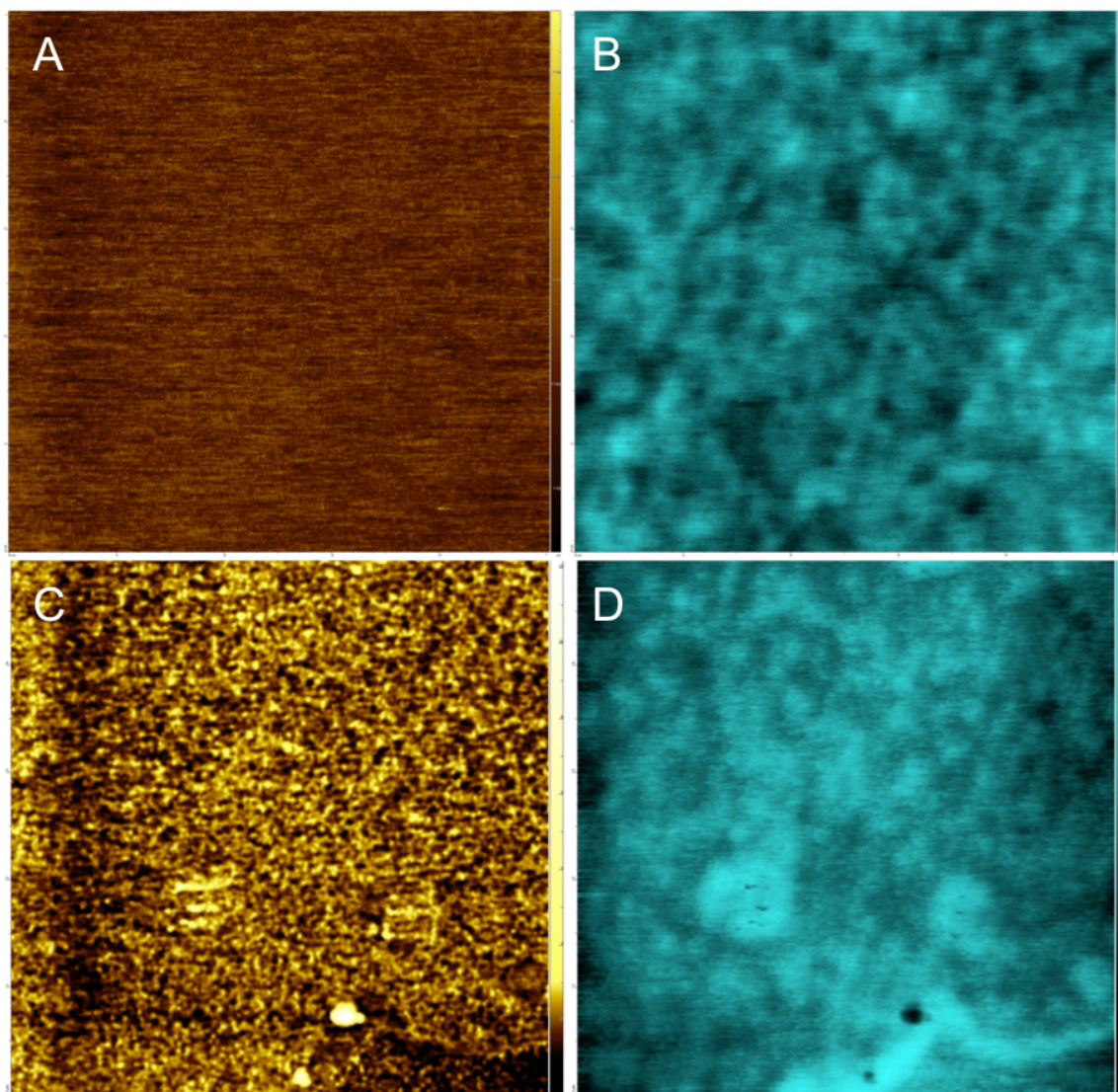


Figure 6.3: AFM and corresponding FM-KPFM illustrating the effect of cholesterol on both the topography and electrical surface potential of a lipid mixture of POPC and SM. AFM images (A) and FM-KPFM images (B) of a POPC-SM (80:20 w/w) mixture are compared to topography captured by AFM and electrical surface potential captured by FM-KPFM of a POPC-SM-Chol (80:10:10 w/w) sample (C and D respectively). AFM and KPFM images were scanned in air in ambient conditions. These images are 2 μm by 2 μm .

This study then moved on to a more complex system, adding DPPC to the previous sample of POPC-SM (Figure 6.4). This DPPC-POPC-SM system was chosen to match lipids commonly found in neuronal cell membranes. As previously mentioned, POPC, DPPC, and

SM are all common constituents of these membranes (Soderberg et al,1991; Prinetti et al, 2001).

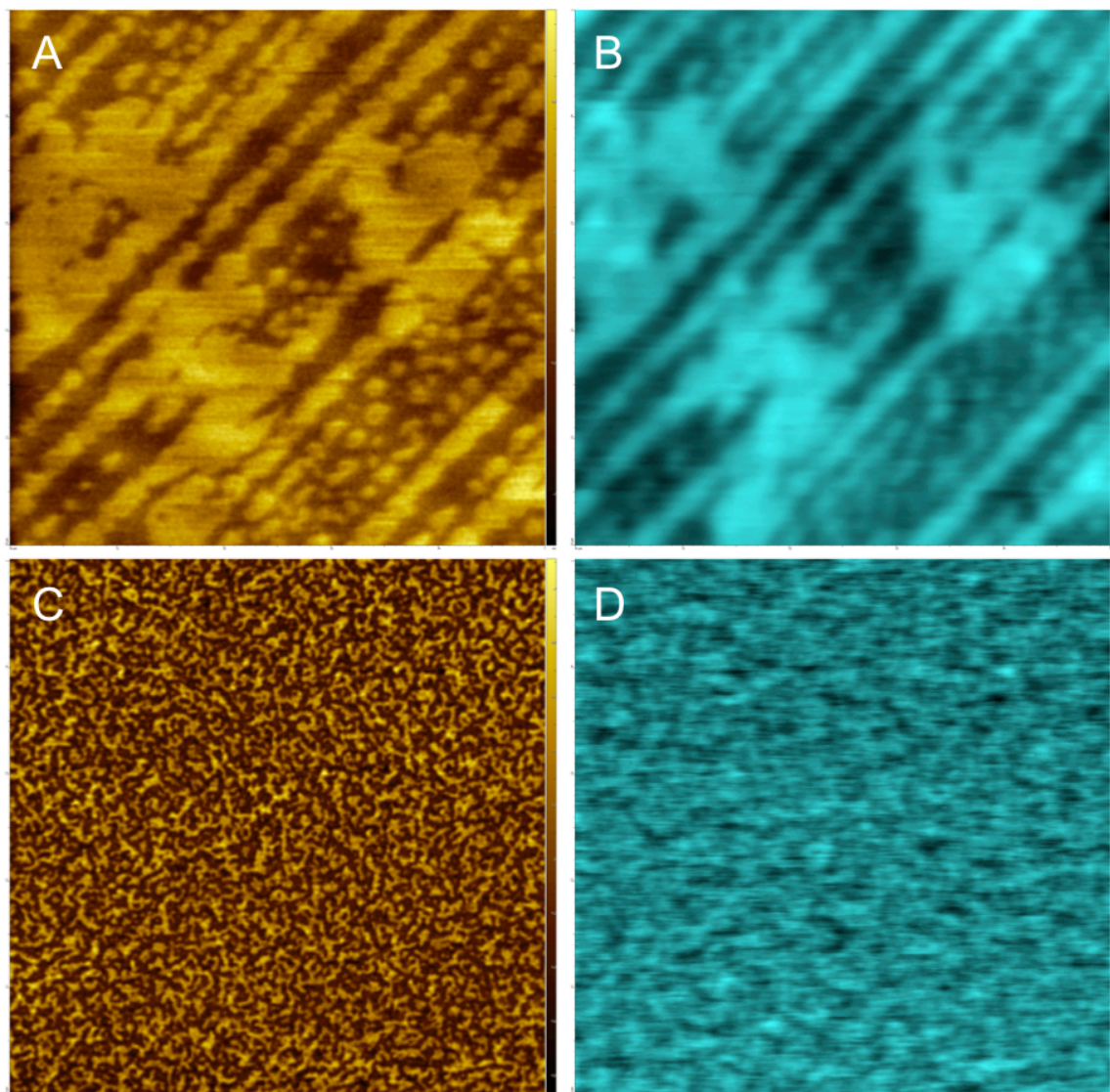


Figure 6.4: AFM and corresponding KPFM illustrating the effect of cholesterol on both the topography and electrical surface potential of a lipid mixture of DPPC, POPC, and SM. AFM images (A) and KPFM images (B) of a DPPC-POPC-SM mixture (40:40:20 w/w) are compared to topography captured by AFM and electrical surface potential captured by KPFM of a DPPC-POPC-SM-Chol (40:40:10:10 w/w) sample (C and D respectively). AFM and KPFM images were scanned in air in ambient conditions. These images are 5 μm by 5 μm.

In the DPPC-POPC-SM sample, two distinct topographical domains are observed (Figure 6.4A). The average difference in height, Δh , of these topographical domains was 0.92 ± 0.03 nm, with lateral dimensions of the higher domains reaching up to 1800 by 2085 nm in area. Because there are two distinct topographical domains but three constituents in this system, most likely the higher domains consist of DPPC and SM which both exist in gel phase at room temperature, while the lower domains are primarily POPC, which exists in fluid phase at room temperature. This idea is supported by comparing the domain roughness values for each domain – the higher domain has a roughness that is almost double that of the lower domains, which is consistent with the idea of two constituents being present in the higher domains versus a single constituent in the lower domain. The surface potential map for this sample (Figure 6.4B) shows electrostatic domains in corresponding locations to the topographical domains. This very ordered surface potential map showed an average difference in electrical surface potential, ΔV , of 215.45 ± 13.12 mV.

In the DPPC-POPC-SM-Chol sample, the addition of cholesterol completely disrupts the organized, large topographical domains seen in the cholesterol-free sample, and instead, small, more plentiful domains that are randomly arranged are observed (Figure 6.4C). The height of the domains is not significantly affected by the addition of cholesterol, with an average Δh of 1.09 ± 0.10 nm compared to the 0.92 nm observed in the cholesterol free sample. However, the lateral dimensions were greatly affected: in the presence of cholesterol, the higher domains only reached sizes of 110 by 115 nm, much smaller than the 1800 by 2085 nm in area observed in the DPPC-POPC-SM sample. This suggests that the addition of cholesterol affected the degree of phase separation of the POPC and DPPC molecules. It is well known that of the three lipids present, Chol will preferentially interact with SM (Ohvo-Rekilä et al, 2002); this fact may also suggest that in the absence of Chol, SM was driving the degree of phase separation of POPC and DPPC by its interactions with them, specifically DPPC. In the presence of cholesterol, however, it no longer does so, which led to a more random arrangement of the lipid molecules in this system. KPFM analysis for this system shows that cholesterol also disrupted the electrostatic domains seen in the DPPC-POPC-SM sample. Instead, at this image size of 5 μm by 5 μm , we see what appear to be random fluctuations in surface potential that do not seem to align with topography as they previously

did in cholesterol's absence (Figure 6.4D). However, when looking at the system at a smaller scale and higher resolution of $2\ \mu\text{m}$ by $2\ \mu\text{m}$, it can be seen that there are correlations between the topography of this system (Figure 6.5A) and the ΔV of the system (Figure 6.5B), showing that there are not just random fluctuations in V present.

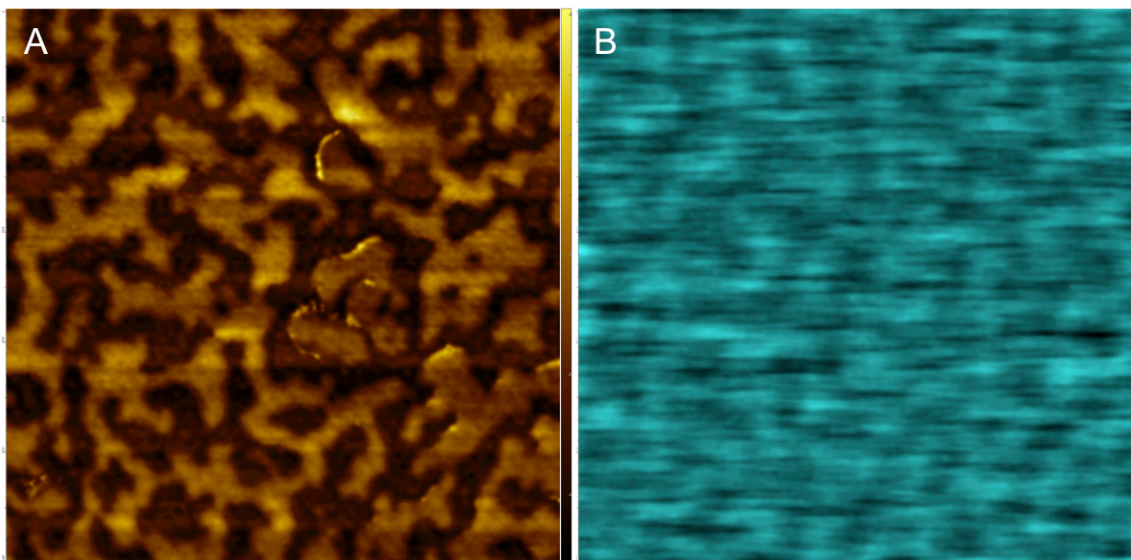


Figure 6.5: Smaller scale image of AFM and corresponding KPFM data for a DPPC-POPC-SM-Chol sample. This image, at a $2\ \mu\text{m}$ by $2\ \mu\text{m}$ scale, shows a closer look at the small topographical domains resolved by AFM (A) of a sample of DPPC-POPC-SM-Chol and the corresponding electrical surface potential features (B) resolved by KPFM that were unable to be visualized at a larger scale, as seen in Figure 6.4.

Despite this correlation between topography and electrical surface potential, the average ΔV was determined to be only $78.74 \pm 4.14\ \text{mV}$, a much smaller difference than the $215.45\ \text{mV}$ observed in the DPPC-POPC-SM sample. This shows that cholesterol can disrupt the electrical surface potential of a sample as well as simply enhancing the differences observed in the DPPC-DOPC-Chol and POPC-SM-Chol samples.

Finally, cholesterol's effect on the V of lipid mixtures containing a charged lipid was examined. DPPC, POPC, and SM all have a neutral net charge, so differences in their surface potential arise from the dipole moments of the lipids. It is also of interest to see if cholesterol can influence the surface potential of a sample that contains a lipid with a

charged head group. To determine this, this study looked at a sample of DPPC (containing a head group with a net neutral charge) and DOPG (containing a head group with a net negative charge). AFM and FM-KPFM images of this system are shown in Figure 6.6.

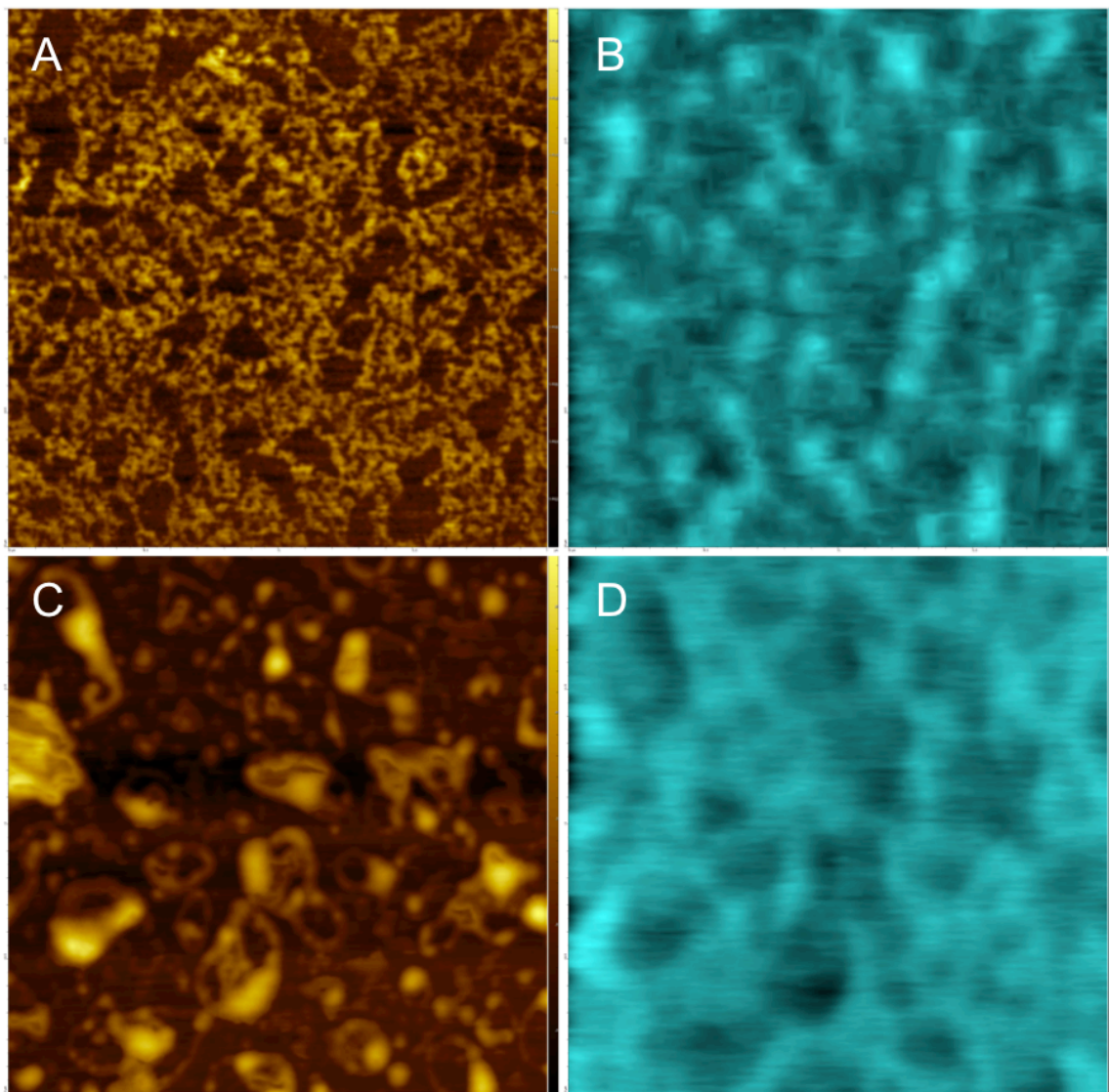


Figure 6.6: AFM and corresponding FM-KPFM illustrating the effect of cholesterol on both the topography and electrical surface potential of a lipid mixture of DPPC and negatively charged DOPG. AFM images (A) and FM-KPFM images (B) of a DPPC-DOPG mixture (50:50 w/w) are compared to topography captured by AFM and electrical surface potential captured by FM-KPFM of a DPPC-DOPG-Chol (40:40:20 w/w) sample (images C and D respectively). AFM and FM-KPFM images were scanned in air in ambient conditions. These images are 2 μm by 2 μm .

Figure 6.6A shows the topography for the pure DPPC-DOPG system; here, distinct differences in topography are observed that likely arise due to the phase separation of gel phase DPPC and fluid phase DOPG. The average Δh for these features was determined to be $0.80 \text{ nm} \pm 0.04 \text{ nm}$. The corresponding KPFM image shows differences in potential (Figure 6.6B) that correspond to the topography differences. On average, there is an average ΔV of $138.67 \pm 6.79 \text{ mV}$.

In the DPPC-DOPG-Chol image, more consistent phase separation is observed, leading to more organized domains, arranged randomly over the surface of the sample, than in the cholesterol-free sample (Figure 6.6C). These surface features have an average Δh of $1.18 \pm 0.06 \text{ nm}$. Interestingly, some areas of the sample show multilayer formation; this feature is normally seen at higher pressures, when the pressure being exerted on the lipid monolayer becomes too much for the lipid mixture and it folds upon itself – forming multilayers in the process – in order to alleviate the high pressure.

The corresponding FM-KPFM image shows electrostatic domains in areas that correlate with topographical domains (Figure 6.6D). Though cholesterol's effect on the ΔV – an average of $117.55 \pm 8.65 \text{ mV}$ for this sample – is only slightly smaller than the 138.67 mV for the DPPC-DOPG sample, it does show that cholesterol influences surface potential in lipid systems containing charged head groups.

Table 6.2: Summary of the Effect of Cholesterol on All Systems Studied. Average difference in height (in nm) and average difference in electric surface potential (in mV) is shown for both the cholesterol-free sample and the cholesterol-present sample. All report effects of cholesterol, unless otherwise indicated, are significant with a confidence level of at least 90% (based on t-test statistical analysis where $N > 50$).

	Average Difference in Height Δh (nm)	Average Difference in Electrical Surface Potential ΔV (mV)
DPPC-DOPC	1.22 ± 0.03	41.60 ± 5.39
DPPC-DOPC-Chol	0.97 ± 0.06	67.25 ± 7.03
<i>Effect of Cholesterol = Decrease in Δh, Increase in ΔV</i>		
POPC-SM	0.35 ± 0.02	22.07 ± 1.11
POPC-SM-Chol	0.57 ± 0.05	35.70 ± 2.02
<i>Effect of Cholesterol = Increase in Δh, Increase in ΔV</i>		
DPPC-POPC-SM	0.92 ± 0.03	215.45 ± 13.12
DPPC-POPC-SM-Chol	1.09 ± 0.10	78.74 ± 4.14
<i>Effect of Cholesterol = No Significant Effect on Δh, Decrease in ΔV</i>		
DPPC-DOPG	0.80 ± 0.04	138.67 ± 6.79
DPPC-DOPG-Chol	1.18 ± 0.06	117.55 ± 8.65
<i>Effect of Cholesterol = Increase in Δh, Decrease in ΔV</i>		

Overall, this study found that cholesterol affects both the height and the difference in potential in all systems, including the most complex system (three lipids) studied. As can be seen in Table 6.2, cholesterol had significant effects on the difference in height in all but one lipid mixture, that being the most complex mixture of DPPC-POPC-SM. However, for changes in difference in surface potential, cholesterol had a significant effect on all the samples studied. Cholesterol's ability to affect the difference in potential of a sample relates to its dipole moment and its effect on the dipole moment of the lipids in the system in question. In general, the dipole moment of a lipid molecule is based on three regions of the molecules: (1) the orientation of the head group region's carbonyl groups; (2) the ester linkage attaching the head group to the lipid tails; and (3) the terminal end of the fatty acid chains of the lipid molecule (Sukhorukov et al, 2001). Because of the cholesterol's orientation in the monolayer, interacting with both the head group and the region of the head

group ester linkage to the fatty acid tails, it has the ability to affect both the dipole moment of other molecules as well as the tilt (which is important in the molecules' "normal dipole moment").

Cholesterol is able to interact with single molecules or cause clustering of molecules, as seen in the formation of lipid rafts and domains. As a result, cholesterol can induce a region's electrical surface potential, forming what are seen as electrostatic domains. In general, it is possible to measure the effect that cholesterol has on a single molecule's electrical surface potential or on a single lipid system's membrane dipole potential, as seen in Starke-Peterkovic et al.'s work (2006); however, when it comes to multiple molecules, it becomes a much more complex issue. This would be the case with domains within the membranes, which could contain thousands of interacting molecules. This is why studies of electrical surface potential and domains are often done with molecular dynamic simulations.

Overall, this study has shown that cholesterol has a measureable effect in all the systems studied. This indicates that cholesterol has measureable effects on the physicochemical properties of lipid systems, even as they increase in complexity of composition. This further supports the idea that cholesterol's presence in the membrane, and in particular its fundamental effect on the electrical surface potential of the membrane, may be largely involved in the membranes interactions with polar or charged biomolecules in nature.

Chapter 7.0 Multicomponent lipid membrane models mimicking “healthy” and “diseased” neuronal membrane states for the study of amyloid toxicity in Alzheimer’s disease.

Summary

It is known that the cellular membrane interacts with amyloid peptides, which are implicated in Alzheimer's disease. We developed and tested multi-component lipid models to mimic healthy and diseased states of the cell membrane in order to study the role of the lipid membrane in amyloid toxicity in relation to Alzheimer's disease. Using atomic force microscopy and Kelvin probe force microscopy, we showed that morphology and electrical surface potential distribution are different in healthy and Alzheimer's disease models, and that these models interact differently with amyloid over time. Using the black lipid membrane technique, we measured the changes in membrane permeability upon amyloid binding and demonstrated that healthy lipid models have higher resistance to amyloid toxicity than Alzheimer's disease model membranes.

Experimental Design and Contributions

Under the supervision of Dr. Z. Leonenko, I designed this experiment, as well as developed the models that hypothesize a healthy and diseased state of a neuronal cell membrane. I carried out the AFM and KPFM monolayer experiments and their data analysis, along with the AFM membrane experiments and amyloid incubation, and their data analysis. These two studies were supplemented with Black Lipid Membrane electrophysiology work that was done by Alexander Negoda from Dalhousie University, under the supervision of Dr. Evgeny Pavlov. I then wrote up all the data for this chapter of my thesis in the format of a manuscript, with the plans to later submit it to a peer-reviewed journal for publishing.

7.1 Introduction

Alzheimer's disease (AD) is a progressive neurodegenerative disease that is connected with severe impairment and deterioration of memory and cognitive function (Coyle et al, 1982; Prince 2009). One of the main features of Alzheimer's disease (AD) is the formation of amyloid-beta ($A\beta$) protein plaques in neurons and cerebral blood vessels (Puglielli et al, 2005). $A\beta$ fibrils are the product of the cleavage of APP (amyloid precursor protein) by a secretase, whose activity and function may be modulated by the lipid environment (Eckert et al, 2010) and the function of both the $A\beta$ peptides and APP itself are still not fully known. $A\beta$ fibrils aggregate to form plaques on the neuron cellular surfaces and can be detected in AD patients (Skovronsky et al, 2000; Baltes et al, 2011). The current widely-agreed upon pathway of fibril formation is that monomers released by the cleavage activity of secretases can oligomerize, and through a series of polymerization, elongation, and bundling processes, amyloid fibrils are formed. Fibrils are approximately 10 nm in diameter and over 100 nm – up to microns – in length (Hardy & Higgins 1992). When these fibrils aggregate together, the aggregates they form are known as plaques; plaques have been found in the affected tissues of over 20 diseases and are insoluble, affecting a great number of regular tissue functions (Hardy & Higgins 1992). $A\beta$ oligomers, fibrils, and plaques serve as a cellular hallmark of AD. Recently it has been shown that oligomers are more toxic to cells than larger fibrils (Rushworth & Hooper 2010), which suggests that the majority of cell damage occurs before the plaques found on neurons and cerebral blood vessels even form. There are currently no drugs to cure or prevent AD; any form of treatment for AD is limited to managing the symptoms. Prospective strategies to prevent amyloid toxicity include arresting the formation of toxic oligomers as well as preventing the damage oligomers cause to cellular membranes. In this work, we discuss the role of lipid membranes in amyloid toxicity.

It is known that amyloid plaques are found on neuron cellular surfaces of individuals diagnosed with AD, and it is accepted that the cellular membrane plays an important role in amyloid toxicity, as specific lipid components (such as gangliosides, like monosialotetrahexosylganglioside [GM1]) bind with $A\beta$ and form a seed structure for plaque formation (Yanagisawa et al, 1995; Yanagisawa & Ihara 1998). Many studies have looked at the effect of the membrane in general and of lipid rafts on AD (Eckert et al 2010; Kim et al

2006; Vestergaard et al, 2008; Friedman et al, 2009; Rushworth & Hooper 2010; Tofoleanu and Buchete 2012; Vestergaard et al, 2010; Terzi et al, 1997; Hane et al, 2011; Matsuzaki 2007). However, there is much left to be determined and the exact role of the lipid membrane and its structure, including membrane rafts, is not clear. Previous studies on the brain membrane lipid composition of AD patients reveal changes in lipid composition as compared to normal controls, such lowering of several types of phospholipids (Pettegrew et al, 2001) and a decrease in SM content due to increased sphingomyelinase activity (He et al, 2010). However, changes in membrane lipid composition occur before the onset of AD symptoms and its corresponding cellular pathology. Recently, researchers demonstrated the predictive power of such changes in lipid composition as an early indicator of AD, showing that decreases in the proportion of various phospholipids and their metabolic derivatives as well as changes in various protein levels in blood plasma, precludes the onset of AD in elderly patients (Mapstone et al, 2014).

Neuronal cells form the core of the nervous system and are one of the primary cell types found in the brain. Neurons can be divided into three functional regions: the dendrites, where signals are received; the cell body or soma, through which a signal is propagated; and the axon, where signals are sent to the dendrites of subsequent neurons. In general, three major lipid types are found in neuronal cell membranes: phospholipids, sterols, and sphingolipids. Studies have shown that phospholipids present in the neuronal cell membrane contain mostly saturated fatty acids, such as dipalmitoylphosphatidylcholine (DPPC); and 18:1 monounsaturated fatty acids, such as 1-palmitoyl-2-oleoyl-sn-glycero-3-phosphocholine (POPC, which contains one saturated chain and one 18:1 monounsaturated chain) or 1,2-dioleoyl-sn-glycero-3-phosphocholine (DOPC, containing two 18:1 monounsaturated chains) (Soderberg et al, 1991; Prinetti et al, 2001). Glycerophospholipids, including phosphatidylserine, phosphatidylinositol, and phosphatidylethanolamine, are restricted to the cytoplasmic (inner) leaflet of the membrane, while most sphingolipids are found in the exoplasmic (outer) leaflet (Vestergaard et al, 2008). Cholesterol, which interacts strongly with sphingolipids, tends to be present in slightly higher levels in the outer leaflet than the inner leaflet (Vestergaard et al, 2008). Gangliosides, a type of sphingolipid, are found nearly exclusively in the outer leaflet of the plasma membrane (Ariga et al, 2008). The cell membrane composition varies depending on what portion of the neuron is in question,

especially in terms of protein content, so the total amount of lipid present in each portion also differs. However, the lipid composition of the different portions of a neuronal membrane only vary slightly – for example, in embryonic rat studies via total lipid extract of dorsal root ganglion cells, the lipid composition of the soma consists of 15.4% cholesterol, 4.8% galactolipid, and 57.1% phospholipid, while neurite (either dendrite or axon) lipid composition consists of 22.1% cholesterol, 7.7% galactolipid, and 56.4% total phospholipid (Calderon et al, 1997). The majority of these differences can be attributed to the difference in the amount of plasma membrane present in general in each of these cell portions (Calderon et al, 1997).

Monolayers and bilayers (model membranes) are widely used to mimic the cellular membrane. Although the cellular membrane is composed of lipids and various proteins, the biophysical properties of the lipid membrane itself are important in many health-related processes (for example, the cellular absorption of drugs, ethanol, and general anesthetics).

While lipid models are very valuable for studying the mechanism of amyloid toxicity, current model membranes cannot be easily related to *in vivo* animal and cellular studies, due to the fact that very simple models are used, often involving a single or few lipids (Vestergaard et al, 2008; Friedman et al, 2009; Maltseva et al, 2004; Qiu et al, 2009; Chi et al, 2007; Fantini et al, 2010; Eckert et al, 2010; Hane et al, 2011; Matsuzaki et al, 2007; Vestergaard et al, 2010; Chakravarthy et al, 2007). For example, using a model membrane containing DOPC and DPPC, where phase separation between the two lipids occurs (akin to lipid raft formation), A β aggregates were found to associate more often with the gel phase (DPPC) regions of the membrane (Choucair et al, 2007). This result lends support to the claim that A β associates preferentially with raft-like structures *in vitro*, but does not address the complexity of lipid rafts *in vivo*. Other previous studies have investigated the interactions of A β in the presence of various simple model membrane systems: for example, it has been shown that in membranes with different charge properties created using one or two types of charged lipid, charge affects both the shape and growth rate of A β aggregations on the model membrane (Hane et al, 2011). As this study and others of simple model membranes involved one- or two-component lipid systems, evaluating more complex model membranes will help bridge our understanding of model systems and *in vivo* systems. Sasahara et al. have used optical and fluorescence microscopy, as well as QCM (quartz crystal microbalance) to

investigate the behaviour of A β in association with a lipid model containing DOPC, DOPS (1,2-dioleoyl-sn-glycero-3-phospho-L-serine), SM, and Chol as well as GM1 (Sasahara et al, 2013). In this more complex model system, specific phase separation properties were observed, A β was found to associate with GM1-rich lipid rafts and restrict the mobility of these lipids throughout the membrane, and partial disintegration of the membrane occurred where A β deposits were found (Sasahara et al, 2013).

There are no suitable models for the healthy and diseased states of neuronal membranes available in the literature, despite the fact that analysis of lipid compositions in healthy and AD human and animal brain tissues show that lipid composition changes in aging and AD (Ariga et al, 2008; Soderberg et al, 1991; Cunnane et al, 2012). Another study showed substantial changes in the amount of phosphatidylethanolamine lipids in the inner leaflet of the membrane in diseased brains as compared to a control brain; however, there was little to no change in the lipid content of the outer leaflet where amyloid species would interact with the cell (Soderberg et al, 1991). Gangliosides are an area of special interest, with some contradicting results as to what occurs to their levels as a result of AD. Reductions in the amount of gangliosides present in the membrane have been observed in several regions of AD brains compared to that of control brains (Svennerholm et al, 1994; Kalanaj et al, 1991; Mlinac and Bonjar 2010; Kracun et al, 1991) while other studies have suggested ganglioside plays a role in the formation of plaques and an increase in GM1 results in an increase of amyloid aggregation *in vitro* (Ariga et al, 2008; Yanagisawa et al, 1995; Yanagisawa et al, 1998). GM1-containing lipid rafts also associate with amyloid aggregates *in vitro*, affecting the lipid raft distribution in the model membrane (Sasahara et al, 2013).

The goal of this work was to build a model that included all major lipids present in the outer leaflet of neuronal cell membranes— phospholipids, sterols, and sphingolipids – corresponding to healthy and diseased states. Based on previous reports (Lingwood & Simons 2010; Sasahara et al, 2013, Yanagisawa 2011) we developed a membrane model that incorporates DPPC, POPC, sphingomyelin, cholesterol, and ganglioside GM1. These lipids are found in neuronal cell membranes in proportions discussed above (Soderberg et al, 1991; Prinetti et al, 2001; Vestergaard et al, 2008; Ariga et al, 2008). *This work hypothesizes that the cellular membrane has different physical and structural properties, due to aging and/or*

AD, as compared to healthy membrane. This may directly affect amyloid toxicity. Amyloid oligomers may be toxic to the cellular membrane in “diseased” or AD membrane states and not to the “healthy” membrane state. This group hypothesizes that the change from the healthy to the diseased membrane state may lead not only to altering the lipid membrane composition, but also the structure, morphology and physical properties of the membrane, such as fluidity and permeability, as well lipid domain (raft) formation. Lipid rafts have been linked to various diseases including AD (Ehehalt et al, 2003; Kim et al, 2006; Wakabayashi & Matsuzaki 2007; Malchiodi-Albedi et al, 2009). These changes may directly affect the interaction of the membrane with A β and thus its toxicity. The mechanism of A β toxicity may be similar to the mechanism of action of antimicrobial peptides, which recognize bacterial and host membranes due to the differences in their lipid compositions and physical properties (Kagan 2012; Caillon et al, 2013; Last & Miraker 2013).

In order to test this hypothesis multicomponent lipid models to mimic “healthy” and “diseased” states of plasma membranes were created based on studies of changes in membrane constituents as a result of AD, with the goal to elucidate if there are any significant structural and morphological differences between these models as well as the differences in A β binding and the damage that A β produces to the healthy vs. AD model membranes.

7.2 Materials and Methods

7.2.1 Lipid Solution Preparation. 1,2-dipalmitoyl-*sn*-glycero-3-phosphocholine (DPPC), 1-palmitoyl-2-oleoyl-*sn*-glycero-3-phosphocholine (POPC), sphingomyelin (SM), cholesterol (Chol), and ganglioside monosialotetrahexosylganglioside (GM1) were purchased from Avanti Polar Lipids (Alabaster, AL) in powder form. Complex mixtures of these five constituents were made for analysis, and are outlined in Table 7.2. All other chemicals used were of reagent grade.

7.2.2 Supported lipid monolayers for Atomic Force Microscopy (AFM) and Kelvin Probe Force Microscopy (KPFM) imaging. Phospholipid monolayers were supported on freshly cleaved mica (Ashville-Schoonmaker Mica Co., Newport News, VA) by the method of Langmuir-Blodgett (LB) deposition using a KSV-Nima LB microtrough (Biolin Scientific,

Stockholm, Sweden). For sample preparation, solutions of lipid dissolved in chloroform at a concentration of 1 mg/mL (lipid/chloroform) were spread at the surface of the subphase and depositions were taken at a pressure control of 35 mN/m with a dipper arm speed of 2 mm/min. The mica slide was allowed to air-dry for 10 minutes before being placed in a dessicator for a 24-hour period, prior to further analysis.

7.2.3 Supported lipid bilayers and amyloid incubation for AFM imaging. Hydrated phospholipid bilayers were supported on freshly cleaved mica via vesicle fusion, which utilizes uniformly sized vesicles in Nanopure water. A β_{1-42} (rPeptide, Bogart GA) was pretreated to ensure monomeric form (according to Fezoui procedure) and suspended in HEPES buffer (20 mM HEPES, 100 mM NaCl, pH 7.4) at a concentration of 40 mM (amyloid/buffer). 100 μ L of the amyloid solution was added to pre-formed membranes and incubated for increasing time periods; at the end of the time period for each membrane, excess amyloid was gently rinsed away in order to stop the fibrilization process, with complete hydration maintained at all times. The final membrane was hydrated in Nanopure water. At least three separate incubation investigations were performed for each set of samples.

7.2.4 AFM and KPFM Imaging – Monolayer Samples. AFM imaging was conducted of monolayers supported on mica affixed to a conductive plate to allow for KPFM to be performed simultaneously, using SmartSPM 1000 (AIST-NT) in air at room temperature and normal humidity using a MikroMasch gold coated cantilever (HQ:NSC14/Cr-Au, MikroMasch USA, Lady's Island, SC) with a resonance frequency of 160 kHz and a spring constant of 5.0 N/m. Monolayer imaging was conducted in ambient air at normal humidity. The AIST-NT instrument allows for simultaneous AFM-KPFM imaging to be collected (where each scan line is done in a two-pass technique, where the first pass scans for topography and the second scan for surface potential); as such, AFM and KPFM images of the sample correspond to the sample location. AFM imaging of hydrated membrane and amyloid incubated membrane samples on a mica substrate were performed using Magnetic-Alternating-Current (MAC) mode on an Agilent AFM/SPM 5500 using Keysight Type II MAC mode rectangular cantilevers (force constant of 2.8 N/m and a resonance frequency in water of 30 kHz). Membrane imaging was conducted at ambient room temperature in liquid

(Nanopure water), with hydration of the membrane maintained at all times throughout imaging.

7.2.5 AFM/KPFM Data Processing and Analysis. Data collected was processed using SPIP and AIST-NT image processing software. The topography images were plane corrected by means of global levelling and global bow removal and filtered using noise reduction caused while scanning with high resolution Z-scale (picometers). KPFM images were not processed with any filters, to ensure the proper potential measurements; the raw data was used for average surface roughness analysis to investigate differences between electrical surface potential. Statistical analysis of AFM topography and KPFM electrical surface potential images and surface roughness was done using Gwyddion and AIST-NT image processing software. Data was collected on 2 μm by 2 μm and 5 μm by 5 μm high-resolution images of monolayer and membrane samples (for Δh through cross-section analysis, $n = 50$; for ΔV through roughness analysis, $n > 10$). All quantitative results are presented as mean \pm standard error, with significance determined using ANOVA tests. Any results determined to be significant are reported with a 95% confidence level.

7.2.6 Planar lipid bilayers for Black Lipid Membrane (BLM) study. Planar BLM were formed from a 15 mg/mL lipid solution in n-decane (Aldrich). The solution bilayer was formed across the 200 μm aperture of a Delrin cup (Warner Instruments, Hamden, CT) by direct application of lipids. Both *cis* (voltage command side) and *trans* (virtual ground) compartments of the cup cuvette contained 150 mM NaCl, 2 mM CaCl_2 , 10 mM Tris-HCl pH 7.4. 5 μM $\text{A}\beta$ was added to the *cis* compartment of the cuvette. All measurements were performed at room temperature.

7.2.7 BLM recording and data analysis. Currents flowing across BLM lipid bilayers were recorded with a Planar Lipid Bilayer Workstation (Warner Instruments, Hamden, CT). The *cis* compartment was connected to the head stage input and the *trans* compartment was held at virtual ground via a pair of matched Ag/AgCl electrodes. Signals from voltage-clamped BLM were high-pass-filtered at 2.1 kHz using an eight-pole Bessel filter LPF-8 (Warner Instruments), digitized (Data Translation digitizer) and recorded on PC after digitization using a homemade analog-to-digital converter acquisition software. For the statistical

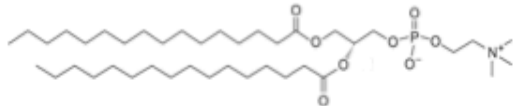
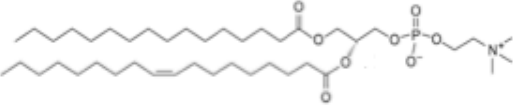
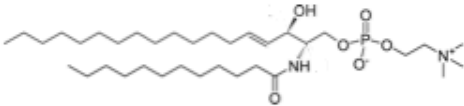
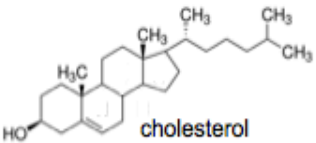
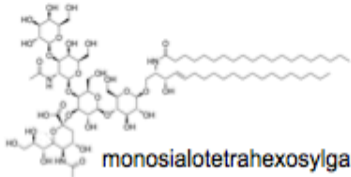
analysis data were averaged from at least three independent experiments and analyzed using Origin software. Experiments were performed in three separate trials for each sample. Each recorded trace was analyzed to get obtain the mean value of conductance. Results are expressed as mean \pm standard error of the mean (S.E.M.), with significance determined using ANOVA tests.

7.3 Results and Discussion

Though there have been numerous studies on the interaction of lipid monolayers and membranes with amyloid peptides in relation to Alzheimer's research (Vestergaard et al, 2008; Friedman et al, 2009; Maltseva et al, 2004; Qiu et al, 2009; Chi et al, 2007; Fantini et al, 2010; Eckert et al, 2010; Hane et al, 2011; Matsuzaki et al, 2007; Vestergaard et al, 2010; Chakravarthy et al, 2007), many studies are carried out using simpler systems, consisting of one or few lipids. For example, studies have been conducted looking at amyloid interactions with DPPC systems and DOPC systems (Hane et al 2011; Choucair et al, 2007; Sheikh et al, 2012), DPPC-POPC systems (Kotarek & Moss 2010), and POPC-POPS systems (Dante et al, 2011). Studies have also looked at systems of ganglioside in combination with another lipid, like GM1-POPC and GM1-DPPC systems (Chi et al, 2007; Morita et al, 2012). However, studies involving more complex, multicomponent lipid systems are necessary to truly match the complexity of a neuronal cell membrane, which consists of many lipids as well as other components like cholesterol and proteins. Based on the lipids commonly found in the outer leaflet of neuronal cell membranes (discussed in the introduction), we developed more complex model lipid membranes, consisting of five constituents, in order to try and approach this complexity.

For this investigation, we looked at three different multicomponent lipid systems consisting of DPPC, POPC, sphingomyelin (SM), cholesterol (Chol), and ganglioside monosialotetrahexosylganglioside (GM1), in order to begin to approach this neuronal cell membrane complexity. The structure and some important properties of these lipids are shown in Table 7.1.

Table 7.1: Structures and Properties of Lipids Studied. This table outlines information about the 5 constituents of the systems studied: DPPC, POPC, SM, Chol, and GM1. Phospholipid phase at ambient room temperature is indicated as samples were studied under these conditions. Dipole moment value is included due to its relevance in the KPFM study portion of this work. Lipid structures were adapted from Avanti Polar Lipids. (¹Beitinger et al, 1989; ²Vogel et al, 1988; ³Brockman 1994; ⁴Paiva et al, 2013; ⁵Prenner et al, 2007).

Structure and name	Abbreviation	Phase at 25°C	Phase transition temperature (°C)	Dipole moment (D)
 1,2-dipalmitoyl-sn-glycero-3-phosphocholine	DPPC	Gel	41	+0.82 ¹
 1-palmitoyl-2-oleoyl-sn-glycero-3-phosphocholine	POPC	Fluid	-2	+0.473 ³
 N-(dodecanoyl)-sphing-4-enine-1-phosphocholine	SM	Gel	~ 37	+0.30 ⁵
 cholesterol	Chol	-	-	+0.40 ⁴
 monosialotetrahexosylganglioside	GM1	Fluid	~ 20	-0.171 ¹

We developed models to reflect a healthy membrane, a membrane beginning to enter the diseased state (with a decrease in GM1 content, noted as “diseased 1”), and a membrane of an increasingly diseased state (with a decrease in both GM1 and SM content, noted as “diseased 2”), based on observations of membrane changes as the result of AD observed *in*

vivo (Ariga et al, 2008; Soderberg et al, 1991). Each model consists of differing ratios of the same model composition: DPPC-POPC-SM-Chol-GM1, shown in Table 7.2.

Table 7.2: Detailed description of complex lipid systems studied. Lipid mixtures are all comprised of the same components but differ in their ratios (by weight) based on documented changes in membrane composition as a result of AD.

Lipids	Ratio
DPPC – POPC – SM – Chol – GM1	37 : 37 : 10 : 10 : 6
-mimics a “healthy” neuron	
DPPC – POPC – SM – Chol – GM1	39 : 39 : 10 : 10 : 2
-mimics a neuron beginning to enter the “diseased” state with a decrease in the GM1 content (Diseased 1)	
DPPC – POPC – SM – Chol – GM1	42 : 42 : 4 : 10 : 2
-mimics an increasingly “diseased” neuron with a decrease in both GM1 and SM content (Diseased 2)	

The DPPC – POPC – SM – Chol – GM1 mixture with ratios of 37:37:10:10:6 is our proposed model for a healthy neuronal cell membrane and is the basis for comparison when it comes to the diseased models. As previously mentioned, these five constituents are commonly found in the outer leaflet of a general neuronal cell membrane, and were chosen for that reason. Mass/mass ratios were utilized to allow for easier comparison to our earlier works (Hane et al, 2011; Drolle et al, 2012) and general relative ratios were decided upon based on extrapolation from studies of lipid content in neuronal cells (Calderon et al, 1997). It is known that Chol preferentially interacts with SM over other lipids (to be specific, the interaction of cholesterol with phospholipids, in decreasing order of preference, is: SM > PC > PS > PE) so it is of interest to see if the preferential interactions of SM and Chol can be visualized (Ohvo-Rekila et al 2002).

The second sample, with a ratio of 39:39:10:10:2 (i.e. a decrease in GM1) was chosen because of the previously mentioned study that showed that reductions in the amount of gangliosides present in the membrane have been observed in several regions of AD brains compared to that of control brains (Ariga et al, 2008). Furthermore, the above sample of

DPPC-POPC-SM-Chol also may serve as a hypothetical model for a neuronal membrane of a patient with progressed Alzheimer's, as studies have suggested that the levels of GM1 tend to decrease as AD progresses until GM1 is no longer present in the membrane (Fantini et al, 2010, Ariga et al, 2008). It should be noted that the decrease in the amount of GM1 comes at the expense of an increase in the relative amount of phospholipid (i.e. DPPC and POPC content). Though research has shown that there are changes in the phospholipid content in a membrane, it was shown to be primarily negatively charged lipids found on the inner membrane (i.e. phosphatidylserines) rather than phosphatidylcholines; despite this, we chose to maintain the cholesterol and sphingomyelin content as we would expect changes in their relative amount to have a larger impact on the system morphology, especially in relation to lipid rafts, than the phosphocholines.

Lastly, the final sample has a decrease in both GM1 and SM compared to our hypothetical model of a healthy neuronal membrane, with a DPPC – POPC – SM – Chol – GM1 ratio of 42:42:4:10:2. This decreased amount of SM was chosen because studies have shown that AD may be associated with a decrease in SM content due to increased sphingomyelinase activity (He et al, 2010). It is important to note that analysis on a system with an increase in cholesterol was also conducted; however, it did not show any significant difference, both qualitatively and quantitatively, from the healthy system and thus was not further studied in this work.

We used both scanning probe microscopy methods and black lipid membrane studies to look at changes in structure and electrostatic properties between these lipid systems in monolayer form and to investigate changes in membrane permeability and topography upon amyloid binding to the membrane. Figure 7.1 depicts the changes in topography, investigated using atomic force microscopy (AFM), and electrical surface potential, investigated using Kelvin probe force microscopy (KPFM), observed between the three models.

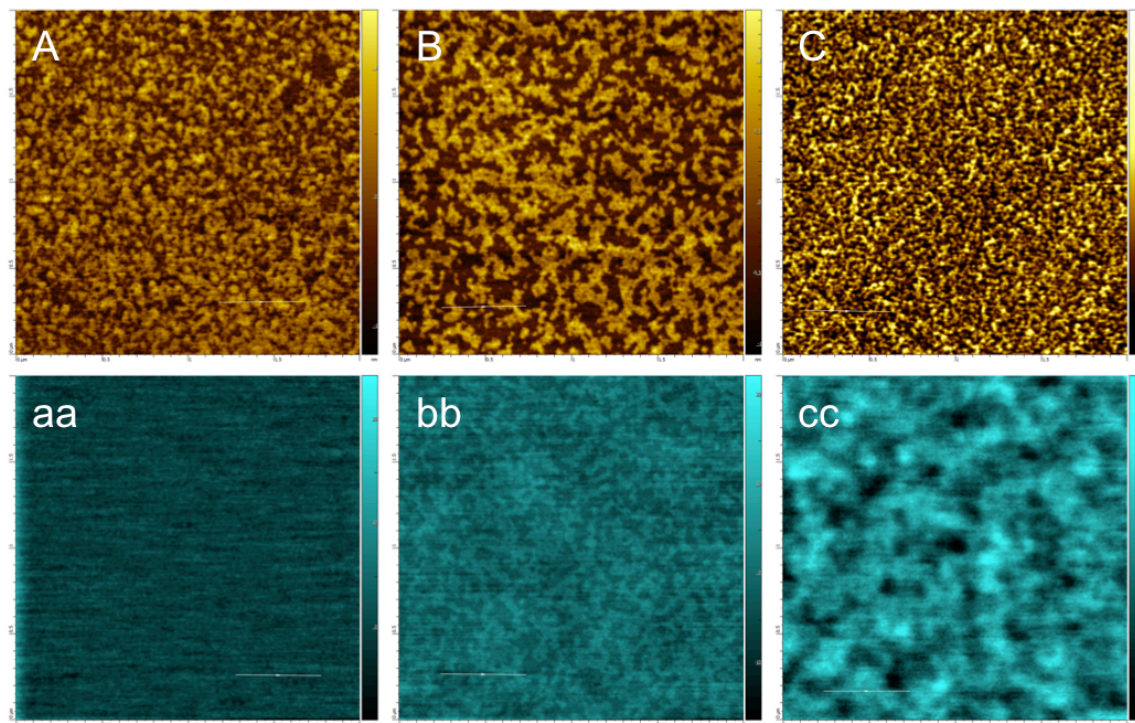


Figure 7.1: Comparison of topography and electrical surface potential results for each system studied. This image depicts the AFM topography (in gold) and KPFM electrical surface potential (in blue) results for healthy (A/aa), diseased 1 (B/bb), and diseased 2 (C/cc) model systems. All images displayed are $2\ \mu\text{m} \times 2\ \mu\text{m}$.

The healthy model (Figure 7.1A) shows small nanodomains spread across the monolayer with an average differences in height (Δh) of $0.986 \pm 0.02\ \text{nm}$, likely arising due to preferential interactions of the lipids with one another. As pure DPPC and POPC are normally in separate phases at ambient room temperature – liquid crystalline (L_c) and liquid disordered (L_d) respectively – phase separation would also be expected to contribute to the nanodomain formation, creating “higher” domains (the L_c domains, or due to the presence of cholesterol in the sample, cholesterol-induced liquid-ordered phase domains, L_o) and “lower” domains (the L_d regions). The lateral dimensions of the higher domains present ranged from 22.5 nm by 40.1 nm (width [X] x length [Y]) up to over 200 nm by 52 nm. These higher domains are likely to be rich in DPPC, SM, and Chol molecules, which are in L_o phase at room temperature when in the presence of cholesterol (as seen in Table 7.1), as well as GM1 molecules, known to associate with saturated phospholipids, SM, and Chol in lipid rafts. The lower regions (darker areas of the topography) between the higher domains for the most part

were very small, primarily less than 20 nm across; however, in certain few areas, larger lower domains between could be seen, up to 150 nm across. These lower regions are likely areas of high concentration of POPC molecules, which are in L_d phase at room temperature. In terms of KPFM results, this model shows some minor fluctuations in electrical surface potential (V) across the surface of our system (Figure 7.1aa), though no discernable patterns in difference in V are observed, despite all the constituents of the membrane having differing dipole moments (see Table 7.2). The V average roughness (ΔV , variances in electrical surface potential) of the sample was 24.64 ± 1.10 mV (as seen in Table 7.3).

In the diseased 1 model (Figure 7.1B), the formation of irregularly shaped higher domains are observed, more organized and larger in area than seen in the healthy model, reaching up to 525 nm across in size. This increase in organization also led to an increase in the number of lower regions between the higher domains (devoid of similar surface features) of between 35 and 200 nm across, with lower domains of larger dimensions (closer to 200 nm) more common. The higher domains also appear slightly more ordered than those in the healthy model, with average Δh values of 1.051 ± 0.016 nm, though they are not significantly different from the differences in height observed in the healthy model (0.986 nm). These observations may be attributed to less GM1 present in these domains saturated with Chol and SM, allowing for the preferential interaction of Chol and SM to be more visible in the higher domains in topography, causing the increased ordering. The diseased 1 sample (Figure 7.1bb) displayed organized, nanoscale electrostatic domains (domains less than 1000 nm in terms of lateral dimensions) that correspond to the nanodomains seen in the topography for this sample. This translated into a higher overall ΔV of 70.47 ± 5.41 mV, which is the highest average difference in electrical surface potential roughness observed for all the samples. As this system is hypothesized to model the environment where the small oligomeric species of amyloid – thought to be most toxic – begin to interact with the cell membrane, having a larger deviation across the sample in terms of electrical surface potential is expected, as it would have a greater likelihood of attracting charged amyloid species.

The size of lower regions are also quite interesting in terms of having larger areas of less organized locations in the lipid system where amyloid may be able to insert itself more

readily to form ion channels. According to Connelly et al., amyloid is able to directly interact with a DOPC lipid bilayer and insert itself to form ion-conductive pores with an average outer diameter of 7.8 - 8.3 nm (Connelly et al, 2012). We hypothesize that amyloid would most easily be able to form pores in less ordered areas of the membrane; thus, the lower regions seen in our monolayer systems, which are rich in disordered lipids, would serve as such locations. As well, the larger the disordered regions, the more potential pores could be formed.

The diseased 2 model (Figure 7.1C) showed a disruption of the larger, more ordered domains from the diseased 1 model to a topography of similarly irregularly shaped features though smaller in area (in terms of lateral dimensions) and more plentiful in number. The domains tend to be quite narrow, with an average width of about 25 nm, and did not exceed 180 nm in length. The size of the lower domains (between the higher domains) also decreased when compared to the diseased 1 system, with widths ranging from 27 to 40 nm. We also observe a drastic decrease in the average difference in height of the surface features when compared to the other samples studied. The microdomains observed in the diseased 2 model had an average Δh of 0.500 ± 0.03 nm, which is significantly different than both the healthy model system and the diseased 1 model system. This is likely due to the lower amounts of SM present in these domains, causing a decrease in order that leads to a decrease in difference in domain height and the larger domain lateral dimensions. For KPFM, this model showed notable patches across the sample of differing electrical surface potential (V) (Figure 7.1cc); however, these fluctuations in V did not correlate with the diseased 2 model's corresponding topography image (Figure 7.1C) and yielded an average difference in potential, ΔV , of 11.63 ± 0.59 mV, the smallest average ΔV observed between all the samples, including the healthy system. As this is the sample corresponding to a "fully" diseased 2 system, having even less variation in potential than the healthy system may contribute to alterations in the cell's interactions with charged molecules, like the charged A β peptide in AD.

Table 7.3 compares the average Δh and ΔV values for each of the three systems studied.

Table 7.3: Summary of Statistical Analysis of Mixed Lipid Monolayer Samples. In terms of topographical domains, those of the healthy and diseased 1 model are not significantly different; the diseased 2 model is significantly different from both. All three systems' differences in electrical surface potential are significantly different from one another.

	Healthy Model	Diseased 1 Model	Diseased 2 Model
<i>Topographical Domains</i>			
Δh	0.986 ± 0.02 nm	1.051 ± 0.016 nm	0.500 ± 0.03 nm
<i>Features in Electrical Surface Potential</i>			
ΔV (uncorrected)	24.64 ± 1.10 mV	70.47 ± 5.41 mV	11.63 ± 0.59 mV

Next, we used Black Lipid Membrane (BLM) techniques to study the effects of A β on lipid bilayer conductance. This method allows for the measurement of ion currents across the membrane and membrane permeability to ions. Two chambers that are filled with buffer solution are separated by a partition that has a very small aperture made in a thin layer of hydrophobic material; the lipid bilayer forms across this hole and an electrode is put into both chambers to allow for measurement of the electrical properties of this bilayer (Winterhalter 2000). This set up can be visualized in Figure 7.2.

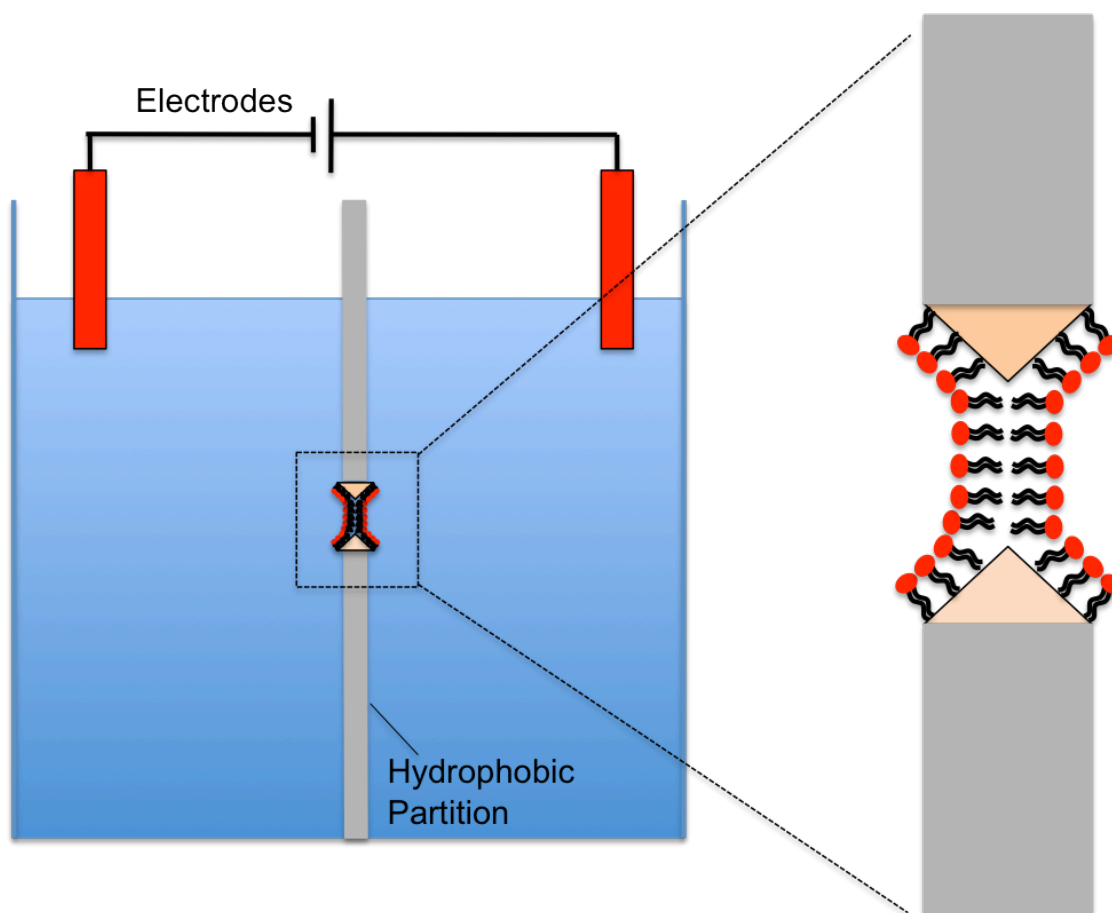


Figure 7.2: Experimental Set Up of a Black Lipid Membrane (BLM) Experiment. This figure depicts how a BLM study would be set up: two chambers containing buffer solution are separated by a hydrophobic partition that has a small hole in it, over which a bilayer is formed. Electrodes submerged in both chambers allow for measuring electrical properties of the bilayer formed. (Adapted from Winterhalter 2000).

We compared currents measured across lipid bilayers of three different compositions corresponding to our models studied in the monolayer portion of this experiment. These systems, in bilayer form, were studied in the absence and the presence of amyloid- β_{1-42} peptide in order to investigate changes in membrane permeability caused by amyloid binding. Ion current, which corresponds to and is directly affected by pore openings, was measured for the membranes.

Interestingly, we found significant conductance in the “healthy” system without the addition of the A β (Figure 7.3A). The addition of 5 μM A β to this model led to an increase in

conductance level; however, the increase was not significant (Figure 7.3A Left panel, $p=0.053$, $n=4$).

For the diseased 1 membrane model, we found that the addition of amyloid to the system caused a significant increase in the conductance of the membrane, which increased with time. This is visible in Figure 7.3B ($p=5*10^{-6}$, $n=11$), which illustrates an increase in conductance after 15 minutes of amyloid incubation versus 5 minutes.

Finally, for the diseased 2 model, we also observed that the addition of amyloid led to a significant increase in the conductance of the membrane over time in comparison to the conductance measured in this system in the absence of any peptide. This is depicted in Figure 7.3C (2C, $p=0.003$, $n=8$).

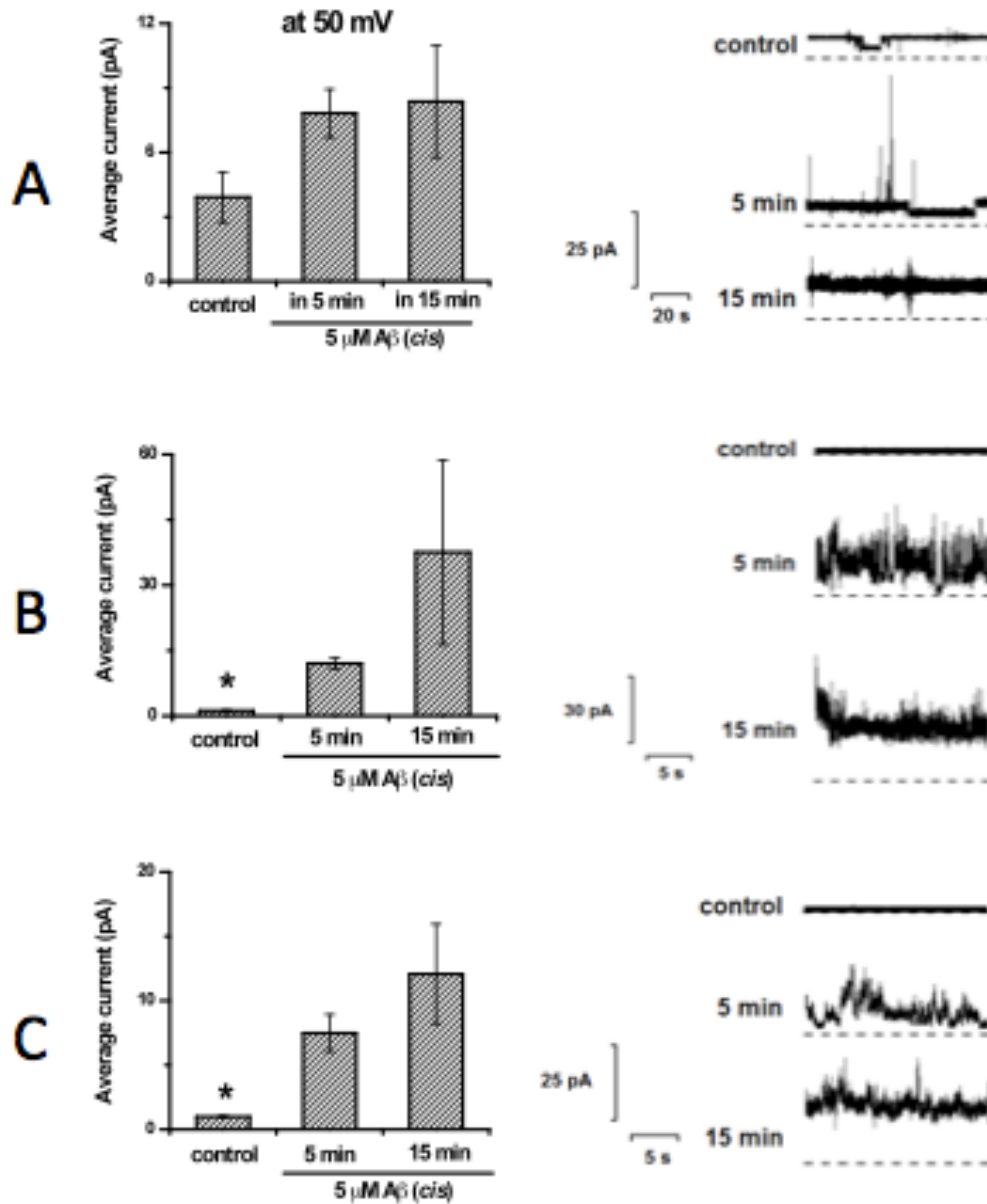


Figure 7.3: Ion currents observed across the membrane with “Healthy” lipid composition (A), “Diseased 1” lipid composition (B), and “Diseased 2” composition (C). Lipid membranes were suspended between symmetric aqueous solution of 150 mM NaCl, 2 mM CaCl₂, 10 mM Tris pH 7.4. Left panel for each section shows average current at the voltage amplitude of 50 mV under control conditions (no additions), in 5 min after induction of conductance by the A β , in 15 min after induction of conductance by the A β . Representative currents at 50 mV have shown at the right panel. * indicates significantly lower current.

As previously mentioned, we also noticed that the current on all of the tested membrane models increased gradually with time as the membrane disintegrated. A comparison of the amyloid incubated models and their membrane conductance is shown in Figure 7.4.

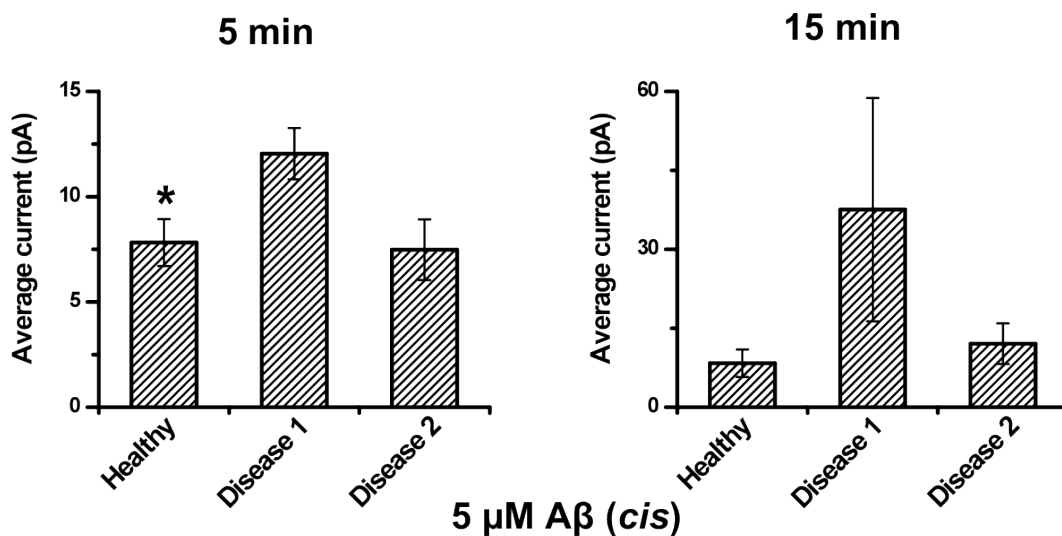


Figure 7.4: Comparison of the currents induced by 5 μM of $\text{A}\beta$ on different model membranes at voltage amplitude of 50 mV. * indicates significantly lower current of the healthy system versus the disease 1 system.

Of the three models, we found that the highest current amplitude was observed in the “diseased 1” model membranes (Fig 7.4, Left: $p=0.03$, $n=11$; Right: $p=0.3$, $n=3$). . This observation suggests that $\text{A}\beta$ has the highest pore forming activity on the membranes with this lipid ratio among the tested models. This is consistent with our findings from the monolayer study, where we saw that the diseased 1 system had larger regions of the less ordered, lower domains (Figure 7.1). These less ordered areas could serve as sites where amyloid would be able to more readily form pores than in the more ordered regions of the system.

Finally, because it was observed via BLM that amyloid damage is present in two of the systems studied (due to the significant increase in conductance with the addition of amyloid observed in those two systems), we wanted to visualize what is happening in the membrane when amyloid is introduced and what the differences between the three systems are. It is thought that, similar to what was seen in the monolayer study portion of this investigation,

the systems in bilayer form would differ from one another in both topography and in electrical surface potential. Because amyloid is a charged species, with a complex charge distribution, we believe these fluctuations in electrical surface potential would affect the interaction of the amyloid species with the membrane, leading to different binding patterns for each. Figure 7.5 shows an example of a potential arrangement of lipids in a complex system and how the different regions of the membrane with their differing electrical surface potential can serve as preferential initial binding sites for amyloid species.

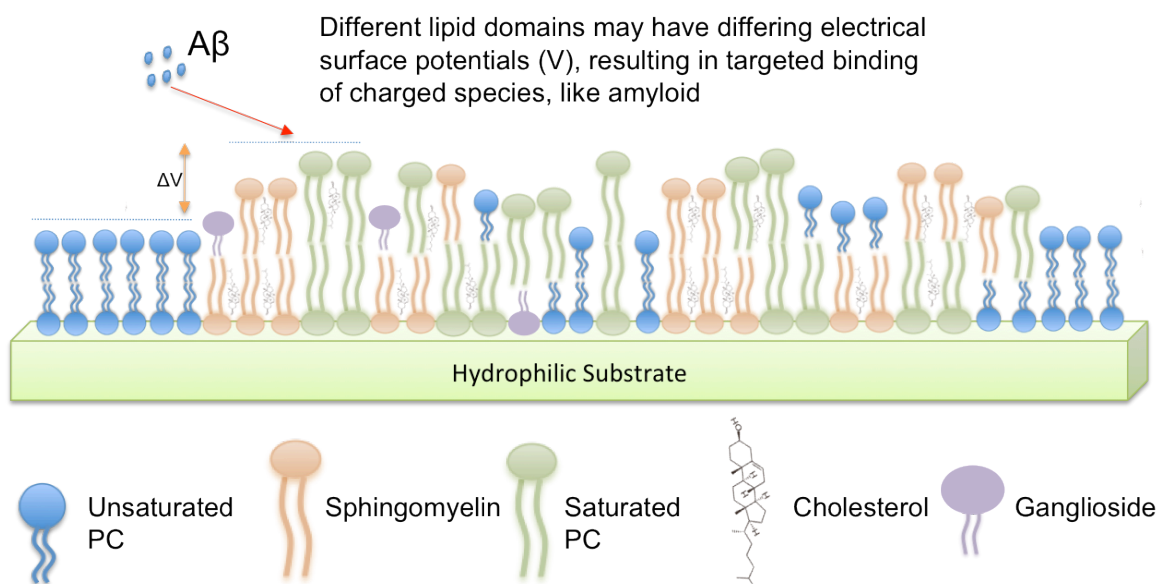


Figure 7.5: Schematic of amyloid beta interacting with a model membrane (not to scale).

This depicts a potential arrangement of lipids consistent with those present in our model systems at one particular location of a bilayer. Here we show that we hypothesize that the arrangement of the lipids, based on factors like preferential interaction and phase separation, leads to membrane nonhomogeneity. This nonhomogeneity leads to fluctuation in surface features, but also can lead to fluctuations in electrical surface potential, which may affect initial points of interaction for charged species, like amyloid beta. Note that this schematic is a hypothesized model for how a particular area of the membrane may be organized.

Membranes were formed for each of the three complex lipid systems and incubated solutions of amyloid in its monomeric form atop the membrane for four time periods: 1, 4, 6, and 24 hours. We then imaged them using the AFM in liquid, in order to maintain membrane hydration. Through atomic force microscopy in a liquid environment, four main factors were

investigated: 1) how amyloid binds to the membrane; 2) the amount of amyloid binding and accumulating over time; 3) the morphology of the amyloid species interacting with the membrane; and 4) whether the presence of amyloid-induced membrane damage.

The differences in amyloid accumulation over time, measured from surface roughness, are shown in Figure 7.6 and quantitatively in Table 7.4.

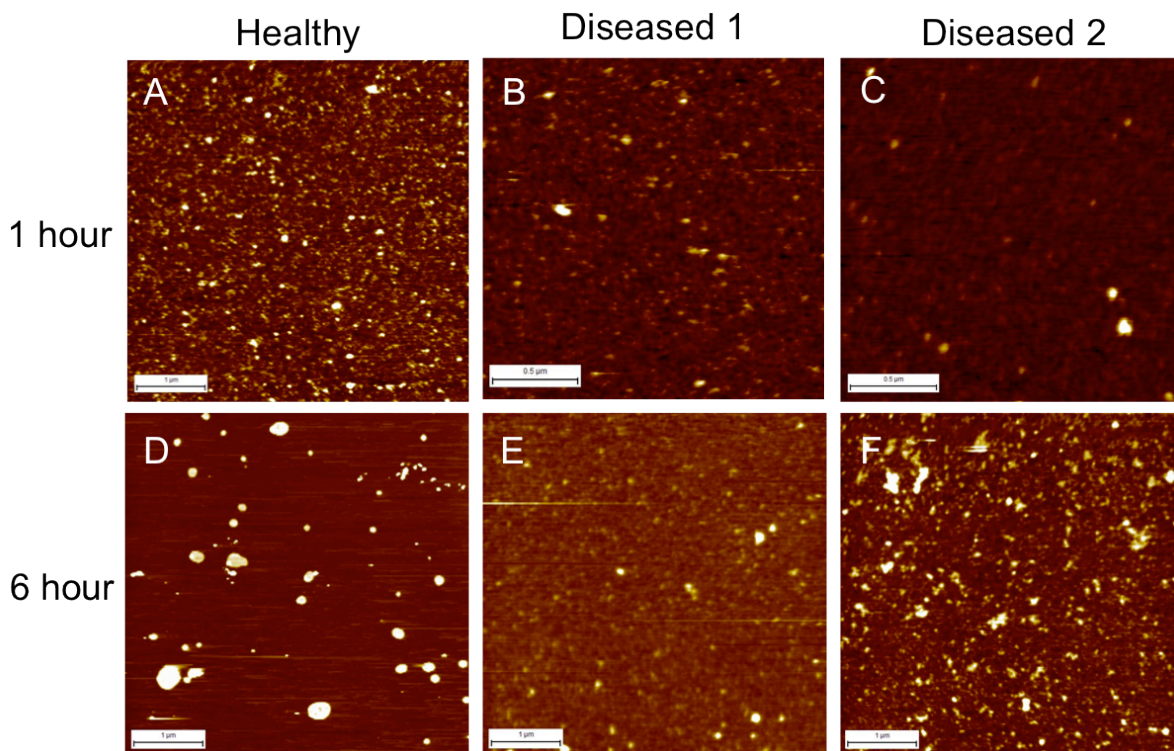


Figure 7.6: Comparison of Amyloid Incubation on Three Different Model Membranes for Increasing Time Periods (1 and 6 Hours). This figure illustrates the difference in amyloid accumulation between 1 and 6 hours of incubation time on a healthy model membrane (A and D respectively), a diseased 1 membrane (B and E) and a diseased 2 membrane (C and F). Image sizes are shown via the ruler scale bar in the left bottom hand corner of each image. Quantitative information for this data (i.e. differences in heights of surface features) are shown in Table 7.4.

In the healthy system, we observe that the surface roughness increases over time and larger clusters are formed over time. This means that amyloid accumulation progressively increases with increasing incubation time. After 1 hour of incubation (Figure 7.6A) we see a layer of

aggregates randomly spread across the surface of the membrane, with a roughness of 0.2674 ± 0.05 nm. With increasing time, we still see a random accumulation of amyloid oligomers and aggregates on the membrane, with the roughness increasing as incubation time increases: after 4 hours of incubation, average surface roughness is 0.5362 ± 0.11 nm; after 6 hours of incubation (Figure 7.6D), roughness is 0.5412 ± 0.074 nm; and after 24 hours of incubation, amyloid accumulation gave a surface roughness of 1.596 ± 0.19 nm. This is indicative of amyloid accumulated on the top of the membrane surface and an increase in the size of the amyloid species and clusters.

Table 7.4: Amyloid Deposition Over Time. This table depicts the amount of amyloid deposited onto incubated model membranes for four time periods. Amyloid accumulation is quantified via surface roughness measurements,. Data is presented as mean \pm S.E.M.

	Healthy (nm)	Diseased 1 (nm)	Diseased 2 (nm)
1 Hour	0.2674 ± 0.05	0.4873 ± 0.027	0.3815 ± 0.033
4 Hour	0.5362 ± 0.11	0.4249 ± 0.03	1.366 ± 0.12
6 Hour	0.5412 ± 0.074	0.5776 ± 0.11	0.366 ± 0.045
24 Hour	1.596 ± 0.19	0.4438 ± 0.19	0.5455 ± 0.026

In the diseased 1 system, we see a change in the accumulation pattern (based on surface roughness) over time, in comparison to the healthy system. After 1 hour of incubation (Figure 7.6B), we have a higher surface roughness than the same incubation time in the healthy model, with an average surface roughness of 0.4873 ± 0.027 nm. This indicates more amyloid accumulation than in the healthy system, though there is no discernable difference in the size and shape of amyloid species on the surface, as in both systems, we see small, spherical and irregularly shaped oligomers and aggregates that are, on average, 100 nm in diameter. However, as time progresses the roughness actually fluctuates between decreases and minor increases: after 4 hours of incubation, we see a decrease in surface roughness to 0.4249 ± 0.03 nm; after 6 hours (Figure 7.6E), the surface roughness increases slightly to 0.5776 ± 0.11 nm; and after 24 hours of incubation time, the average roughness decreases again to its lowest of all the time periods, to 0.4438 ± 0.19 nm. This is indicative of amyloid

species actually causing deformations in the membrane; these deformations lead to amyloid being able to penetrate slightly into the membrane and as a result, sink down, one of the three proposed mechanism of amyloid interaction with the membrane (Drolle et al, 2014). It has been proposed that amyloid either tends to adsorb onto the surface of the lipid membrane (as seen in the healthy model), partially penetrate into the membrane, causing membrane disruption and irregular pore formation, which is likely what we see here in the diseased 1 model, or finally, the formation of a complete ion channel in the membrane (Drolle et al, 2014). This can be visualized in Figure 2.5 in chapter 2 of this thesis. Though not easily visualized in the AFM images shown here because of a uniform layer of amyloid species across the membrane, defects and pores may also have been formed in this diseased 1 membrane. This also agrees with the data from the BLM studies, where the amyloid had the highest pore forming activity in the diseased 1 membrane.

Finally, in the diseased 2 model, we see an initial large accumulation of amyloid species, indicated by an initial large increase in roughness, followed by a dramatic decrease. After 1 hour of incubation (Figure 7.6C), the surface roughness was 0.3815 ± 0.033 nm, which almost quadrupled to 1.366 ± 0.12 nm after 4 hours. This indicates an initial large accumulation of amyloid on the surface of the membrane, without much membrane damage (see Figure 2.5A in chapter 2 of this thesis for a schematic interpretation of this type of amyloid interaction). However, after 6 hours (Figure 7.6F), we see a large decrease in roughness of the system, with an average roughness of 0.366 ± 0.045 nm. This indicates that at this point, amyloid clusters sink into the membrane and cause large deformations in the membrane, leading to a dramatic decrease in surface roughness, similar to what we see in fluid membrane reference (of the three possible amyloid interaction pathways). After 24 hours, the roughness increased slightly to 0.5455 ± 0.026 nm, suggesting a continuation of accumulation atop the amyloid-disrupted and deformed membrane. Due to penetration in the membrane, amyloid induces defects and deformation of the membrane, which agrees well with the BLM data, which showed that the diseased 2 sample had a significantly higher conductance with the addition of amyloid than in its absence, possibly caused by this large membrane deformation.

7.4 Conclusions

In this investigation, summarized in Table 7.5, we studied three complex lipid models mimicking a healthy neuron membrane, a diseased 1 membrane, and a diseased 2 membrane. Through our AFM studies, we found that, when compared to the healthy model, the diseased 1 model revealed a more organized distribution of larger domains with larger spaces in between the domains and corresponding electrical surface potential domains to the topographical domains. For the diseased 2 membrane, the domains were smaller and more plentiful, which resulted in a smaller spacing between the domains. Features in electrical surface potential did not correspond to the topographical domains as was observed in the diseased 1 model; however, this system had the largest variation in electrical surface potential.

Table 7.5: Summary of Results. This table summarizes the results of this multi-method study: AFM/KPFM study on topographical and electrical surface potential features of the models in monolayer form; Black Lipid Membrane analysis on the conductance of each model and the effect of amyloid on this conductance; and an AFM study on amyloid incubation over time on each model system.

	Healthy Model	Diseased 1 Model	Diseased 2 Model
Monolayer – AFM / KPFM Analysis			
Topographical Δh	0.986 ± 0.02 nm	1.051 ± 0.016 nm	0.500 ± 0.03 nm Lower than Healthy Model
Electrostatic Surface Potential ΔV	24.64 ± 1.10 mV	70.47 ± 5.41 mV Higher than Healthy Model	11.63 ± 0.59 mV Lower than Healthy Model
Black Lipid Membrane (BLM) Analysis			
Pore Forming Activity (PFA)	No significant increase in PFA with addition of amyloid	Highest PFA of three systems studied Significant increase in PFA with addition of amyloid	Significant increase in PFA with addition of amyloid
Amyloid Incubation on Model Membranes			
Deposition Pattern Over Time measured via Roughness Measurements	Increase with time	Fluctuate between increases and decreases over time Indicative of amyloid penetrating into membrane	Initial increase followed by large decrease Indicative of an initial accumulation event preceding membrane disruption/penetration

Through our BLM studies, we saw that the diseased 1 model has the highest pore forming activity in the presence of A β of the three systems studied. This is consistent with our previously mentioned hypothesis that the larger spacing between topographical domains of this system would give an increased area of less ordered lipids where amyloid would be able to form pores in the membrane. As only the two diseased systems shown significant increase in pore forming activity with the addition of amyloid (whereas the healthy system did not), supports the idea that the differences in membrane composition can have a strong effect on

the interaction of the amyloid peptides with the membrane and the extent to which the peptides can cause damage and alteration of normal cell function by changing membrane permeability.

Finally, through amyloid incubation on hydrated membrane studies, we found differences in amyloid accumulation between the three systems investigated. In the healthy system, we saw an increase in roughness over time, indicating a progressive accumulation of amyloid species atop the membrane. However, in the diseased 1 membrane, we saw fluctuations in roughness over time, indicating the likelihood of the amyloid penetrating into the membrane and causing disruptions. This disruption of the membrane over time agrees with what was seen in the BLM studies, which showed that this model had the highest pore forming activity. The diseased 2 system showed signs of both accumulation types, with an initial accumulation atop the membrane with time, followed by large membrane deformations, likely caused by the accumulation reaching a point where it caused disruptions then sank into the membrane. The differences in amyloid accumulation type as well as differences in membrane disruption further show what an effect the lipid composition of the membrane has on its interaction with amyloid species.

In summary, the diseased models are more susceptible to interaction with amyloid and their damaging effects than the healthy model, which may play a role in amyloid toxicity.

Chapter 8.0: Thesis Conclusions

The aim of this thesis was to provide an insight into the interaction of amyloid peptides with the lipid membrane in relation to amyloid toxicity in Alzheimer's disease. More specifically, we showed the important effects of cholesterol and lipid composition on amyloid binding to the membrane and developed novel systems to mimic healthy and diseased states of a neuronal membrane to study amyloid toxicity.

In more detail, this thesis first gave an in depth review into Alzheimer's disease and how nanotechnology-related methods of study have already been used to examine the disease and its molecular mechanism. While there has been abundant research in this area, there is still much left to be discovered, which is evident by the lack of treatment and cure for this disease.

The comparative effects of cholesterol and melatonin on lipid systems were investigated utilizing neutron scattering techniques. Cholesterol's effect on the membrane has been widely studied; however, melatonin's effect was still unclear. In this work, we provided a direct comparison of cholesterol and melatonin's effects and we showed that in contrast to cholesterol's thickening effect on the membrane, melatonin has a thinning effect, causing disorder between the lipid molecules. This effect of melatonin may play into its suggested neuroprotective effect against amyloid.

The effect of lipid head group charge and lipid phase was investigated in single lipid systems. It was found that there is a similar increase in amyloid accumulation on membranes composed of neutral lipids in gel phase and membranes made up of fluid phase lipids with negatively charged head groups. Differing from these results were the observations for membranes of lipids in fluid phase both with positively charged and neutral head groups: in these systems, amyloid deposits of reduced height were observed, suggesting the fusing of the amyloid into the lipid membrane surface. These results showed clearly that lipid phase and head group charge have a measureable effect on amyloid interactions with the membrane. The effect of cholesterol on single lipid systems was also studied. In DOPC membranes with cholesterol present, targeted binding of amyloid was observed, which was not seen in a pure DOPC membranes. By mapping the electrical surface potential of the

systems, cholesterol induced electrostatic domains in the lipid systems were observed; these domains could act as a targeted binding site for the complexly charged amyloid peptides.

More complex systems were then investigated, from two constituent systems up to five constituent systems, with the goal of building up to a lipid system that would mimic the lipid composition in a neuronal cell membrane. First, lipid monolayer systems of increasing complexity in the presence and absence of cholesterol were studied to determine cholesterol's effect on both the topography and surface features of the samples, as well as the electrical surface potential of the samples. It was found that in all the systems studied, cholesterol had a visible effect on the surface features of the systems as well as a measureable effect on the electrical surface potential, even in systems consisting of lipids with a charged head group. This further supports the idea that cholesterol plays an important role in the formation of electrostatic domains in the membrane that may be involved in the membrane's interaction with charged species.

Membrane models of the neuronal membrane were then developed and studied; the models were created to mimic hypothesized compositions in healthy and Alzheimer's diseased states. It was first shown that the three models differed in terms of topographical features and electrical surface potential. It was then shown that the three models in bilayer form had differing membrane permeabilities when in the presence of amyloid. It was found that the healthy model actually has higher resistance to amyloid toxicity than the diseased models. Finally, amyloid interactions were directly studied on membranes of the model systems and it was found that the three systems all had different types and amounts of amyloid, with the diseased models showing evidence of amyloid disruption and deformation to the membrane itself. These results together show that the lipid composition of a membrane can have a very strong effect on the membrane's interaction with amyloid, especially in terms of susceptibility to damage.

Chapter 9.0: Future Work

The findings presented in this thesis provide very interesting points from which many more studies can expand. It would be very desirable to continue looking at systems of increasing complexity so as to continue to be able to better match physiological complexity while still utilizing model systems. Other areas of future work and interest include the investigation of systems that include additional protective agents, like anti-oxidants or other biomolecules like melatonin and DHA.

For a currently incurable disease like Alzheimer's, any insight into areas that can potentially protect against negative amyloid effects are of great interest. The developed models also provide a new avenue for Alzheimer's research in terms of the ultimate goal of finding prospective treatments or preventative measures by illustrating that changes in membrane lipid composition can have a great effect on biomolecular-membrane interactions. These models show the need for further research in what causes these changes in membrane composition and, more importantly, how these alterations may be avoided.

References

- Abramov AY, Ionov M, Pavlov E, Duchon MR. (2011). Membrane cholesterol content plays a key role in the neurotoxicity of β -amyloid: implications for Alzheimer's disease. *Aging Cell*, 10(4): 595-603.
- Abu-Hamad S, Arbel N, Calo D, Arzoine L, Israelson A, Keinan N, Ben-Romano R, Friedman O, Shoshan-Barmatz, V. (2009). The VDAC1 N-terminus is essential both for apoptosis and the protective effect of anti-apoptotic proteins. *J. Cell. Sci.*, 122:1906-1916.
- Adamcik J, Jung J-M, Flakowski J, De Los Rios P, Dietler G, Mezzenga R (2010). Understanding amyloid aggregation by statistical analysis of atomic force microscopy images, *Nature Nanotech.*, 5:423–428.
- Aguilar LF, Pino JA, Soto-Arriaza MA, Cuevas FJ, Sanchez S, Sotomayor CP. (2012). Differential Dynamic and Structural Behavior of Lipid-Cholesterol Domains in Model Membranes. *PLoS ONE*, 7(6): e40254.
- Ah-Fat, N. M. W., Craig, D. Q. M., & Taylor, K. M. G. (1994). An investigation into the effects of surfactants on phospholipid monolayers using a Langmuir-Blodgett film balance. *Int. J. Pharm.*, 107(3), 239–242.
- Ahyayauch H, Raab M, Busto J, Andraka N, Arrondo J, Masserini M, Tvaroska I, Goñi F. (2013). Binding of β -Amyloid (1–42) Peptide to Negatively Charged Phospholipid Membranes in the Liquid-Ordered State: Modeling and Experimental Studies. *Biophys. J*, 103:453–463.
- Akkas SB, Inci S, Zorlu F, Severcan F. (2007). Melatonin affects the order, dynamics and hydration of brain membrane lipids. *J. Mol. Struct.*, 834-836: 207–215.
- Allsop D, Landon M, Kidd M. (1983). The isolation and amino acid composition of senile plaque core protein. *Brain Res.*, 259(2): 348-352.
- Als-Nielsen, J., & McMorrow, D. (2001). *Elements of Modern X-Ray Physics*. John Wiley & Sons, Ltd.
- Alwarawrah M, Dai J, Huang J. (2010). A molecular view of the cholesterol condensing effect in DOPC lipid bilayers. *J. Phys. Chem. B*, 114(22): 7516–7523.
- Alzheimer A. (1907). Uber eine eigenartige Erkrankung der Hirnrinde. *Allgemeine Zeitschrift fur Psychiatrie und Psychisch-gerichtliche Medizin*, 64:146-148.
- Ambroggio EE, Kim DH, Separovic F, Barrow CJ, Barnham KJ, Bagatolli LA, Fidelio GD. (2005). Surface behaviour and lipid interaction of Alzheimer beta-amyloid peptide 1-42: a membrane-disrupting peptide. *Biophys. J.*, 88(4): 2706-2713.

- Antzutkin ON, Balbach JJ, Leapman RD, Rizzo NW, Reed J, Tycko, R. (2000). Multiple quantum solid-state NMR indicates a parallel, not antiparallel, organization of beta-sheets in Alzheimer's beta-amyloid fibrils. *P. Natl. Acad. Sci. U.S.A.*, 97(24):13045-13050.
- Ariga T, McDonald MP, Yu RK. (2008). Role of ganglioside metabolism in the pathogenesis of Alzheimer's disease—a review. *J. Lipid Res.*, 49(6): 1157 – 1175.
- Arispe N, Rojas E, Pollard HB. (1993). Alzheimer disease amyloid β protein forms calcium channels in bilayer membranes: Blockade by tromethamine and aluminum. *P. Natl. Acad. Sci. U.S.A.*, 90:567-571
- Arispe N, Doh M. (2002). Plasma membrane cholesterol controls the cytotoxicity of Alzheimer's disease A β (1-40) and (1-42) peptides. *FASEB J.*, 16:1526-1536
- Arispe N. (2004). Architecture of the Alzheimer's A β Ion Channel Pore. *J Mem Biol*, 197:33–Bacon GE. 1962. Neutron Diffraction. *Oxford University Press*.
- Baltes C, Princz-Kranz, F, Rudin M, Mueggler T. (2011). Detecting Amyloid-Beta Plaques in Alzheimer's Disease. *Methods Mol. Biol.*, 711: 511–533.
- Baoukina S, Mendez-Villuendas E, Bennett WFD, Tieleman DP. (2013). Computer simulations of the phase separation in model membranes. *Faraday Discuss.*, 161: 63–75.
- Baoukina S, Mendez-Villuendas E, Tieleman DP. (2012). Molecular View of Phase Coexistence in Lipid Monolayers. *J. Am. Chem. Soc.*, 134(42): 17543–17553.
- Bartzokis G. (2004). Age-related myelin breakdown: a developmental model of cognitive decline and Alzheimer's disease. *Neurobiol. Aging*, 25(1):5-18.
- Bay DC, Court DA. (2002). Origami in the outer membrane: the transmembrane arrangement of mitochondrial porins. *Biochem. Cell Biol.*, 80(5):551-562.
- Behl C, Davis JB, Lesley R, Schubert D. (1994). Hydrogen peroxide mediates amyloid beta protein toxicity. *Cell*, 77(6):817-827.
- Beitinger H, Vogel V, Mobius, Hinrich D, Rahmann H. (1989). Surface potentials and electric dipole moments of ganglioside and phospholipid monolayers: contribution of the polar headgroup at the water/lipid interface. *Biochem. Biophys. Acta.*, 948: 293 – 300.
- Benloucif S, Burgess HJ, Klerman EB, Lewy AJ, Middleton B, Murphy PJ, Parry BL, et al. (2008). Measuring melatonin in humans. *J. Clin. Sleep Med.*, 4(1), 66–69.
- Bennett WFD, Tieleman DP. Computer simulations of lipid membrane domains. (2013). *Biochim. Biophys. Acta.*, 1828: 1765-1776.

- Benoit M, Gabriel D, Gerisch G, Gaub HE. (2000). Discrete interactions in cell adhesion measured by single-molecule force spectroscopy. *Nature Cell Biol.*, 2(6):313-317.
- Berhanu WM, Hansmann UH. (2012). Structure and dynamics of amyloid- β segmental polymorphisms. *PLoS ONE*, 7(7):e41479.
- Berthelot K, Cullin C, Lecomte S. (2013). What does make an amyloid toxic: morphology, structure or interaction with membrane? *Biochimie*, 95(1):12-19.
- Binning G, Quate CF, Gerber C. (1986). Atomic force microscope. *Phys. Rev. Lett.*, 56:930-933.
- Bitan G, Kirkitadze MD, Lomakin A, Vollers SS, Benedek GB, Teplow DB. (2003). Amyloid beta-protein (A β) assembly: A β 40 and A β 42 oligomerize through distinct pathways. *P. Natl. Acad. Sci. U.S.A.*, 100(1):330-335.
- Blackley HK, Patel N, Davies MC, Roberts CJ, Tendler SJ, Wilkinson MJ, Williams PM. (1999). Morphological development of β (1-40) amyloid fibrils. *Exp. Neurology*, 158(2):437-443.
- Blackley HK, Sanders GH, Davies MC, Roberts CJ, Tendler SJ, Wilkinson, M. J. (2000). In-situ atomic force microscopy study of beta-amyloid fibrillization. *J. Mol. Biol.*, 298(5):833-840.
- Bokvist M, Lindström F, Watts A, Grobner, G. (2004) Two Types of Alzheimer's β -Amyloid (1–40) Peptide Membrane Interactions: Aggregation Preventing Transmembrane Anchoring Versus Accelerated Surface Fibril Formation. *J. Mol. Biol.*, 335:1039–1049.
- Bongiorno D, Ceraulo L, Ferrugia M, Filizzola F, Ruggirell A, Liveri VT. (2005). Localization and interactions of melatonin in dry cholesterol/lecithin mixed reversed micelles used as cell membrane models. *J. Pineal Res.*, 38(4), 292–298.
- Bonn M, Roke S, Berg O, Juurlink L, Stamouli A, Mueller M. (2004). A vibrational study of cholesterol-lipid interactions in a monolayer: a molecular view of condensation. *Phys. Chem. B*, 108:19083–10985.
- Brockman H. (1994). Dipole potential of lipid membranes. *Chem. Phys. Lipids*, 73: 57 – 79.
- Bragg WH, Bragg WL. (1913). The Reflexion of X-rays by Crystals. *Proc R. Soc. Lond. A*, 88(605): 428–438.
- Brown AC, Towles KB, Wrenn SP. (2007). Measuring raft size as a function of membrane composition in PC-Based systems: Part II - Ternary systems. *Langmuir*, 23(22): 11188–11196.

- Brown CL, Aksay IA, Saville DA, Hecht MH. (2002). Template-directed assembly of a de novo designed protein. *J. Am. Chem. Soc.*, 124(24):6846-6848.
- Brookmeyer, R., Ziegler-Graham, K., Johnson, E., & Arrighi, H. M. (2007). Forecasting the Global Burden of Alzheimer's Disease. *Public Health*, 130.
- Bucciantini M, Giannoni E, Chiti F, Baroni F, Formigli L, Zurdo J, Taddei N, Ramponi G, Dobson CM, Stefani, M. (2002). Inherent toxicity of aggregates implies a common mechanism for protein misfolding diseases. *Nature*, 416(6880):507-511.
- Buchsteiner, A., Hauß, T., & Dencher, N. (2012). Influence of amyloid-b peptides with different lengths and amino acid sequences on the lateral diffusion of lipids in model membranes. *Soft Matter*, 8:424-429.
- Buell AK, Dhulesia A, White DA, Knowles TP, Dobson CM, Welland, M. E. (2012). Detailed analysis of the energy barriers for amyloid fibril growth. *Angew Chemie*, 51(21):5247-5251.
- Bunge, Mueller P, Stoeckl M, Herrmann A, Huster D. (2008). Characterization of the ternary mixture of sphingomyelin, POPC, and cholesterol: Support for an inhomogeneous lipid distribution at high temperatures. *Biophys. J.*, 94(7): 2680–2690.
- Burke KA, Yates EA, Legleiter J. (2013). Amyloid-forming proteins alter the local mechanical properties of lipid membranes. *Biochem*, 52(5):808-817.
- Bush AI, Tanzi RE. (2008). Therapeutics for Alzheimer's disease based on the metal hypothesis. *Neurotherapeutics*, 5(3):421-432.
- Butterfield DA, Yatin SM, Varadarajan S, Koppal, T. (1999). Amyloid beta-peptide-associated free radical oxidative stress, neurotoxicity, and Alzheimer's disease. *Methods in Enzymology*, 309:746-768.
- Cadenhead, G. (1985). *Structure and Properties of Cell Membranes*. Boca Raton, FL:CRC Press.
- Cai M, Zhao W, Shang X, Jiang J, Ji H, Tang Z, Wang H. (2012). Direct Evidence of Lipid Rafts by in situ Atomic Force Microscopy. *Small*, 8(8): 1243-1250.
- Caillon L, Killian JA, Lequin O, Khemtémourian L. (2013). Biophysical investigation of the membrane-disrupting mechanism of the antimicrobial and amyloid-like peptide dermaseptin S9. *PLoS ONE*, 8(10): e75528.
- Calderon RO, Attema B, DeVries GH. (1995). Lipid Composition of Neuronal Cell Bodies and Neurites from Cultured Dorsal Root Ganglia. *J. Neurochem.*, 64(1): 424 – 429.

- Campioni S, Mannini B, Zampagni M, Pensalfini A, Parrini C, Evangelisti E et al. (2010). A causative link between the the structure of aberrant protein oligomers and their toxicity. *Nat. Chem. Biol.*, 6:140-147.
- Capone R, Jang H, Kotler SA, Connelly L, Teran Arce F, Ramachandran S, Kagan BL, et al. (2012). All-d-Enantiomer of β -Amyloid Peptide Forms Ion Channels in Lipid Bilayers. *J. Chem. Theory Comput.*, 8(3): 1143-1152.
- Carrell R (1998) Conformational changes and disease - serpins, prions and Alzheimer's. *Curr Opin Struct Biol.*, 8: 799-809.
- Casadio R, Jacoboni I, Messina A, De Pinto V. A 3D model of the voltage-dependent anion channel (VDAC). *FEBS Lett.*, 520:1-7.
- Cecchi C, Nichino D, Zampagni M, Bernacchioni C, Evangelisti E, Pensalfini A, Liguri G, Gliozzi A, Stefani M, and Relini, A. (2009) A protective role for lipid raft cholesterol against amyloid-induced membrane damage in human neuroblastoma cells. *Biochim. Biophys. Acta*, 1788:2204–2216.
- Chi EY, Frey SL, Lee KYC. (2007). Ganglioside G(M1)-mediated amyloid-beta fibrillogenesis and membrane disruption. *Biochem.*, 46(7): 1913–24.
- Chiang, P. K., Lam, M. A., & Luo, Y. (2008). The many faces of amyloid beta in Alzheimer's disease. *Curr. Mol. Med.*, 8(6), 580–584.
- Chiti F, Dobson CM. (2006). Protein misfolding, functional amyloid, and human disease. *Annual Rev. Biochem.*, 75:333-366.
- Choo-Smith LP, Garzon-Rodriguez W, Glabe CG, Surewicz WK. (1997). Acceleration of amyloid fibril formation by specific binding of A β (1-40) peptide to ganglioside-containing membrane vesicles. *J. Biol. Chem.*, 272(37):22987-22990.
- Choucair A, Chakrapani M, Chakravarthy B, Katsara J, Johnston LJ. (2007). Preferential accumulation of A β (1-42) on gel phase domains of lipid bilayers: an AFM and fluorescence study. *Biochim. Biophys. Acta*, 1768(1):146-154.
- Connelly L, Jang H, Arce FT, Capone R, Kotler SA, Ramachandran S, ... Lal R. (2012). Atomic Force Microscopy and MD Simulations Reveal Pore-Like Structures of All-D-Enantiomer of Alzheimer's β -Amyloid Peptide: Relevance to the Ion Channel Mechanism of AD Pathology. *J. Phys. Chem. B*, 116: 1728–1735.
- Connolly MR, Smith CG. (2010). Nanoanalysis of graphene layers using scanning probe techniques. *Phil. Trans. Roy. Soc. London A*, 368(1932):5379-5389.
- Cordy JM, Hooper NM, Turner AJ. (2006). The involvement of lipid rafts in Alzheimer's disease. *Mol. Memb. Biol.*, 23(1):111-122.

- Costa EJX, Shida CS, Biaggi MH, Ito AS, Lamy-Freund MT. (1997). How melatonin interacts with lipid bilayers - a study by fluorescence and ESR spectroscopies. *FEBS Lett.*, 416: 103–106.
- Coyle T, DeLong MR. (1982). Alzheimer's Disease and Senile Dementia: Loss of Neurons in the Basal Forebrain. *Science*, 215(4537): 1237 – 1239.
- Crespo R, Rocha FA, Damas AM, Martins PM. (2012). A generic crystallization-like model that describes the kinetics of amyloid fibril formation. *J. Biol. Chem.*, 287(36):30585-30594.
- Cruz L, Urbanc B, Borreguero JM, Lazo ND, Teplow DB, Stanley HE. (2005) Solvent and mutation effects on the nucleation of amyloid-protein folding. *Proc. Natl. Acad. Sci. U.S.A.*, 102: 18258-18263.
- Cunnane SC, Schneider JA, Tangney C, Tremblay-Merciera J, Fortiera M, Bennett DA, Morris MC. (2012). Plasma and brain fatty acid profiles in mild cognitive impairment and Alzheimer's disease. *J. Alzheimer's Dis.*, 29: 691–697.
- Curtain C, Ali F, Smith D, Bush A, Masters C, Barnham K. (2003) Metal ions, pH, and cholesterol regulate the interactions of Alzheimer's disease amyloid-beta peptide with membrane lipid. *J. Biol. Chem.*, 278: 2977-2982.
- Dahlgren KN, Manelli AM, Stine WB, Baker LK, Krafft GA, LaDu MJ. (2002). Oligomeric and fibrillar species of amyloid- β peptides differentially affect neuronal viability. *J. Biol. Chem.*, 277:32046-32053.
- Dante S, Hauss T, Dencher NA. (2006). Cholesterol inhibits the insertion of the Alzheimer's peptide Ab(25–35) in lipid bilayers. *Eur. Biophys. J.*, 35: 523-531.
- Dante S, Hauss T, Steitz R, Canale C, Dencher NA. (2011). Nanoscale structural and mechanical effects of beta-amyloid (1-42) on polymer cushioned membranes: a combined study by neutron reflectometry and AFM Force Spectroscopy. *Biochim. Biophys. Acta.*, 1808(11): 2646-55
- Davinelli S, Intrieri M, Russo C, Di Costanzo A, Zella D, Bosco P, Scapagnini G. (2011). The “Alzheimer's disease signature”: potential perspectives for novel biomarkers. *Immunity & Aging*, 8:7-17.
- Davis JH, Clair JJ, Juhasz J. (2009). Phase Equilibria in DOPC/DPPC-d62/Cholesterol Mixtures. *Biophys. J.*, 96: 521–539.
- De Meyer G, Shapiro F, Vanderstichele H, Vanmechelen E, Engelborghs S, De Deyn PP, Coart E, Hansson O, Minthon L, Zetterberg H, Blennow K, Shaw L, Trojanowski JQ. (2010). Diagnosis-independent Alzheimer disease biomarker signature in cognitively normal elderly people. *Arch. Neuro.*, 67(8):949-956.

- De Lima VR, Caro MSB, Munford ML, Desbat B, Dufourc E, Pasa AA, Creczynski-Pasa TB. (2010). Influence of melatonin on the order of phosphatidylcholine-based membranes. *J. Pineal Res.*, 49(2), 169–175.
- De Lima VR, Caro MSB, Tavares MIB, Creczynski-Pasa TB. (2007). Melatonin location in egg phosphatidylcholine liposomes: possible relation to its antioxidant mechanisms. *J. Pineal Res.*, 43(3), 276–282.
- Demel RA, De Kruff B. (1976) The function of sterols in membranes. *Biochim. Biophys. Acta*, 457:109–132.
- Di Paolo G, Kim TW. (2011). Linking lipids to Alzheimer’s disease: cholesterol and beyond. *Nat. Rev. Neurosci.*, 12(5), 284–296.
- Dobson CM. (2001). The structural basis of protein folding and its links with human disease. *Phil. Trans. Roy. Soc. London B*, 356(1406):133-145.
- Dobson CM, Karplus M. (1999). The fundamentals of protein folding: bringing together theory and experiment. *Curr. Opin. Struc. Biol.*, 9(1):92-101.
- Dragicevic N, Copes N, O’Neal-Moffitt G, Jin J, Buzzeo R, Mamcarz M, Tan J, et al. (2011). Melatonin treatment restores mitochondrial function in Alzheimer’s mice: a mitochondrial protective role of melatonin membrane receptor signaling. *J. Pineal Res.*, 51(1), 75–86.
- Drolle E, Gaikwad R, Leonenko Z. (2012). Nanoscale electrostatic domains in cholesterol-laden lipid membranes create a target for amyloid binding. *Biophys. J.*, 103(4):L27-29.
- Drolle E, Hane F, Lee B, Leonenko Z. (2014). Atomic force microscopy to study molecular mechanisms of amyloid fibril formation and toxicity in Alzheimer’s disease. *Drug Metab. Rev.*, 46(2): 207–223.
- Drolle E, Kučerka N, Hoopes MI, Choi Y, Katsaras J, Karttunen M, Leonenko Z. (2013). Effect of melatonin and cholesterol on the structure of DOPC and DPPC membranes. *Biochim. Biophys. Acta*, 1828: 2247 – 2254.
- Dyrks T, Dyrks E, Masters CL, Beyreuther K. (1993). Amyloidogenicity of rodent and human beta A4 sequences. *FEBS Lett.*, 324(2):231-236.
- Eckert GP, Wood WG, Mueller WE. (2010). Lipid Membranes and Beta-Amyloid: A Harmful Connection. *Curr. Protein Pept. Sci.*, 11(5), 319–325.
- Ege C, Majewski J, Wu G, Kjaer K, Lee KY. (2005). Templating effect of lipid membranes on Alzheimer’s amyloid beta peptide. *Chemphyschem*, 6(2):226-229.
- Ehehalt R, Keller P, Haass C, Thiele C, Simons K. (2003). Amyloidogenic processing of the Alzheimer beta-amyloid precursor protein depends on lipid rafts. *J. Cell Biol.*, 160: 113–123.

- Esparza TJ, Zhao H, Cirrito JR, Cairns NJ, Bateman RJ, Holtzman DM, Brody DL. (2013). Amyloid- β oligomerization in Alzheimer dementia versus high-pathology controls. *Annals of Neurology*, 73(1):104-119.
- Fantini J, Yahi N. (2010). Molecular insights into amyloid regulation by membrane cholesterol and sphingolipids: common mechanisms in neurodegenerative diseases. *Expert Rev. Mol. Med.*, 12: e27.
- Farooqui AA, Wells K, Horrocks LA. (1995) Breakdown of membrane phospholipids in Alzheimer disease. *Mol. Chem. Neuropathol.*, 23(2-3):155-173.
- Farooqui AA, Liss L, Horrocks LA. (1988) Neurochemical aspects of Alzheimer's disease: Involvement of membrane phospholipids. *Metabolic Brain Disease*. 3(1):19-35.
- Fassbender K, Masters C, Beyreuther, K. (2001). Alzheimer's disease: molecular concepts and therapeutic targets. *Naturwissenschaften*, 88: 261-267.
- Feigenson GW. (2006) Phase behavior of lipid mixtures. *Nature Chem Biol.*, 2, 560-563.
- Feng Z, Zhang JT. (2004). Protective effect of melatonin on beta-amyloid-induced apoptosis in rat astrogloma C6 cells and its mechanism. *Free Radical Bio. Med.*, 37(11), 1790–1801.
- Fezoui Y, Hartley D, Harper J, Khurana R, Walsh D, Condron M, Selkoe D, Lansbury P, Fink A, Teplow D. (2007). An improved method of preparing the amyloid p-protein for fibrillogenesis and neurotoxicity experiments. *Amyloid: Int. J. Exp. Clin. Invest.*, 7: 166-178.
- Finot E, Leonenko Y, Moores B, Eng L, Amrein M, Leonenko Z. (2010) Effect of cholesterol on electrostatics in lipid-protein films of a lung surfactant. *Langmuir*, 26:1929–1935.
- Friedman R, Pellarin R, Caffisch A. (2009). Amyloid aggregation on lipid bilayers and its impact on membrane permeability. *J. Mol. Biol.*, 387(2): 407–415.
- Galano A, Tan DX, Reiter RJ. (2011). Melatonin as a natural ally against oxidative stress: a physicochemical examination. *J. Pineal Res.*, 51(1): 1–16.
- García JJ, Reiter RJ, Guerrero JM, Escames G, Yu BP, Oh CS, Munoz-Hoyos A. (1997). Melatonin prevents changes in microsomal membrane fluidity during induced lipid peroxidation. *FEBS Lett.*, 408: 297–300.
- García JJ, Reiter RJ, Ortiz GG, Oh CS, Tang L, Yu BP, Escames G. (1998). Melatonin enhances tamoxifen's ability to prevent the reduction in microsomal membrane fluidity induced by lipid peroxidation. *J. Membrane Biol.*, 162(1): 59–65.
- Garcia R, Perez R. (2002). Dynamic atomic force microscopy methods. *Surf. Sci. Rep.*, 47, 197–301.

- Gellermann, G. P., Appel, T. R., Tannert, A., Radestock, A., Hortschansky, P., Schroeckh, V., Leisner, C., et al. (2005). Raft lipids as common components of human extracellular amyloid fibrils. *P. Natl. Acad. Sci. U.S.A.*, 102(18): 6297–6302.
- Geng J, Zhao C, Ren J, Qu X. (2010). Alzheimer's disease amyloid beta converting left-handed Z-DNA back to right-handed B-form. *Chem. Comm.*, 46:7187-7189.
- Giacomelli CE, Norde W. (2005). Conformational changes of the amyloid β -peptide (1-40) adsorbed on solid surfaces. *Macromolecular Bioscience*, 5(5): 401-407.
- Giordani C, Wakai C, Yoshida K, Okamura E, Matubayasi N, Nakahara M. (2008) Cholesterol location and orientation in aqueous suspension of large unilamellar vesicles of phospholipid revealed by intermolecular nuclear Overhauser effect. *J. Phys. Chem. B*, 112(9): 2622–2628.
- Glenner GG, Wong CW. (1984). Alzheimer's disease: initial report of the purification and characterization of a novel cerebrovascular amyloid protein. *Biochem. Biophys. Res. Comm.*, 120(3): 885-890.
- Goldsbury C, Kitsler J, Aebi U, Arvinte T, Cooper GJS. (1999). Watching amyloid fibrils grow by time-lapse atomic force microscopy. *J. Mol. Biol.*, 285:33-39.
- Gorbenko G, Kinnunen P. (2006). The role of lipid-protein interactions in amyloid-type protein fibril formation. *Chem. Phys. Lipids*, 141: 72-82.
- Greenough MA, Camakaris J, Bush AI. (2012). Metal dyshomeostasis and oxidative stress in Alzheimer's disease. *Neurochem. Int.*, 62(5): 540-555.
- Gunasekara L, Schurch S, Schoel W, Nag K, Leonenko Z, Haufs M, Amrein M. (2005). Pulmonary surfactant function is abolished by an elevated proportion of cholesterol. *Biochim. Biophys. Acta*, 1737: 27-35.
- Hammarstrom P, Ali MM, Mishra R, Svensson S, Tengvall P, Lundstrom, I. (2008). A catalytic surface for amyloid fibril formation. *J. Phys.: Conference Series*, 100(5): 052039.
- Hane F, Tran G, Attwood SJ, Leonenko Z. (2013). Cu^{2+} affects amyloid- β (1-42) aggregation by increasing peptide-peptide binding forces. *PLoS ONE*, 8(3): e59005.
- Hane F, Drolle E, Gaikwad R, Faught E, Leonenko Z. (2011). Amyloid- β aggregation on model lipid membranes: an AFM study. *J. Alzheimers Dis.*, 26: 485-494.
- Hansma HG, Hoh JH. (1994). Biomolecular imaging with the atomic force microscope. *An Rev Biophys Biomol Strut*, 23:115-140.
- Hardy J, Allsop D. (1991). Amyloid deposition as the central event in the aetiology of Alzheimer's disease. *Trends in Pharmacological Sciences*, 12(10):383-388.

- Hardy JA, Higgins GA. (1992). Alzheimer's Disease: The Amyloid Cascade Hypothesis. *Science*, 256(5054): 184–185.
- Harper JD, Lieber CM, Lansbury Jr PT, (1997). Atomic force microscopic imaging of seeded fibril formation and fibril branching by the Alzheimer's disease amyloid- β protein, *Chem. Biol.*, 4 (12):951–959.
- Harper JD, Lansbury PT Jr. (1997). Models of amyloid seeding in Alzheimer's disease and scrapie: mechanistic truths and physiological consequences of the time-dependent solubility of amyloid proteins. *Ann. Rev. Biochem.*, 66:385-407.
- Harroun TA, Katsaras J, Wassall SR. (2006). Cholesterol hydroxyl group is found to reside in the center of a polyunsaturated lipid membrane. *Biochemistry*, 45(4): 1227–1233.
- He X, Huang Y, Li B, Gong CX, Schuchman EH. (2010). Deregulation of sphingolipid metabolism in Alzheimer's disease. *Neurobiol. Aging*, 31(3): 398 – 408.
- Hinterdorfer P, Dufrene Y. (2006). Detection and localization of single molecular recognition events using atomic force microscopy. *Nature Methods*, 3(5):347-355.
- Hooper NM. (1999). Detergent-insoluble glycosphingolipid/cholesterol-rich membrane domains, lipid rafts and caveolae (review). *Mol. Membr. Biol.*, 16 (2): 145-156.
- Hussain SAR. (2007). Effect of melatonin on cholesterol absorption in rats. *J. Pineal Res.*, 42(3): 267–271.
- Ionov M, Klajnert B, Gardikis K, Hatziantoniou S, Palecz B, Salakhutdinov B, Cladera J, Zamaraeva M, Demetzos C, Bryszewska M. (2010). Effect of amyloid beta peptides A β 1–28 and A β 25–40 on model lipid membranes. *J. Therm. Anal. Calorim.*, 99:741-747.
- Irwin JA, Wong HE, Inchan K. (2013). Different fates of Alzheimer's disease amyloid- β fibrils remodeled by biocompatible small molecules. *Biomacromolecules*, 14(1):264-274.
- Jacobson K, Mouritsen OG, Anderson RGW. (2007). Lipid rafts: at a crossroad between cell biology and physics. *Nature*, 9(1): 7-14.
- Jang H, Arce FT, Ramachandran S, Capone R, Azimova R, Kagan BL, Nussinov R, Lal R. (2010). Truncated β -amyloid peptide channels provide an alternative mechanism for Alzheimer's disease and Down syndrome. *P. Natl. Acad. Sci. U.S.A.*, 107(14):6538-6543.
- Jang H, Arce FT, Mustata M, Ramachandran S, Capone R, Nussinov R, Lal R. (2011). Antimicrobial protegrin-1 forms amyloid-like fibrils with rapid kinetics suggesting a functional link. *Biophys. J.*, 100(7):1775-1783.

- Jang H, Connelly L, Arce FT, Ramachandran S, Kagan BL, Lal R, Nussinov R. (2013). Mechanisms for the Insertion of Toxic, Fibril-like β -Amyloid Oligomers into the Membrane. *Chem. Theory Comput.* 9:822–833)
- Ji SR, Wu Y, Sui SF. (2002a). Study of beta-amyloid peptide (A β 40) insertion into phospholipid membranes using monolayer technique. *Biochem. (Mosc.)*, 67:1283-1288.
- Ji S-R, Wu Y, Sui S. (2002b). Cholesterol is an important factor affecting the membrane insertion of beta-amyloid peptide (A β 1-40), which may potentially inhibit the fibril formation. *J. Biol. Chem.*, 277(8), 6273–6279.
- Joanne P, Galanth C, Goasdoue N, Nicolas P, Sagan S, Lavielle S, Chassaing G, El Amri C, Alves ID. (2009). Lipid reorganization induced by membrane-active peptides probed using differential scanning calorimetry. *Biochim. Biophys. Acta – Biomembr.*, 1788(9): 1772–1781.
- Joannis JJ, Coppock PS, Yin F, Mori M, Zamorano A, Kindt JT. (2011). Atomistic simulation of cholesterol effects on miscibility of saturated and unsaturated phospholipids: implications for liquid-ordered/liquid-disordered phase coexistence. *J. Am. Chem. Soc.*, 133(10): 3625–3634.
- Johansson J. (2003) Molecular determinants for amyloid fibril formation: lessons from lung surfactant protein C. *Swiss Med Wkly.*, 133: 275-282.
- JPK Instruments. (2005). The NanoWizard AFM handbook, Version 1.3.
- Juhász J, Sharom FJ, Davis JH. (2009). Quantitative characterization of coexisting phases in DOPC/DPPC/cholesterol mixtures: Comparing confocal fluorescence microscopy and deuterium magnetic resonance. *Biochem. Biophys. Acta: Biomembr.*, 1788(12): 2541–2552.
- Kagan BL. (2012). Antimicrobial properties of amyloid peptides. *Mol. Pharmaceutics*, 9(4): 708 – 717.
- Kakio A, Nishimoto S, Yanagisawa K, Kozutsumi Y, Matsuzaki K. (2002). Interactions of amyloid beta-protein with various gangliosides in raft-like membranes: importance of GM1 ganglioside-bound form as an endogenous seed for Alzheimer amyloid. *Biochem.*, 41(23):7385-7890.
- Kakio A, Nishimoto S, Kozutsumi Y, Matsuzaki, K. (2003). Formation of membrane-active form of amyloid beta-protein in raft-like model membranes. *Biochem. Biophys. Res. Com.*, 303:514-518.
- Kapoor S, Werkmüller A, Denter C, Zhai Y, Markgraf J, Weise K, Opitz N, Winter R. (2011). Temperature-pressure phase diagram of a heterogeneous anionic model

- biomembrane system: Results from a combined calorimetry, spectroscopy and microscopy study. *Biochem. Biophys. Acta: Biomembr.*, 1808(4): 1187–1195.
- Karasek M. (2004). Melatonin, human aging, and age-related diseases. *Exp. Gerontol.*, 39(11-12): 1723–1729.
- Karmakar S, Raghunathan V. (2003). Cholesterol-induced modulated phase in phospholipid membranes. *Phys. Rev. Lett.*, 91(9): 098102.
- Kayed R, Head E, Thompson JL, McIntire TM, Milton SC, Cotman CW, Glabe CG. (2003). Common structure of soluble amyloid oligomers implies common mechanism of pathogenesis. *Science*, 300(5618): 486-489.
- Kayed R, Sokolov Y, Edmonds B, McIntire TM, Milton SC, Hall JE, Glabe CG. (2004). Permeabilization of lipid bilayers is a common conformation-dependent activity of soluble amyloid oligomers in protein misfolding diseases. *J. Biol. Chem.*, 279:46363-46366.
- Kayed R, Pensalfini A, Margol L, Sokolov Y, Sarsoza F, Head E, Hall J, Glabe C. (2009). Annular Protofibrils Are a Structurally and Functionally Distinct Type of Amyloid Oligomer. *J. Biol. Chem.*, 284:4230–4237.
- Kim SI, Yi JS, Ko YG. (2006). Amyloid beta oligomerization is induced by brain lipid rafts. *J. Cell. Biochem.*, 99: 1878–1889.
- Kinnunen PKJ. (2009). Amyloid Formation on Lipid Membrane Surfaces. *The Open Biology Journal*. 2:163-175.
- Knopman DS, DeKosky ST, Cummings JL, Chui H, Corey-Bloom J, Relkin N, Small GW, Miller B, Stevens JC. (2001). Practice parameter: Diagnosis of dementia (an evidence-based review). *Neurology*, 56:1143-1153.
- Kojro E, Gimpl G, Lammich S, Marz W, Fahrenholz F. (2001). Low cholesterol stimulates the nonamyloidogenic pathway by its effect on the alpha-secretase ADAM 10. *Proc. Natl Acad. Sci. USA*, 98:5815-5820.
- Kondratova AA, Kondratov RV. (2012). The circadian clock and pathology of the ageing brain. *Nat. Rev. Neurosci.*, 13(5): 325-335.
- Koudinov AR, Berezov TT, Koudinova NV. (1998). Alzheimer's amyloid beta and lipid metabolism: a missing link? *FASEB J.*, 12(12):1097-1099.
- Kowalewski T, Holtzman DM. (1999) In situ atomic force microscopy study of Alzheimer's β -amyloid peptide on different substrates: new insights into mechanism of β -sheet formation. *Proc. Natl Acad. Sci. U.S.A.*, 96:3688-3693.

- Koynova R, Caffrey M. (2002) An index of lipid phase diagrams. *Chem Phys Lipids*, 115: 107-219.
- Kracun I, Rosner H, Drnovsek V, Heffer-Lauc M, Cosovic C, Lauc G. (1991). Human brain gangliosides in development, aging and iseases. *Int. J. Dev. Biol.*, 35: 289–295.
- Kremer JJ, Pallitto MM, Sklansky DJ, Murphy RM. (2000). Correlation of beta-amyloid aggregate size and hydrophobicity with decreased bilayer fluidity of model membranes. *Biochem.*, 39(33):10309-10318.
- Kučerka N, Marquardt D, Harroun TA, Nieh MP, Wassall SR, De Jong DH, Schäfer LV et al. (2010). Cholesterol in bilayers with PUFA chains: doping with DMPC or POPC results in sterol reorientation and membrane-domain formation. *Biochemistry*, 49(35): 7485–7493.
- Kučerka N, Marquardt D, Harroun TA, Nieh MP, Wassall SR, Katsaras J. (2009). The functional significance of lipid diversity: orientation of cholesterol in bilayers is determined by lipid species. *J. Am. Chem. Soc.*, 131(45): 16358–16359.
- Kučerka N, Nagle JF, Feller SE, Balgavý P. (2004). Models to analyze small-angle neutron scattering from unilamellar lipid vesicles. *Phys. Rev. E*, 69(5): 1–9.
- Kučerka N, Nagle JF, Sachs JN, Feller SE, Pencer J, Jackson A, Katsaras J. (2008). Lipid bilayer structure determined by the simultaneous analysis of neutron and X-ray scattering data. *Biophys. J.*, 95(5): 2356–2367.
- Kučerka N, Nieh MP, Katsaras J. (2010). Small-angle scattering from homogenous and heterogeneous lipid bilayers. In A. Iglič & H. T. Tien (Eds.), *Advances in Planar Lipid Bilayers and Liposomes* (Vol. 12, pp. 201–236). Elsevier Inc.
- Kučerka N, Nieh MP, Pencer J, Sachs JN, Katsaras J. (2009). What determines the thickness of a biological membrane. *Gen. Physiol. Biophys.*, 28(2), 117–125.
- Kučerka N, Pencer J, Nieh MP, Katsaras, J. (2007). Influence of cholesterol on the bilayer properties of monounsaturated phosphatidylcholine unilamellar vesicles. *Eur. Phys. J. E*, 23(3): 247–254.
- Kučerka N, Pencer J, Sachs JN, Nagle JF, Katsaras J. (2007). Curvature effect on the structure of phospholipid bilayers. *Langmuir*, 23(3): 1292–1299.
- Kuo YM, Emmerling MR, Vigo-Pelfrey C, Kasunic TC, Kirkpatrick JB, Murdoch GH, Ball MJ, Roher AE. (1996). Water-soluble Abeta (N-40, N-42) oligomers in normal and Alzheimer disease brains. *J. Biol. Chem.*, 271(8):4077-4081.
- Kusomoto Y, Lomakin A, Teplow DB, Benedek GB. (1998). Temperature dependence of amyloid β -protein fibrillization. *P. Natl. Acad. Sci. U.S.A.*, 95:12277-12282.
- Langner M, Kubica K. (1999). The electrostatics of lipid surfaces. *Chem. Phys. Lipids*, 101(1): 3-35.

- Lal R, Arnsdorf MF. (2010). Multidimensional atomic force microscopy for drug discovery: A versatile tool for defining targets, designing therapeutics and monitoring their efficacy. *Life Sci.*, 86:545-562.
- Lambert MP, Barlow AK, Chromy BA, Edwards C, Freed, Liosatos M, Morgan TE, Rozovsky I, Trommer B, Viola KL, Wals P, Zhang C, Finch CE, Krafft GA, Klein WL. (1998) Diffusible, nonfibrillar ligands derived from A β 1–42 are potent central nervous system neurotoxins. *Proc. Natl. Acad. Sci. U.S.A.*, 95: 6448-6453.
- Lansbury PT Jr. (1997). Inhibition of amyloid formation: a strategy to delay the onset of Alzheimer's disease. *Curr. Opin. Chem. Biol.*, 1(2): 260-267.
- Last NB, Miranker AD. (2013). Common mechanism unites membrane poration by amyloid and antimicrobial peptides. *Proc. Natl. Acad. Sci. U S A.*, 110(16): 6382–6387.
- Leblanc RM, Huo Q. (2006). Langmuir and Langmuir-Blodgett Films of Proteins and Enzymes. *Encyclopedia of Surface and Colloid Science*. P. Somasundaran (Ed). (Vol 5, pp 3233 - 3260).
- Lemmich J, Mortensen K, Ipsen JH, Hønger T, Bauer R, Mouritsen OG. (1997). The effect of cholesterol in small amounts on lipid-bilayer softness in the region of the main phase transition. *Eur. Biophys. J.*, 25(4): 293–304.
- Léonard A, Escrive C, Laguerre M, Pebay-Peyroula E, Néri W, Pott T, Katsaras J, et al. (2001). Location of cholesterol in DMPC membranes. A comparative study by neutron diffraction and molecular mechanics simulation. *Langmuir*, 17(6): 2019–2030.
- Leonenko ZV, Carnini A, Cramb DT. (2000). Supported planar bilayer formation by vesicle fusion: the interaction of phospholipid vesicles with surfaces and the effect of gramicidin on bilayer properties using atomic force microscopy. *Biochim. Biophys. Acta*, 1509(1-2), 131–147.
- Leonenko Z, Rodenstein M, Döner J, Eng L, Amrein M. (2006). The electrical surface potential of pulmonary surfactant. *Langmuir*, 22:10135-10139.
- Levine H 3rd. (1995). Soluble multimeric Alzheimer beta(1-40) pre-amyloid complexes in dilute solution. *Neurobiol. Aging*, 16(5):755-764.
- Levy D, Briggman KA. (2007). Cholesterol/phospholipid interactions in hybrid bilayer membranes. *Langmuir*, 23(13): 7155–7161.
- Lin H, BR, Lal R. (2001). Amyloid β protein forms ion channels: implications for Alzheimer's diseases pathophysiology. *Pathophysiology FASEB J.*, 15(13): 2433-2444.

- Lingwood D, Simons K. (2010). Lipid Rafts as a Membrane-Organizing Principle. *Science*, 327:46–50.
- Linse S, Cabaleiro-Lago C, Xue W, Lynch I, Lindman S, Thulin E, Radford SE, Dawson KE. (2007). Nucleation of protein fibrillation by nanoparticles. *P. Natl. Acad. Sci. U.S.A.*, 104(21):8691-8696.
- Lipowski R. (1995). Structure and dynamics of membranes—from cells to vesicles 1 – 65. North-Holland, Amsterdam: Elsevier.
- Loo DT, Copani A, Pike CJ, Whittemore ER, Walencewicz AJ, Cotman CW. (1993). Apoptosis is induced by β -amyloid in cultured central nervous system neurons. *P. Natl. Acad. Sci. U.S.A.*, 90:7951-7955.
- Lorenzo A, Yankner B. (1996). Amyloid fibril toxicity in Alzheimer's Disease and Diabetes. *Ann. N.Y. Acad. Sci.*, 77: 89-95.
- Lynn GW, Heller W, Urban V, Wignall GD, Weiss K, Myles DAA. (2006). Bio-SANS—A dedicated facility for neutron structural biology at Oak Ridge National Laboratory. *Physica B*, 385-386: 880–882.
- Malchiodi-Albedi F, Contrusciere V, Raggi C, Fecchi K, Rainaldi G, Paradisi S, Matteucci A, Santini MT, Sargiacomo M, Frank C, Gaudiano MC, Diociaiuti M. (2010). Lipid raft disruption protects mature neurons against amyloid oligomer toxicity. *Biochim. Biophys. Acta*, 1802: 406–415.
- Maltseva E, Brezesinski G. (2004). Adsorption of amyloid beta (1-40) peptide to phosphatidylethanolamine monolayers. *Chemphyschem.* 5(8): 1185–1190.
- Maltseva E, Kerth A, Blume A, Mohwald, H, Brezesinski, G. (2005) Adsorption of Amyloid β (1–40) Peptide at Phospholipid Monolayers. *ChemBioChem.*, 6:1817–1824.
- Mapstone M, Cheema AK, Fiandaca MS, Zhong X, Mhyre TR, MacArthur LH, ... Federoff, HJ. (2014). Plasma phospholipids identify antecedent memory impairment in older adults. *Nat. Med.*, 20(4): 415–8.
- Marrink SJ, De Vries AH, Harroun TA, Katsaras J, Wassall SR. (2008). Cholesterol shows preference for the interior of polyunsaturated lipid membranes. *J. Am. Chem. Soc.*, 130(1): 10–11
- Martinez-Seara H, Róg T, Karttunen M, Vattulainen I, Reigada R. (2010). Cholesterol induces specific spatial and orientational order in cholesterol/phospholipid membranes. *PloS One*, 5(6), e11162.
- Martinez-Seara H, Róg T, Pasenkiewicz-Gierula M, Vattulainen I, Karttunen M, Reigada. (2008). Interplay of unsaturated phospholipids and cholesterol in membranes: effect of the double-bond position. *Biophys. J.*, 95(7), 3295–3305.

- Masters CL, Simms G, Weinman NA, Multhaup G, McDonald BL, Beyreuther K. (1985). Amyloid plaque core protein in Alzheimer disease and Down syndrome. *P. Natl. Acad. Sci. U.S.A.*, 82:4245-4249.
- Mastrangelo IA, Ahmed M, Sato T, Liu W, Wang C, Hough P, Smith SO. (2006). High-resolution atomic force microscopy of soluble A β 42 oligomers. *J. Mol. Biol.*, 358(1): 106-119.
- Matsuzaki K. (2007). Physicochemical interactions of amyloid beta-peptide with lipid bilayers. *Biochim. Biophys. Acta*, 1768(8): 1935–42.
- Mattson MP. (2004). Pathways towards and away from Alzheimer's disease. *Nature*, 430(7000): 631-639.
- McIntosh TJ, Vidal A, Simon SA. (2003). Sorting of lipids and transmembrane peptides between detergent-soluble bilayers and detergent-resistant rafts. *Biophys. J.*, 85: 1656–1666.
- McMasters MJ, Hammer RP, McCarley RL. (2005). Surface-induced aggregation of beta amyloid peptide by co-substituted alkanethiol monolayers supported on gold. *Langmuir*, 21(10):4464-4470.
- McMullen TPW, Lewis RNAH, McElhaney, RN. (2004). Cholesterol-phospholipid interactions, the liquid -ordered phase and lipid rafts in model and biological membranes. *Cur. Opin. Colloid Interface Sci.*, 8:459-468.
- Meyer E. (1992). Atomic Force Microscopy. *Prog. Surf. Sci.*, 41, 3–49.
- Mlinac K, Bognar SK. (2010). Role of gangliosides in brain aging and neurodegeneration. *Transl. Neurosci.*, 1(4): 300–307.
- Moore B, Drolle E, Attwood SJ, Simons J, Leonenko Z. (2011). Effect of surfaces on amyloid fibril formation. *PLoS ONE*, 6(10):e25954.
- Moore B, Hane F, Eng L, Leonenko Z. 2010. Kelvin Probe Force Microscopy in Application to Biomolecular Films: Frequency Modulation, Amplitude Modulation, and Lift Mode. *Ultramicroscopy*, 110: 708-711.
- Morita M, Hamada T, Tendo Y, Hata T, C. MC, Takagi M. (2012). Selective localization of Alzheimer's amyloid beta in membrane lateral compartments. *Soft Matter*, 8: 2816-2819.
- Mouritsen OJ. (2010). The liquid-ordered state comes of age. *Biochem. Biophys. Acta: Biomembr.*, 1798(7): 1286–1288.
- Mucke L, Selkoe DJ. (2012). Neurotoxicity of amyloid β -protein: synaptic and network dysfunction. *Cold Spring Harb. Perspect. Med.*, 2(7): a006338.

- Mukherjee S, Chattopadhyay, A. (2005). Monitoring cholesterol organization in membranes at low concentrations utilizing the wavelength-selective fluorescence approach. *Chem. Phys. Lipids*, 134(1), 79–84.
- Muller WE, Eckert GP, Scheuer K, Cairns NJ, Maras A, Gattaz WF. (1998). Effects of beta-amyloid peptides on the fluidity of membranes from frontal and parietal lobes of human brain. High potencies of A beta 1-42 and A beta 1-43. *Amyloid*, 5(1):10-15.
- Mutisya EM, Bowling AC, Beal MF. (1994). Cortical cytochrome oxidase activity is reduced in Alzheimer's disease. *J. Neurochem.*, 63(6):2179-2184.
- Neugroschl J, Sano M. (2010) Current treatment and recent clinical research in Alzheimer's disease. *Mt. Sinai J. Med.*, 77, 3-16.
- Nieh MP, Yamani Z, Kučerka N, Katsaras J, Burgess D, Breton H. (2008). Adapting a triple-axis spectrometer for small angle neutron scattering measurements. *Rev. Sci. Instrum.*, 79(9): 095102.
- Niemela PS, Ollila S, Hyvo MT, Karttunen M, Vattulainen I. (2007). Assessing the nature of lipid raft membranes. *PLoS Comput. Biol.*, 3(2), e34.
- Nonnenmacher M, O'Boyle MP, Wickramasinghe HK. 1991. Kelvin probe force microscopy. *Appl. Phys. Lett.*, 58: 2921.
- Norlin N, Hellberg M, Filippov A, Sousa AA, Grobner G, Leapman RD, Almqvist N, Antzutkin ON. (2012). Aggregation and fibril morphology of the Arctic mutation of Alzheimer's A β peptide by CD, TEM, STEM and in situ AFM. *J. Struct. Biol.*, 180(1):174-189.
- Nusrat A, Parkos CA, Verkade P, Foley CS, Liang TW, Whitehouse-Innis W, Eastburn KK, Madara JL. (2000). Tight junctions are membrane microdomains. *J. Cell Sci.*, 113: 1771 – 1781.
- O'Brien RJ, Wong PC. (2011). Amyloid precursor protein processing and Alzheimer's disease. *Ann. Rev. Neurosci.*, 34:185-204.
- Ohvo-Rekila H, Ramstedt B, Leppimaki P, Slotte J. (2002). Cholesterol Interactions with Phospholipids in Membranes. *Prog. Lipid Res.*, 41:66–97.
- Olcese JM, Cao C, Mori T, Mamcarz M, Maxwell A, Runfeldt MJ, Wang L, et al. (2009). Protection against cognitive deficits and markers of neurodegeneration by long-term oral administration of melatonin in a transgenic model of Alzheimer disease. *J. Pineal Res.*, 47(1): 82–96.
- Ono K, Condrón MM, Teplow DB. (2009). Structure-neurotoxicity relationships of amyloid beta-protein oligomers. *P. Natl. Acad. Sci. U.S.A.*, 106(35):14745-14750.

- Paiva D, Brezesinski G, Pereira MC, Rocha S. (2013). Langmuir Monolayers of Monocationic Lipid Mixed with Cholesterol or Fluorocholesterol: DNA Adsorption Studies. *Langmuir*, 20: 1920 – 1925.
- Pannuzzo M, Milardi D, Raudino A, Karttunen M, La Rosa, C. (2013). Analytical model and multiscale simulations of A β peptide aggregation in lipid membranes: towards a unifying description of conformational transitions, oligomerization and membrane damage. *Phys. Chem. Chem. Phys.*, 15(23): 8940-8951.
- Paravastu A, Leapman R, Yau W, Tycko R. (2008). Molecular structural basis for polymorphism in Alzheimer's beta-amyloid fibrils. *P. Natl. Acad. Sci. U.S.A.*, 105:18349-18354.
- Patel GJ, Behrens-Kneip S, Holst O, Kleinschmidt JH. (2009). The Periplasmic Chaperone Skp Facilitates Targeting, Insertion, and Folding of OmpA into Lipid Membranes with a Negative Membrane Surface Potential. *Biochem.*, 48(43):10235–10245.
- Petkova AT, Leapman RD, GuoZ, Yau W-M, Mattson MP, Tycko R, (2005). Self-propagating, molecular-level polymorphism in Alzheimer's β -amyloid fibrils. *Science*, 307 (5707):262-265.
- Pfleeger RL, Mandel L. 1967. Interference of independent photon beams, *Phys. Rev.*, 159(5): 1084–1088.
- Poeggeler B, Miravalle L, Zagorski MG, Wisniewski T, Chyan YJ, Zhang Y, Shao H, et al. (2001). Melatonin reverses the profibrillogenic activity of apolipoprotein E4 on the Alzheimer amyloid A β peptide. *Biochem.*, 40(49): 14995–15001.
- Poojari C, Kukol A, Strodel B. (2013). How the amyloid- β peptide and membranes affect each other: An extensive simulation study. *Biochim. Biophys. Acta – Biomem.*, 1828:327–339.
- Powers ET, Kelly JW. (2001). Medium-dependent self-assembly of an amphiphilic peptide: direct observation of peptide phase domains at the air-water interface. *J. Am. Chem. Soc.*, 123(4):775-776.
- Prenner E, Honsek G, Honig D, Mobius D, Lohner K. (2007). Imaging of the domain organization in sphingomyelin and phosphatidylcholine monolayers. *Chem Phys Lipids*, 145: 106 – 118.
- Prinetti A, Chigorno V, Prioni S, Loberto N, Marano N, Tettamanti G, Sonnino S. (2001). Changes in the Lipid Turnover, Composition, and Organization, as Sphingolipid-enriched Membrane Domains, in Rat Cerebellar Granule Cells Developing in Vitro. *J. Biol. Chem.*, 276(24): 21136 – 21145.

- Pronchik J, He X, Giurleo JT, Talaga DS. (2010). In vitro formation of amyloid from alpha-synuclein is dominated by reactions at hydrophobic interfaces. *J. Am. Chem. Soc.*, 132(28): 9797-9803.
- Puglielli L, Tanzi RE, Kovacs DM. (2003). Alzheimer's disease: the cholesterol. *Nat. Neurosci.*, 6(4), 345–351.
- Qin Z, Hu D, Zhu M, Fink AL. (2007). Structural characterization of the partially folded intermediates of an immunoglobulin light chain leading to amyloid fibrillation and amorphous aggregation. *Biochem.*, 46(11):3521-3531.
- Qiu L, Buie C, Reay A, Vaughn M, Cheng KH. (2011). Molecular Dynamics Simulations Reveal the Protective Role of Cholesterol in beta-Amyloid Protein-Induced Membrane Disruptions in Neuronal Membrane Mimics. *J. Phys. Chem. B*, 115:9795–9812.
- Qiu L, Lewis A, Como J, Vaughn MW, Huang J, Somerharju P, Virtanen J, Cheng KH. (2009). Cholesterol modulates the interaction of beta-amyloid peptide with lipid bilayers. *Biophys. J.*, 96(10): 4299–4307.
- Quist A, Doudevski I, Lin H, Azimova R, Ng D, Frangione B, Kagan B, Ghiso J, Lal, R. (2005). Amyloid ion channels: A common structural link for protein-misfolding disease. *P. Natl. Acad. Sci. U.S.A.*, 102(30):10427-10432.
- Quist A, Chand A, Ramachandran S, Daraio C, Jin S, Lal R. (2007). Atomic Force Microscopy Imaging and Electrical Recording of Lipid Bilayers Supported over Microfabricated Silicon Chip Nanopores: Lab-on-a-Chip System for Lipid Membranes and Ion Channels. *Langmuir*, 23: 1375-1380.
- Radhakrishnan A, Anderson TG, McConnell HM. (2000). Condensed complexes, rafts, and the chemical activity of cholesterol in membranes. *P. Natl. Acad. Sci. U.S.A.*, 97(23): 12422–12427.
- Radmacher M. (2007). Studying the Mechanics of Cellular Processes by Atomic Force Microscopy. *Methods in Cell Biology*. 83: 347 – 372.
- Rauch H, Petrascheck D. (1979). Neutron Diffraction. *Topics in Current Physics*, Ch 9. Springer Publishing, Berlin, Germany.
- Rauk A. (2009). The chemistry of Alzheimer's disease. *Chem. Soc. Rev.*, 38(9): 2698-2715.
- Refolo L, Malester B, LaFrancois J, Bryant-Thomas T, Wang R, Tint G, Sambamurti K, Duff K, Pappolla MA. (2000). Hypercholesterolemia accelerates the Alzheimer's amyloid pathology in a transgenic mouse model. *Neurobiol. Dis.*, 7: 321-331.
- Regelin A. (2000) Biophysical and lipofection studies of DOTAP analogs. *Biochim. Biophys. Acta*, 1464: 151-164.

- Relini A, Cavalleri O, Rolandi R, Gliozzi. (2009). The two-fold aspect of the interplay of amyloidogenic proteins with lipid membranes. *Chem. Phys. Lip.*, 158:1-9.
- Ridgley DM, Barone JR. (2013). Evolution of the amyloid fiber over multiple length scales. *ACS Nano*, 7(2):1006-1015.
- Risselada HJ, Marrink SJ. (2008). The molecular face of lipid rafts in model membranes. . *Proc. Natl. Acad. Sci. U S A.*, 105(45): 17367–17372.
- Roberson ED, Mucke L. (2006). 100 years and counting: prospects for defeating Alzheimer's disease. *Science*, 314(5800): 781-784.
- Rocha S, Krastev R, Thunemann AF, Pereira C, Mohwald H, Brezesinski G. (2005). Adsorption of amyloid β -peptide at polymer surfaces: a neutron reflectivity study. *Chemphyschem.*, 6(12):2527-2534.
- Roher AE, Chaney MO, Kuo YM, Webster SD, Stine WB, Haverkamp LJ, Woods AS, Cotter RJ, Tuohy JM, Krafft GA, Bonnell BS, Emmerling MR. (1996). Morphology and toxicity of A β (1-42) dimer derived from neurotic and vascular amyloid deposits of Alzheimer's disease. *J. Biol. Chem.*, 271:20631-20635.
- Rosales-Corral SA, Acuña-Castroviejo D, Coto-Montes A, Boga JA, Manchester LC, Fuentes-Broto L, Korkmaz A, et al. (2012). Alzheimer's disease: pathological mechanisms and the beneficial role of melatonin. *J. Pineal Res.*, 52(2): 167–202.
- Rugar D, Hansma P. (1990). Atomic Force Microscopy. *Phys. Today*, 43(10), 23–30.
- Rushworth JV, Hooper NM. (2011). Lipid Rafts: Linking Alzheimer's Amyloid- β Production, Aggregation, and Toxicity at Neuronal Membranes. *Int. J. Alzheimers Dis.*, 2011(1): 603052.
- Ryan T, Friedhube A, Lind M, Howlett G, Masters C, Roberts B. (2012). Small Amphipathic Molecules Modulate Secondary Structure and Amyloid Fibril-forming Kinetics of Alzheimer Disease Peptide A- β 1–42. *J. Biol. Chem.*, 287:16947–16954.
- Sack RL, Lewy AJ, Erb DL, Vollmer WM, Singer CM. (1986). Human melatonin production decreases with age. *J. Pineal Res.*, 3(4): 379–388.
- Sackmann E. (1995). Biological Membranes Architecture and Function. In R. Lipowski & E. Sackmann (Eds.), *Structure and dynamics of membranes - from cells to vesicles* (Vol. 1A., Vol. 1, pp. 1 – 65).
- Sahin I, Severcan F, Kazancı N. (2007). Melatonin induces opposite effects on order and dynamics of anionic DPPG model membranes. *J. Mol. Struct.*, 834-836: 195–201.
- Saija A, Tomaino A, Trombetta D, Pellegrino ML, Tita B, Caruso S, Castelli F. (2002). Interaction of melatonin with model membranes and possible implications in its photoprotective activity. *Eur. J. Pharm. Biopharm.*, 53(2): 209–215.

- Sasahara K, Morigaki K, Shinya K. (2013) Effects of membrane interaction and aggregation of amyloid β -peptide on lipid mobility and membrane domain structure. *Phys. Chem. Chem.*, 15(23): 8929-8939.
- Sayre LM, Perry G, Smith MA. (1999). Redox metals and neurodegenerative disease. *Curr. Opin. Chem. Biol.*, 3(2):220-225.
- Seelig A. (1987) Local anesthetics and pressure: a comparison of dibucaine binding to lipid monolayers and bilayers. *Biochim. Biophys. Acta*, 899: 196-204.
- Segers-Nolten I, van der Werf K, van Raaij M, Subramaniam V. (2007). Quantitative characterization of protein nanostructures using atomic force microscopy. *Conf. Proc. IEEE Eng. Med. Biol. Soc.*, 2007:6609-6612.
- Selkoe DJ. (1980). Altered protein composition of isolated human cortical neurons in Alzheimer disease. *Ann. Neurol.* 8(5):468-478.
- Selkoe DJ. (1991). The molecular pathology of Alzheimer's disease. *Neuron*, 6(4):487-498.
- Sepulveda J, Parodi RW, Peoples C, Opazo LG, Aguayo, L. (2010). Synaptotoxicity of Alzheimer beta amyloid can be explained by its membrane perforating property. *PLoS ONE*, 5:e11820
- Serrano-Pozo A, Frosch MP, Masliah E, Hyman BT. (2011). Neuropathological alternation in Alzheimer disease. *Cold Spring Harb. Perspect. Med.*, 1(1):a006189.
- Severcan F, Sahin I, Kazanci N. (2005). Melatonin strongly interacts with zwitterionic model membranes--evidence from Fourier transform infrared spectroscopy and differential scanning calorimetry. *Biochim. Biophys. Acta*, 1668(2): 215–222.
- Sharp JS, Forrest JA, Jones RA. (2002). Surface denaturation and amyloid fibril formation of insulin at model lipid-water interfaces. *Biochem.*, 41(52): 15810-15819.
- Sheikh K, Giordani C, McManus J, Hovgaard M, Jarvis J. (2012). Differing modes of interaction between monomeric A β 1–40 peptides and model lipid membranes: an AFM study. *Chem. Phys. Lipids*, 165: 142– 150.
- Shen L, Adachi T, Bout DV, Zhu X. (2012). A mobile precursor determines amyloid- β peptide fibril formation at interfaces. *J. Am. Chem. Soc.*, 134(34): 14172-14178.
- Shulga N, Wilson-Smith R, Pastorino JG. (2009). Hexokinase II detachment from the mitochondria potentiates cisplatin induced cytotoxicity through a caspase-2 dependent mechanism. *Cell Cycle*, 8(20):3355-3364.
- Silvius J. (1982) Thermotropic phase transitions of pure lipids in model membranes and their modifications by membrane proteins. *In: Lipid-Protein Interactions*, John Wiley & Sons, Inc., New York.

- Simakova O, Arispe NJ. (2007). The cell-selective neurotoxicity of the Alzheimer's Abeta peptide is determined by surface phosphatidylserine and cytosolic ATP levels. Membrane binding is required for Abeta toxicity. *J. Neurosci.*, 27(50): 13719–13729.
- Simons K, Toomre D. (2000). Lipid rafts and signal transduction. *Nat. Rev. Mol. Cell Biol.*, 1: 31-41.
- Simons K, Vanmeer G. (1988). Lipid sorting in epithelial cells. *Biochem.*, 27(17): 6197-6202.
- Singer SJ, Nicolson GL. (1972). The fluid mosaic model of the structure of cell membranes. *Science*, 175(4023): 720–731.
- Sipe JD, Benson MD, Buxbaum JN, Ikeda S, Merlini G, Saraiva MJ, Westermark P. (2010). Amyloid fibril protein nomenclature: 2010 recommendations from the nomenclature committee of the International Society of Amyloidosis. *Amyloid*, 17(3-4): 101-104.
- Skovronsky DM, Zhang B, Kung MP, Kung HF, Trojanowski JQ, Lee VMY. (2000). In vivo detection of amyloid plaques in a mouse model of Alzheimer's disease. *Proc. Natl. Acad. Sci. U.S.A.*, 97(13): 7609–7614.
- Soderberg M, Edlund C, Kristensson K, Dallner G. (1991). Fatty acid composition of brain phospholipids in aging and in Alzheimer's disease. *Lipids.*, 26(6): 421 – 425.
- Sokolov Y, Kozak JA, Kaye R, Chanturiya A, Glabe C, Hall JE. (2006). Soluble amyloid oligomers increase bilayer conductance by altering dielectric structure. *J. Gen. Physiol.*, 128(6): 637-647.
- Soscia SJ, Kirby JE, Washicosky KJ, Tucker SM, Ingelsson M, Hyman B, Burton MA, Goldstein LE, Duong S, Tanzi RE, Moir RD. (2010). The Alzheimer's disease-associated amyloid β -protein is an antimicrobial peptide. *PLoS ONE*, 5(3):e5905.
- Sriram I, Schwartz DK. (2012). Line tension between coexisting phases in monolayers and bilayers of amphiphilic molecules. *Surf. Sci. Rep.*, 67(6): 143–159.
- Stefani M. (2012). Structural features of cytotoxicity of amyloid oligomers: Implications in Alzheimer's disease and other diseases with amyloid deposits. *Prog. Neurobiol.*, 99(3):226-245.
- Starke-Peterkovic T, Turner N, Vitha MF, Waller MP, Hibbs DE, Clarke RJ. (2006). Cholesterol Effect on the Dipole Potential of Lipid Membranes. *Biophys J.*, 90(11): 4060–4070.
- Stine WB, Snyder SW, Lador US, Wade WS, Miller MF, Perun TJ, Holzman TF, Krafft GA. (1996). The nanometer-scale structure of amyloid-beta visualized by atomic force microscopy. *J. Protein Chem.*, 15(2): 193-203.

- Stine WB, Dahlgren KN, Krafft GA, LaDu MJ. (2002). In vitro characterization of conditions for amyloid- β peptide oligomerization and fibrillogenesis. *J. Biol. Chem.*, 278:11612-11622.
- Suga K, Umakoshi H. (2013). Detection of Nanosized Ordered Domains in DOPC/DPPC and DOPC/Ch Binary Lipid Mixture Systems of Large Unilamellar Vesicles Using a TEMPO Quenching Method. *Langmuir*, 29(15): 4830–4838.
- Sukhorukov VL, Kürschner M, Dilsky S, Lisec T, Wagner B, Schenk WA, Benz R, Zimmermann U. (2001). Phloretin-induced changes of lipophilic ion transport across the plasma membrane of mammalian cells. *Biophys. J.*, 81(2): 1006–1013.
- Svennerholm L, Gottfries CG. (1994). Membrane lipids, selectively diminished in Alzheimer brains, suggest synapse loss as a primary event in early-onset form (type I) and demyelination in late-onset form (type II). *J. Neurochem.*, 62(3): 1039–1047.
- Tanzi RE, McClatchey AI, Lamperti ED, Villa-Komaroff L, Gusella JF, Neve RL. (1988). Protease inhibitor domain encoded by an amyloid protein precursor mRNA associated with Alzheimer's disease. *Nature*, 331(6156): 528-530.
- Terzi E, Holzemann G, Seelig J. (1995). Self-association of beta-amyloid peptide (1-40) in solution and binding to lipid membranes. *J. Mol. Biol.*, 252(5): 633-642.
- Thinnes FP, Gotz H, Kayser H, Benz R, Schmidt WE, Kratzin HD, Hilschmann N. (1989). Identification of human porins. I. Purification of a porin from human B-lymphocytes (Porin 31HL) and the topochemical proof of its expression on the plasmalemma of the progenitor cell. *Biol. Chem. Hoppe-Seyler*, 370(12): 1253-1264.
- Tofoleanu F, Buchete NV. (2012). Alzheimer A β peptide interactions with lipid membranes: Fibrils, oligomers and polymorphic amyloid channels. *Prion*. 6(4): 339-345.
- Tristram-Nagle SA. (2007). Preparation of oriented, fully hydrated lipid samples for structure determination using X-ray scattering. *Methods Mol. Biol.*, 400: 63–75.
- Uversky VN, Li J, Fink AL. (2001). Evidence for a partially folded intermediate in alpha-synuclein fibril formation. *J. Biol. Chem.*, 276(14):10737-10744.
- Veatch S and Keller S. (2005a). Miscibility phase diagrams of giant vesicles containing sphingomyelin. *Phys. Rev. Lett.*, 94(14): 148101.
- Veatch S and Keller S. (2005b). Seeing spots: Complex phase behavior in simple membranes. 2005b. *Biochim. Biophys. Acta: Mol. Cell Res.*, 1746(3): 172–185.
- Veatch SL, Polozov IV, Gawrisch K, Keller SL. (2004). Liquid Domains in Vesicles Investigated by NMR and Fluorescence Microscopy. *Biophys. J.*, 86(5): 2910-2922.
- Veatch SL, Soubias O, Keller SL, Gawrisch K. (2007). Critical fluctuations in domain-forming lipid mixtures. *Proc. Natl. Acad. Sci. U S A.*, 104(45): 17650–17655.

- Verdier Y, Penke B. (2004). Binding sites of amyloid beta-peptide in cell plasma membrane and implications for Alzheimer's disease. *Curr. Protein Pept. Sci.*, 5(1):19-31.
- Vestergaard M, Hamada T, Takagi M. (2008). Using model membranes for the study of amyloid beta- Lipid interactions and neurotoxicity. *Biotechnol. Bioeng.*, 99(4): 753 – 763.
- Vestergaard MC, Morita M, Hamada T, Takagi M. (2010). Alzheimer's Amyloid beta: Lipid membrane interactions, detected in real-time. *2010 International Symposium on Micro-NanoMechatronics and Human Science*, 144–148.
- Vogel V, Mobius D. (1988). Local surface potentials and electric dipole moments of lipid monolayers: Contributions of the water/lipid and the lipid/air interfaces. *J. Colloid Interface Sci.*, 126(2): 408 – 420.
- Vogt K, Jeworrek C, Garamus VM, Winter R. (2010). Microdomains in Lipid Vesicles: Structure and Distribution Assessed by Small-Angle Neutron Scattering. *J. Phys. Chem. B*, 114(16): 5643–5648.
- Wakabayashi M, Matsuzaki K. (2007). Formation of amyloids by A β -(1–42) on NGF-differentiated PC12 cells: roles of gangliosides and cholesterol. *J. Mol. Biol*, 371: 924–933.
- Walsh DM, Klyubin I, Fadeeva JV, Cullen WK, Anwyl R, Wolfe MS, Rowan MJ, Selkoe DJ. (2002). Naturally secreted oligomers of amyloid beta protein potently inhibit hippocampal long-term potentiation in vivo. *Nature*, 416(6880): 535-539.
- Walsh DM, Klyubin I, Fadeeva JV, Rowan MJ, Selkoe DJ (2002) Amyloid- β oligomers: their production, toxicity and therapeutic inhibition. *Biochem. Soc. Trans.*, 30: 552-557.
- Walsh DM, Selkoe DJ. (2004). Oligomers on the brain: the emerging role of soluble protein aggregates in neurodegeneration. *Protein Pept. Lett.*, 11(3):213-228.
- Wang Q, Fan X, Gao W, Chen J. (2006). Characterization of bioscoured cotton fabrics using FT-IR ATR spectroscopy and microscopy techniques, *Carbohydrate Research*, 341: 2170– 2175.
- Wang Q, Walsh DM, Rowan MJ, Selkoe DJ, Anwyl R. (2004). Block of long-term potentiation by naturally secreted and synthetic amyloid beta-peptide in hippocampal slices is mediated via activation of the kinases c-Jun N-terminal kinase, cyclin-dependent kinase 5, and p38 mitogen-activated protein kinase as well as metabotropic glutamate receptor type 5. *J. Neurosci.*, 24(13):3370-3378.
- Wang Q, Zhao J, Yu Z, Zhao C, Li L, Zheng J. (2010). Alzheimer A β (1-42) monomer adsorbed on the self-assembled monolayers. *Langmuir*, 26(15):12722-12732.

- Wang Z, Zhou C, Wang C, Wan L, Fang X, Bai C. (2003). AFM and STM study of β -amyloid aggregation on graphite. *Ultramicroscopy*, 97(1-4):73-79.
- Wells K, Farooqui AA, Liss L, Horrocks LA. (1995). Neural membrane phospholipids in Alzheimer's disease. *Neurochemical Research*. 20(11):1329-1333.
- Whitehouse PJ, Price DL, Struble RG, Clark AW, Coyle T, DeLong MR. (1982). Alzheimer's Disease and Senile Dementia: Loss of Neurons in the Basal Forebrain. *Science*, 215(4537), 1237–1239.
- Williams T, Johnson B, Urbanc B, Jenkins A, Connell S, Serpell L. (2011). A β 42 oligomers, but not fibrils, simultaneously bind to and cause damage to ganglioside-containing lipid membranes. *Biochem. J.*, 439:67-77.
- Williamson R, Usardi A, Hanger D, Anderton, B. (2008). Membrane-bound β -amyloid oligomers are recruited into lipid rafts by a fyn-dependent mechanism. *FASEB J.*, 22:1552–1559.
- Winterhalter M. (2000). Black Lipid Membranes. *Curr. Opin. Colloid Interface Sci.*, 5: 250 – 255.
- Worcester DL, Franks NP. (1976). Structural analysis of hydrated egg lecithin and cholesterol bilayers II. Neutron diffraction. *J. Mol. Biol.*, 100: 359–378.
- Yamaguchi T, Yagi H, Goto Y, Matsuzaki K, Hoshino M. (2010). A disulfide-linked amyloid- β peptide dimer forms a protofibril-like oligomer through a distinct pathway from amyloid fibril formation. *Biochem.*, 49(33):7100-7107.
- Yanagisawa K. (2011). Pathological significance of ganglioside clusters in Alzheimer's disease. *J. Neurochem.*, 116: 806–812.
- Yanagisawa K, Ihara Y. (1998). GM1 ganglioside- bound amyloid β -protein in Alzheimer's disease brain. *Neurobiol. Aging*, 19: S65–S67.
- Yanagisawa K, Odaka A, Suzuki N, Ihara Y. (1995). GM1 ganglioside-bound amyloid beta-protein (A β): a possible form of preamyloid in Alzheimer's disease. *Nat. Med.*, 1(10): 1062-1066.
- Yang T, Hong S, O'Malley T, Sperling RA, Walsh DM, Selkoe DJ. (2013). New ELISAs with high specificity for soluble oligomers of amyloid β -protein detect natural A β oligomers in human brain but not CSF. *Alzheimer's & Dementia*, 9(2): 99-112.
- Yeagle PL. (1985). Cholesterol and the cell membrane. *Biochim. Biophys. Acta*, 822, 267–287.
- Yip CM, Elton EA, Darabie AA, Morrison MR, McLaurin J. (2001). Cholesterol, a modulator of membrane-associated A β -fibrillogenesis and neurotoxicity. *J. Mol. Biol.*, 311(4):723-734.

- Yokoyama K, Welchons DR. (2007). The conjugation of amyloid beta protein on the gold colloidal nanoparticles' surfaces. *Nanotech.*, 18(10):105101.
- Yu X, Wang Q, Lin Y, Zhao J, Zhao C, Zheng J. (2012). Structure, orientation, and surface interaction of Alzheimer Amyloid- β peptides on the graphite. *Langmuir*, 28(16):6595-6605.
- Yu X, Zheng J. (2012). Cholesterol Promotes the Interaction of Alzheimer β -Amyloid Monomer with Lipid Bilayer. *J. Mol. Biol.*, 421: 561–571.
- Zampagni M, Evangelisti E, Cascella R, Liguri G, Becatti M, Pensalfini A, Uberti D, Cenini G, Memo M, Bagnoli S, Nacmias B, Sorbi S, Cecchi C. (2010). Lipid rafts are primary mediators of amyloid oxidative attack on plasma membrane. *J. Mol. Med.*, 88:597-608.
- Zerweck U, Loppacher C, Otto T, Grafstrom S, Eng L. (2005). Accuracy and resolution limits of Kelvin probe force microscopy. *Phys. Rev. B*, 71(12): 125424-125433.
- Zhao L, Long H, Mu Y, Yue Chew L. (2012). The Toxicity of Amyloid-beta Oligomers. *Int. J. Mol. Sci.*, 13:7303-7327.
- Zhong Q, Inniss D, Kjoller K, Elings VB. (1993). Fractured polymer / silica fiber surface studied by tapping mode atomic force microscopy. *Surf. Sci. Lett.*, 290, L688–L692.
- Zhu M, Souillac PO, Ionescu-Zanetti C, Carter SA, Fink AL. (2002). Surface-catalyzed amyloid fibril formation. *J. Biol. Chem.*, 277(52): 50914-50922.

Appendix A: Additional Information on Sample Preparation

A.1 Monolayer Formation via Langmuir-Blodgett Deposition

A.1.1 Solid-Supporting Sample Formation (on a Mica Substrate)

1. Fully clean off the trough and the barriers using chloroform and Kimwipes
 - Kimwipes are used because they do not release any particles that could contaminate the surface of your trough rather than cleaning it
 - When cleaning the trough, make sure that no droplets of chloroform are left – if this happens, the chloroform will evaporate and any contaminants that were in the droplet will be left on the trough
2. Fill the trough with “clean” water
 - Water used should either be distilled (such as Ultrapure or Nanopure water, in which virtually all impurities are removed from the water) or deionized (removes minerals from water quickly, giving water that is quite similar to distilled water, however normal deionizing process do not necessarily remove uncharged organic molecules)
3. Use a new Wilhelmy paper plate (for the pressure sensor) and submerge it in the subphase, allowing it to absorb the water and equilibrate
 - It is best to use a new plate every time you switch to a new sample
 - The plate is fully equilibrated with the subphase when the pressure reading stabilizes (wait time typically ~ 10 minutes)
4. After pressure equilibration, raise the pressure sensor so that the plate is completely out of the water and zero the pressure sensor
5. Re-submerge the plate and then slowly raise the pedestal so that the plate leaves the water again
 - The subphase will exert forces on the plate, essentially pulling down on the plate as it is being raised out of the water
 - Just as the plate leaves the subphase, the forces on the plate are at the ideal surface pressure and the optimal surface tension can be measured
6. According to the value the pressure sensor is reading, clean off the surface of the subphase using the aspirator or continue on with adding your sample to the surface

- The ideal surface tension for pure water at a temperature of 20°C is 72.8 mN/m; at 25°C, it is 72.0 mN/m; and at 37°C (healthy body temperature), it is 70.0 mN/m
 - Please note that the previously mentioned surface tension values are for *ideal* conditions, therefore it is very unlikely to achieve these exact values in practice
 - It is also good practice to check that the surface pressure of the clean subphase does not change when the trough is compressed and when it is open; therefore, close the trough barriers and watch to see if the pressure changes; it is best for the pressure to not alter more than 0.1 mN/m
 - To ensure that your surface does not get contaminated after you have already cleaned it, it is best to have the trough in a protective enclosure, like the protective cabinet
7. Taking your solid substrate, attach it to the dipping mechanism, ensuring that it is clean and contaminant free. Lower the dipping arm so that the mica is almost fully submerged in the subphase of the trough; the only portion of the mica not submerged is that portion that is attached to the clamp
- By freshly cleaving the mica, untouched and unspoiled layers of the substrate are revealed, while are atomically flat (necessary for AFM studies)
8. Add desired amount of lipid (mixture) solution to subphase of trough and allow for equilibration (~ 10 minutes for a microtrough)
- To ensure that the lipids spread across the surface of the subphase, add drops very slowly to the surface and without touching the subphase at all
 - The pressure will spike as soon as the sample is added and then go back down; dependent on the amount added to the trough, the pressure reading may not return to 0 – this is normal
 - **Never** re-zero the pressure sensor once sample has been added to the surface of the trough
9. Using the applicable pressure (i.e. for membrane comparisons, the pressure is typically 35 mN/m), set up a pressure control for the trough (the barrier arms will close, causing a decrease in surface area that will translate in an increase in pressure for the sample until the desired pressure is reached, at which time the barrier arms will hold that pressure steady)
10. Using the dipper menu of the trough, choose the creep up option

- This will slowly raise the sample at a constant speed; the substrate will travel through the monolayer of lipid atop the trough subphase and collect a sample of the monolayer at the desired specific pressure
 - Speed of the dipper can be altered but typically the dipper is set at 2 mm/min for a crawl up
11. After deposition is completed (i.e. the dipper has fully raised the solid substrate out of the trough), allow the substrate to air dry (within the confines of the trough's protective enclosure) for ten minutes
- You can also use a very gentle stream of N₂ gas to dry off the sample; however, the substrate tends to be very fragile and anything more than a very gentle stream of gas can cause damage to the sample
12. Store in a dessicator for at least 24 hours prior to further analysis (i.e. with the AFM)

A.1.2 Trough Cleaning Procedures

1. When first using the trough, you first want to clean the PTFE surface using HPLC chloroform that is in the chloroform wash bottle
- Do not use the chloroform that is from sample preparation – this will cause contaminations and it will no longer be suitable for sample use
 - Moisten a Kimwipe with chloroform and clean off the base of the trough as well as the barriers (make sure that the wipe is saturated enough so that it will not dry while you are wiping down the trough)
 - As you are cleaning, wipe with different portions of the Kimwipe (so that you are cleaning with “fresh” areas and not just relocating contaminants)
2. Fill the trough with Nanopure water outside the barrier contained area (so that no contaminants are poured directly
- If you are concerned about the cleanliness of the trough (i.e. if you are unsure of what sample was experimented with on the trough previously), this water can be removed by completely closing the barriers and vacuuming off the water at the surface in the contained area until all the water is removed → then, refill the trough with Nanopure water

3. Syringes used must be rinsed three times with chloroform before use but also immediately after use

- After using the syringe, the chloroform portion of the sample will evaporate quickly, leaving only sample on the walls of the syringe, which is very hard to remove!

4. After using the trough, you **MUST** close the barriers completely and remove the water by vacuuming off the surface of the liquid

- This ensures that any lipids or sample on the surface of the trough is removed first
- If this is not done (i.e. water is removed from the bulk phase), the sample of the surface will contaminate the surface of the PTFE, and is then very hard to clean off

A.1.3 Kelvin Compatible Samples

In order to conduct Kelvin probe force microscopy studies on the monolayer samples in air, a solid-supported mica sample must be attached to a conductive plate to allow for conductivity of the sample and an electric current to flow between the sample and conducting tip.

After 24 hours of drying time in a dessicator, carefully take mica sample (always wearing gloves to prevent contamination) and attach a conductive substrate to the bottom of the mica (ideally using conductive tape). These may be circular conductive plates (can be purchased from Sigma-Aldrich) or as simple as a piece of aluminum foil with dimensions slightly larger than that of the piece of mica. In the case of the foil, the mica should be attached to the very centre of the piece of foil with pieces of conductive tape. The excess foil on each side can then be folded over and secured in each corner with an additional piece of conductive tape.

A.2 Membrane Formation via Vesicle Fusion

A.2.1 Preparing a Vesicle Solution

→ the mixed lipid vesicle solutions are each made at a concentration of 0.5 mg/mL

From Powdered Lipid

1a) The appropriate amount of powdered lipids are measured into small vials

- An appropriate amount is typically ~ 2 mg

- Measure by first weighing the empty storage bottle, zero the balance and then add powdered lipid into the bottle
 - If using weigh paper / weigh boats, tend to lose material when transferring in to bottle

From Lipids Suspended in Chloroform

1b) Make lipid stock solutions in chloroform (usually go with a 1 mg/mL concentration – measure powdered lipid into an empty storage bottle, as in step 1a and add in the appropriate amount of chloroform to make the concentration 1 mg/mL)

- Evaporate off the chloroform
- Store lipid solutions in chloroform in -20°C freezer when not in use

→ using this method makes mixed lipid vesicle solutions MUCH easier to prepare

-the following is an example of how to make a complex mixture from single lipid stock solutions:

Lipids	Ratio
DPPC – POPC – SM – Chol – GM1	37 : 37 : 10 : 10 : 6

-these sample ratios are based on weight

-for typical sample preparation, we make stock solutions of lipids at a concentration of 1 mg/mL in chloroform and then combine specific amounts to make the mixtures

- For example, for the “healthy” neuron mixture, to make it, I would combine from their stock solutions:
 - 370 µL DPPC
 - 370 µL POPC
 - 100 µL SM
 - 100 µL Chol
 - 60 µL GM1

2. Add Nanopure water / buffer to make concentration of solution 0.5 mg/mL

- i.e. if have 3 mg of lipid, add 6 mL of solvent

→ This initial combination results in the formation of vesicles of varying sizes and multilamellar bodies, causing the solution to appear cloudy

- add in a freshly cleaned (rinsed three times in ethanol and three times in whatever solvent is being used – water or buffer)
3. In order to create a solution of vesicles of uniform size, the lipid solution is sonicated for 10-minute intervals
 4. Between these periods of sonication the solution is stirred at room temperature for 15 minutes
→ This cycle is repeated until the solution became clear indicating the presence of uniform vesicles.
 5. Optional Step: The solution is then filtered using 0.2 μm filter caps on syringes.
 - This step is not always necessary – if after 24+ hours of vesicle solution prep time the solution is still cloudy, then filtering may be the only option for getting uniformly sized vesicles
 6. Store in fridge

A.2.2 Membrane Preparation using Vesicle Solution

1. Obtain hydrophilic substrate or thiol modified substrate that will allow for lipid binding
 - Excellent substrate is freshly cleaved mica (atomically flat and hydrophilic)
 - For membrane analysis, because it must be kept in constant hydration, liquid imaging on the AFM must be used; typically AFMs have their own liquid cell (to prevent leakage) so ideally the substrate would be modified to fit the liquid cell perfectly (i.e. for Agilent AFM – mica can be cut in a circular shape to exactly fit the cell)
2. Add aliquot of vesicle solution to surface of substrate and allow it to incubate for 10 minutes
 - typically 100 μL for 10 minutes – if surface coverage does not look adequate or if after 10 minutes, evaporation seems to be an issue, can alter amount and time of incubation (i.e. 300 μL for 10 minutes)
 - if using a vesicle solution that has been stored in the fridge overnight, sonicate it for 10 minutes prior to using it
3. After the incubation time period, gently rinse away the excess vesicle solution with solvent at least three times
 - avoid too much force or a direct harsh stream of solvent on the membrane – this can cause holes

- Can fill a syringe with the solvent and use that to direct the stream at the side of the liquid cell and let the solvent seep into the cell and run over
- **Need to maintain hydration at all times**
 - Typically cannot be stored for longer than 48 hours (all the while in constant hydration)

A.3 Amyloid Preparation

1. The peptide is treated according to the Fezoui procedure to ensure it is in a monomeric form (essential for studies looking at effects on fibrilization)
2. Add HEPES buffer to a 0.5 mg vial of $A\beta_{1-42}$
 - Amount of buffer added depends on desired final concentration of the amyloid
 - i.e. for amyloid incubations on healthy vs diseased membranes (chapter 7), a 40 mM solution of $A\beta_{1-42}$ was used:
 - 0.5 mg $A\beta_{1-42}$ + 2.77 mL HEPES buffer yielded the desired concentration
3. The solution is sonicated for 1 minute
4. Amyloid should be immediately used
 - incubation time starts as soon as buffer is added and sonicated
 - if doing membrane studies, the amyloid must be added to the pre-made membranes immediately
 - typically, 100 μ L of amyloid solution is added to the membrane (must add same amount to every membrane being studied for consistency and control of variables)

A.4 Buffer Preparation

The major buffer used for amyloid experiments in this thesis is HEPES (4-(2-hydroxyethyl)-1-piperazineethanesulfonic acid) buffer. The following is a preparation outline for making 1L of the buffer at a concentration of 20 mM HEPES and 100 mM NaCl, pH 7.4:

1. Dissolve 4.766 g HEPES in 800 mL distilled water
2. Add in 5.844 g NaCl to solution
3. Mix well (using magnetic plate stirrer and stir-bar)
4. Adjust pH to 7.4 using NaOH
5. Add distilled water to bring total volume up to 1.00 L

$$n = m / M$$

$$C = n/V$$

$$V = 1.00L$$

$$\text{HEPES: } M = 238.3 \text{ g/mol}$$

$$m = 4.766 \text{ g}$$

$$n = 0.02 \text{ mol}$$

$$C = 0.02 \text{ mol/L}$$

$$= 20 \text{ mM}$$

$$\text{NaCl: } M = 58.44 \text{ g/mol}$$

$$m = 5.844 \text{ g}$$

$$n = 0.10 \text{ mol}$$

$$C = 0.10 \text{ mol/L}$$

$$= 100 \text{ mM}$$